frontiers | Research Topics

Experimental models and model organisms in cardiac electrophysiology: Opportunities and challenges

Edited by
Ruben Coronel, Igor R. Efimov, Fanny Vaillant, Chris Jopling, Yoram Etzion, Bianca J. J. M. Brundel, Jolanda Van Der Velden and Flavien Charpentier

Published in
Frontiers in Physiology

ISSN 1664-8714
ISBN 978-2-8325-3523-3
DOI 10.3389/978-2-8325-3523-3

About Frontiers

Frontiers is more than just an open access publisher of scholarly articles: it is a pioneering approach to the world of academia, radically improving the way scholarly research is managed. The grand vision of Frontiers is a world where all people have an equal opportunity to seek, share and generate knowledge. Frontiers provides immediate and permanent online open access to all its publications, but this alone is not enough to realize our grand goals.

Frontiers journal series

The Frontiers journal series is a multi-tier and interdisciplinary set of open-access, online journals, promising a paradigm shift from the current review, selection and dissemination processes in academic publishing. All Frontiers journals are driven by researchers for researchers; therefore, they constitute a service to the scholarly community. At the same time, the *Frontiers journal series* operates on a revolutionary invention, the tiered publishing system, initially addressing specific communities of scholars, and gradually climbing up to broader public understanding, thus serving the interests of the lay society, too.

Dedication to quality

Each Frontiers article is a landmark of the highest quality, thanks to genuinely collaborative interactions between authors and review editors, who include some of the world's best academicians. Research must be certified by peers before entering a stream of knowledge that may eventually reach the public - and shape society; therefore, Frontiers only applies the most rigorous and unbiased reviews. Frontiers revolutionizes research publishing by freely delivering the most outstanding research, evaluated with no bias from both the academic and social point of view. By applying the most advanced information technologies, Frontiers is catapulting scholarly publishing into a new generation.

What are Frontiers Research Topics?

Frontiers Research Topics are very popular trademarks of the *Frontiers journals series*: they are collections of at least ten articles, all centered on a particular subject. With their unique mix of varied contributions from Original Research to Review Articles, Frontiers Research Topics unify the most influential researchers, the latest key findings and historical advances in a hot research area.

Find out more on how to host your own Frontiers Research Topic or contribute to one as an author by contacting the Frontiers editorial office: frontiersin.org/about/contact

Experimental models and model organisms in cardiac electrophysiology: Opportunities and challenges

Topic editors

Ruben Coronel — University of Amsterdam, Netherlands
Igor R. Efimov — Northwestern University, United States
Fanny Vaillant — Université de Bordeaux, France
Chris Jopling — Institut National de la Santé et de la Recherche Médicale (INSERM), France
Yoram Etzion — Ben-Gurion University of the Negev, Israel
Bianca J. J. M. Brundel — Amsterdam University Medical Center, Netherlands
Jolanda Van Der Velden — VU Medical Center, Netherlands
Flavien Charpentier — INSERM U1087 Institut du Thorax, France

Citation

Coronel, R., Efimov, I. R., Vaillant, F., Jopling, C., Etzion, Y., Brundel, B. J. J. M., Van Der Velden, J., Charpentier, F., eds. (2023). *Experimental models and model organisms in cardiac electrophysiology: Opportunities and challenges*. Lausanne: Frontiers Media SA. doi: 10.3389/978-2-8325-3523-3

Table of contents

frontiers | Frontiers in Physiology

TYPE Editorial
PUBLISHED 06 September 2023
DOI 10.3389/fphys.2023.1254596

OPEN ACCESS

EDITED AND REVIEWED BY
Jordi Heijman,
Maastricht University, Netherlands

*CORRESPONDENCE
Bianca J. J. M. Brundel,
b.brundel@amsterdamumc.nl

RECEIVED 07 July 2023
ACCEPTED 24 July 2023
PUBLISHED 06 September 2023

CITATION
Brundel BJJM, Jopling C, Efimov IR, Charpentier F and Etzion Y (2023), Editorial: Experimental models and model organisms in cardiac electrophysiology: opportunities and challenges.
Front. Physiol. 14:1254596.
doi: 10.3389/fphys.2023.1254596

Editorial: Experimental models and model organisms in cardiac electrophysiology: opportunities and challenges

Bianca J. J. M. Brundel[1]*, Chris Jopling[2], Igor R. Efimov[3,4], Flavien Charpentier[5] and Yoram Etzion[6]

[1]Department of Physiology, Amsterdam Cardiovascular Sciences, Amsterdam University Medical Centers, VU Universiteit, Amsterdam, Netherlands, [2]Institute of Functional Genomics, University of Montpellier, CNRS, INSERM, LabEx ICST, Montpellier, France, [3]Department of Biomedical Engineering, Northwestern University, Chicago, IL, United States, [4]Department of Medicine, Northwestern University, Chicago, IL, United States, [5]Nantes Université, CNRS, INSERM, L'institut Du Thorax, Nantes, France, [6]Department of Physiology and Cell Biology, Ben-Gurion University of the Negev, Beer-Sheva, Israel

KEYWORDS

experimental models, cardiac electrophysiology, arrhythmia, model organisms, cardiac electrophysiologic technique

Editorial on the Research Topic
Experimental models and model organisms in cardiac electrophysiology: opportunities and challenges

Cardiac diseases are the main cause of death worldwide and their incidence and prevalence are likely to increase because of ageing of the population and unhealthy changes in lifestyle. Prevailing theories about the mechanisms of cardiac disease onset, encompass molecular and electrophysiological changes in the cardiac tissue and cells. Insights into the underlying molecular mechanisms are essential to create a deeper understanding of key concepts of cardiac disease development. Moreover, mechanistic insights may drive the development of novel technologies to explore further mechanisms as well as diagnostic and therapeutic tools for cardiac disease management in the clinic.

In this Research Topic "*Experimental Models and Model Organisms in Cardiac Electrophysiology: Opportunities and Challenges*" various experimental model systems are discussed that enable mechanistic studies on molecular mechanisms and electrophysiological changes that drive cardiac diseases. Experimental model systems include induced pluripotent stem cell (iPSC)-derived cardiomyocytes, as well as cultured neonatal monolayers of cardiomyocytes and fibroblasts. The contribution of Carvalho et al. describes the potential of iPSC-derived cardiomyocytes from healthy donors as a disease model to study electrical properties. By testing the action potential variability of 780 cardiomyocytes from six healthy heart donors, they observed that the action potential data per cell line, per differentiation protocol and per batch fluctuates. This has important consequences for mechanistic studies on arrhythmias. Further standardization of iPSC cardiomyocyte culture is needed for arrhythmia research. In line with Carvalho, the paper of Isamili et al. points out the biological and methodological issues researchers have to consider when working with iPSC-derived cardiomyocytes. Challenges include the variation in ion-channel currents, action potential durations, and atrial

phenotype of atrial cardiomyocytes compared to isolated adult human cardiomyocytes. Despite these drawbacks, the authors are hopeful as they expect that the concerted expertise of experimental electrophysiologists and stem cell experts will eventually solve the challenges.

An innovative emerging model system in arrhythmia research is the use of (human) living myocardial tissue slices. Amesz et al. provide an overview of the potential of utilizing living myocardial slices in electrophysiological studies. The authors state that human atrial and ventricular tissue slices of 150–400 µm thickness (6–17 cardiomyocyte layers) can be used for action potential recordings, optical mapping, and extracellular field potential mapping. So far, living myocardial tissue slices hold the promise to facilitate detailed research on cardiac arrhythmias. Optogenetic light-based pacing is an emerging technique to manipulate cardiac activity in a spatial- and temporal-specific manner and improve our understanding of arrhythmogenic mechanisms. Marchal et al. show their results on the application of low-intensity, sub-threshold illumination to selectively manipulate cardiac electrical activity in defined areas of the heart. This approach enables the study of conduction slowing and repolarization heterogeneities during cardiac disease.

In addition to innovative model systems and technologies as described above, novel methodological insight into the interpretation of ECG data may improve the identification of cardiac arrhythmias. Mulla et al. review differences in rate-adaptation of ECG properties in mice and rats compared to humans. Although mice and rats have been used for decades as model systems to study cardiac arrhythmias, conflicting data on QT interval rate-dependence still exists, and therefore the authors state that the empirical ways by which QT intervals are corrected in rodent studies should be revisited. In addition to improved interpretation of ECG data in rodents, optimal programmed electrical stimulation is a prerequisite to assess atrial fibrillation susceptibility. Murphy et al. provide important insight into the optimal pacing protocol to elicit an atrial fibrillation phenotype in mice. Their main message is that for each study, an individualized protocol should be developed. Amorós-Figueras et al. describe a pig model for atrial arrhythmia by scarring of the atrium. Scarring is induced via selective occlusion of the atrial branches, resulting in atrial infarction in the left atrium, and low voltage of bipolar electrograms in affected areas. This model may have potential applicability for studying atrial arrhythmia mechanisms. According to Alameh et al. improved characterization of ion channel activity is required to more accurately study the role of hERG, the pore-forming subunit of the rapid component of the delayed rectifier K^+ current, in ventricular repolarization. Mutations in hERG are associated with Long QT syndrome, but most identified variants have unknown or unclear functional consequences and are thus classified as variants of unknown significance. The authors advocate for a unique homogeneous protocol that could ultimately facilitate Long QT syndrome management. Lastly, Ernault et al. study the impact of atrial fibrosis on the development of atrial fibrillation. They describe that the selective disruption of primary cilia in fibroblasts via Ift88 knock-out induces extracellular matrix production, decreases conduction velocity, increases the number of block lines, and increases the risk or reentrant arrhythmias without changing the action potential (AP) characteristics of co-cultured cardiomyocytes with fibroblasts. The data suggest that dysregulation of primary cilia causes fibrosis and hinders myocardial conduction, thereby producing an arrhythmogenic substrate.

In summary, multiple model systems and technical approaches have been developed to study molecular and electrophysiological changes that drive cardiac arrhythmia in recent years. Novel mechanistic findings are important as they will fuel the identification of druggable and diagnostic targets, to ultimately improve clinical arrhythmia management. Hereto, a novel standardized methodology for the design of the models, induction of arrhythmias, and interpretation of the data is of prime importance. This Research Topic provides insights into all items relevant for solid translational research on cardiac arrhythmias.

Author contributions

BB: Writing–original draft, Writing–review and editing. IE: Writing–review and editing. YE: Writing–review and editing. CJ: Writing–review and editing. FC: Writing–review and editing. All authors contributed to the article and approved the submitted version.

Funding

BB is funded by the Dutch Heart Foundation (2020-2020B003, DnAFix project), and NWO (NWA.1389.20.157 CIRCULAR). FC is funded by the ANR (ANR-19-CE14-0031-02 & ANR-22-CE17-0051-01).

Conflict of interest

The authors declare that the research was conducted in the absence of any commercial or financial relationships that could be construed as a potential conflict of interest.

Publisher's note

frontiers | Frontiers in Physiology

TYPE Mini Review
PUBLISHED 11 October 2022
DOI 10.3389/fphys.2022.1002203

OPEN ACCESS

EDITED BY
Brian P. Delisle,
University of Kentucky, United States

REVIEWED BY
Alex Carll,
University of Louisville, United States
Bastiaan J Boukens,
University of Amsterdam, Netherlands

*CORRESPONDENCE
Wesam Mulla,
mulla@post.bgu.ac.il
Yoram Etzion,
tzion@bgu.ac.il

SPECIALTY SECTION
This article was submitted to Cardiac Electrophysiology, a section of the journal Frontiers in Physiology

RECEIVED 24 July 2022
ACCEPTED 30 August 2022
PUBLISHED 11 October 2022

CITATION
Mulla W, Murninkas M, Levi O and Etzion Y (2022), Incorrectly corrected? QT interval analysis in rats and mice. *Front. Physiol.* 13:1002203. doi: 10.3389/fphys.2022.1002203

Incorrectly corrected? QT interval analysis in rats and mice

Wesam Mulla[1,2]*, Michael Murninkas[1,2], Or Levi[1,2] and Yoram Etzion[1,2]*

[1]Cardiac Arrhythmia Research Laboratory, Department of Physiology and Cell Biology, Faculty of Health Sciences, Ben-Gurion University of the Negev, Beer-Sheva, Israel, [2]Regenerative Medicine and Stem Cell Research Center, Ben-Gurion University of the Negev, Beer-Sheva, Israel

QT interval, a surrogate measure for ventricular action potential duration (APD) in the surface ECG, is widely used to identify cardiac abnormalities and drug safety. In humans, cardiac APD and QT interval are prominently affected by heart rate (HR), leading to widely accepted formulas to correct the QT interval for HR changes (QT corrected - QTc). While QTc is widely used in the clinic, the proper way to correct the QT interval in small mammals such as rats and mice is not clear. Over the years, empiric correction formulas were developed for rats and mice, which are widely used in the literature. Recent experimental findings obtained from pharmacological and direct pacing experiments in unanesthetized rodents show that the rate-adaptation properties are markedly different from those in humans and the use of existing QTc formulae can lead to major errors in data interpretation. In the present review, these experimental findings are summarized and discussed.

KEYWORDS

rodent cardiac electrophysiology, ECG, QT interval, effective refractory period, action potential duration, rate-adaptation

Introduction

QT interval measurement is an important aspect of any ECG evaluation and interpretation. It has significant clinical importance, as there is a correlation between the QT interval value and the risk of developing ventricular arrhythmias and sudden cardiac death (Viskin, 2009; Lester et al., 2019). The importance of the QT interval did not come to light for several decades after the first description of the morphology of the human ECG by Willem Einthoven in 1885 (Lester et al., 2019). Louise Wolff, an American cardiologist who described the WPW syndrome with Parkinson and White, was probably the first person to measure the QT interval (G Postema and AM Wilde, 2014). However, the clinical importance of the QT interval was not fully understood until further work by Jervell and Lange-Nielsen in the late 1950s (Jervell and Lange-Nielsen, 1957), and by Romano, Gemme, Pongiglione, and Ward in the 1960s (Romano, 1963; Ward, 1964). Several types of long QT syndrome have since been described, and the recognition of the relationship between QT prolongation and serious ventricular arrhythmias has strengthened. Moreover, a series of patients treated with the antiarrhythmic drug quinidine were reported to have syncope due to ventricular tachycardia in the setting of a prolonged QT interval in 1964 (Selzer and

Wray, 1964). The morphology of quinidine-induced ventricular tachycardia had a peculiar undulating appearance which in 1966 was termed Torsades de Pointes (TdP) by Desertennes (Dessertenne, 1966). In the subsequent decades, additional classes of medications including antibiotics and psychotropic drugs were linked to TdP and a number of these agents were subsequently withdrawn by the Food and Drug Administration (FDA) (Fung et al., 2001). Drug-induced prolongation of the QT interval is usually caused by the drug's ability to inhibit IKr, the rapid component of the delayed rectifier potassium current. In humans, this component is encoded by human ether-a-go-go related gene (hERG) (Redfern et al., 2003). In 2007, the FDA formed an internal review team responsible for overseeing the clinical assessment of QT prolongation for all drugs that the agency reviewed, thus assessment of QT prolongation has rapidly become an essential part of the development of new drugs (Darpo, 2010). Although it recommends correcting of the QT interval for HR, it also concedes that such correction can yield misleading results (Food and Drug Administration, 2005). Moreover, literature-based assessments indicate that only non-rodent mammalian models can mimic QT interval prolongation and TdP caused by human therapeutics (Davis, 1998; De Ponti et al., 2001; Webster et al., 2002; Redfern et al., 2003). IKr plays a small role if any in rodents and most studies agree that these models are inappropriate for the study of drug-induced TdP (Hoffmann and Warner, 2006).

QT interval rate dependence in humans

The QT interval consists of two components: the QRS complex and the T wave, which reflect ventricular depolarization and repolarization, respectively. Duration of the QT interval can vary widely in each individual (Al-Khatib et al., 2003). Many determinants contribute to this variation, including HR, age, sex, autonomic nervous activity, circadian rhythm, drugs, electrolyte variations, myocardial disease, and congenital syndromes (Al-Khatib et al., 2003; Tomaselli Muensterman and Tisdale, 2018). The greatest variation occurs with HR as it is the principal modulator of repolarization duration (Locati et al., 2017). The QT interval dependence on HR reflects the APD dependence on cycle length (CL), a fundamental property of cardiac muscle in humans and large mammals (Franz et al., 1988; Locati et al., 2017). Like APD, QT interval also decreases at shorter CL and prolongs as the CL increases. The kinetics of APD/QT interval adaptation consists of a fast response followed by a gradual course towards a new steady-state value (Franz et al., 1988; Seethala et al., 2011). Mechanisms underlying this adaptive response include inactivation of the L-type calcium current as well as activation of the slow component of the delayed rectifier K^+ current ($Kv7.1/I_{ks}$). In addition, it appears that mechanisms affecting intracellular Na^+ accumulation are important determinants of the slow phase of adaptation (Pueyo et al., 2010; O'Hara and Rudy, 2012; Schmitt et al., 2014). ADP and QT interval do not adapt solely on the basis of changes in CL. Exercise and adrenergic stimulation which promote both tachycardia and QT interval shortening are known to induced adaptation beyond that observed during pacing (Seethala et al., 2011). This phenomena involves autonomic stimulation of Kv7.1 (Vyas and Ackerman, 2006). Many QTc formulae have been developed to normalize the QT interval to rate-dependent changes with variable utility in the clinic (Rautaharju et al., 2009; G Postema and AM Wilde, 2014; Locati et al., 2017). The most commonly used correction method in the clinic is the QT Bazett's formula (G Postema and AM Wilde, 2014; Locati et al., 2017) in which QTc is calculated as the QT interval in seconds divided by the square root of the preceding CL in seconds (Bazett, 1920). When HR is particularly fast or slow, the Bazett's formula may over or underestimate the baseline QT, respectively. However, regardless of this limitation it still remains the current standard in clinical practice (G Postema and AM Wilde, 2014; Locati et al., 2017).

Myocardial repolarization in rats and mice

Although the overall principles of myocardial excitation are the same in all mammalian species, the role of repolarizing currents markedly differ between humans and rodents (Boukens et al., 2014). This is presumably dictated by the great variations in HR and HR modulation among species. Humans have a resting HR of ≈60 bpm, whereas rats and mice have a HR of on average 6 and 10 times higher, respectively (Kaese and Verheule, 2012; Milani-Nejad and Janssen, 2014; Konopelski and Ufnal, 2016). In addition, while rats and mice can increase their HR by around 40%–50% and 30%–40% respectively, humans can increase their HR by up to 300% (Milani-Nejad and Janssen, 2014; Janssen et al., 2016). These differences require repolarizing K^+ ionic currents with different kinetics in order to adapt the APD appropriately. In rats and mice, the major repolarizing K^+ ionic currents are the transient outward K^+ current (I_{to}) and ultra-rapid potassium current (I_{kur}), and the ventricular APD has a triangular shape, with short repolarization and no clear plateau phase (Watanabe et al., 1983; Varró et al., 1993; Knollmann et al., 2001). Importantly, most rodent studies involve direct pacing under anesthesia, or *ex-vivo*/*in-vitro* preparations, overlooking the effects of autonomic

TABLE 1 Summary of studies in which QT interval, ERP and APD rate relation were evaluated in rats and mice.

	Experiment	Unanesthetized			Anesthetized			*Ex-vivo*/*In-vitro*		
	Parameter	**Pacing**	**Pharmacologic**	**Physiologic**	**Pacing**	**Pharmacologic**	**Physiologic**	**Pacing**	**Pharmacologic**	**Physiologic**
Rats	QT interval	↔ Mulla et al. (2018)	↔ Wallman et al. (2021)	↔ Fein et al. (1991), Adeyemi et al. (2020), Wallman et al. (2021)	↔ Hayes et al. (1994)	↔ Kmecova and Klimas (2010)	↔ Ohtani et al. (1997)			
	Atrial ERP	↔ Murninkas et al. (2020)	↔ Etzion et al. (2008)		↔ Etzion et al. (2008)					
					↓ Li et al. (2020)					
	Ventricular ERP	↔ Mulla et al. (2018)			↑↔ Ypma (1972)			↑ ↔ Ypma (1972)		
	Atrial APD							↔↓ Huang et al. (2006)		↔ Couch et al. (1969)
	Ventricular APD				↔ Rapuzzi and Rindi (1967)			↑ Shimoni et al. (1994), Shimoni et al. (1995), Shigematsu et al. (1997), Fauconnier et al. (2003)	↔ Sakatani et al. (2006)	↔ Couch et al. (1969)
								↔ Blesa et al. (1970), Pucelik et al. (1982), Shigematsu et al. (1997), Pacher et al. (1999), Benoist et al. (2011), Benoist et al. (2012), Walton et al. (2013), Hardy et al. (2018)	↔↓ Howlett et al. (2022)	
								↑↓ Watanabe et al. (1983)	↓ Wang and Fitts (2017)	
								↔↓ Keung and Aronson (1981), Howlett et al. (2022)		
								↓ Payet et al. (1981), Watanabe et al. (1983), Wang and Fitts (2017)		

(Continued on following page)

10.3389/fphys.2022.1002203

TABLE 1 (*Continued*) Summary of studies in which QT interval, ERP and APD rate relation were evaluated in rats and mice.

	Experiment	Unanesthetized			Anesthetized			*Ex-vivo*/*In-vitro*		
Parameter		**Pacing**	**Pharmacologic**	**Physiologic**	**Pacing**	**Pharmacologic**	**Physiologic**	**Pacing**	**Pharmacologic**	**Physiologic**
Mice	QT interval	↔ Mulla et al. (2018)	↔ Roussel et al. (2016)	↔ Roussel et al. (2016), Schroder et al. (2021), Warhol et al. (2021) ↓ Mitchell et al. (1998) ↑↔↓ Sudhir et al. (2020)	↔ Speerschneider and Thomsen (2013)	↑ Speerschneider and Thomsen (2013) ↔ Warhol et al. (2021)			↔ Joyce et al. (2021)	
	Atrial ERP				↔ Etzion et al. (2008) ↓ Berul et al. (1996)			↔ Syeda et al. (2016), Obergassel et al. (2021)		
	Ventricular ERP	↔ Mulla et al. (2018)			↓ Berul et al. (1996)			↔ Waldeyer et al. (2009)		
	Atrial APD							↔ Syeda et al. (2016) ↓ Knollmann et al. (2007), Obergassel et al. (2021)		
	Ventricular APD				↔↓ Nuyens et al. (2001)			↔ Wagner et al. (2006), Kulkarni et al. (2018), Joyce et al. (2021) ↓ Knollmann et al. (2007), Sabir et al. (2008), Waldeyer et al. (2009), Mulla et al. (2018)	↔ Sudhir et al. (2020), Joyce et al. (2021) ↓ Francis Stuart et al. (2018)	↑ Francis Stuart et al. (2018)

Typical rate adaptation ↓ Flat rate adaptation ↔ Atypical rate adaptation ↑

10.3389/fphys.2022.1002203

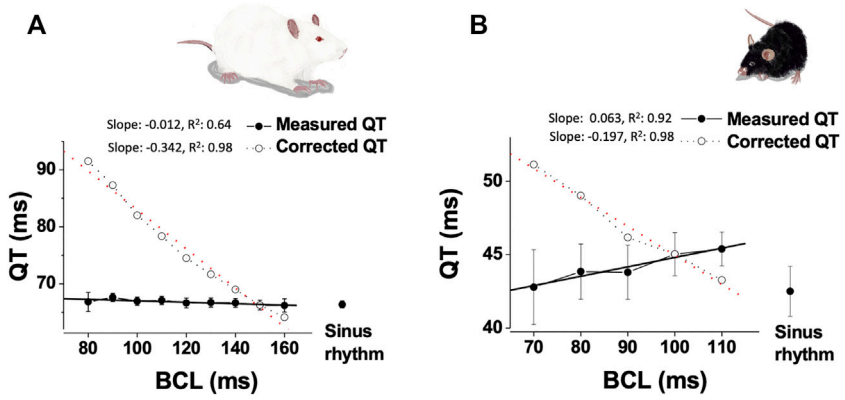

FIGURE 1
Absence of QT interval dependence on HR in paced unanesthetized rodents. **(A)**. Data from instrumented, unanesthetized male SD rats that were subjected to atrial pacing at different CL (n = 10): Mean ± SE of measured QT and calculated QTc (based on the formula of Kmecova and Klimas (Kmecova and Klimas, 2010)), plotted as a function of CL. Linear regression data (slope, R^2) are presented for both QT and calculated QTc. **(B)**. Data from instrumented, unanesthetized male C57BL/J mice that were subjected to atrial pacing at different CL (n = 9): Mean ± SE of measured QT and calculated QTc [based on the formula of Mitchell et al. (1998)], plotted as a function of CL. Linear regression data (slope, R^2) are presented for both QT and calculated QTc. Experimental findings were adapted from Mulla et al. (2018).

stimulation. Indeed, there is some evidence that IKs mediates repolarization in rat cardiomyocytes under β-adrenergic stimulation (Xu et al., 2016). In addition, among mice, the most phosphorylated protein upon β1-adrenergic receptor activation of the heart is Kv7.1 (Lundby et al., 2013). Nevertheless, the *in-vivo* effect of I_{Ks} on the QT of mice is questionable considering the notable QT prolongation observed in response to β-adrenergic stimulation (Speerschneider and Thomsen, 2013). Adrenergic stimulation also resulted in phosphorylation of I_{Na} (Nav1.5), an additional potential mechanism by which changes in autonomic balance may affect repolarization duration (Lundby et al., 2013). Thus, the mechanisms governing APD in the unanesthetized rodent seem to be far more complex than I_{to}/I_{Kur} -dependent repolarization.

Rate-adaptation studies of ADP and QT interval in rodents

As mentioned above the basic electrophysiological components governing ADP in the rodent myocardium are relatively well known. Still, *in-vivo* rate-dependence of the APD and QT are rather poorly defined in these species. As already mentioned, one possible explanation for this is the technical challenge in performing advanced EP studies in unanesthetized rodents. In addition, results may vary substantially depending on the used methodology (i.e., type of anesthesia, type of perfused solution) and indeed, data regarding the electrophysiological properties of rodents show marked variations in the literature (Kaese and Verheule, 2012). Although the determinants of the rate-dependence of APD differ between small rodents and humans (as described above) there are various publications supporting the notion that typical rate-adaptation still exists in rodents (Table 1). However, various publications have demonstrated no rate-adaptation or even atypical rate-adaptation (i.e., increased APD at shorter CL). This variability raise the question whether discrepancies between studies might be secondary to differences in techniques (e.g., techniques that interfere with endogenous autonomic modulation such as anesthetics, large doses of exogenous catecholamines, overcontrolling for circadian rhythm). In any case, these discrepancies stresses the importance of obtaining data from unanesthetized rodents under physiological conditions in order to arrive at reliable conclusions. Another major challenge and source of uncertainty in evaluations of the relationship between HR and repolarization of rodent and particularly mice is identification of the end of the T wave. Because of the high HRs, motion artifact, and other sources of signal noise with telemetry devices, obtaining clean ECG signals in conscious rodents can be particularly challenging. As well, the end of the negative murine T wave is more subtle and therefore elusive to automated software detection than in humans and other mammals with more overt, positive T waves.

Discussion

The dependence of QT interval of HR is debatable in rats and mice (Hayes et al., 1994; Ohtani et al., 1997; Mitchell et al., 1998; Kmecova and Klimas, 2010; Speerschneider and Thomsen, 2013; Roussel et al., 2016; Mulla et al., 2018). For example, Mitchell et al. (Mitchell et al., 1998) used the natural daily variation in HR in unanesthetized mice

and found a strong correlation between the QT interval and HR, where slower HRs were associated with longer QT intervals. In contrast, Roussel et al. (Roussel et al., 2016) examined the same natural daily variation in HR as well as changes induced by tachycardic agents (norepinephrine or nitroprusside) and concluded that increased HR was not associated with apparent shortening of the QT interval. Nevertheless, at least for the circadian data it might be possible that analysis of light and dark phases separately for QT-RR relationships may over-control for endogenous changes in rate and repolarization mediated by circadian fluctuations in rhythm and autonomic modulation. Sudhir et al. (Sudhir et al., 2020) recently explored adaptation of QT to physical stress in mice overexpressing SUR2A, a regulatory subunit of sarcolemmal ATP-sensitive K + (K_{ATP}) channels. Although the results show highly complex pattern of changes over time in both transgenic and control mice, only corrected QT intervals (using Mitchell's formula) are presented in the study, limiting ability to evaluate the effects of exercise on the native QT interval. In rats, a QT interval correction formula suggested by Kmecova and Klimas (Kmecova and Klimas, 2010) was validated using pharmacological manipulations affecting HR. Interestingly, adrenergic stimulation with isoproterenol as well as selectively manipulation of the HR by ivabradine, did not affect the QT interval in this study. Technical challenges largely limited direct pacing experiments as a mean of evaluating QT rate-dependence in rodents. However, Mulla et al. (2018) managed to explore the QT interval of freely moving rats and mice during atrial pacing at various CL values through a unique chronically implanted device. The findings of this work indicated absence of conventional rate-adaptation of the QT interval over a wide range of physiologically relevant frequencies. Moreover, ventricular ERP (a surrogate of ventricular APD) also demonstrated absence of typical rate-dependence. Calculating the QTc interval according to the formulae suggested by Kmecova and Klimas (Kmecova and Klimas, 2010) for rats and by Mitchell et al. (1998) for mice, resulted in marked difference between the measured QT interval and the QTc interval for a wide range of atrial pacing rates in both species (Figure 1). At the present, it is hard to conclude what is the optimal way of QT correction in rodent and if correction is required at all. However, it appears that the existing and widely use correction formulas can introduce marked errors. This issue seems specifically relevant for Mitchell formula for mice that appears to overcorrect QT, indicating a great need for a better QT correction formula for mice. Overall, we suggest that any correction formula used should be validated in that species under baseline conditions using comparable analytic methods and measurement techniques as those applied during/after experimental treatments. As well, we suggest that as a standard, corrected QT results should be presented along with those for uncorrected QT. Importantly, to the best of our knowledge direct data on the relationship between QT and HR in the unanesthetized Guinea pig are lacking in literature. Given the existence of I_{kr} and I_{ks} in the myocardium and their broad utility for QT prolongation studies, we believe that understanding the precise HR-QT relationship of this animal model in future studies will be of high value as well.

In conclusion, conflicting data still exists regarding the dependence between QT interval and HR in rodents. Multiple physiological and technical complexities and challenges prevents clear conclusions regarding this issue based on the currently available data. However, large body of evidence support the notion that the extensive use of existing correction formulae may introduce significant errors and thus further and more systematic exploration of this issue would be of high value.

Author contributions

WM. drafted manuscript; MM, OL, and YE. edited and revised manuscript; WM, MM, OL, and YE. approved final version of manuscript.

Acknowledgments

The authors thank Layan Faris for the illustrations in the figure.

Conflict of interest

The authors declare that the research was conducted in the absence of any commercial or financial relationships that could be construed as a potential conflict of interest.

Publisher's note

References

Adeyemi, O., Parker, N., Pointon, A., and Rolf, M. (2020). A pharmacological characterization of electrocardiogram PR and QRS intervals in conscious telemetered rats. *J. Pharmacol. Toxicol. Methods* 102, 106679. doi:10.1016/j.vascn.2020.106679

Al-Khatib, S. M., Lapointe, N. M. A., Kramer, J. M., and Califf, R. M. (2003). What clinicians should know about the QT interval. *Jama* 289, 2120–2127. doi:10.1001/jama.289.16.2120

Bazett, H. C. (1920). An analysis of the time relations of electrocardiograms. *Heart* 7, 353–370.

Benoist, D., Stones, R., Drinkhill, M., Bernus, O., and White, E. (2011). Arrhythmogenic substrate in hearts of rats with monocrotaline-induced pulmonary hypertension and right ventricular hypertrophy. *Am. J. Physiol. Heart Circ. Physiol.* 300, H2230–H2237. doi:10.1152/ajpheart.01226.2010

Benoist, D., Stones, R., Drinkhill, M. J., Benson, A. P., Yang, Z., Cassan, C., et al. (2012). Cardiac arrhythmia mechanisms in rats with heart failure induced by pulmonary hypertension. *Am. J. Physiol. Heart Circ. Physiol.* 302, H2381–H2395. doi:10.1152/ajpheart.01084.2011

Berul, C. I., Aronovitz, M. J., Wang, P. J., and Mendelsohn, M. E. (1996). *In vivo* cardiac electrophysiology studies in the mouse. *Circulation* 94, 2641–2648. doi:10.1161/01.cir.94.10.2641

Blesa, E. S., Langer, G. A., Brady, A. J., and Serena, S. D. (1970). Potassium exchange in rat ventricular myocardium: Its relation to rate of stimulation. *Am. J. Physiol.* 219, 747–754. doi:10.1152/ajplegacy.1970.219.3.747

Boukens, B. J., Rivaud, M. R., Rentschler, S., and Coronel, R. (2014). Misinterpretation of the mouse ECG:'musing the waves of *Mus musculus*. *J. Physiol.* 592, 4613–4626. doi:10.1113/jphysiol.2014.279380

Couch, J. R., West, T. C., and Hoff, H. E. (1969). Development of the action potential of the prenatal rat heart. *Circ. Res.* 24, 19–31. doi:10.1161/01.res.24.1.19

Darpo, B. (2010). The thorough QT/QTc study 4 years after the implementation of the ICH E14 guidance. *Br. J. Pharmacol.* 159, 49–57. doi:10.1111/j.1476-5381.2009.00487.x

Davis, A. S. (1998). The pre-clinical assessment of QT interval prolongation: A comparison of *in vitro* and *in vivo* methods. *Hum. Exp. Toxicol.* 17, 677–680. doi:10.1177/096032719801701205

De Ponti, F., Poluzzi, E., and Montanaro, N. (2001). Organising evidence on QT prolongation and occurrence of torsades de Pointes with non-antiarrhythmic drugs: A call for consensus. *Eur. J. Clin. Pharmacol.* 57, 185–209. doi:10.1007/s002280100290

Dessertenne, F. (1966). Ventricular tachycardia with 2 variable opposing foci. *Arch. Mal. Coeur Vaiss.* 59, 263–272.

Etzion, Y., Mor, M., Shalev, A., Dror, S., Etzion, O., Dagan, A., et al. (2008). New insights into the atrial electrophysiology of rodents using a novel modality: The miniature-bipolar hook electrode. *Am. J. Physiol. Heart Circ. Physiol.* 295, H1460–H1469. doi:10.1152/ajpheart.00414.2008

Fauconnier, J., Bedut, S., Le Guennec, J.-Y., Babuty, D., and Richard, S. (2003). Ca2+ current-mediated regulation of action potential by pacing rate in rat ventricular myocytes. *Cardiovasc. Res.* 57, 670–680. doi:10.1016/s0008-6363(02)00731-9

Fein, A., Hecht, Z., Varon, D., Eyal, E., Nebel, L., and Manoach, M. (1991). A correlation between the structure of myocardial cells and prolonged QT interval in young rats. *Int. J. Cardiol.* 32, 13–22. doi:10.1016/0167-5273(91)90039-r

Food, and Drug Administration, H. (2005). International conference on harmonisation; guidance on E14 Clinical Evaluation of QT/QTc interval prolongation and proarrhythmic potential for non-antiarrhythmic drugs; availability. notice. *Fed. Regist.* 70, 61134–61135.

Francis Stuart, S. D., Wang, L., Woodard, W. R., Ng, G. A., Habecker, B. A., and Ripplinger, C. M. (2018). Age-related changes in cardiac electrophysiology and calcium handling in response to sympathetic nerve stimulation. *J. Physiol.* 596, 3977–3991. doi:10.1113/JP276396

Franz, M. R., Swerdlow, C. D., Liem, L. B., and Schaefer, J. (1988). Cycle length dependence of human action potential duration *in vivo*. Effects of single extrastimuli, sudden sustained rate acceleration and deceleration, and different steady-state frequencies. *J. Clin. Invest.* 82, 972–979. doi:10.1172/JCI113706

Fung, M., Thornton, A., Mybeck, K., Wu, J. H.-H., Hornbuckle, K., and Muniz, E. (2001). Evaluation of the characteristics of safety withdrawal of prescription drugs from worldwide pharmaceutical markets-1960 to 1999. *Drug Inf. J.* 35, 293–317. doi:10.1177/009286150103500134

G Postema, P., and Am Wilde, A. (2014). The measurement of the QT interval. *Curr. Cardiol. Rev.* 10, 287–294. doi:10.2174/1573403x10666140514103612

Hardy, M. E., Pervolaraki, E., Bernus, O., and White, E. (2018). Dynamic action potential restitution contributes to mechanical restitution in right ventricular myocytes from pulmonary hypertensive rats. *Front. Physiol.* 9, 205. doi:10.3389/fphys.2018.00205

Hayes, E., Pugsley, M., Penz, W., Adaikan, G., and Walker, M. (1994). Relationship between QaT and RR intervals in rats, Guinea pigs, rabbits, and primates. *J. Pharmacol. Toxicol. Methods* 32, 201–207. doi:10.1016/1056-8719(94)90088-4

Hoffmann, P., and Warner, B. (2006). Are hERG channel inhibition and QT interval prolongation all there is in drug-induced torsadogenesis? A review of emerging trends. *J. Pharmacol. Toxicol. Methods* 53, 87–105. doi:10.1016/j.vascn.2005.07.003

Howlett, L. A., Kirton, H. M., Al-Owais, M. M., Steele, D., and Lancaster, M. K. (2022). Action potential responses to changes in stimulation frequency and isoproterenol in rat ventricular myocytes. *Physiol. Rep.* 10, e15166. doi:10.14814/phy2.15166

Huang, C., Ding, W., Li, L., and Zhao, D. (2006). Differences in the aging-associated trends of the monophasic action potential duration and effective refractory period of the right and left atria of the rat. *Circ. J.* 70, 352–357. doi:10.1253/circj.70.352

Janssen, P. M., Biesiadecki, B. J., Ziolo, M. T., and Davis, J. P. (2016). The need for speed: Mice, men, and myocardial kinetic reserve. *Circ. Res.* 119, 418–421. doi:10.1161/CIRCRESAHA.116.309126

Jervell, A., and Lange-Nielsen, F. (1957). Congenital deaf-mutism, functional heart disease with prolongation of the QT interval, and sudden death. *Am. Heart J.* 54, 59–68. doi:10.1016/0002-8703(57)90079-0

Joyce, W., Scholman, K. T., Jensen, B., Wang, T., and Boukens, B. J. (2021). α1-adrenergic stimulation increases ventricular action potential duration in the intact mouse heart. *FACETS* 6, 823–836. doi:10.1139/facets-2020-0081

Kaese, S., and Verheule, S. (2012). Cardiac electrophysiology in mice: A matter of size. *Front. Physiol.* 3, 345. doi:10.3389/fphys.2012.00345

Keung, E., and Aronson, R. (1981). Non-uniform electrophysiological properties and electrotonic interaction in hypertrophied rat myocardium. *Circ. Res.* 49, 150–158. doi:10.1161/01.res.49.1.150

Kmecova, J., and Klimas, J. (2010). Heart rate correction of the QT duration in rats. *Eur. J. Pharmacol.* 641, 187–192. doi:10.1016/j.ejphar.2010.05.038

Knollmann, B. C., Katchman, A. N., and Franz, M. R. (2001). Monophasic action potential recordings from intact mouse heart: Validation, regional heterogeneity, and relation to refractoriness. *J. Cardiovasc. Electrophysiol.* 12, 1286–1294. doi:10.1046/j.1540-8167.2001.01286.x

Knollmann, B. C., Schober, T., Petersen, A. O., Sirenko, S. G., and Franz, M. R. (2007). Action potential characterization in intact mouse heart: Steady-state cycle length dependence and electrical restitution. *Am. J. Physiol. Heart Circ. Physiol.* 292, H614–H621. doi:10.1152/ajpheart.01085.2005

Konopelski, P., and Ufnal, M. (2016). Electrocardiography in rats: A comparison to human. *Physiol. Res.* 65, 717–725. doi:10.33549/physiolres.933270

Kulkarni, K., Xie, X., Fernandez De Velasco, E. M., Anderson, A., Martemyanov, K. A., Wickman, K., et al. (2018). The influences of the M2R-GIRK4-RGS6 dependent parasympathetic pathway on electrophysiological properties of the mouse heart. *PloS one* 13, e0193798. doi:10.1371/journal.pone.0193798

Lester, R. M., Paglialunga, S., and Johnson, I. A. (2019). QT assessment in early drug development: The long and the short of it. *Int. J. Mol. Sci.* 20, 1324. doi:10.3390/ijms20061324

Li, X., Deng, C.-Y., Xue, Y.-M., Yang, H., Wei, W., Liu, F.-Z., et al. (2020). High hydrostatic pressure induces atrial electrical remodeling through angiotensin upregulation mediating FAK/Src pathway activation. *J. Mol. Cell. Cardiol.* 140, 10–21. doi:10.1016/j.yjmcc.2020.01.012

Locati, E. T., Bagliani, G., and Padeletti, L. (2017). Normal ventricular repolarization and QT interval: Ionic background, modifiers, and measurements. *Card. Electrophysiol. Clin.* 9, 487–513. doi:10.1016/j.ccep.2017.05.007

Lundby, A., Andersen, M. N., Steffensen, A. B., Horn, H., Kelstrup, C. D., Francavilla, C., et al. (2013). *In vivo* phosphoproteomics analysis reveals the cardiac targets of β-adrenergic receptor signaling. *Sci. Signal.* 6, rs11. doi:10.1126/scisignal.2003506

Milani-Nejad, N., and Janssen, P. M. (2014). Small and large animal models in cardiac contraction research: Advantages and disadvantages. *Pharmacol. Ther.* 141, 235–249. doi:10.1016/j.pharmthera.2013.10.007

Mitchell, G. F., Jeron, A., and Koren, G. (1998). Measurement of heart rate and QT interval in the conscious mouse. *Am. J. Physiol.* 274, H747–H751. doi:10.1152/ajpheart.1998.274.3.H747

Mulla, W., Gillis, R., Murninkas, M., Klapper-Goldstein, H., Gabay, H., Mor, M., et al. (2018). Unanesthetized rodents demonstrate insensitivity of QT interval and ventricular refractory period to pacing cycle length. *Front. Physiol.* 9, 897. doi:10.3389/fphys.2018.00897

Murninkas, M., Gillis, R., Lee, D. I., Elyagon, S., Bhandarkar, N. S., Levi, O., et al. (2020). A new implantable tool for repeated assessment of supraventricular electrophysiology and atrial fibrillation susceptibility in freely moving rats. *Am. J. Physiology-Heart Circulatory Physiology* 320, H713–H724. doi:10.1152/ajpheart.00676.2020

Nuyens, D., Stengl, M., Dugarmaa, S., Rossenbacker, T., Compernolle, V., Rudy, Y., et al. (2001). Abrupt rate accelerations or premature beats cause life-threatening

arrhythmias in mice with long-QT3 syndrome. *Nat. Med.* 7, 1021–1027. doi:10.1038/nm0901-1021

O'hara, T., and Rudy, Y. (2012). Quantitative comparison of cardiac ventricular myocyte electrophysiology and response to drugs in human and nonhuman species. *Am. J. Physiol. Heart Circ. Physiol.* 302, H1023–H1030. doi:10.1152/ajpheart.00785.2011

Obergassel, J., O'reilly, M., Sommerfeld, L. C., Kabir, S. N., O'shea, C., Syeda, F., et al. (2021). Effects of genetic background, sex, and age on murine atrial electrophysiology. *EP Eur.* 23, 958. doi:10.1093/europace/euaa369

Ohtani, H., Kotaki, H., Sawada, Y., and Iga, T. (1997). A comparative pharmacokinetic-pharmacodynamic study of the electrocardiographic effects of epinastine and terfenadine in rats. *J. Pharm. Pharmacol.* 49, 458–462. doi:10.1111/j.2042-7158.1997.tb06824.x

Pacher, P., Ungvari, Z., Nanasi, P., and Kecskemeti, V. (1999). Electrophysiological changes in rat ventricular and atrial myocardium at different stages of experimental diabetes. *Acta Physiol. Scand.* 166, 7–13. doi:10.1046/j.1365-201x.1999.00538.x

Payet, M., Schanne, O., and Ruiz-Ceretti, E. (1981). Frequency dependence of the ionic currents determining the action potential repolarization in rat ventricular muscle. *J. Mol. Cell. Cardiol.* 13, 207–215. doi:10.1016/0022-2828(81)90217-0

Pucelik, P., Jezek, K., and Bartak, F. (1982). Postnatal development of electrophysiological manifestations of the working ventricular myocardium of albino rats. *Physiol. Bohemoslov.* 31, 217–224.

Pueyo, E., Husti, Z., Hornyik, T., Baczkó, I., Laguna, P., Varró, A., et al. (2010). Mechanisms of ventricular rate adaptation as a predictor of arrhythmic risk. *Am. J. Physiol. Heart Circ. Physiol.* 298, H1577–H1587. doi:10.1152/ajpheart.00936.2009

Rapuzzi, G., and Rindi, G. (1967). Inluence of increasing heart rate on the alterations of the cardiac ventricular fibre-cells action potentials induced by thiamine deficiency. *Q. J. Exp. Physiol. Cogn. Med. Sci.* 52, 277–284. doi:10.1113/expphysiol.1967.sp001913

Rautaharju, P. M., Surawicz, B., Gettes, L. S., Bailey, J. J., Childers, R., Deal, B. J., et al. (2009). AHA/ACCF/HRS recommendations for the standardization and interpretation of the electrocardiogram: Part IV: The ST segment, T and U waves, and the QT interval a scientific statement from the American heart association electrocardiography and arrhythmias committee, council on clinical cardiology; the American college of cardiology foundation; and the heart rhythm society endorsed by the international society for computerized electrocardiology. *J. Am. Coll. Cardiol.* 53, 982–991. doi:10.1016/j.jacc.2008.12.014

Redfern, W., Carlsson, L., Davis, A., Lynch, W., Mackenzie, I., Palethorpe, S., et al. (2003). Relationships between preclinical cardiac electrophysiology, clinical QT interval prolongation and torsade de pointes for a broad range of drugs: Evidence for a provisional safety margin in drug development. *Cardiovasc. Res.* 58, 32–45. doi:10.1016/s0008-6363(02)00846-5

Romano, C. (1963). Rare cardiac arrhythmias of the pediatric age. II: Syncopal attacks due to paroxysmal ventricular fibrillation (Presentation of 1st case in Italian pediatric literature). *Clin. Pediatr. (Bologna)* 45, 656–683.

Roussel, J., Champeroux, P., Roy, J., Richard, S., Fauconnier, J., Le Guennec, J.-Y., et al. (2016). The complex QT/RR relationship in mice. *Sci. Rep.* 6, 25388. doi:10.1038/srep25388

Sabir, I. N., Li, L. M., Grace, A. A., and Huang, C. L.-H. (2008). Restitution analysis of alternans and its relationship to arrhythmogenicity in hypokalaemic Langendorff-perfused murine hearts. *Pflugers Arch.* 455, 653–666. doi:10.1007/s00424-007-0327-y

Sakatani, T., Shirayama, T., Yamamoto, T., Mani, H., Shiraishi, H., and Matsubara, H. (2006). Cardiac hypertrophy diminished the effects of isoproterenol on delayed rectifier potassium current in rat heart. *J. Physiol. Sci.* 56, 173–181. doi:10.2170/physiolsci.RP002405

Schmitt, N., Grunnet, M., and Olesen, S.-P. (2014). Cardiac potassium channel subtypes: New roles in repolarization and arrhythmia. *Physiol. Rev.* 94, 609–653. doi:10.1152/physrev.00022.2013

Schroder, E. A., Wayland, J. L., Samuels, K. M., Shah, S. F., Burgess, D. E., Seward, T., et al. (2021). Cardiomyocyte deletion of Bmal1 exacerbates QT-and RR-interval prolongation in scn5a+/dkpq mice. *Front. Physiol.* 853, 681011. doi:10.3389/fphys.2021.681011

Seethala, S., Shusterman, V., Saba, S., Mularski, S., and Němec, J. (2011). Effect of β-adrenergic stimulation on QT interval accommodation. *Heart rhythm.* 8, 263–270. doi:10.1016/j.hrthm.2010.10.012

Selzer, A., and Wray, H. W. (1964). Quinidine syncope: Paroxysmal ventricular fibrillation occurring during treatment of chronic atrial arrhythmias. *Circulation* 30, 17–26. doi:10.1161/01.cir.30.1.17

Shigematsu, S., Kiyosue, T., Sato, T., and Arita, M. (1997). Rate-dependent prolongation of action potential duration in isolated rat ventricular myocytes. *Basic Res. Cardiol.* 92, 123–128. doi:10.1007/BF00788629

Shimoni, Y., Firek, L., Severson, D., and Giles, W. (1994). Short-term diabetes alters K+ currents in rat ventricular myocytes. *Circ. Res.* 74, 620–628. doi:10.1161/01.res.74.4.620

Shimoni, Y., Severson, D., and Giles, W. (1995). Thyroid status and diabetes modulate regional differences in potassium currents in rat ventricle. *J. Physiol.* 488, 673–688. doi:10.1113/jphysiol.1995.sp020999

Speerschneider, T., and Thomsen, M. B. (2013). Physiology and analysis of the electrocardiographic T wave in mice. *Acta Physiol.* 209, 262–271. doi:10.1111/apha.12172

Sudhir, R., Du, Q., Sukhodub, A., Jovanović, S., and Jovanović, A. (2020). Improved adaptation to physical stress in mice overexpressing SUR2A is associated with changes in the pattern of Q-T interval. *Pflugers Arch.* 472, 683–691. doi:10.1007/s00424-020-02401-5

Syeda, F., Holmes, A. P., Yu, T. Y., Tull, S., Kuhlmann, S. M., Pavlovic, D., et al. (2016). PITX2 modulates atrial membrane potential and the antiarrhythmic effects of sodium-channel blockers. *J. Am. Coll. Cardiol.* 68, 1881–1894. doi:10.1016/j.jacc.2016.07.766

Tomaselli Muensterman, E., and Tisdale, J. E. (2018). Predictive analytics for identification of patients at risk for QT interval prolongation: A systematic review. *Pharmacotherapy* 38, 813–821. doi:10.1002/phar.2146

Varró, A., Lathrop, D., Hester, S., Nanasi, P., Papp, J., and Varro, A. (1993). Ionic currents and action potentials in rabbit, rat, and Guinea pig ventricular myocytes. *Basic Res. Cardiol.* 88, 93–102. doi:10.1007/BF00798257

Viskin, S. (2009). The QT interval: Too long, too short or just right. *Heart rhythm.* 6, 711–715. doi:10.1016/j.hrthm.2009.02.044

Vyas, H., and Ackerman, M. J. (2006). Epinephrine QT stress testing in congenital long QT syndrome. *J. Electrocardiol.* 39, S107–S113. doi:10.1016/j.jelectrocard.2006.05.013

Wagner, S., Dybkova, N., Rasenack, E. C., Jacobshagen, C., Fabritz, L., Kirchhof, P., et al. (2006). Ca 2+/calmodulin-dependent protein kinase II regulates cardiac Na+ channels. *J. Clin. Invest.* 116, 3127–3138. doi:10.1172/JCI26620

Waldeyer, C., Fabritz, L., Fortmueller, L., Gerss, J., Damke, D., Blana, A., et al. (2009). Regional, age-dependent, and genotype-dependent differences in ventricular action potential duration and activation time in 410 Langendorff-perfused mouse hearts. *Basic Res. Cardiol.* 104, 523–533. doi:10.1007/s00395-009-0019-1

Wallman, M., Scheuerer, S., Martel, E., Pairet, N., Jirstrand, M., and Gabrielsson, J. (2021). An integrative approach for improved assessment of cardiovascular safety data. *J. Pharmacol. Exp. Ther.* 377, 218–231. doi:10.1124/jpet.120.000348

Walton, R. D., Benson, A., Hardy, M., White, E., and Bernus, O. (2013). Electrophysiological and structural determinants of electrotonic modulation of repolarization by the activation sequence. *Front. Physiol.* 4, 281. doi:10.3389/fphys.2013.00281

Wang, X., and Fitts, R. H. (2017). Ventricular action potential adaptation to regular exercise: Role of β-adrenergic and KATP channel function. *J. Appl. Physiol.* 123, 285–296. doi:10.1152/japplphysiol.00197.2017

Ward, O. (1964). A new familial cardiac syndorome in children. *J. Ir. Med. Assoc.* 54, 103–106.

Warhol, A., George, S. A., Obaid, S. N., Efimova, T., and Efimov, I. R. (2021). Differential cardiotoxic electrocardiographic response to doxorubicin treatment in conscious versus anesthetized mice. *Physiol. Rep.* 9, e14987. doi:10.14814/phy2.14987

Watanabe, T., Delbridge, L. M., Bustamante, J. O., and Mcdonald, T. F. (1983). Heterogeneity of the action potential in isolated rat ventricular myocytes and tissue. *Circ. Res.* 52, 280–290. doi:10.1161/01.res.52.3.280

Webster, R., Leishman, D., and Walker, D. (2002). Towards a drug concentration effect relationship for QT prolongation and torsades de pointes. *Curr. Opin. Drug Discov. Devel.* 5, 116–126.

Xu, H., Zhao, M., Liang, S., Huang, Q., Xiao, Y., Ye, L., et al. (2016). The effects of puerarin on rat ventricular myocytes and the potential mechanism. *Sci. Rep.* 6, 35475. doi:10.1038/srep35475

Ypma, J. (1972). Adaptation of refractory period of rat ventricle to changes in heart rate. *Am. J. Physiol.* 223, 894–897. doi:10.1152/ajplegacy.1972.223.4.894

frontiers | Frontiers in Physiology

TYPE Original Research
PUBLISHED 17 November 2022
DOI 10.3389/fphys.2022.1057200

OPEN ACCESS

EDITED BY
Fu Siong Ng,
Imperial College London,
United Kingdom

REVIEWED BY
Robin Mark Shaw,
The University of Utah, United States
Henrique Girao,
University of Coimbra, Portugal

*CORRESPONDENCE
Ruben Coronel,
rubencoronel@gmail.com
Joris R. De Groot,
j.r.degroot@amsterdamumc.nl

†These authors have contributed equally to this work and share first authorship

‡These authors share last authorship

SPECIALTY SECTION
This article was submitted to Cardiac Electrophysiology, a section of the journal Frontiers in Physiology

RECEIVED 29 September 2022
ACCEPTED 07 November 2022
PUBLISHED 17 November 2022

CITATION
Ernault AC, Kawasaki M, Fabrizi B, Montañés-Agudo P, Amersfoorth SCM, Al-Shama RFM, Coronel R and De Groot JR (2022), Knockdown of Ift88 in fibroblasts causes extracellular matrix remodeling and decreases conduction velocity in cardiomyocyte monolayers. *Front. Physiol.* 13:1057200. doi: 10.3389/fphys.2022.1057200

Knockdown of Ift88 in fibroblasts causes extracellular matrix remodeling and decreases conduction velocity in cardiomyocyte monolayers

Auriane C. Ernault†, Makiri Kawasaki†, Benedetta Fabrizi, Pablo Montañés-Agudo, Shirley C. M. Amersfoorth, Rushd F. M. Al-Shama, Ruben Coronel*‡ and Joris R. De Groot*‡

Department of Clinical and Experimental Cardiology, Heart Center, Amsterdam Cardiovascular Sciences, Amsterdam UMC, University of Amsterdam, Amsterdam, Netherlands

Background: Atrial fibrosis plays an important role in the development and persistence of atrial fibrillation by promoting reentry. Primary cilia have been identified as a regulator of fibroblasts (FB) activation and extracellular matrix (ECM) deposition. We hypothesized that selective reduction of primary cilia causes increased fibrosis and facilitates reentry.

Aim: The aim of this study was to disrupt the formation of primary cilia in FB and examine its consequences on ECM and conduction in a co-culture system of cardiomyocytes (CM) and FB.

Materials: Using short interfering RNA (siRNA), we removed primary cilia in neonatal rat ventricular FB by reducing the expression of *Ift88* gene required for ciliary assembly. We co-cultured neonatal rat ventricular cardiomyocytes (CM) with FB previously transfected with *Ift88* siRNA (siIft88) or negative control siRNA (siNC) for 48 h. We examined the consequences of ciliated fibroblasts reduction on conduction and tissue remodeling by performing electrical mapping, microelectrode, and gene expression measurements.

Results: Transfection of FB with siIft88 resulted in a significant 60% and 30% reduction of relative *Ift88* expression in FB and CM-FB co-cultures, respectively, compared to siNC. Knockdown of *Ift88* significantly increased the expression of ECM genes *Fn1*, *Col1a1* and *Ctgf* by 38%, 30% and 18%, respectively, in comparison to transfection with siNC. Conduction velocity (CV) was significantly decreased in the siIft88 group in comparison to siNC [11.12 $\pm$ 4.27 cm/s ($n = 10$) vs. 17.00 $\pm$ 6.20 ($n = 10$) respectively, $p < 0.05$]. The fraction of sites with interelectrode activation block was larger in the siIft88 group than in the siNC group ($6.59 \times 10^{-2} \pm 8.01 \times 10^{-2}$ vs. $1.18 \times 10^{-2} \pm 3.72 \times 10^{-2}$ respectively, $p < 0.05$). We documented spontaneous reentrant arrhythmias in two cultures in the siIft88 group and in none of the siNC group. Action potentials were not significantly different between siNC and siIft88 groups.

Conclusion: Disruption of cilia formation by siIft88 causes ECM remodeling and conduction abnormalities. Prevention of cilia loss could be a target for prevention of arrhythmias.

KEYWORDS

atrial fibrillation, fibrosis, fibroblasts, primary cilia, cardiac

Introduction

Atrial fibrillation (AF) is the most common arrhythmia, with an estimated 46.3 million individuals suffering from this condition worldwide (Kornej et al., 2020). AF not only significantly reduces the quality of life, but also results in an increased morbidity and mortality (Benjamin et al., 1998). AF is a progressive disease which starts as a non-sustained arrhythmia originating from ectopic activity, and often progresses to a sustained state *via* structural remodeling of the atria (Krogh-Madsen et al., 2012; Heijman et al., 2021).

Atrial fibrosis, the concert of proliferation of fibroblasts and differentiation into myofibroblasts and the pathological accumulation of extracellular matrix (ECM), is the main component of structural remodeling in AF (Nattel et al., 2008). Fibrosis causes heterogeneous conduction delay, facilitating the occurrence and maintenance of AF. Cardiac (myo) fibroblasts are the main cell population responsible for ECM production and fibrosis formation in AF. TGF-β1 and angiotensin II are the main drivers for cardiac fibroblasts to form such pathological accumulation of ECM (Burstein and Nattel, 2008).

Primary cilium is a small organelle that extends from a cell's surface, and functions as a chemo- and mechano-sensors. Our proteome and transcriptome analysis of atrial tissue of patients with or without AF (non-AF) shows that the gene-sets of ciliogenesis, including *IFT88*, are down-regulated in AF compared to non-AF patients (Kawasaki et al., 2021; van den Berg et al., 2021). The dysregulation of primary cilia has been implicated in the fibrosis formation in various tissues, such as liver and kidney (Teves et al., 2019; Collins and Wann, 2020). Furthermore, our simultaneous study has indicated that the proportion of atrial fibroblasts with primary cilia is decreased in the left atrial tissue of persistent AF patients compared to non-AF patients, and the disruption of primary cilia in human atrial fibroblasts enhances their capacity to produce ECM. Thus, disruption of primary cilia in FB could activate them and cause accumulation of ECM, resulting in the formation of fibrosis in AF. However, it remains unclear what the direct consequences of FB with disrupted primary cilia are on cardiac conduction and action potential properties in multicellular preparations.

The aim of this study was to selectively decrease primary cilia in FB and examine its consequences on conduction and action potential properties in a co-culture system of cardiomyocytes (CM) and FB isolated from neonatal rats.

Here, we report that the selective disruption of primary cilia in FB by RNAi targeting *Ift88* induces ECM production, decreases conduction velocity, increases number of block lines and increases the risk or reentrant arrhythmias without changing the action potential (AP) characteristics of CM. Our data suggest that dysregulation of primary cilia causes fibrosis and hinders myocardial conduction, thereby facilitating the occurrence of re-entry and formation of the arrhythmogenic substrate.

Materials and methods

Neonatal rat ventricular myocytes and fibroblasts isolation

All animal experiments were approved by the local Animal Experiments Committee (Academic Medical Center, University of Amsterdam) and carried out in compliance with the Guide for the Care and Use of Laboratory Animals and in accordance with national and institutional guidelines. Neonatal rat ventricular CM and FB were isolated from 2-days-old Wistar rats (Janvier labs). Pups were anesthetized by isoflurane and hearts were excised after decapitation. Ventricles were cut in pieces and dissociated using trypsin (1 mg/ml; Sigma) and collagenase type 2 (1 mg/ml; Worthington). Cells were resuspended in TUNG culture medium (M199 medium, Gibco) supplemented with 10% heat inactivated fetal bovine serum (FB, Gibco), 1% HEPES (Gibco), 5,000 U/L penicillin-G (Sigma), 2 mg/L vitamin B12 (Sigma-Aldrich), 3.5 g/L glucose, 1% non-essential amino acids (Gibco), 1% L-glutamine (Gibco). The cell suspension was pre-plated for 2 h to physically separate the rapidly adhering FB from CM. CM in suspension were collected and plated on multi-electrode arrays (MEAs, Multi-Channel Systems MCS GmbH, Reutlingen, Germany) and on 24-well tissue culture plates coated with fibronectin (125 μg/ml BD Biosciences, Breda, Netherlands) at a density of 2.29×10^5 cells per cm^2. CM and FB were cultured at 37°C and 5% CO_2.

Transfection

In order to suppress the formation of primary cilia in FB, we downregulated the expression of the intraflagellar transport protein 88 gene (*Ift88*) required for ciliary assembly (Marshall, 2008). FB were transfected with 5 nM short interfering RNA (siRNA) for Ift88 (siIft88) (Silencer™ Select siIFT88,

TABLE 1 Primer sequences.

Primer	Sequence
COL1A1 Fw	CTGAGCCAGCAGATCGAGAA
COL1A1 Rv	TCGCTTCCATACTCGAACTGG
CTGF Fw	GCGCCTGTTCTAAGACCTGT
CTGF Rv	TGCACTTTTTGCCCTTCTTAATGT
GJA1 Fw	ACTTCAGCCTCCAAGGAGTTC
GJA1 Rv	GGTGGAGTAGGCTTGGACCT
FN1 Fw	CCACCATCACTGGTCTGGAG
FN1 Rv	GGGTGTGGAAGGGTAACCAG
HPRT Fw	TGACTATAATGAGCACTTCAGGGATTT
HPRT Rv	CGCTGTCTTTTAGGCTTTGTACTTG
IFT88 Fw	CTGGCAGTGATAGTGGCCAGA
IFT88 Rv	GCATTTGCCTATTTCTTTGTTCCC
CACNA1G Fw	AGGCAGAGGAAATCGGCAAA
CACNA1G Rv	CTGTCCCCATCACCATCCAC
KCNJ11 Fw	ATCAGTCCAGAGGTTGGTGC
KCNJ11 Rv	TAATGCCCTTTCGGGACAGC
KCNQ1 Fw	GATCAGTCCATCGGGAAGCC
KCNQ1 Rv	GGTCCAGTTGTGTCACCTTGT
KCNJ2 Fw	TGTGTTACAGACGAGTGCCC
KCNJ2 Rv	CAGAGTTTGCCGTCCCTCAT
SCN1B Fw	AACACCAGCGTCGTCAAGAA
SCN1B Rv	TTCCGAGGCATTCTCTTGTGC
SCN5A Fw	TCTTCCGGTTCAGTGCCACC
SCN5A Rv	GGATGGTGCACATGATGAGCATG

ThermoFisher Scientific, Cat#. 4390771, SiRNA ID. s157133) and with 5 nM negative control siRNA (siNC) (Silencer™ Negative Control, ThermoFisher Scientific, Cat#. AM4611) using Lipofectamine RNAiMAX reagent (Invitrogen, Cat#. 13778).

Co-culture of fibroblasts and cardiomyocytes

Twenty-four hours after transfection, cells were digested with trypsin, collected and counted for co-culture experiments. FB were resuspended in 1 ml of TUNG culture medium and added to the CM culture plates/MEAs at a ratio of 1:0.27 (CM:FB). After 48 h of co-culture, cells were collected for RNA isolation. Electrical mapping and microelectrode measurements were also performed.

qRT-PCR

Total RNA was extracted from co-cultured CM and FB with TRI reagent (Sigma-Aldrich) following manufacturer's protocol. RNA was used to generate cDNA using Superscript II (Invitrogen). qRT-PCR was performed on a LightCycler 480 (Roche) with SYBR Green I Master (Roche). Results were analyzed using LinRegPCR software. Primer sequences are included in Table 1. Relative gene expression was calculated using reference gene *Hprt*. Gene expression in the siIFT88 experiments was normalized to siNC for each cell isolation, and expressed as fold change (FC).

Protein analysis

Protein were isolated using TRI reagent (Sigma-Aldrich) following manufacturer's protocol.

Protein concentration was measured by Pierce™ BCA Protein Assay Kit (Thermo Scientific) following manufacturer's instructions.

Western blotting

Western blotting was performed following standard protocols. In short, proteins were separated by electrophoresis in 4%–15% Mini-PROTEAN TGX Precast Protein Gels (Bio-Rad) and transferred to PVDF membranes with the TransBlot Turbo Transfer System (Bio-Rad). Membranes were blocked in TBST 5% milk Protifar (Nutricia) for 1 h at room temperature, then they were incubated with the primary antibodies overnight at 4°C, and finally with HRP-conjugated secondary antibodies for 1 h at room temperature. Western blots were developed with ECL prime western blotting detection agent (Amersham Biosciences) in ImageQuant LAS 4000 (GE Healthcare Life Sciences). Western blots were quantified using Fiji (ImageJ). Antibody references are listed in Table 2.

Simple western analysis

Proteins were separated by size and detected with a WES system (ProteinSimple, San Jose, CA, United States) using a 12–230 kDa separation module with the primary and secondary antibodies mentioned in Table 2. Protein signal analysis and quantification was performed with the Compass software v.4.0.0 (Protein Simple).

Immunofluorescence assays

Cells were fixed in 4% paraformaldehyde, washed and permeabilized (0.2% Triton X-100 in PBS), blocked with 4% goat serum and incubated overnight with the primary antibodies in a humidity chamber at 4°C. Coverslips were incubated for 1 h with secondary antibodies at room temperature, followed by DAPI (Molecular probes) staining. Images were acquired with a Leica DM6000B. The proportion of non-ciliated fibroblasts was quantified using ImageJ.

TABLE 2 Antibodies.

Antibody	Dilution	References
Anti-connexin-43	1:1000 (Simple Wes) 1:250 (IF)	Sigma-Aldrich C6219
Anti-calnexin	1:250 (Simple Wes)	Sigma-Aldrich 208880
Anti-α-actinin	1:1000 (IF)	Sigma-Aldrich A7811
Anti-acetylated α-tubulin	1:1000 (IF)	Abcam 24610
Anti-vimentin	1:1000 (IF)	Abcam ab92547
Anti-IFT88	1:500 (WB)	Proteintech 13967-1-AP
Anti-GAPDH	1:10 000 (WB)	Fitzgerald 10R-G109A
Anti-rabbit-HRP	1:10 000 (WB)	Amersham NA9340V
Anti-mouse-HRP	1:10 000 (WB)	Amersham NA9310V

IF, immunofluorescence.

Electrical mapping

Electrical mapping was performed as previously described (Ernault et al., 2022). Briefly, 10 min before measurements, CM-FB culture media were replaced by a modified Tyrode's solution (36.5°C) containing (mM): NaCl 140, KCl 5.4, CaCl2 1.8, MgCl2 1.0, glucose 5.5, HEPES 5.0; pH 7.4. Spontaneous electrical activity was recorded from CM-FB co-cultured on MEAs (60 electrodes terminals) (60EcoMEA-Glass-gr, Multi Channel Systems MCS GmbH). A reference electrode was place inside the MEA, not in contact with the cells. Unipolar electrograms were recorded simultaneously with a 256-channel amplifier (BioSemi, 24 bit dynamic range, 122.07 nV LSB, total noise 0.5 μV). Signals were recorded with a sampling frequency of 2048 Hz [bandwidth (−3 dB) DC–400 Hz].

Data analysis were performed using a custom-made data analysis program written in Matlab 2006b [The MathWorks Inc, Natick, MA, United States (Potse et al., 2002)]. At each local unipolar electrogram, activation time (AT) was determined as the interval from a reference time zero to the minimum derivative of the QRS-complex of the local unipolar electrogram, and used to construct activation maps. Conduction velocity (CV) was determined along lines perpendicular to isochronal lines by dividing the distance by the difference in local AT. Number of block lines was assessed by counting the number of 30 ms block lines separating adjacent electrodes within one spontaneously active monolayer. The number of 30 ms block line was normalized to the total number of recording electrodes.

Microelectrode measurements

Spontaneous APs were measured in CM-FB monolayers using glass pipette microelectrodes (Harvard apparatus GC100F- 10). These micro-electrodes were filled with 3M KCl, typical tip resistance was 15–25 MΩ. An AgCl-covered silver wire was used as a reference electrode. Resting membrane potential (RMP) was taken as the most negative membrane potential recorded at each recording position. Maximum AP upstroke velocity (V_{max}) was measured and AP duration was determined at 40, 60, and 80% (APD_{40}, APD_{60}, APD_{80}) of repolarization. All signal analyses were performed using a custom-made data analysis program written in Matlab 2006b [The MathWorks Inc, Natick, MA, United States (Potse et al., 2002)].

Statistics

Statistical analyses were performed with GraphPad Prism (GraphPad Software, San Diego, CA, United States). Data are given as mean ± SD unless indicated otherwise. Number of observations and repeated experiments are given in the figure legends. Data were tested for normality using a Shapiro-Wilk normality test. If normal distribution was verified, the 2-tailed Student's *t*-test was performed. If the data were not normally distributed, statistical significance was assessed using the 2-tailed Mann-Whitney test. $p < 0.05$ was considered significant.

Results

Knockdown of Ift88 in fibroblasts is associated with extracellular matrix production

To evaluate the knockdown efficiency of siIft88 in FB, we measured *Ift88* expression in FB only (mRNA and protein) and in CM-FB co-culture (mRNA). Transfection of FB with siIft88 resulted in a 60% significant reduction of (mRNA) *Ift88* expression in FB after 48 h of culture [2.18×10^{-3} ±

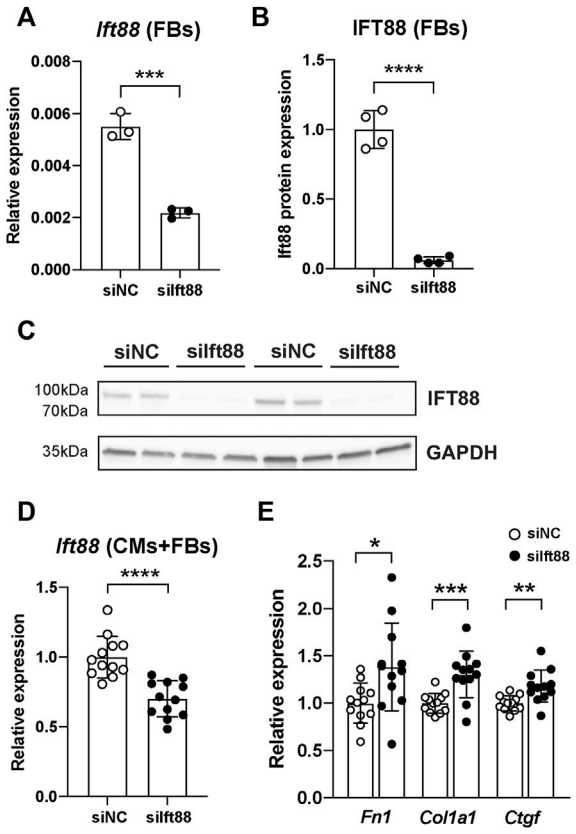

FIGURE 1
Reduction of *Ift88* expression in FB leads to increased ECM genes expression in CM and FB co-culture. **(A)** Relative expression of (mRNA) *Ift88* in FB previously transfected with siNC or siIft88. Data are mean ± SD. $n = 6$ from tree independent CM/FB isolation, Student's *t*-test. **(B,C)** Relative expression of (protein) IFT88 in FB previously transfected with siNC or siIft88. Data are mean ± SD. $n = 4$ from two independent CM/FB isolation, Student's *t*-test. Full unedited blots are provided in Supplementary Figure S1. **(D)** Relative expression of (mRNA) *Ift88* in CM-FB co-cultures after FB transfection with siNC or siIft88. Data are mean ± SD. $n = 12$ from four independent CM/FB isolation, Student's *t*-test. **(E)** Relative expression of ECM genes *Fn1*, *Col1a1* and *Ctfg* after 48 h of co-culture of CM-FB. Data are mean ± SD. $n = 12$ from four independent CM/FB isolation, Student's *t*-test. *$p < 0.05$, **$p < 0.01$, ***$p < 0.001$, ****$p < 0.0001$

1.89×10^{-4} (siIft88) vs. $5.50 \times 10^{-3} \pm 4.99 \times 10^{-4}$ (siNC), $p < 0.001$, $n = 6$] in comparison to the group transfected with siNC (Figure 1A). In addition, transfection of FB with siIft88 resulted in a 94% significant reduction of IFT88 protein expression in FB [0.06 ± 0.02 (siIft88) vs. 1.0 ± 0.13 (siNC), $p < 0.0001$, $n = 8$] in comparison to siNC (Figures 1B,C; Supplementary Figure S1). Furthermore, transfection of FB with siIft88 resulted in a 30% significant reduction of relative *Ift88* expression in the combined CM-FB co-culture, (FC = 0.07 ± 0.13, $p < 0.0001$, $n = 12$) in comparison to the group transfected with siNC (Figure 1B).

Next, we assessed whether *Ift88* reduction in fibroblasts was associated with reduction of primary cilia. Knockdown of *Ift88* in fibroblasts led to a significant increase in the proportion of non-ciliated fibroblasts in comparison to siNC (Supplementary Figure S2) [0.12 ± 0.03 (siIft88) vs. 0.07 ± 0.02 (siNC), $p < 0.0001$].

Knockdown of *Ift88* significantly increased the relative expression of ECM genes *Fn1*, *Col1a1* and *Ctgf* by 38%, 30% and 18%, respectively, in comparison to siNC (*Fn1*: FC = 1.38 ± 0.46, $p < 0.05$; *Col1a1*: FC = 1.30 ± 0.25, $p < 0.001$; *Ctgf*: FC = 1.18 ± 0.17, $p < 0.01$; $n = 12$) (Figure 1C).

Co-culture of cardiomyocytes and fibroblasts with reduced cilia show heterogeneous conduction slowing and reentry

To examine the effect of disrupted cilia formation in FB on conduction, we performed electrical mapping of CM co-cultured with FB pretreated with siIft88 or siNC. Activation maps generated from the siIft88 co-cultures showed isochrone crowding, revealing a slower conduction in siIft88 than in siNC co-cultures (Figures 2A,B).

On average, CV was 17.00 ± 6.20 cm/s in the siNC co-cultures, while it was 11.12 ± 4.27 cm/s in the siIft88 co-cultures (Figure 2C). CV was significantly lower in the siIft88 than in the siNC co-cultures ($p < 0.05$, $n = 10$).

Next, number of block lines was assessed by counting the number of 30 ms block lines in the activation maps, as shown in Figure 2B (right). Number of block lines was $1.18 \times 10^{-2} \pm 3.72 \times 10^{-2}$ in the siNC co-cultures, while it was $6.59 \times 10^{-2} \pm 8.01 \times 10^{-2}$ lines of block per electrode in the siIft88 co-cultures. Number of block lines was significantly higher in the siIft88 co-cultures than in the siNC ($p < 0.05$, $n = 10$).

Cardiomyocytes monolayers co-cultured with fibroblasts with reduced cilia are more prone to reentrant arrhythmias

Figure 3A shows example representative activation maps of a spontaneous rhythm in one MEA in the siIft88 group. Activation times (small numbers) in both panels indicate activation times relative to the same reference time. The white letters indicate electrodes from which selected unipolar electrograms are depicted in panel B. The activation maps show two cycles with reentrant activation patterns in one CM-FB co-culture from the siIft88 group. Activation is continuous from the last activated site in the left panel to the first activated site in the right panel. Electrograms selected along the reentrant circuit are shown in Figure 3B and show that the diastolic interval is spanned by local activation, as expected during reentry. Overall, we observed two spontaneous reentrant activation patterns in two different CM-FB co-cultures in the siIft88 group and none in the siNC group (Figure 3C).

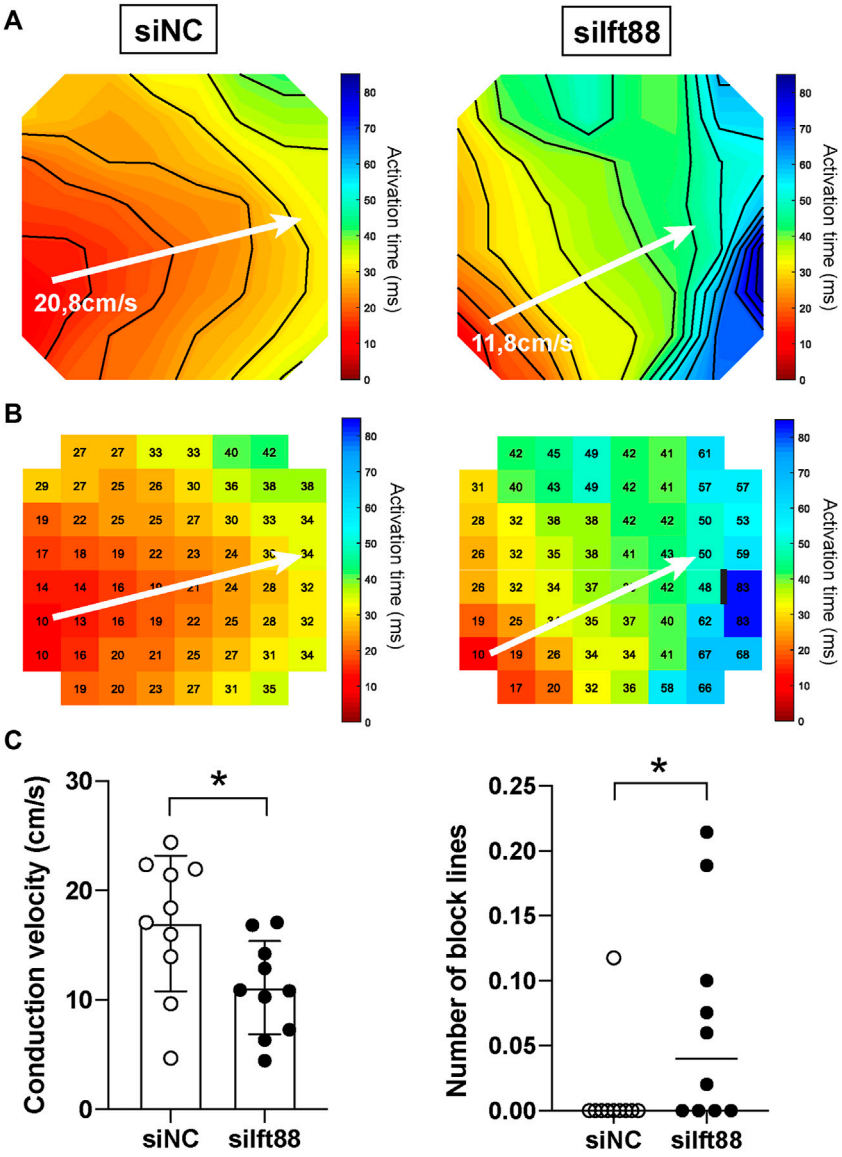

FIGURE 2
Reduced conduction velocity in CM monolayers co-cultured with decreased Ift88 FB. **(A,B)** Representative activation maps obtained after electrical mapping of spontaneously active CM co-cultured for 48 h with FB previously transfected with siNC or siIft88. Colors indicate activation times, according to the scale at right. Isochrones, 5 ms. White arrows indicate where conduction velocity was measured. Black line indicates 30 ms conduction block. Interelectrode distance of 700 μM. **(C)** Conduction velocity (CV) and number of block lines in spontaneously active CM monolayers co-cultured for 48 h with FB transfected with siNC or siIft88. Data are mean ± SD for CV and median for number of block lines, n = 10 monolayers from three independent CM/FB isolation. Student's t-test for CV, Mann-Whitney test for number of block lines. Factor correction was carried out on CV to avoid inter-isolations differences.

Knockdown of Ift88 in fibroblasts is not associated with changes of action potential characteristics nor reduced electrical coupling

Figure 4A shows representative examples of microelectrode AP measurements in CM-FB co-cultures from siNC and siIft88 groups. Overall, there were no significant differences in APD_{40} [92.03 ± 17.60 (siNC) vs. 82.24 ± 11.25 ms (siIft88)], APD_{60} [124.6 ± 20.21 (siNC) vs. 119.1 ± 14.83 ms (siIft88)], nor in APD_{80} [189.4 ± 20.54 (siNC) vs. 201.1 ± 39.50 ms (siIft88)] between siNC and siIft88 co-cultures ($n \geq 9$) (Figure 4B).

The observed reduction in conduction velocity (Figure 2) was not associated with significant depolarization of CM nor

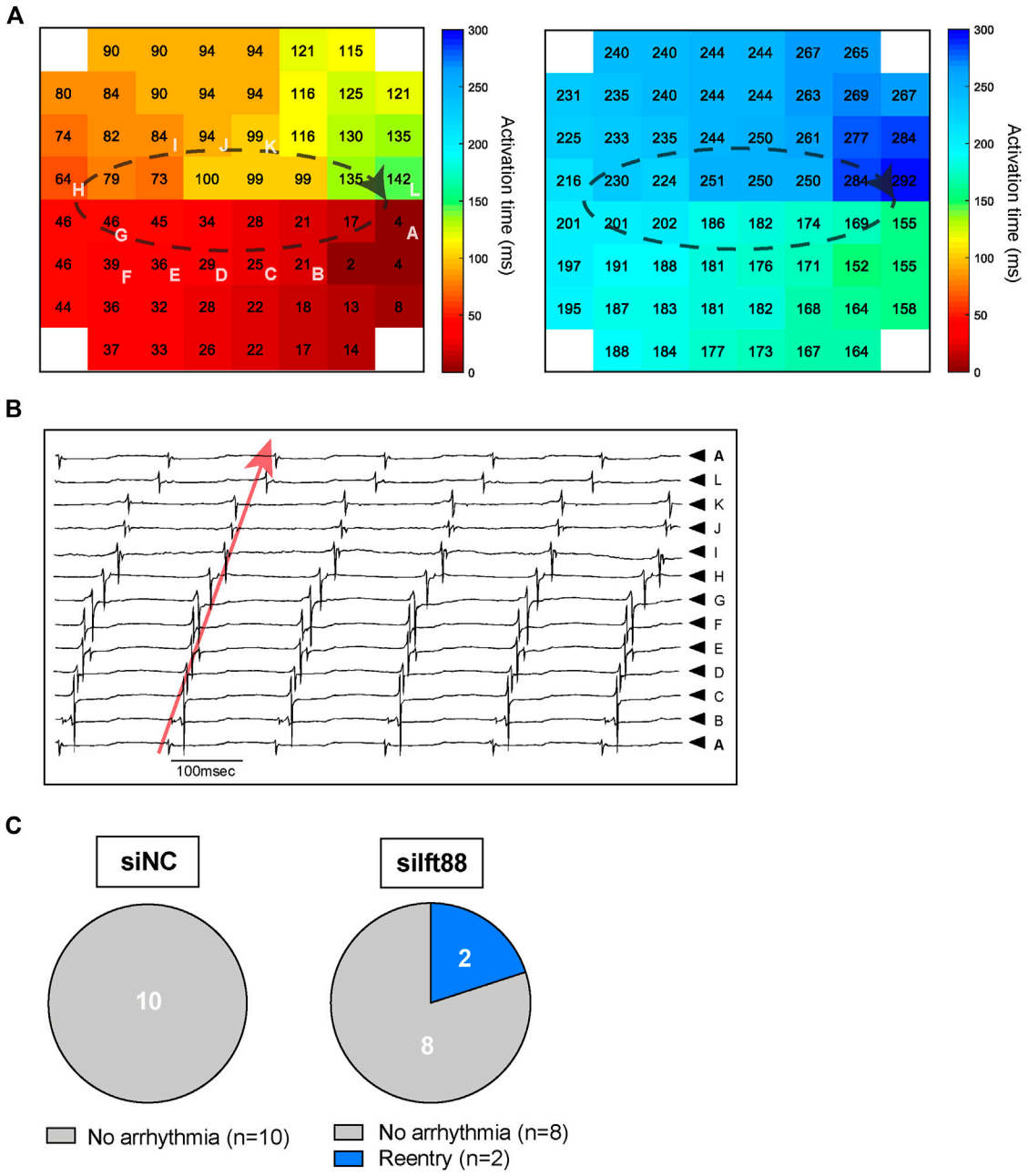

FIGURE 3
Reentry in CM co-cultured with silft88 FB. **(A)** Activation maps of two following beats showing reentrant circuit and obtained from one CM monolayer co-cultured for 48 h with FB previously transfected with silft88. Colors indicate activation times, according to the scale at right. Dashed black line indicated reentrant conduction pattern. Letters indicate electrodes from which selected unipolar electrograms are depicted in **(B)**. **(B)** Electrograms selected along the reentry circuit. Red arrow shows that the diastolic interval is spanned within local activation (electrogram from electrode A is repeated on top and at the bottom) as expected during reentry. The letters next to the electrograms indicate electrodes from which selected unipolar electrograms are shown **(A)**. **(C)** Proportion of CM-FB co-cultures showing reentrant arrhythmia or no arrhythmia in the siNC and silft88 groups.

reduction of AP amplitude. Overall, the RMP was −57.96 ± 15.92 mV in the siNC co-cultures, while it was −59.23 ± 14.30 mV in the siIft88 co-cultures ($n \geq 9$). The averaged AP amplitude was 78.94 ± 18.52 mV in the siNC co-cultures while it was 76.73 ± 17.83 mV in the siIft88 co-cultures (Figure 4C). V_{max} and cycle length were also not significantly different between the two groups [19.24 ± 6.719 (siNC) vs. 25.43 ± 17.79 V/s (siIft88) and 3.96 ± 3.84 (siNC) vs. 2.25 ± 1.84 s (siIft88), respectively] (Figures 4D,E).

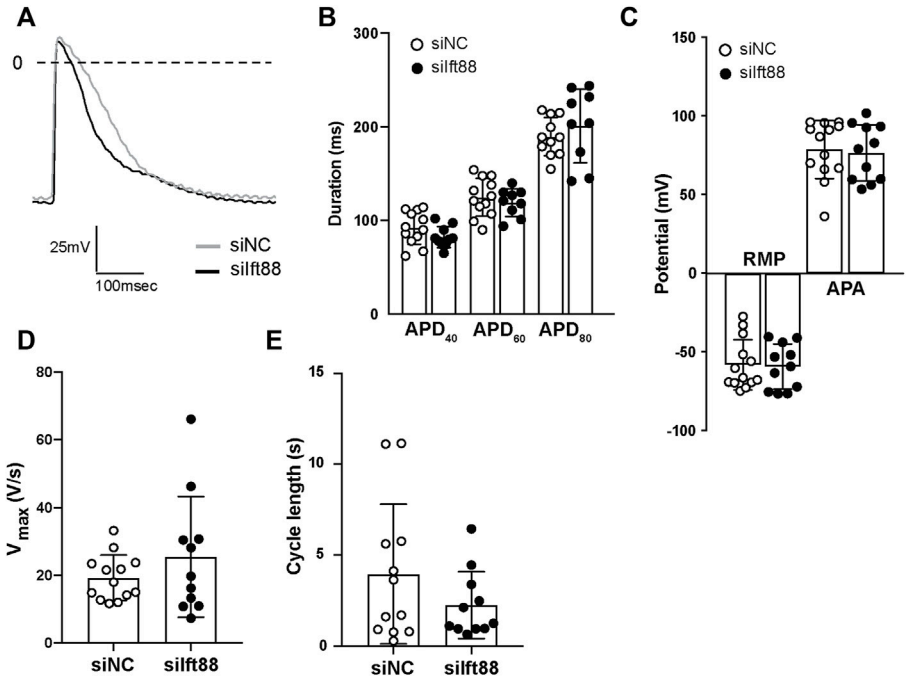

FIGURE 4
Co-culture between FB with reduced (mRNA) *Ift88* expression and CM does not lead to changes of the action potential characteristics. **(A)** Representative spontaneous APs recorded in CM monolayers co-cultured for 48 h with FB previously transfected with siNC or siIft88. **(B–E)** Effect of co-culture on spontaneous APs duration at 40%, 60%, and 80% (APD_{40}, APD_{60}, and APD_{80}) of repolarization **(B)**, resting membrane potential (RMP), AP amplitude (APA) **(C)**, maximal upstroke velocity (V_{max}) **(D)** and cycle length **(E)**. $n \geq 9$ microelectrode measurements from two independent CM/FB isolation. Data are mean ± SD.

Connexin43 (main protein component of gap junctions in neonatal rat ventricular CM) expression and distribution were not different between siNC and siIft88 co-cultures (Supplementary Figures S3, S4). Finally, the expression of major cardiomyocytes ion channels (*Kcnj11*, *Kcnq1*, *Kcnj2*, *Cacna1g*, *Scn1b*, *Scn5a*) was not significantly different between siIft88 and siNC groups (Supplementary Figure S5).

Discussion

In this study, we show that the disruption of cilia formation in FB *via* targeting *Ift88* with siRNA is associated with enhanced ECM gene expression and conduction delay in CM-FB co-cultures, without changes of AP characteristics.

The cardiac ECM is a dynamic and complex network which plays an important role in providing structural support to cardiac cells, and regulates gene expression as well as gap junction organization (Forte et al., 2012). Remodeling of the ECM under pathological conditions alters cardiac fibers organization, leading to heterogeneous conduction delay and enhanced anisotropy, increasing the risk of arrhythmias.

Dysregulation of primary cilia in cardiac diseases and fibrosis formation has been implicated in various studies. For instance, primary cilia are important for embryonic development (Komatsu and Mishina, 2013) and the patients affected by a ciliopathy, a genetic condition caused by dysfunction of primary cilia, often manifest congenital heart disease and multi-organ fibrosis (Seeger-Nukpezah and Golemis, 2012; Klena et al., 2017). Several age-dependent diseases, such as atherosclerosis was shown to be driven by loss of primary cilia in aortic endothelial cells (Dinsmore and Reiter, 2016), suggesting that primary cilia suppress pro-atherosclerotic signaling. Biological processes underlying atrial fibrosis formation, such as epithelial-mesenchymal transition, differentiation of fibroblasts into myofibroblasts, and ECM synthesis depend on primary cilia (Ten Dijke et al., 2012).

Co-culture of CM and FB with a reduction of primary cilia by knockdown of Ift88 leads to increased ECM gene expression of *Fn1*, *Col1a1* and *Ctgf* (Figure 1). This is in accordance with previous work showing that conditional knockout of *Ift88* in mouse heart leads to increased production of ECM substrates collagen I and versican (Toomer et al., 2017). Consistently, silencing *Ift88* in chondrocytes leads to increased expression of ECM components *Mmp13*, *Adamts5*, *ColX*, and *Runx2* (Chang et al., 2012; Collins and Wann, 2020). These results suggest that

primary cilia are dynamic cellular appendages which restrain and fine-tune FB activation and ECM production. Consistent with these previous reports, we previously observed that FB from patients with persistent AF express fewer primary cilia in association with more ECM production compared to FB from non-AF patients (data not shown).

Our results are in seemingly contradiction with the study by Villalobos et al. where the conditional knockout of polycistine1 (PC1 encoded by pkd1, pkd1-cKO) in activated cardiac fibroblasts reduces scar size in a myocardial infarction (MI) model. However, this reduction was not attributable to reduced fibrosis. PC1 together with polycistine2 (PC2, encoded by pkd2) form a transient receptor potential ion channel and mediate the mechano-sensation *via* primary cilia, but they are not involved in the formation of primary cilia (Surya M. Nauli et al. Nature Genetics, 2003). Therefore, from the paper by Villalobos et al. it remains unclear whether a loss of primary cilia in the activated cardiac fibroblasts increases or decreases cardiac fibrosis.

We observed differences in *Ift88* transcript levels between FB cultures and CM-FB co-cultures (Figure 1). We speculate that these differences are caused by *Ift88* expression in cardiomyocytes in which *Ift88* was not knocked-down.

Co-culture of CM with FB transfected with siIft88 led to conduction abnormalities (slower CV, increased number of block lines) (Figure 2) and subsequent increased risk of reentrant arrhythmias (Figure 3), without changes in AP characteristics (Figure 4) and without reduction in *Gja1* expression (Supplementary Figure S1). This demonstrates that the observed CV reduction and increased risk of arrhythmia is not subsequent to electrical remodeling of CM (i.e., reduction of intercellular electrical coupling between CM or depolarization of CM). Instead, the CV reduction and increased number of block lines observed in the siIft88 CM-FB co-cultures is likely due to the increased ECM production from activated fibroblasts following the dysregulation of primary cilia. Excessive ECM deposition separates CM and may lead to tortuous patterns of activation which results in conduction delay and blocks. These findings are in accordance with literature showing that conduction velocity is impaired when (myo)fibroblast concentration increases and fibrosis occurs (Spencer et al., 2017).

Study limitations

While knockdown of IFT88 is known to cause loss of primary cilia in fibroblasts, we cannot exclude that there are other, secondary, effects caused by this gene knockdown which could modify fibroblast behavior.

Extracellular matrix remodeling was in this study assessed by gene expression measurement, without quantifying the ECM architecture or composition. Further study should investigate and perform quantitative analysis on the ECM architecture and composition in the two groups.

Conclusion

Protecting the function of primary cilia and repairing the disrupted cilia is a potential therapy to prevent the onset of AF and to reverse the fibrosis formation in the advanced AF, respectively.

Data availability statement

The raw data supporting the conclusion of this article will be made available by the authors, without undue reservation.

Ethics statement

The animal study was reviewed and approved by the local Animal Experiments Committee (Academic Medical Center, University of Amsterdam).

Author contributions

AE, MK, RC, and JG designed the project. AE, MK, BF, PM-A, SA, and RA-S performed the experiments. AE, MK, PM-A, and BF acquired and analyzed the data. AE wrote the paper with input from all authors. All authors provided critical feedbacks on the manuscript and approved its submission.

Funding

This study was supported by Netherlands Organization for Health Research and Development (ZonMW/NWO, 106.146.310) awarded to JG.

Conflict of interest

JG received research grants through his institution from Abbott, Atricure, Boston Scientific, Bayer, Daiichi Sankyo, Johnson & Johnson, Medtronic Servier, and received speaker/consultancy fees from Atricure, Bayer, Daiichi Sankyo, Johnson

& Johnson and Medtronic outside the submitted work. AHGD is a consultant for Atricure.

The remaining authors declare that the research was conducted in the absence of any commercial or financial relationships that could be construed as a potential conflict of interest.

Publisher's note

All claims expressed in this article are solely those of the authors and do not necessarily represent those of their affiliated organizations, or those of the publisher, the editors and the reviewers. Any product that may be evaluated in this article, or claim that may be made by its manufacturer, is not guaranteed or endorsed by the publisher.

Supplementary material

The Supplementary Material for this article can be found online at: https://www.frontiersin.org/articles/10.3389/fphys.2022.1057200/full#supplementary-material

References

Benjamin, E. J., Wolf, P. A., D'agostino, R. B., Silbershatz, H., Kannel, W. B., and Levy, D. (1998). Impact of atrial fibrillation on the risk of death: The framingham heart study. *Circulation* 98, 946–952. doi:10.1161/01.cir.98.10.946

Burstein, B., and Nattel, S. (2008). Atrial fibrosis: Mechanisms and clinical relevance in atrial fibrillation. *J. Am. Coll. Cardiol.* 51, 802–809. doi:10.1016/j.jacc.2007.09.064

Chang, C. F., Ramaswamy, G., and Serra, R. (2012). Depletion of primary cilia in articular chondrocytes results in reduced Gli3 repressor to activator ratio, increased Hedgehog signaling, and symptoms of early osteoarthritis. *Osteoarthr. Cartil.* 20, 152–161. doi:10.1016/j.joca.2011.11.009

Collins, I., and Wann, A. K. T. (2020). Regulation of the extracellular matrix by ciliary machinery. *Cells* 9, E278. doi:10.3390/cells9020278

Dinsmore, C., and Reiter, J. F. (2016). Endothelial primary cilia inhibit atherosclerosis. *EMBO Rep.* 17, 156–166. doi:10.15252/embr.201541019

Ernault, A. C., Verkerk, A. O., Bayer, J. D., Aras, K., Montañés-Agudo, P., Mohan, R. A., et al. (2022). Secretome of atrial epicardial adipose tissue facilitates reentrant arrhythmias by myocardial remodeling. *Heart rhythm.* 19, 1461–1470. doi:10.1016/j.hrthm.2022.05.011

Forte, G., Pagliari, S., Ebara, M., Uto, K., Tam, J. K., Romanazzo, S., et al. (2012). Substrate stiffness modulates gene expression and phenotype in neonatal cardiomyocytes *in vitro*. *Tissue Eng. Part A* 18, 1837–1848. doi:10.1089/ten.TEA.2011.0707

Heijman, J., Linz, D., and Schotten, U. (2021). Dynamics of atrial fibrillation mechanisms and comorbidities. *Annu. Rev. Physiol.* 83, 83–106. doi:10.1146/annurev-physiol-031720-085307

Kawasaki, M., Meulendijks, E. R., Van Den Berg, N. W. E., Nariswari, F. A., Neefs, J., Wesselink, R., et al. (2021). Neutrophil degranulation interconnects over-represented biological processes in atrial fibrillation. *Sci. Rep.* 11, 2972. doi:10.1038/s41598-021-82533-5

Klena, N. T., Gibbs, B. C., and Lo, C. W. (2017). Cilia and ciliopathies in congenital heart disease. *Cold Spring Harb. Perspect. Biol.* 9, a028266. doi:10.1101/cshperspect.a028266

Komatsu, Y., and Mishina, Y. (2013). Establishment of left-right asymmetry in vertebrate development: The node in mouse embryos. *Cell. Mol. Life Sci.* 70, 4659–4666. doi:10.1007/s00018-013-1399-9

Kornej, J., Börschel, C. S., Benjamin, E. J., and Schnabel, R. B. (2020). Epidemiology of atrial fibrillation in the 21st century: Novel methods and new insights. *Circ. Res.* 127, 4–20. doi:10.1161/CIRCRESAHA.120.316340

Krogh-Madsen, T., Abbott, G. W., and Christini, D. J. (2012). Effects of electrical and structural remodeling on atrial fibrillation maintenance: A simulation study. *PLoS Comput. Biol.* 8, e1002390. doi:10.1371/journal.pcbi.1002390

Marshall, W. F. (2008). Basal bodies platforms for building cilia. *Curr. Top. Dev. Biol.* 85, 1–22. doi:10.1016/S0070-2153(08)00801-6

Nauli, S. M., Alenghat, F. J., Luo, Y., Williams, E., Vassilev, P., Li, X., et al. (2003). Polycystins 1 and 2 mediate mechanosensation in the primary cilium of kidney cells. *Nat. genet.* 33 (2), 129–137. doi:10.1038/ng1076

Nattel, S., Burstein, B., and Dobrev, D. (2008). Atrial remodeling and atrial fibrillation: Mechanisms and implications. *Circ. Arrhythm. Electrophysiol.* 1, 62–73. doi:10.1161/CIRCEP.107.754564

Potse, M., Linnenbank, A. C., and Grimbergen, C. A. (2002). Software design for analysis of multichannel intracardial and body surface electrocardiograms. *Comput. Methods Programs Biomed.* 69, 225–236. doi:10.1016/s0169-2607(02)00014-7

Seeger-Nukpezah, T., and Golemis, E. A. (2012). The extracellular matrix and ciliary signaling. *Curr. Opin. Cell Biol.* 24, 652–661. doi:10.1016/j.ceb.2012.06.002

Spencer, T. M., Blumenstein, R. F., Pryse, K. M., Lee, S. L., Glaubke, D. A., Carlson, B. E., et al. (2017). Fibroblasts slow conduction velocity in a reconstituted tissue model of fibrotic cardiomyopathy. *ACS Biomater. Sci. Eng.* 3, 3022–3028. doi:10.1021/acsbiomaterials.6b00576

Ten Dijke, P., Egorova, A. D., Goumans, M. J., Poelmann, R. E., and Hierck, B. P. (2012). TGF-B signaling in endothelial-to-mesenchymal transition: The role of shear stress and primary cilia. *Sci. Signal.* 5, pt2. doi:10.1126/scisignal.2002722

Teves, M. E., Strauss, J. F., 3rd, Sapao, P., Shi, B., and Varga, J. (2019). The primary cilium: Emerging role as a key player in fibrosis. *Curr. Rheumatol. Rep.* 21, 29. doi:10.1007/s11926-019-0822-0

Toomer, K. A., Fulmer, D., Guo, L., Drohan, A., Peterson, N., Swanson, P., et al. (2017). A role for primary cilia in aortic valve development and disease. *Dev. Dyn.* 246, 625–634. doi:10.1002/dvdy.24524

Van Den Berg, N. W. E., Kawasaki, M., Fabrizi, B., Nariswari, F. A., Verduijn, A. C., Neefs, J., et al. (2021). Epicardial and endothelial cell activation concurs with extracellular matrix remodeling in atrial fibrillation. *Clin. Transl. Med.* 11, e558. doi:10.1002/ctm2.558

frontiers | Frontiers in Physiology

TYPE Original Research
PUBLISHED 16 December 2022
DOI 10.3389/fphys.2022.1077069

OPEN ACCESS

EDITED BY
Flavien Charpentier,
INSERM U1087 Institut du Thorax, France

REVIEWED BY
Jean-Sebastien Rougier,
University of Bern, Switzerland
Mark Hoogendijk,
Erasmus Medical Center, Netherlands

*CORRESPONDENCE
A. B. Carvalho,
carvalhoab@biof.ufrj.br

SPECIALTY SECTION
This article was submitted to Cardiac Electrophysiology, a section of the journal Frontiers in Physiology

RECEIVED 22 October 2022
ACCEPTED 08 December 2022
PUBLISHED 16 December 2022

CITATION
Carvalho AB, Coutinho KCdS, Barbosa RAQ, Campos DBPd, Leitão IdC, Pinto RS, Dos Santos DS, Farjun B, De Araújo DdS, Mesquita FCP, Monnerat-Cahli G, Medei EH, Kasai-Brunswick TH and De Carvalho ACC (2022), Action potential variability in human pluripotent stem cell-derived cardiomyocytes obtained from healthy donors.
Front. Physiol. 13:1077069.
doi: 10.3389/fphys.2022.1077069

Action potential variability in human pluripotent stem cell-derived cardiomyocytes obtained from healthy donors

A. B. Carvalho[1,2,3]*, Keyla Cristiny da Silva Coutinho[1], Raiana Andrade Quintanilha Barbosa[1], Dilza Balteiro Pereira de Campos[1], Isabela de Carvalho Leitão[1], R. S. Pinto[1], D. Silva Dos Santos[1], Bruna Farjun[1], Dayana da Silva De Araújo[1], Fernanda Cristina Paccola Mesquita[1], G. Monnerat-Cahli[1], E. H. Medei[1,2,3], Tais Hanae Kasai-Brunswick[1,2,3] and A. C. Campos De Carvalho[1,2,3,4]

[1]Carlos Chagas Filho Institute of Biophysics, Federal University of Rio de Janeiro, Rio de Janeiro, Brazil, [2]National Center for Structural Biology and Bioimaging, Federal University of Rio de Janeiro, Rio de Janeiro, Brazil, [3]National Institute of Science and Technology in Regenerative Medicine, Rio de Janeiro, Brazil, [4]National Institute of Cardiology, Rio de Janeiro, Brazil

Human pluripotent stem cells (PSC) have been used for disease modelling, after differentiation into the desired cell type. Electrophysiologic properties of cardiomyocytes derived from pluripotent stem cells are extensively used to model cardiac arrhythmias, in cardiomyopathies and channelopathies. This requires strict control of the multiple variables that can influence the electrical properties of these cells. In this article, we report the action potential variability of 780 cardiomyocytes derived from pluripotent stem cells obtained from six healthy donors. We analyze the overall distribution of action potential (AP) data, the distribution of action potential data per cell line, per differentiation protocol and batch. This analysis indicates that even using the same cell line and differentiation protocol, the differentiation batch still affects the results. This variability has important implications in modeling arrhythmias and imputing pathogenicity to variants encountered in patients with arrhythmic diseases. We conclude that even when using isogenic cell lines to ascertain pathogenicity to variants associated to arrythmias one should use cardiomyocytes derived from pluripotent stem cells using the same differentiation protocol and batch and pace the cells or use only cells that have very similar spontaneous beat rates. Otherwise, one may find phenotypic variability that is not attributable to pathogenic variants.

KEYWORDS

iPSC (induced pluripotent stem cell), cardiomyocytes, action potential (AP), variability, cell lines, differentiation methods, differentiation batches, healthy donors

Introduction

Since the advent of human embryonic stem (ES) cells (Thomson et al., 1998) and the reprograming of human adult cells to a pluripotent state by Yamanaka's group (Takahashi et al., 2007), human pluripotent stem cells (PSC) have been used extensively in multiple areas of biology and medicine (for a review see (Takahashi and Yamanaka, 2016). Methods to differentiate the PSC into cardiomyocytes have been described by different laboratories with efficiencies ranging from 60%–99% (Kattman et al., 2011; Burridge et al., 2011; 2014; Lian et al., 2012), indicating a residual population of non-cardiomyocyte cell types in the most robust differentiation methods, even after metabolic selection (Tohyama et al., 2013). Additionally, there is still variability in the differentiation process depending on donor and donor cell source (Ohno et al., 2013; Sanchez-Freire et al., 2014). Furthermore, although methods to enrich atrial and ventricular cardiomyocyte populations have been described (Lee et al., 2017; Zhao et al., 2019) none ascertain a pure population of chamber specific cardiomyocytes. On top of all these factors the differentiation process leads to an immature phenotype, typical of fetal cardiomyocytes, and although protocols using long term culturing, electric stimulation, mechanical loading, scaffold stiffness, 3-dimensional culturing, epigenetic regulators, metabolic maturation media and neurohormonal stimulation have been developed (Yang et al., 2014; Weinberger et al., 2017; Feyen et al., 2020), combining all these procedures in one single protocol is virtually unattainable.

Considering all these factors it is not surprising that electrophysiologic properties of PSC-derived cardiomyocytes are highly variable. In this article, we report the action potential variability of 780 cardiomyocytes derived from PSC obtained from six healthy donors. One PSC is an ES cell line while the other five lines are induced pluripotent stem (iPS) cells. These six lines were compared as group since they share similar pluripotent properties (Takahashi et al., 2007). We analyze the overall distribution of action potential data, the distribution of AP data per cell line, per differentiation protocol and batch. This analysis indicates that even using the same cell line and differentiation protocol, the differentiation batch still affects the results. This variability has important implications in modeling arrhythmias and imputing pathogenicity to variants encountered in patients with arrhythmic diseases.

Materials and methods

All data generated or analyzed during this study are included in this published article or in its Supplementary Material.

Cell lines and culture

The human PSC lines used in this study are described in Supplementary Table S1. HES3 NKX2-5$^{eGFP/w}$ was kindly donated to us by Dr. David Elliot (Elliott et al., 2011). The other cells lines were generated in our laboratory from peripheral blood mononuclear cells using Sendai virus (Thermo Scientific) (Mesquita et al., 2019; Cruvinel et al., 2020) (Kasai-Brunswick

TABLE 1 Descriptive statistics for the entire dataset.

Parameter	Min	1st Q	Median	3rd Q	Max	Mean	SD
MDP (mV)	−94	−63.84	−57.53	−51.07	−40.1	−57.89	9.26
APA (mV)	70.08	81.38	90.29	98.59	125	90.63	11.53
dV/dt max (mV/s)	4.4×10^3	1.2×10^4	1.7×10^4	3.1×10^4	2.3×10^5	2.3×10^4	1.8×10^4
dV/dt min (mV/s)	3.7×10^2	9.5×10^2	1.3×10^3	1.7×10^3	4.7×10^3	1.4×10^3	6×10^2
APD10 (ms)	20.29	68.47	83.67	108.55	628.50	97.76	52.45
APD20 (ms)	32.06	101.05	123.4	158.95	671	138.58	61.82
APD30 (ms)	45.82	125.78	151.8	203.93	704.9	176.56	81.26
APD40 (ms)	56.73	141.2	170.7	236.45	752.6	202.32	96.61
APD50 (ms)	64.8	150.9	184.8	254.3	1134	220.1	110.29
APD60 (ms)	73.21	158.97	193.3	266.25	1185	231.74	116.41
APD70 (ms)	82.43	167.10	202	281.07	1205	241.76	119.83
APD80 (ms)	94.61	17.65	212.05	295.32	1224	253.38	123.19
APD90 (ms)	112.8	191.9	241.3	324.9	1290	280.4	136.74
Cycle length (ms)	309.7	1001	1515	1965.5	8634	1597.5	821.39

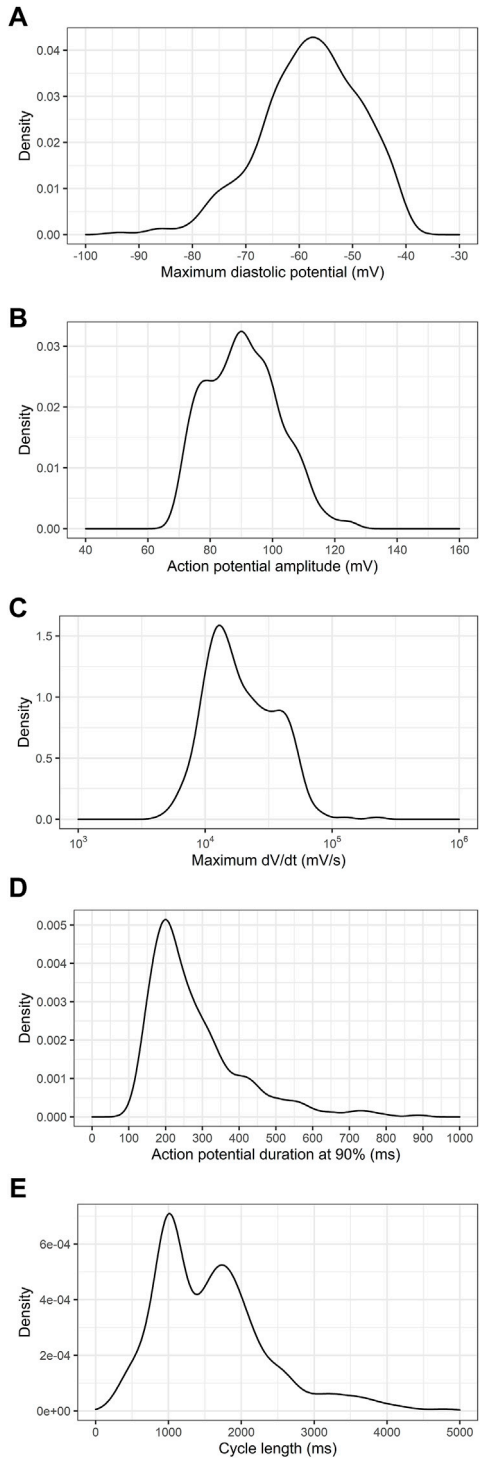

FIGURE 1
Density distribution of action potential parameters from PSC-derived cardiomyocytes. **(A)** Maximum diastolic potentials (MDP), **(B)** action potential amplitudes (APA), **(C)** maximum dV/dt (dV/dt max), **(D)** action potential duration at 90% repolarization (APD90) and **(E)** cycle length are shown for the whole dataset, comprising 780 electrophysiological recordings.

et al., 2018). PSC were cultured in mouse embryonic fibroblast feeder layers under standard conditions (Thomson et al., 1998).

Cardiac differentiation

Two well established cardiac differentiation protocols were used in this study, henceforth referred to as Kattman (Kattman et al., 2011) and Lian (Lian et al., 2012). Both are based on stimulation followed by inhibition of the Wnt pathway using cytokines and/or small molecules. Detailed conditions for each cell line are provided in Supplementary Table S2.

Action potential recordings

A total of 780 PSC-derived cardiomyocytes were recorded, 138 from ES and 652 from iPS cells (Supplementary Table S3). For Kattman's protocol, embryoid bodies were digested with collagenase 1 and trypsin-EDTA and plated in Matrigel 2 days in advance to recover from the digestion process. For Lian's protocol, monolayers were dissociated with trypsin-EDTA and also plated in Matrigel for 2 days. Cells were perfused with Tyrode's solution (in mM: 140 NaCl, 5.4 KCl, 1.8 $CaCl_2$, 1.0 $MgCl_2$, 11.0 glucose, 10.0 HEPES, pH 7.4) at 37.0°C ± 1.0°C saturated with oxygen at a perfusion flow rate of 0.5 ml/min. Transmembrane potential was recorded using glass microelectrodes (40–80 MΩ DC resistance) filled with 2.7 M KCl connected to a Microelectrode Amplifier (MultiClamp 700B, Molecular Devices). Amplified signals were digitized (1440 digidata A/D interface, Axon Instruments) and stored in a computer for later analysis using LabChart 7.3 software (ADInstruments). The following parameters were analyzed from at least 10 consecutive action potentials from each cell: maximum diastolic potential (MDP), action potential amplitudes (APA), maximum dV/dt (dV/dtmax), minimum dV/dt (dV/dtmin), action potential duration (APD) at 10 through 90% repolarization, and cycle length. Electrophysiologic data were used from cells having MDP between −100 and −40 mV, APA between 70 and 130 mV, and dV/dt max below 250 V/s.

Statistics

Statistical analyses were conducted using R (https://www.r-project.org) with RStudio (https://www.rstudio.com) as a visual interface. Raw data, R packages and code used for analyses are provided in the Supplementary Material. Action potential data were compared using Student's

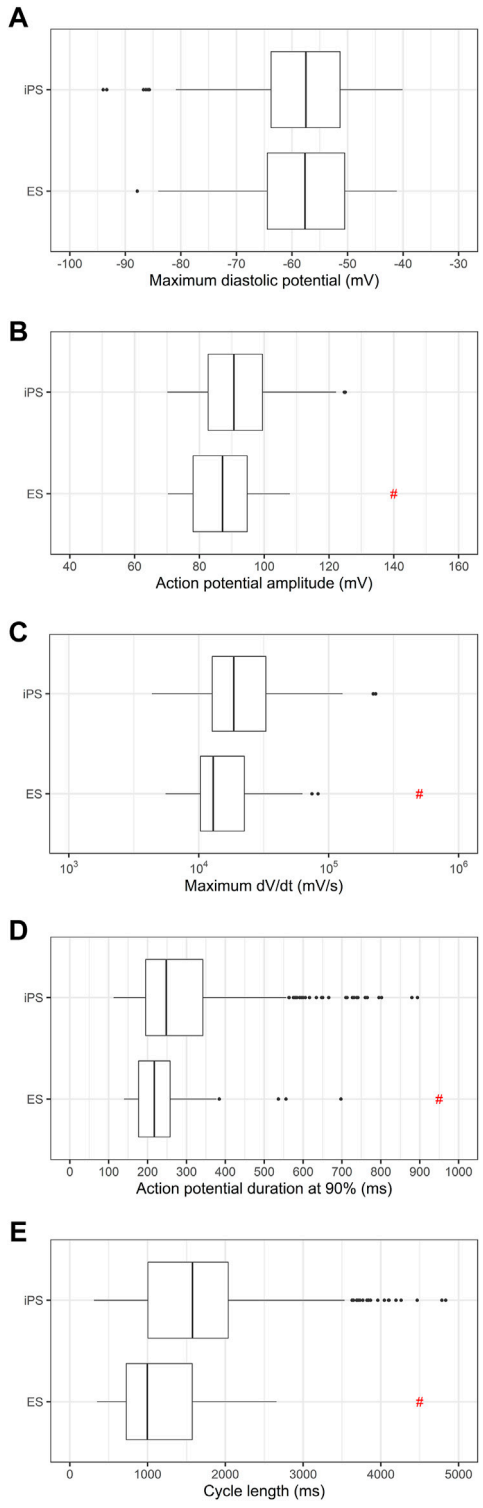

FIGURE 2
Comparison of electrophysiologic parameters between ES and iPS-derived cardiomyocytes. **(A)** Maximum diastolic potentials (MDP), **(B)** action potential amplitudes (APA), **(C)** maximum dV/dt (dV/dt max), **(D)** action potential duration at 90% repolarization (APD90) and **(E)** cycle length are shown. It is important to note that differentiation protocols varied between the two cell types, and herefore the significance of the differences may be attributable to the varying protocols used for differentiation. # indicates $p < 0.05$ using Student's *t*-test.

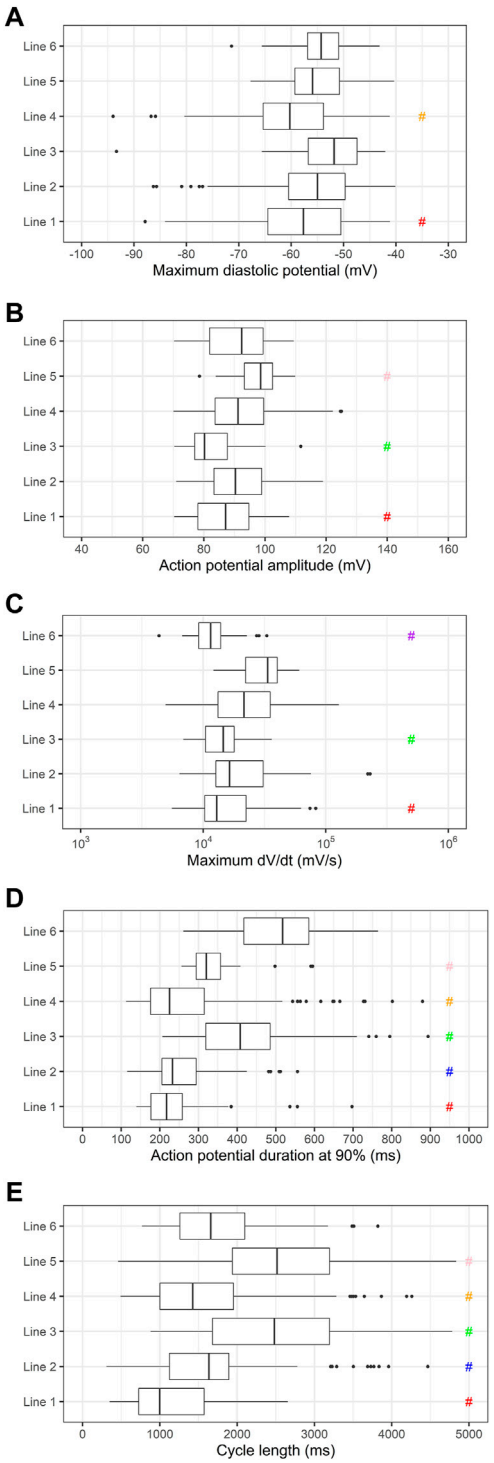

FIGURE 3
Comparison of electrophysiologic parameters of cardiomyocytes differentiated from individual cell lines. **(A)** Maximum diastolic potentials (MDP), **(B)** action potential amplitudes (APA), **(C)** maximum dV/dt (dV/dt max), **(D)** action potential duration at 90% repolarization (APD90) and **(E)** cycle length are shown. # indicates $p < 0.05$ using one-way ANOVA followed by Tukey's post test. Significant differences were observed in the following parameters: MDP (red: 1 vs. 3, orange: 4 vs. 2, 3 and 6), APA (red: 1 vs. 2, 4 and 5, green: 3 vs. 2, 4, 5 and 6, pink: 5 vs. 1, 2 and 3), dV/dt max (red: 1 vs. 2, 4 and 5, green: 3 vs. 2, 4 and 5, purple: 6 vs. 2, 4 and 5), APD90 (red: 1 vs. 3, 5 and 6, blue: 2

(*Continued*)

FIGURE 3 (Continued)
vs. 3, 5 and 6, green: 3 vs. all lines, orange: 4 vs. 3, 5 and 6, pink: 5 vs. all lines), cycle length (red: 1 vs. all lines, blue: 2 vs. 1, 3 and 5, green: 3 vs. 1, 2, 4 and 6, orange: 4 vs. 1, 3 and 5, pink: 5 vs. 1, 2, 4 and 6).

t-test, one-way ANOVA followed by Tukey's post-test to correct for multiple comparisons, or Kruskal-Wallis test. Data were considered statistically significant if *p*-value was below 0.05.

Results

We first analyzed the overall distribution of resting and action potential properties. Table 1 shows descriptive statistics for 780 PSC-derived cardiomyocytes across six different cell lines, four distinct differentiation protocols and several differentiation batches (18–21 batches/3 cell lines). Supplementary Tables S4–S8 show the same descriptive statistics for all six cell lines individually.

We next examined the distribution of the electrophysiologic properties of PSC-derived cardiomyocytes obtained from all six cell lines. Figure 1 shows the distribution of maximum diastolic potentials (MDP), action potential amplitudes (APA), maximum dV/dt (dV/dt max), action potential duration at 90% repolarization (APD90) and cycle length across the entire dataset.

Then, we investigated if the use of ES or iPS could influence in the electrophysiologic parameters of the differentiated PSC-derived cardiomyocytes. Figure 2 shows there is no difference in MDP distribution, but there is significant variability in APA, dV/dt max and cycle length between ES and iPS-derived cardiomyocytes.

To investigate the variability in the electrophysiologic properties of the PSC-derived cardiomyocytes from all 6 cell lines individually, we plotted the values of MDP, APA, dV/dt max, APD90 and cycle length, as shown in Figure 3. As expected from the literature, there are significant differences between some of the lines.

Since MDP is known to influence the action potential amplitude and rate of depolarization, in Figures 4A, B we analyzed the influence of MDP in APA and dV/dt max. Although the correlation coefficients found are low, there is a strong negative correlation between these parameters as expected in cardiac electrophysiology. Figure 4C analyzes the influence of cycle duration in ADP90. There is a strong positive correlation between these parameters but at higher cycle lengths there is clear heteroscedasticity. Supplementary Figure S1 shows the same analysis as Figure 4, but now highlighting the two cell types (ES and iPS, 1a), the four differentiation protocols (1b) and the six cell lines individually (1c). Segmentation by these variables does not differ from the entire dataset.

To investigate the effect of differentiation batch, we analyzed resting and action potential parameters obtained from PSC-derived cardiomyocytes derived from 3 different cell lines submitted to 18–21 differentiation batches. For each cell line, all differentiation batches used the same protocol, but line 1 used Kattman's protocol and lines 2 and 4 used Lian's protocol. As shown in Figure 5, across all parameters analyzed, there is considerable variability depending on batch number.

When we use the same cell line submitted to two distinct differentiation protocols (Lian's and a commercial protocol) we find significant differences in APA, dV/dt max and APD90, as shown in Figure 6.

Given the known influence of cycle length in action potential duration we compared APD90 for two cell lines

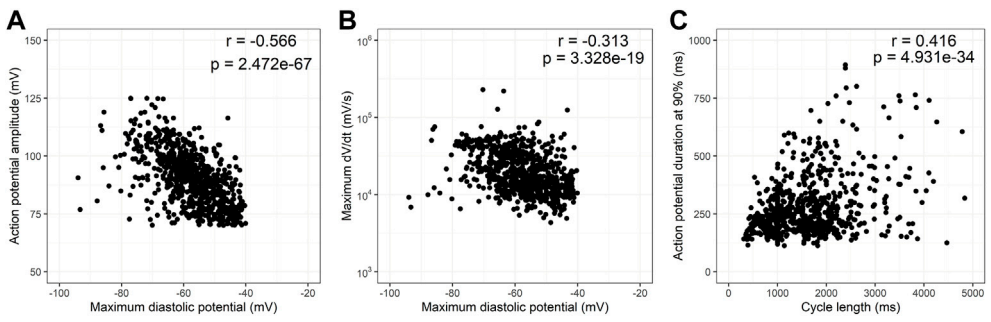

FIGURE 4
Correlation of action potential variables. Scatter plots of action potential amplitudes (APA) and maximum dV/dt (dV/dt max) as a function of maximum diastolic potential (MDP) are shown in **(A,B)**, respectively. **(C)** shows a scatter plot of action potential duration at 90% repolarization (APD90) as a function of cycle length. All correlations are statistically significant although correlation coefficients are low. Heteroscedasticity increases with cycle length especially above 2,000 ms.

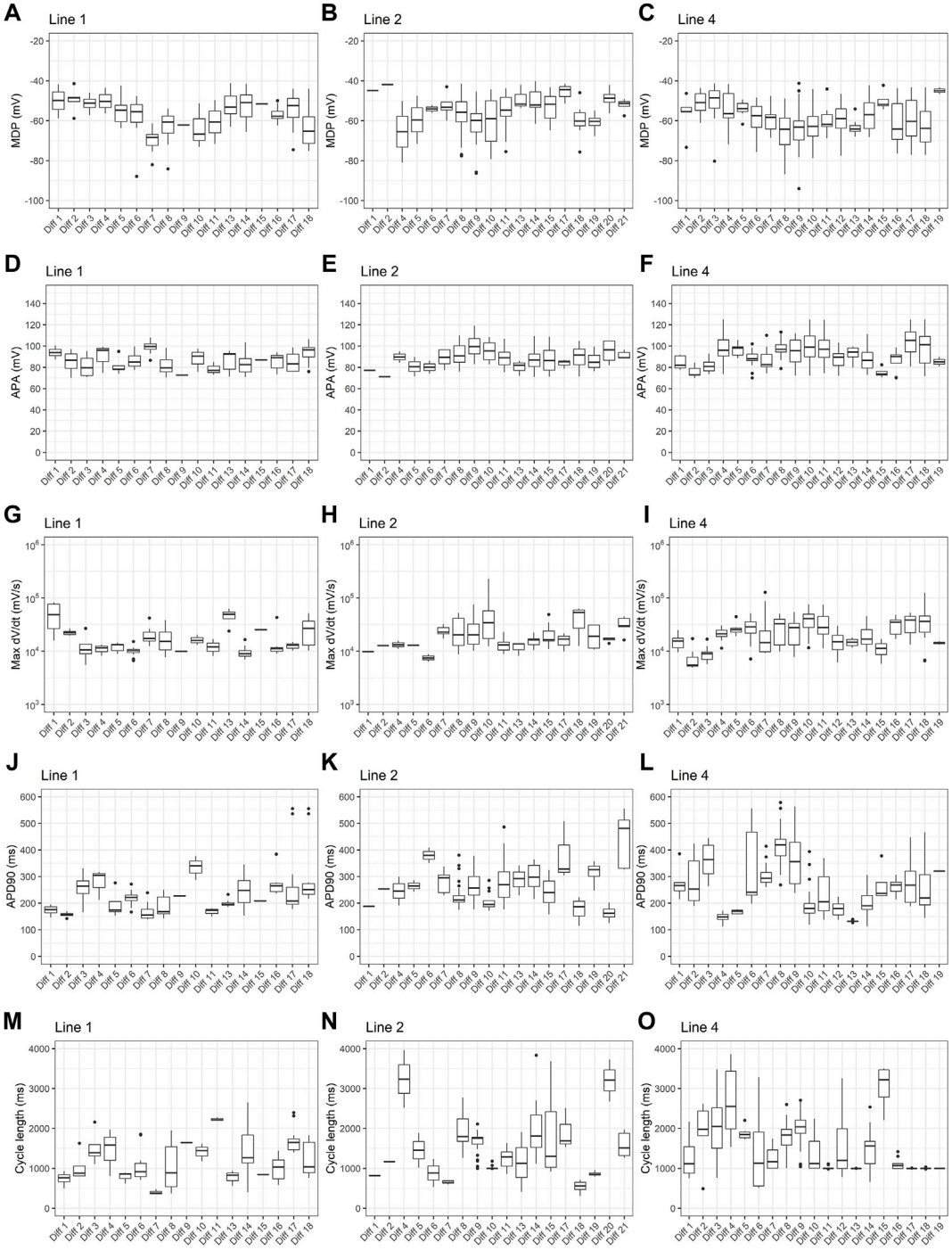

FIGURE 5
Effect of differentiation batch on action potential parameters. Box plots of **(A–C)** maximum diastolic potentials (MDP), **(D–F)** action potential amplitudes (APA), **(G–I)** maximum dV/dt (dV/dt max), **(J–L)** action potential duration at 90% repolarization (APD90) and **(M–O)** cycle length are shown for three different cell lines. For line 1, all batches used Kattman's differentiation protocol. For lines 2 and 4, Lian's protocol was used for all batches.

submitted to the same differentiation protocol under spontaneous and paced conditions. Figure 7A shows significantly greater values for APD90 under spontaneous beating when compared to pacing at 1 Hz. If we restrict spontaneous cycle length to 10% variation of the pacing, APD90 is similar between the two conditions.

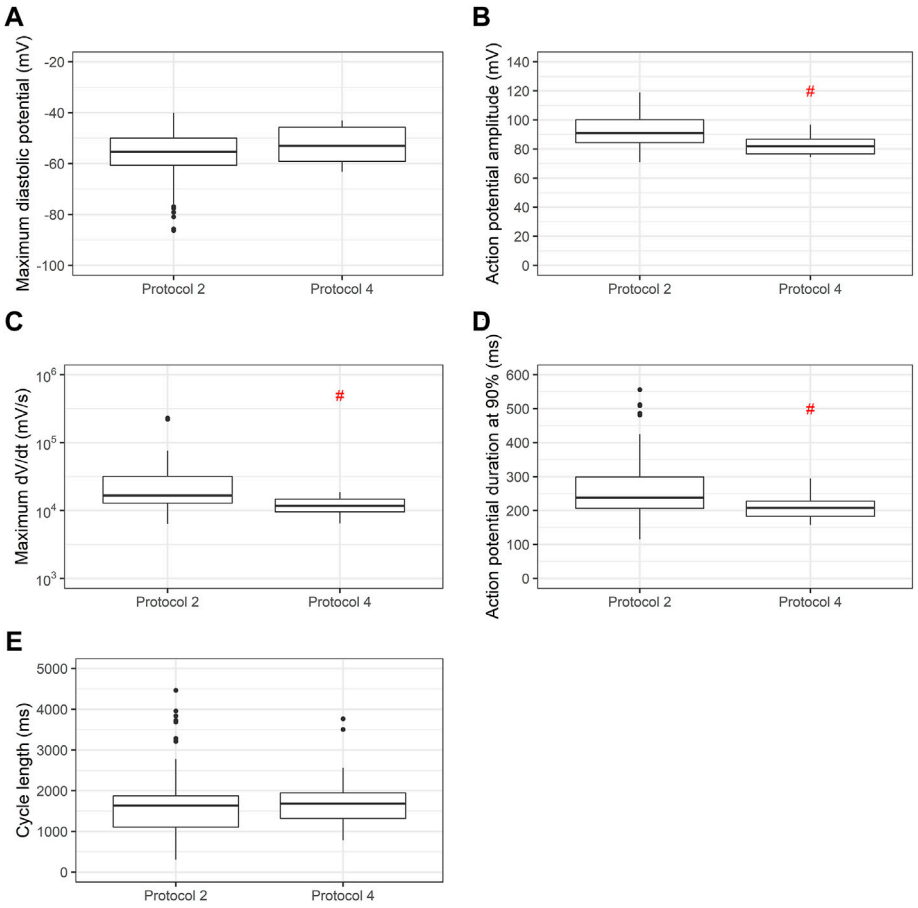

FIGURE 6
Comparison of action potential variables using two differentiation protocols in the same cell line. Box plots of **(A)** maximum diastolic potentials (MDP), **(B)** action potential amplitudes (APA), **(C)** maximum dV/dt (dV/dt max), **(D)** action potential duration at 90% repolarization (APD90) and **(E)** cycle length for cell line 2 using Lian's and a commercial protocol. Red # indicates $p < 0.05$ using Student's t-test.

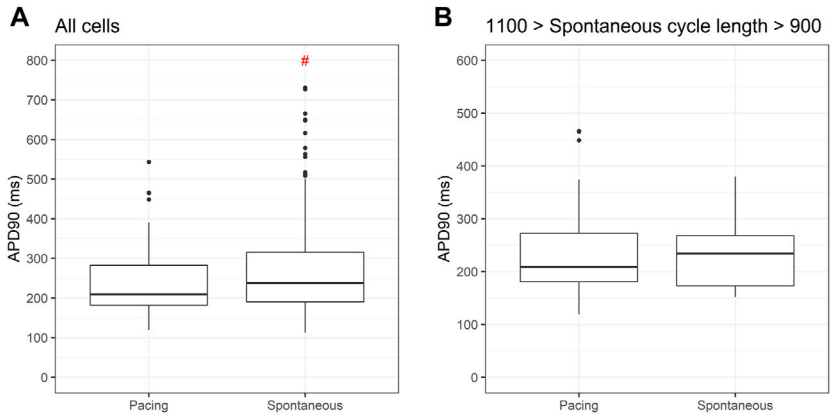

FIGURE 7
Action potential duration at 90% repolarization (APD90) under spontaneous and pacing conditions. Box plots in **(A)** shows significant differences in APD90 between PSC-derived cardiomyocytes beating spontaneously and paced at 1 Hz. In **(B)**, using only spontaneous cycle lengths varying between 0.9 and 1.1 Hz, similar values for APD90 are obtained under both conditions.

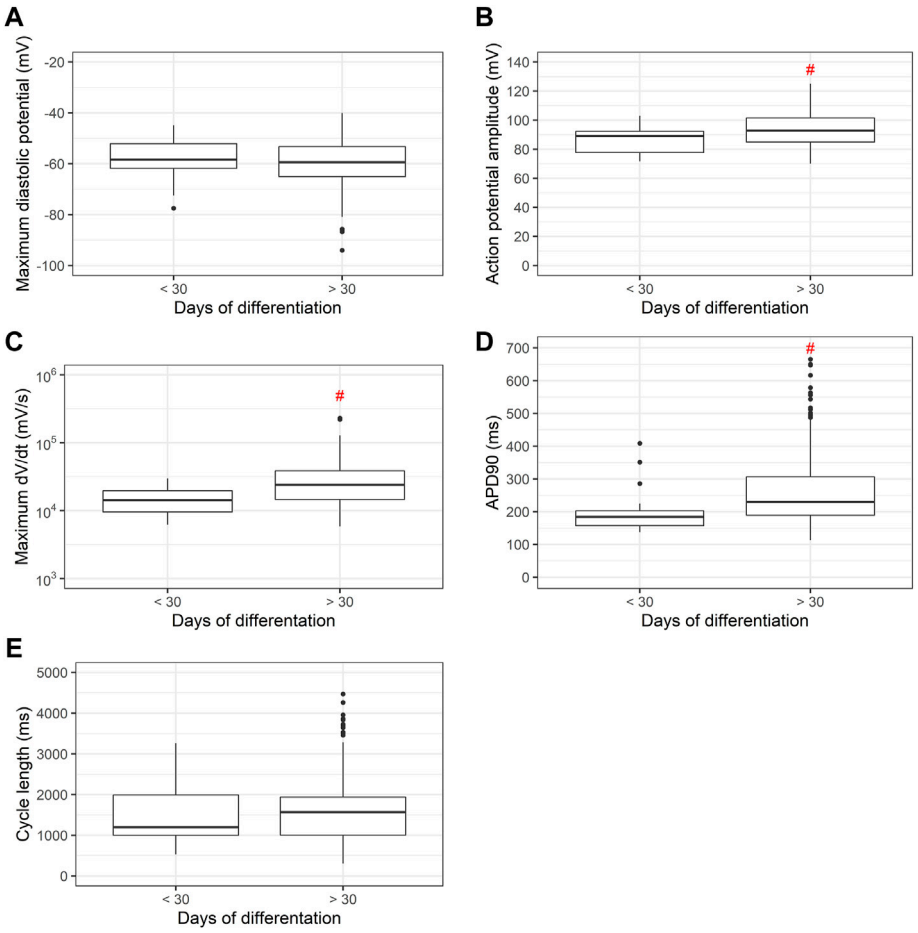

FIGURE 8
(A) Maximum diastolic potentials (MDP), **(B)** action potential amplitudes (APA), **(C)** maximum dV/dt (dV/dt max), **(D)** action potential duration at 90% repolarization (APD90) and **(E)** cycle length as a function of differentiation time. Cardiomyocytes derived from PSC differentiated for less or more than 30 days show significant increases in APA, dV/dt max and APD90 with longer differentiation times.

Since differentiation time is known to produce more mature PSC-derived cardiomyocytes, in Figure 8 we measured MDP, APA, dV/dt max, APD90 and cycle length between PSC-derived cardiomyocytes before and after 30 days of differentiation. After 30 days of differentiation, significant increases in APA, dV/dt max and APD90 are recorded.

Discussion

The use of PSC in disease modelling has become widespread due to the uncertainties of animal models as faithful models of cardiac human diseases (Saura et al., 2022; Houser et al., 2012). In particular, the use of cell types derived from PSC extracted from diseased patients (disease specific PSC) avoids the costly and risky nature of biopsies. Therefore, PSC have attained prominence for disease modeling, especially in monogenic diseases, but also in more complex diseases as the concept of disease in a dish has advanced not only in modeling but also in drug screening. Non-etheless, the use of PSC for disease modeling has limitations that have been addressed in many reviews (Saha and Jaenisch, 2009; Soldner and Jaenisch, 2012; Sharma et al., 2020; Horwitz et al., 2021).

In cardiac pathophysiology, PSC-derived cardiomyocytes have been intensively used to model inherited arrhythmic cardiac diseases since the seminal works of Moretti et al. (2010), Itzhaki et al. (2011) in which they compared the electrophysiologic properties of cardiomyocytes derived from patients with long QT syndrome (LQTS) to those of healthy controls. Since then, the field has become prolific in publications where 1 or a few disease cell lines are compared to 1 or a few controls cell lines. These comparisons have obvious limitations since the diverse genetic backgrounds may introduce confounding factors that influence the observed phenotype.

Using control cells from the families of affected patients may reduce, but not abolish these confounding factors and the field has become stricter about attributing the altered phenotype to the diseased cells. Currently, isogenic cell lines, where the variant encountered in the diseased cell is corrected by gene editing technologies in monogenic diseases should be mandatory to investigate the pathogenicity of variants. The availability of CRISPR based techniques to perform gene editing in PSC has made this possible (Doudna and Charpentier, 2014).

In this article we used control cell lines from six healthy donors and show that there is great variability in physiologic properties of the PSC-derived cardiomyocytes differentiated from these lines, as shown by others (Sanchez-Freire et al., 2014; Sala et al., 2016; Mannhardt et al., 2020). Furthermore, we show that the electrophysiologic data for these six cell lines is also dependent on the differentiation protocol used and on differentiation batch. Similar results have been described by Mannhardt et al. (2017), Mannhardt et al (2020) when measuring contractile properties in control iPS-derived cardiomyocytes and Huo et al. (2016) when evaluating iPS-derived cardiomyocytes from two commercial suppliers. We also show that cycle length influences APD90, and great dispersion is observed with periods above 2,000 ms, indicating that pacing should be preferred when comparing APD from distinct cell lines. Furthermore, electrophysiologic properties of PSC-derived cardiomyocytes are influenced by time after differentiation. Significant increases in APA, dV/dt max and APD90, when comparing differentiation protocols with less or more than 30 days, indicate that a more mature phenotype can be achieved with longer differentiation periods.

Age, sex, cell source and race are other variables that can influence the molecular and physiologic parameters of PSC-derived cardiomyocytes. D'Antonio-Chronowska et al. (D'Antonio-Chronowska et al., 2019) reported the influence of the X chromosome on the differentiation trajectories of human iPS into cardiomyocytes. Pianezzi et al. (2020) suggest that iPS derived from cardiac sources differentiate into more mature cardiomyocytes. But race has not been reported to influence calcium transient kinetics or beat rate in iPS-derived cardiomyocytes by Schaniel et al. (2021) when generating a library of iPS from diverse healthy human individuals. Age does not seem to influence the reprograming of cells to a pluripotent state (Lapasset et al., 2011), and Schaniel et al. (2021) have not reported differences in the function of cardiomyocytes derived from iPS obtained from healthy patients with ages ranging from 22 to 61 years. Our data concerning these variables is limited since we used three cell lines from male and three from female donors, with a large age span, and except for the ES, all reprogrammed from erythroblasts.

An important point to be considered is if the variability here reported is also present in bona-fide cardiomyocytes isolated from adult hearts. Here we are restricted to animal models for comparisons, due to the obvious ethical barriers related to obtaining cardiac tissue from healthy humans. Using ventricular slices of adult mouse hearts, Halbach et al. (2006) report the variability in resting membrane potential (RMP), APA and APD90 at a fixed stimulation frequency, and observe significant differences in APA and APD90 if stimulation frequency varies by 5-fold. Using guinea pigs heart slices, Bussek et al. (2009) also reported the variability in RMP, APA and APD90 in 59 recordings from left ventricular slice preparations. In Supplementary Table S9 we list the standard deviations found in six articles using rat, mouse and guinea pig cardiomyocytes for RMP/MDP, APA, dV/dt max and APD90, although with a limited number of recordings. As shown in the Table, standard deviations are similar between PSC-derived and animal cardiomyocytes for RMP/MDP, APA and dV/dt max. However, standard deviation is considerably higher in APD90 of PSC-derived when compared to animal cardiomyocytes. Since APD90 is a critical parameter for the modeling of arrhythmic events *in vitro*, this variability should be considered when inputting evidence of pathogenicity using this type of functional assay.

We conclude that even when using isogenic cell lines to ascertain pathogenicity to variants associated to arrythmias one should use cardiomyocytes derived from PSC using the same differentiation protocol and batch and pace the cells or use only cells that have very similar spontaneous beat rates. Otherwise, one may find phenotypic variability that is not attributable to pathogenic variants. Al-Owais et al., 2021, Howlett et al., 2022, Saito et al., 2005, Tan et al., 2014.

Data availability statement

The original contributions presented in the study are included in the article/Supplementary Material, further inquiries can be directed to the corresponding author.

Ethics statement

The studies involving human participants were reviewed and approved by the Comissão de Ética em Pesquisa do Instituto Nacional de Cardiologia (IRB of the National Cardiology Institute—Rio de Janeiro, Brazil). The patients/participants provided their written informed consent to participate in this study.

Author contributions

ABC and ACCC devised the project, analyzed data, and wrote the manuscript. KCSC, ICL, RSP, DSS, BF, and GMC

collected electrophysiologic data. RAQB, DBPC, DSA, FCPM, and THKB generated iPS and differentiated into cardiomyocytes. EHM and THKB devised the project and revised the manuscript.

Conflict of interest

The authors declare that the research was conducted in the absence of any commercial or financial relationships that could be construed as a potential conflict of interest.

Publisher's note

All claims expressed in this article are solely those of the authors and do not necessarily represent those of their affiliated organizations, or those of the publisher, the editors and the reviewers. Any product that may be evaluated in this article, or claim that may be made by its manufacturer, is not guaranteed or endorsed by the publisher.

Supplementary material

The Supplementary Material for this article can be found online at: https://www.frontiersin.org/articles/10.3389/fphys.2022.1077069/full#supplementary-material

SUPPLEMENTARY FIGURE S1
Correlation of action potential variables. The upper row shows scatter plots of action potential amplitudes (APA) as a function of maximum diastolic potentials (MDP) for different cell types **(A)**, differentiation protocols **(B)** and cell lines **(C)**. The center row shows scatter plots of maximum dV/dt (dV/dt max) as a function of MDP for different cell types **(D)**, differentiation protocols **(E)** and cell lines **(F)**. The bottom row shows a scatter plot of action potential duration at 90% repolarization (APD90) as a function of cycle length for different cell types **(G)**, differentiation protocols **(H)** and cell lines **(I)**.

References

Al-Owais, M. M., Steele, D. S., Holden, A. V., and Benson, A. P. (2021). Deterministic and stochastic cellular mechanisms contributing to carbon monoxide induced ventricular arrhythmias. *Front. Pharmacol.* 12, 651050. doi:10.3389/fphar.2021.651050

Burridge, P. W., Matsa, E., Shukla, P., Lin, Z. C., Churko, J. M., Ebert, A. D., et al. (2014). Chemically defined generation of human cardiomyocytes. *Nat. Methods* 11, 855–860. doi:10.1038/nmeth.2999

Burridge, P. W., Thompson, S., Millrod, M. A., Weinberg, S., Yuan, X., Peters, A., et al. (2011). A universal system for highly efficient cardiac differentiation of human induced pluripotent stem cells that eliminates interline variability. *Plos One* 6, e18293. doi:10.1371/journal.pone.0018293

Bussek, A., Wettwer, E., Christ, T., Lohmann, H., Camelliti, P., and Ravens, U. (2009). Tissue slices from adult mammalian hearts as a model for pharmacological drug testing. *Cell Physiol. Biochem.* 24, 527–536. doi:10.1159/000257528

Cruvinel, E., Ogusuku, I., Cerioni, R., Rodrigues, S., Gonçalves, J., Góes, M. E., et al. (2020). Long-term single-cell passaging of human iPSC fully supports pluripotency and high-efficient trilineage differentiation capacity. *SAGE Open Med.* 8, 2050312120966456. doi:10.1177/2050312120966456

D'Antonio-Chronowska, A., Donovan, M. K. R., Greenwald, W. W. Y., Nguyen, J. P., Fujita, K., Hashem, S., et al. (2019). Association of human iPSC gene signatures and X chromosome dosage with two distinct cardiac differentiation trajectories. *Stem Cell Rep.* 13, 924–938. doi:10.1016/j.stemcr.2019.09.011

Doudna, J. A., and Charpentier, E. (2014). Genome editing. The new frontier of genome engineering with CRISPR-Cas9. *Science* 346, 1258096. doi:10.1126/science.1258096

Elliott, D. A., Braam, S. R., Koutsis, K., Ng, E. S., Jenny, R., Lagerqvist, E. L., et al. (2011). NKX2-5eGFP/w hESCs for isolation of human cardiac progenitors and cardiomyocytes. *Nat. Methods* 8, 1037–1040. doi:10.1038/nmeth.1740

Feyen, D. A. M., McKeithan, W. L., Bruyneel, A. A. N., Spiering, S., Hörmann, L., Ulmer, B., et al. (2020). Metabolic maturation media improve physiological function of human iPSC-derived cardiomyocytes. *Cell Rep.* 32, 107925. doi:10.1016/j.celrep.2020.107925

Halbach, M., Pillekamp, F., Brockmeier, K., Hescheler, J., Müller-Ehmsen, J., and Reppel, M. (2006). Ventricular slices of adult mouse hearts - a new multicellular *in vitro* model for electrophysiological studies. *Cell Physiol. Biochem.* 18, 1–8. doi:10.1159/000095132

Horwitz, R., Riley, E. A. U., Millan, M. T., and Gunawardane, R. N. (2021). It's time to incorporate diversity into our basic science and disease models. *Nat. Cell Biol.* 1, 1213–1214. doi:10.1038/s41556-021-00803-w

Houser, S. R., Margulies, K. B., Murphy, A. M., Spinale, F. G., Francis, G. S., Prabhu, S. D., et al. (2012). Animal models of heart failure: A scientific statement from the American heart association. *Circ. Res.* 111, 131–150. doi:10.1161/res.0b013e3182582523

Howlett, L. A., Kirton, H. M., Al-Owais, M. M., Steele, D., and Lancaster, M. K. (2022). Action potential responses to changes in stimulation frequency and isoproterenol in rat ventricular myocytes. *Physiol. Rep.* 10 (2), e15166. doi:10.14814/phy2.15166

Huo, J., Kamalakar, A., Yang, X., Word, B., Stockbridge, N., Lyn-Cook, B., et al. (2016). Evaluation of batch variations in induced pluripotent stem cell-derived human cardiomyocytes from 2 major suppliers. *Toxicol. Sci.* 156, 25–38. doi:10.1093/toxsci/kfw235

Itzhaki, I., Maizels, L., Huber, I., Zwi-Dantsis, L., Caspi, O., Winterstern, A., et al. (2011). Modelling the long QT syndrome with induced pluripotent stem cells. *Nature* 471, 225–229. doi:10.1038/nature09747

Kasai-Brunswick, T. H., Santos, D. S., Ferreira, R. P., Araujo, D. S., Dias, G. M., Coutinho, J. L. A., et al. (2018). Generation of patient-specific induced pluripotent stem cell lines from one patient with Jervell and Lange-Nielsen syndrome, one with type 1 long QT syndrome and two healthy relatives. *Stem Cell Res.* 31, 174–180. doi:10.1016/j.scr.2018.07.016

Kattman, S. J., Witty, A. D., Gagliardi, M., Dubois, N. C., Niapour, M., Hotta, A., et al. (2011). Stage-specific optimization of activin/nodal and BMP signaling promotes cardiac differentiation of mouse and human pluripotent stem cell lines. *Cell Stem Cell* 8, 228–240. doi:10.1016/j.stem.2010.12.008

Lapasset, L., Milhavet, O., Prieur, A., Besnard, E., Babled, A., Aït-Hamou, N., et al. (2011). Rejuvenating senescent and centenarian human cells by reprogramming through the pluripotent state. *Genes & Dev.* 25, 2248–2253. doi:10.1101/gad.173922.111

Lee, J., Protze, S. I., Laksman, Z., Backx, P. H., and Keller, G. M. (2017). Human pluripotent stem cell-derived atrial and ventricular cardiomyocytes develop from distinct mesoderm populations. *Cell Stem Cell* 21, 179–194. e4. doi:10.1016/j.stem.2017.07.003

Lian, X., Hsiao, C., Wilson, G., Zhu, K., Hazeltine, L. B., Azarin, S. M., et al. (2012). Robust cardiomyocyte differentiation from human pluripotent stem cells via temporal modulation of canonical Wnt signaling. *Proc. Natl. Acad. Sci.* 109, E1848–E1857. doi:10.1073/pnas.1200250109

Mannhardt, I., Eder, A., Dumotier, B., Prondzynski, M., Krämer, E., Traebert, M., et al. (2017). Blinded contractility analysis in hiPSC-cardiomyocytes in engineered heart tissue format: Comparison with human atrial trabeculae. *Toxicol. Sci.* 158, 164–175. doi:10.1093/toxsci/kfx081

Mannhardt, I., Saleem, U., Mosqueira, D., Loos, M. F., Ulmer, B. M., Lemoine, M. D., et al. (2020). Comparison of 10 control hPSC lines for drug screening in an engineered heart tissue format. *Stem Cell Rep.* 15, 983–998. doi:10.1016/j.stemcr.2020.09.002

Mesquita, F. C. P., Arantes, P. C., Kasai-Brunswick, T. H., Araujo, D. S., Gubert, F., Monnerat, G., et al. (2019). R534C mutation in hERG causes a trafficking defect in iPSC-derived cardiomyocytes from patients with type 2 long QT syndrome. *Sci. Rep.* 9 (1), 19203. doi:10.1038/s41598-019-55837-w

Moretti, A., Bellin, M., Welling, A., Jung, C. B., Lam, J. T., Bott-Flügel, L., et al. (2010). Patient-specific induced pluripotent stem-cell models for long-QT syndrome. *New Engl. J. Med.* 363, 1397–1409. doi:10.1056/nejmoa0908679

Ohno, Y., Yuasa, S., Egashira, T., Seki, T., Hashimoto, H., Tohyama, S., et al. (2013). Distinct iPS cells show different cardiac differentiation efficiency. *Stem Cells Int.* 2013, 659739. doi:10.1155/2013/659739

Pianezzi, E., Altomare, C., Bolis, S., Balbi, C., Torre, T., Rinaldi, A., et al. (2020). Role of somatic cell sources in the maturation degree of human induced pluripotent stem cell-derived cardiomyocytes. *Biochimica Biophysica Acta Bba - Mol Cell Res* 1867, 118538. doi:10.1016/j.bbamcr.2019.118538

Saha, K., and Jaenisch, R. (2009). Technical challenges in using human induced pluripotent stem cells to model disease. *Cell Stem Cell* 5, 584–595. doi:10.1016/j.stem.2009.11.009

Saito, T., Sato, T., Miki, T., Seino, S., and Nakaya, H. (2005). Role of ATP-sensitive K+ channels in electrophysiological alterations during myocardial ischemia: A study using kir6.2-null mice. *Am. J. Physiol. Heart Circ. Physiol.* 288 (1), H352–H357. doi:10.1152/ajpheart.00695.2004

Sala, L., Bellin, M., and Mummery, C. L. (2016). Integrating cardiomyocytes from human pluripotent stem cells in safety pharmacology: Has the time come? *Brit J. Pharmacol.* 174, 3749–3765. doi:10.1111/bph.13577

Sanchez-Freire, V., Lee, A. S., Hu, S., Abilez, O. J., Liang, P., Lan, F., et al. (2014). Effect of human donor cell source on differentiation and function of cardiac induced pluripotent stem cells. *J. Am. Coll. Cardiol.* 64, 436–448. doi:10.1016/j.jacc.2014.04.056

Saura, M., Zamorano, J. L., and Zaragoza, C. (2022). Preclinical models of congestive heart failure, advantages, and limitations for application in clinical practice. *Front. Physiol.* 13, 850301. doi:10.3389/fphys.2022.850301

Schaniel, C., Dhanan, P., Hu, B., Xiong, Y., Raghunandan, T., Gonzalez, D. M., et al. (2021). A library of induced pluripotent stem cells from clinically well-characterized, diverse healthy human individuals. *Stem Cell Rep.* 16, 3036–3049. doi:10.1016/j.stemcr.2021.10.005

Sharma, A., Sances, S., Workman, M. J., and Svendsen, C. N. (2020). Multi-lineage human iPSC-derived platforms for disease modeling and drug discovery. *Cell Stem Cell* 26, 309–329. doi:10.1016/j.stem.2020.02.011

Soldner, F., and Jaenisch, R. (2012). Medicine. iPSC disease modeling. *Science* 338, 1155–1156. doi:10.1126/science.1227682

Takahashi, K., Tanabe, K., Ohnuki, M., Narita, M., Ichisaka, T., Tomoda, K., et al. (2007). Induction of pluripotent stem cells from adult human fibroblasts by defined factors. *Cell* 131, 861–872. doi:10.1016/j.cell.2007.11.019

Takahashi, K., and Yamanaka, S. (2016). A decade of transcription factor-mediated reprogramming to pluripotency. *Nat. Rev. Mol. Cell Biol.* 17, 183–193. nrm. doi:10.1038/nrm.2016.8

Tan, X.-Q., Cheng, X.-L., Zhang, L., Wu, B.-W., Liu, Q.-H., Meng, J., et al. (2014). Multi-walled carbon nanotubes impair Kv4.2/4.3 channel activities, delay membrane repolarization and induce bradyarrhythmias in the rat. *PLoS One* 9 (7), e101545. doi:10.1371/journal.pone.0101545

Thomson, J. A., Itskovitz-Eldor, J., Shapiro, S. S., Waknitz, M. A., Swiergiel, J. J., Marshall, V. S., et al. (1998). Embryonic stem cell lines derived from human blastocysts. *Science* 282, 1145–1147. doi:10.1126/science.282.5391.1145

Tohyama, S., Hattori, F., Sano, M., Hishiki, T., Nagahata, Y., Matsuura, T., et al. (2013). Distinct metabolic flow enables large-scale purification of mouse and human pluripotent stem cell-derived cardiomyocytes. *Cell Stem Cell* 12, 127–137. doi:10.1016/j.stem.2012.09.013

Weinberger, F., Mannhardt, I., and Eschenhagen, T. (2017). Engineering cardiac muscle tissue: A maturating field of research. *Circulation Res.* 120, 1487–1500. doi:10.1161/CIRCRESAHA.117.310738

Yang, X., Pabon, L., and Murry, C. E. (2014). Engineering adolescence maturation of human pluripotent stem cell–derived cardiomyocytes. *Circulation Res.* 114, 511–523. doi:10.1161/CIRCRESAHA.114.300558

Zhao, Y., Rafatian, N., Feric, N. T., Cox, B. J., Aschar-Sobbi, R., Wang, E., et al. (2019). A platform for generation of chamber-specific cardiac tissues and disease modeling. *Cell* 176, 913–927. doi:10.1016/j.cell.2018.11.042

frontiers | Frontiers in Physiology

TYPE Original Research
PUBLISHED 12 January 2023
DOI 10.3389/fphys.2022.1104327

OPEN ACCESS

EDITED BY
Yoram Etzion,
Ben-Gurion University of the Negev, Israel

REVIEWED BY
David Filgueiras-Rama,
Spanish National Centre for Cardiovascular Research, Spain
Lisa A Gottlieb,
University of Copenhagen, Denmark
Avishag Laish-Farkash,
Assuta Ashdod University Hospital, Israel

*CORRESPONDENCE
Gerard Amorós-Figueras,
gamorosf@santpau.cat

†These authors share senior authorship

SPECIALTY SECTION
This article was submitted to Cardiac Electrophysiology, a section of the journal Frontiers in Physiology

RECEIVED 21 November 2022
ACCEPTED 28 December 2022
PUBLISHED 12 January 2023

CITATION
Amorós-Figueras G, Casabella-Ramon S, Company-Se G, Arzamendi D, Jorge E, Garcia-Osuna A, Macías Y, Sánchez-Quintana D, Rosell-Ferrer J, Guerra JM and Cinca J (2023), Electrophysiological and histological characterization of atrial scarring in a model of isolated atrial myocardial infarction.
Front. Physiol. 13:1104327.
doi: 10.3389/fphys.2022.1104327

Electrophysiological and histological characterization of atrial scarring in a model of isolated atrial myocardial infarction

Gerard Amorós-Figueras[1]*, Sergi Casabella-Ramon[1], Georgina Company-Se[2], Dabit Arzamendi[1], Esther Jorge[1], Alvaro Garcia-Osuna[3], Yolanda Macías[4], Damián Sánchez-Quintana[4], Javier Rosell-Ferrer[2], José M. Guerra[1†] and Juan Cinca[1†]

[1]Department of Cardiology, Hospital de la Santa Creu i Sant Pau, IIB-Sant Pau, UAB, CIBERCV, Barcelona, Spain, [2]Electronic and Biomedical Instrumentation Group, Department of Electronics Engineering, Universitat Politècnica de Catalunya, Barcelona, Spain, [3]Biochemistry Department, Hospital de la Santa Creu i Sant Pau, IIB-Sant Pau, Barcelona, Spain, [4]Department of Anatomy and Cell Biology, Faculty of Medicine, University of Extremadura, Badajoz, Spain

Background: Characterization of atrial myocardial infarction is hampered by the frequent concurrence of ventricular infarction. Theoretically, atrial infarct scarring could be recognized by multifrequency tissue impedance, like in ventricular infarction, but this remains to be proven.

Objective: This study aimed at developing a model of atrial infarction to assess the potential of multifrequency impedance to recognize areas of atrial infarct scar. Methods: Seven anesthetized pigs were submitted to transcatheter occlusion of atrial coronary branches arising from the left coronary circumflex artery. Six weeks later the animals were anesthetized and underwent atrial voltage mapping and multifrequency impedance recordings. The hearts were thereafter extracted for anatomopathological study. Two additional pigs not submitted to atrial branch occlusion were used as controls.

Results: Selective occlusion of the atrial branches induced areas of healed infarction in the left atrium in 6 of the 7 cases. Endocardial mapping of the left atrium showed reduced multi-frequency impedance (Phase angle at 307 kHz: from −17.1° ± 5.0° to −8.9° ± 2.6°, $p < .01$) and low-voltage of bipolar electrograms (.2 ± 0.1 mV vs. 1.9 ± 1.5 mV vs., $p < .01$) in areas affected by the infarction. Data variability of the impedance phase angle was lower than that of bipolar voltage (coefficient of variability of phase angle at307 kHz vs. bipolar voltage: .30 vs. .77). Histological analysis excluded the presence of ventricular infarction.

Conclusion: Selective occlusion of atrial coronary branches permits to set up a model of selective atrial infarction. Atrial multifrequency impedance mapping allowed recognition of atrial infarct scarring with lesser data variability than local bipolar voltage mapping. Our model may have potential applicability on the study of atrial arrhythmia mechanisms.

KEYWORDS

atrial branch occlusion, atrial myocardial infarction, ECG, endocardial electrical mapping, multifrequency myocardial impedance, anatomopathology

1 Introduction

Improving electrophysiological identification of areas of atrial fibrosis would be of relevance in the ablation treatment of patients suffering from atrial arrhythmias. Nowadays the electroanatomic cardiac navigators use the information of the local voltage as surrogate marker of fibrosis. However, the voltage cut-off values vary from patient to patient and are dependent on the cardiac rhythm at the time of the procedure. (Lahuerta et al., 2022). Electrophysiological characterization of atrial infarct scarring is hampered by the paucity of animal models mimicking this clinical entity. To date, the basic knowledge on the intrinsic electrophysiological alterations induced by isolated atrial myocardial infarction (MI) are based on short series of experimental studies. (Sinno et al., 2003; Rivard et al., 2007; Nishida et al., 2011; Alasady et al., 2013; Avula et al., 2018; Amorós-Figueras et al., 2020) These studies showed slowing of local atrial conduction, prolongation of the refractory period, (Sinno et al., 2003), and changes in ST segment and voltage of local atrial electrograms. (Amorós-Figueras et al., 2020) More recently new surrogates for the detection of atrial fibrosis have been proposed and these include strain imaging during left atrial reservoir phase, (Laish-Farkash et al., 2021), or atrial magnetic resonance imaging using late gadolinium enhancement LGE-MRI. (Hopman et al., 2022) Endocardial measurement of myocardial electrical impedance allowed recognition of chronic infarction of the ventricle, (Amoros-Figueras et al., 2018), but its ability to detect the infarct scarring in the atria has not been reported.

This study aimed at developing a closed-chest animal model of selective occlusion of atrial coronary branches to detect atrial infarct scarring by endocardial mapping of multifrequency tissue electrical impedance.

2 Materials and methods

2.1 Study population

This study involved 9 domestic swine (Landrace-Large White cross). Seven pigs underwent atrial coronary branch occlusion whereas the remaining two were used as controls for endocardial voltage mapping and multifrequency impedance data. The study protocol was approved by the Animal Care and Use Committee of our institution, and fully conformed to the Guide for the Care and Use of Laboratory Animals, eighth ed. (National Research Council. Washington, DC: The National Academies Press, 2010).

2.2 Experimental procedures

2.2.1 Induction of chronic atrial myocardial infarction

Seven pigs weighing 49 ± 5 kg were premedicated with midazolam (.6 mg/kg) and ketamine (12 mg/kg) intramuscularly. General anesthesia was induced with intravenous propofol (2–4 mg/kg) and was maintained with a mixture of oxygen and sevoflurane inhalation (2.5%–3.5%). The animals were mechanically ventilated through endotracheal intubation and analgesia was maintained during the entire procedure with intravenous fentanyl (0.1 μg/kg/min). A femoral artery was catheterized with a 7F cannula and a 6F hockey stick guiding catheter (Cordis, United States) was introduced. Under fluoroscopic guidance (Philips Endura), the catheter was advanced to the proximal segment of the LCX and a covered stent (PK Papyrus, Biotronik, Germany) was deployed with a catheter balloon (Figure 1A). We selected this stent because it would allow interruption of blood flow in the exiting atrial coronary branches but preserving at the same time the main stream flow into the LCX, avoiding a concomitant ventricular infarction. We verified the existence of atrial coronary branches arising from the LCX in pigs in a previous series of open-chest experiments. (Amorós-Figueras et al., 2020) The small diameter of these atrial vessels was often below the resolution of our fluoroscopic system and images could not be consistently obtained. A 15-lead ECG was continuously recorded during the procedure to verify the absence of ST-changes secondary to acute ventricular myocardial ischemia. Animals were allowed to recover and were treated with antibiotics and analgesics. After a median period of 6 weeks, the 7 pigs underwent sedation and general anesthesia like in the previous intervention. We performed an atrial endocardial mapping of local electrograms and local tissue electrical impedance. Thereafter, the animals were euthanized, and the hearts processed for anatomopathological study (Figure 1B).

2.2.2 Mapping of left atrial electrograms and tissue electrical impedance

These procedures were performed in the 7 pigs with 6-week old atrial coronary branch occlusion and in the 2 control pigs not submitted to coronary intervention. A femoral vein was catheterized and a mapping electrocatheter (Smarttouch®, Biosense-Webster, United States) was advanced into the left atrium through a transeptal access. The electrocatheter was connected to a CARTO three system (Biosense-Webster, United States) to generate 3D high density endocardial mapping of left atrial unipolar and bipolar local electrograms (Electroanatomic map settings: Tissue Proximity Index was activated, Local Activation Time stability was set to 3 ms, Position Stability was set to 2 mm, the map density for voltage maps was 1,646 ± 1,277 points and for impedance maps was 28 ± 9 points, Force Setting was set to Force above minimum threshold, Color Fill Threshold was set to 30). The voltage amplitude (mV) was automatically measured in all endocardial signals and thereafter, voltage and activation maps were constructed. Based on the clinically accepted definition of areas of low voltage in endocardial mapping procedures, (Kottkamp et al., 2017), we considered areas of low atrial voltage those with local bipolar voltage <.5 mV.

Myocardial electrical impedance of the left atrium was measured at selected anatomical regions (atrial appendage, septum, anterior and posterior wall) at frequencies ranging from 1 to 1,000 kHz using the same endocardial mapping electrocatheter. This catheter was connected to an impedance recording system made by our group. (Sanchez et al., 2013) Alternating currents (1 ms duration, 1 mA total peak amplitude) of twenty-six frequencies ranging from 1 to 1,000 kHz were injected between the distal electrocatheter pole and a skin reference electrode (Dispersive pad, 3M) placed on the anterior thoracic region. The resultant changes in current voltage were measured between the distal electrocatheter pole and a second thoracic skin reference electrode (ECG pad, 3M). The local impedance was measured at a sampling rate of 60 Hz during the entire duration of the cardiac cycle and stored at 2 s frames. The impedance magnitude (Z) and the phase angle (PA) were measured at all current frequencies. The Z quantifies the drop of voltage amplitude for a given applied

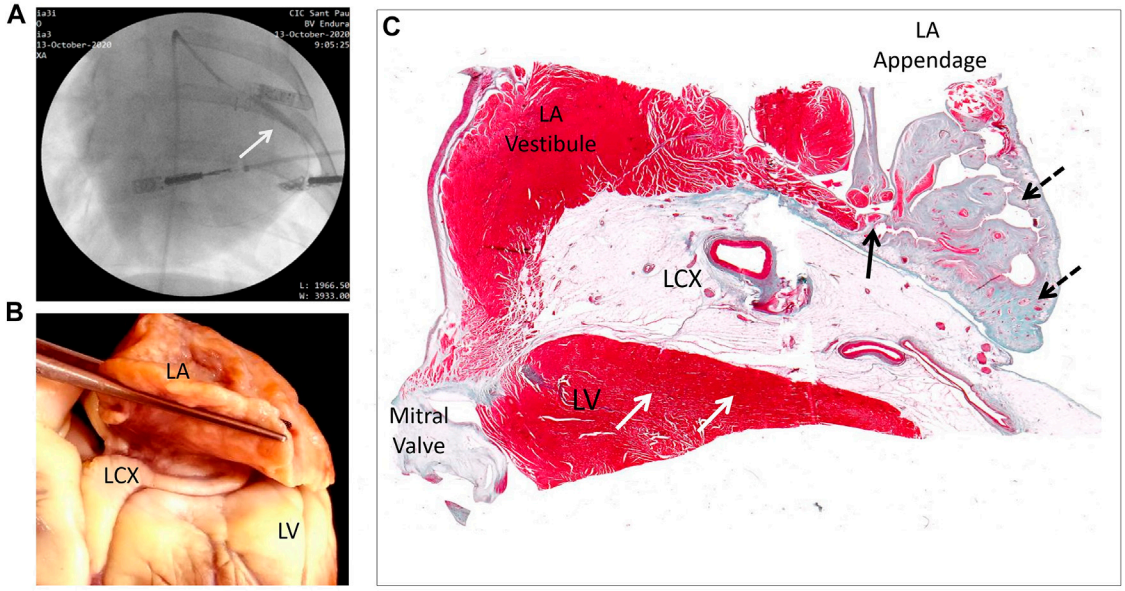

FIGURE 1
Illustration of the experimental procedure and study specimen preparations. **(A)** Fluoroscopic image of one studied pig showing the catheter balloon located in the proximal segment of the LCX while deploying the covered stent (white arrow). **(B)** Photograph showing the anatomical relationship between the left ventricle (LV), left atrium (LA) and the left circumflex coronary artery (LCX) where the covered stent was deployed. **(C)** Microphotograph of a histological preparation (frontal section) showing both areas of infarct infarcted (dashed arrows) and non-infarcted areas (solid arrows) in the left atrial appendage with preserved left ventricular myocardium (white arrows) corresponding to the annular area.

current and the PA reflects the time delay between the voltage and current waves which is influenced by structural characteristics of the myocardial tissue. In an attempt to discriminate between healthy and infarcted atrial regions we selected a phase angle cutoff of −12° at 307 kHz based on a previous study in a pig model of chronic left ventricular infarction. (Amorós-figueras et al., 2017)

To support the assumption that atrial fibrosis accounted for the areas of low-voltage and depressed electrical impedance, we analyzed the left atrial voltage mapping and multifrequency impedance data recorded in two control pigs not submitted to atrial branch occlusion. All voltage and impedance recordings were performed with a stable contact tip-catheter force between 10 and 20 g.

2.2.3 Anatomopathology

The explanted hearts of the 7 pigs with atrial coronary branch occlusion were cleaned from blood and fixed in buffered formalin. The atria were separated at the vestibule level of the ventricles and embedded in a paraffin block. Sections (12 μm) of the entire left atrium were mounted and serially sectioned frontally in 12 μm slices, and then stained with Masson's trichrome (Figure 1C). Morphometric study was performed to evaluate the average extent of atrial fibrosis. In brief, digital images were taken of the sections stained with Masson's and the areas of fibrosis were delimitated in the sections of maximum extent of infarcted area using ImageJ software. (Schneider et al., 2012) The areas of fibrosis were expressed as a percentage of the entire limits of the sectioned atria. The identification of the areas of fibrosis was done by two expert anatomopathologists under direct visualization of the histologic preparation at proper magnification. We also calculated the mapping-derived voltage and impedance scar-areas (excluding pulmonary veins) using the software of the electroanatomic mapping system.

2.3 Statistical analysis

Quantitative data were expressed as the mean ± standard deviation (SD). The degree of variation of the bipolar voltage and impedance magnitude values was assessed by the coefficient of variation (ratio of the standard deviation and its corresponding mean value). The ordinary two-way ANOVA test with Dunnet's multiple comparison correction was used to assess the statistical significance of changes in bipolar voltages, impedance magnitude and phase angle at different current frequencies, and ST-segment displacement. A p-value <.05 was considered significant. All analyses were performed using SPSS v.22.0 software (IBM-SPSS, United States).

3 Results

Nine pigs were included in the study. Occlusion of the LCX atrial branches was performed in 7 cases. Among the latter, 6 completed the entire protocol and one pig was lost during anesthesia induction in the 6-week second intervention, though its heart was included in the anatomopathological study. Two pigs non-submitted to atrial branch occlusion were used for the endocardial mapping studies.

3.1 Anatomopathological findings

We observed areas of necrosis with collagen deposition in the left atrium in 6 out of the 7 pigs (86%) submitted to atrial branch occlusion. Histological analysis ruled out the presence of areas of

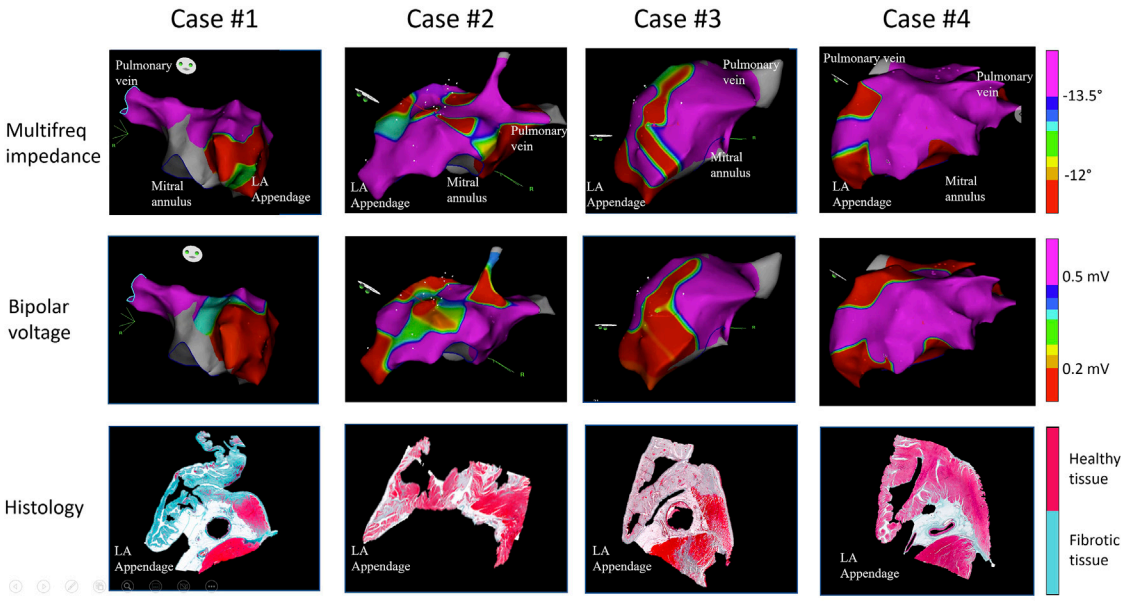

FIGURE 2
Electroanatomical voltage and multifrequency impedance maps of the left atrium and histological preparations of the explanted hearts of four representative pigs submitted to acute transcatheter occlusion of the atrial coronary artery branches arising from the proximal segment of the left circumflex coronary artery, with preserved left ventricular myocardium. The figure shows a correspondence between endocardial areas of low voltage and impedance and location of infarct zones.

ventricular myocardial infarction (Figure 1). In addition, at the time of stent implantation, close monitoring of the 15 lead ECG in all the animals did not show ST segment changes secondary to acute ventricular myocardial ischemia (lead II: .00 ± .02 mV at baseline vs. .00 ± .03 mV after 30 min vs. −.02 ± .02 mV after 6 weeks, both p = ns). Figure 1C is a microphotograph of a pig showing areas of fibrosis affecting the left atrial appendage while preserving left ventricular myocardium. The morphometric analysis of the sections showing the greatest infarct extent in the 6 pigs revealed a mean area of fibrosis of about 38% (range 17%–66%) of the entire microscopic field.

3.2 Voltage and impedance derived scar areas of the left atrium

Figure 2 illustrates representative electroanatomical maps of four pigs submitted to atrial coronary branch occlusion. These show areas of low-multifrequency impedance and low-voltage bipolar electrograms in correspondence with atrial anatomical regions affected by the infarction, as observed in the histology sections. The impedance derived scar areas were significantly smaller than the voltage derived scar areas (impedance vs. voltage derived scar area: 31 ± 12 cm^2 vs. 50 ± 26 cm^2; $p < .05$). Further electroanatomical mapping analysis of the peri-infarct areas by lowering the voltage scar definition revealed that voltage derived scar areas with a voltage <.1 mV improved the overlap with impedance derived scar areas with a phase angle at 307 kHz lower than −12°. The remaining non-infarcted atrial zones depicted greater voltage and impedance values, but these were lower than those observed in two control pigs not submitted to atrial branch occlusion (Table 1).

3.3 Myocardial electrical impedance of the left atrium

Figure 3 shows the bipolar and multifrequency impedance signals in comparable anatomical regions of the left atrium in a pig with occluded atrial coronary branches and in a control pig with non-occluded atrial coronary branches. As shown in Figure 4, the atrial zones affected by the infarction (IZ) showed lower values of the impedance magnitude than non-affected regions (NZ) at all current frequencies. Likewise, the IZ zones showed less negative values of the phase angle at all current frequencies (Table 2). The current frequency range that better discriminated affected and non-affected infarct regions was 1–253 kHz for the impedance magnitude and 200–1,000 kHz for the impedance phase angle. The coefficient of variation of the impedance magnitude was lower than the coefficient of variation of the bipolar voltage in both affected and non-affected infarction regions (coefficient of variation for impedance magnitude at 1,000 kHz vs. bipolar voltage: .30 vs. .77). This can be also observed in Figure 5, where the variability of median values in phase angle of atrial tissue electrical impedance at 307 kHz was lower than the variability of the median values of bipolar voltage.

4 Discussion

4.1 Main findings

This study shows that myocardial infarction restricted to the atrial chambers can be successfully induced by selective transcatheter occlusion of atrial coronary branches in swine. In this closed-chest model, healed atrial MI was associated with decreased magnitude and phase angle of myocardial impedance at all studied frequencies. Impedance data variability was lower than bipolar voltage values.

TABLE 1 Voltage of local left atrial bipolar electrograms in pigs with and without atrial coronary artery branch occlusion.

	Atrial areas with a bipolar voltage cutoff <.5 mV	Atrial areas with a bipolar voltage cutoff ≥.5 mV
Pigs with occluded atrial branches	.2 ± .1 mV (N = 66)	1.9 ± 1.5 mV () (N = 75)
Pigs with non-occluded atrial branches	Not found	3.2 ± 2.2 mV (N = 16)

**, ANOVA $p < .01$ between areas with a bipolar voltage cutoff lower or higher than .5 mV.

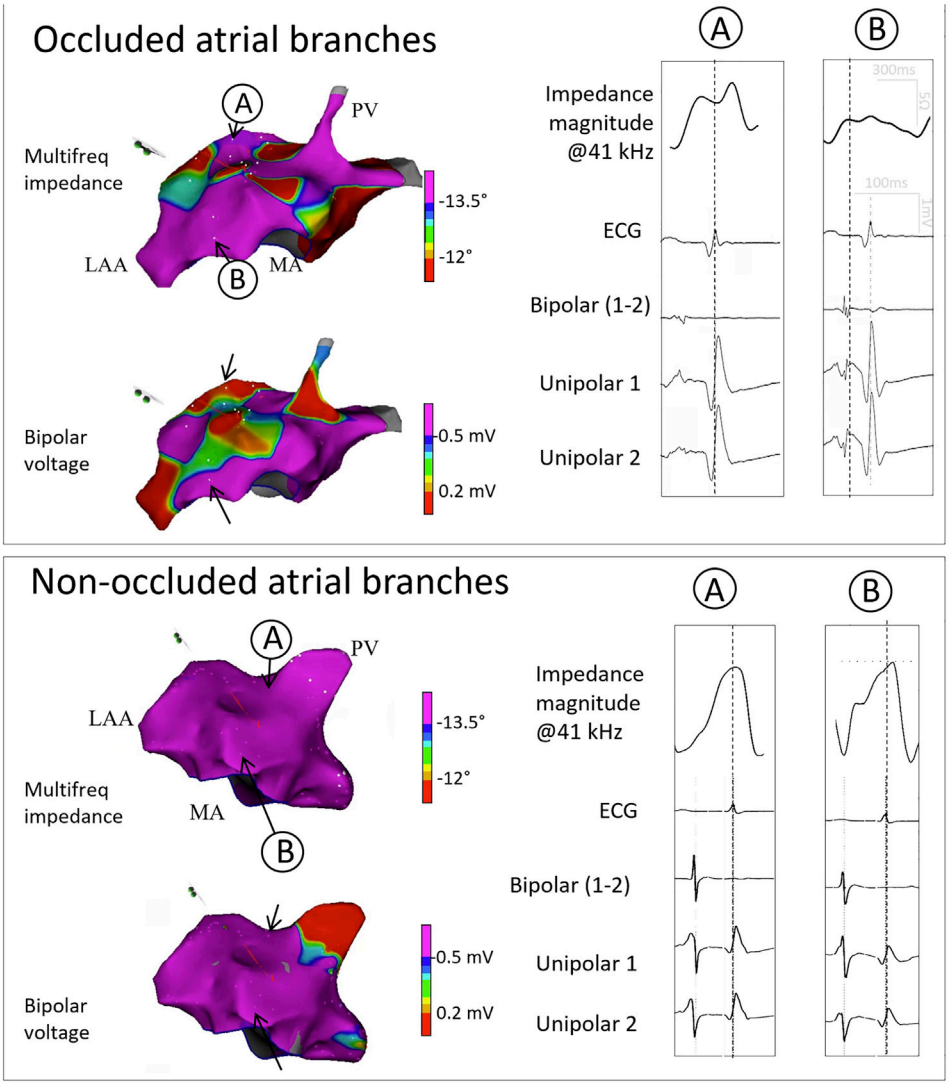

FIGURE 3
Electroanatomical voltage and multifequency maps and corresponding signals in two representative pigs. The upper panel shows the electroanatomical maps and the corresponding multifrequency impedance, ECG, local bipolar and unipolar signals in two selected sites **(A,B)** in a pig with acute transcatheter occlusion of the atrial coronary artery branches arising from the proximal segment of the left circumflex coronary artery. The lower panel shows the electroanatomical maps and the corresponding signals in two selected sites **(A,B)** in a control pig non-submitted to atrial coronary branch occlusion. LAA: Left atrial appendage; MA: Mitral annulus; PV: Pulmonary vein.

4.2 Local electrophysiological findings

Left atrial electroanatomical mapping evidenced areas of low voltage of the local electrograms and decreased multifrequency tissue impedance. Post infarct fibrosis is the most likely substrate for these electrophysiologic alterations since left atrial mapping in 2 control pigs not submitted to atrial branch occlusion evidenced normal voltage of electrograms and impedance in similar anatomical atrial regions. Moreover, the infarcted areas observed in the histological preparations shared a correspondence with the anatomical atrial regions showing low voltage electrograms and reduced impedance. A delayed and heterogeneous local activation inside the ischemic atrial myocardium has been reported in dogs after acute or 8-days old occlusion of atrial coronary branches arising from

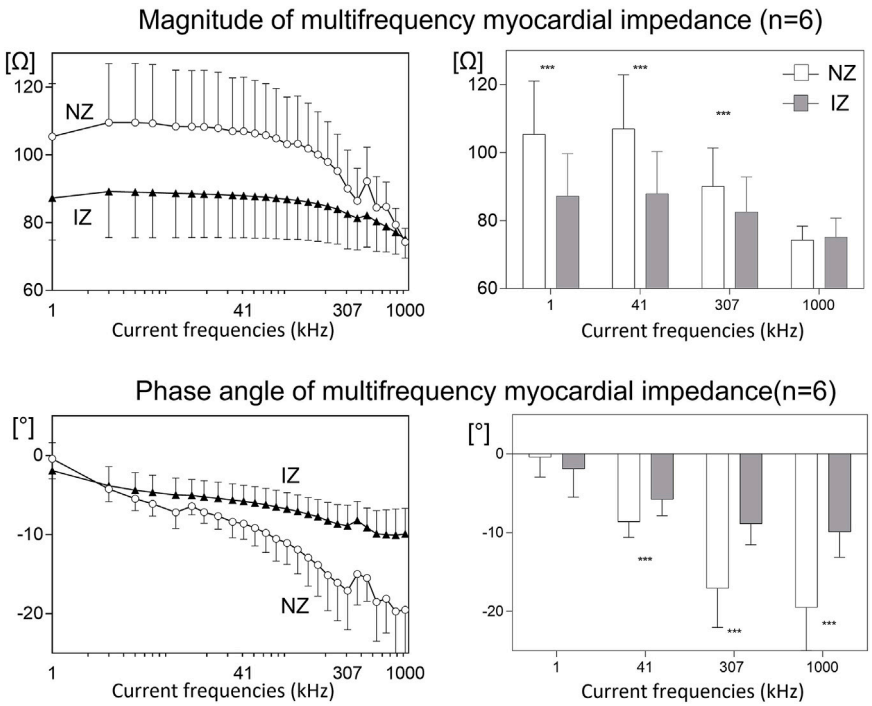

FIGURE 4
Mean values of the impedance magnitude and phase angle at multifrequency in 6 pigs submitted to acute transcatheter occlusion of the atrial coronary artery branches arising from the proximal segment of the left circumflex coronary artery. The left panels show the mean changes in atrial myocardial impedance magnitude (upper) and phase angle (lower at 26 studied current frequencies. The right panels show the mean changes in atrial myocardial impedance magnitude (upper) and phase angle (lower) at four selected current frequencies. NZ: normal zone; IZ: infarcted zone; ***: ANOVA $p <$ .001 between myocardial impedance NZ and IZ areas.

TABLE 2 Magnitude of the atrial myocardial impedance at 1 kHz in pigs with and without atrial coronary artery branch occlusion.

	Atrial areas with a phase angle cutoff < −12°	Atrial areas with a phase angle cutoff ≥ −12°
Pigs with occluded atrial branches	87.3 ± 12.4 Ω (N = 53)	105.4 ± 15.6 Ω (***) (N = 88)
Pigs with non-occluded atrial branches	Not found	119.7 ± 5.5 Ω (N = 16)

**, ANOVA $p <$ .001 between areas with a phase angle cutoff lower or higher than −12°.

the RCA, (Sinno et al., 2003; Nishida et al., 2011), in sheep after acute occlusion of the LCX, (Alasady et al., 2013), and in pigs with submitted to surgical clamping of atrial branches arising from the LCX. (Amorós-Figueras et al., 2020)

The present study addressed the healing phase of atrial infarct and revealed, for the first time, that the low voltage areas also presented low tissue electrical impedance at all current frequencies. Comparable low-voltage and low-impedance findings were found in pigs with 1-month old ventricular myocardial infarction induced by occlusion of the LAD coronary artery (Amoros-Figueras et al., 2018) thus revealing that both, healed atrial and ventricular myocardial infarction share a similar electrophysiologic substrate. We also found that impedance phase angle values presented less variability than bipolar voltage values, for both healthy and infarct scar regions. This finding, as well as the observation that impedance derived scar areas were significantly smaller than classic voltage derived scar areas (<.5 mV), suggest a more accurate assessment of atrial infarct scar by bioimpedance measurement which, in contrast to voltage mapping, are not dependent on the direction the atrial activation front. (Amorós-figueras et al., 2017) The arrhythmogenic potential of this substrate has been consistently documented in clinical and experimental ventricular myocardial infarction. (Guandalini et al., 2019) However, spontaneous atrial ectopic arrhythmias rarely occurred in experimental atrial infarction, though susceptibility to electrical induction and of atrial fibrillation (AF) has been reported. (Sinno et al., 2003) In our study, vulnerability to electrically induced atrial arrhythmias was not tested.

4.3 Anatomopathology

The characteristic structural features of healed atrial infarction in our model were the irregular distribution of the necrotic areas and the sharp delineation of the infarcted border zone. The left atrial appendage was more frequently affected, and the ventricular myocardium was preserved, indicating that deployment of a covered Papyrus stent in the proximal segment of the LCX was a successful method to create a model of isolated atrial myocardial ischemia.

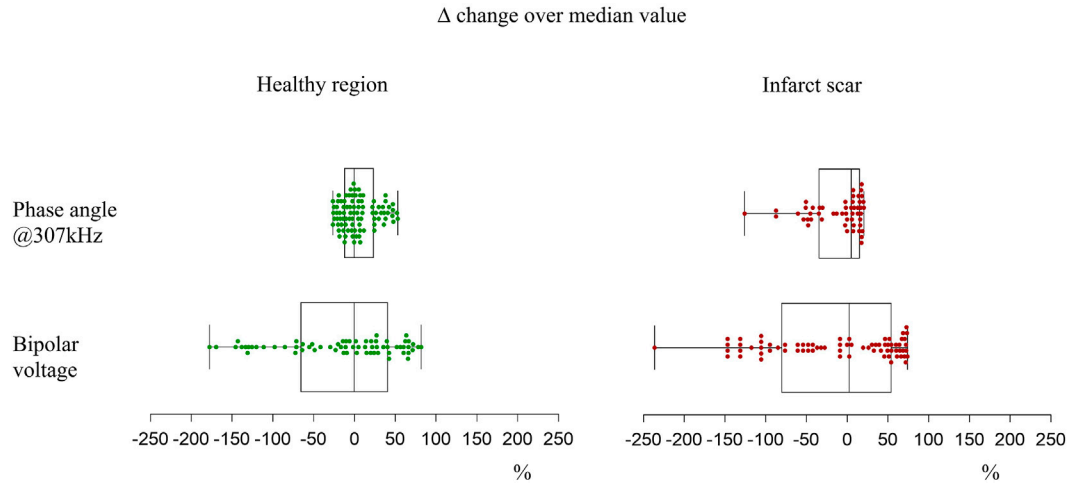

FIGURE 5
Variability of median values of phase angle of atrial tissue electrical impedance at 307 kHz and bipolar voltage of local atrial electrograms. Data are represented in box and whisker plots. Boxes represent 25th to 75th quartiles; horizontal lines within boxes represent the median; whiskers represent the minimum and maximum values.

4.4 Study limitations

The mean values of the bipolar electrograms and myocardial impedance in atrial areas not affected by the infarction in pigs with occluded coronary branches were lower than those recorded in the healthy atria in pigs with non-occluded coronary atrial branches. This could reflect an electrotonic effect of the infarcted tissue over the neighboring normal zones, or the existence of a non-transmural distribution of the infarct fibrosis over the endocardial non-affected zones.

Due to the individual anatomical variability in the distribution of atrial coronary branches and to their rich inter-anastomotic network, the atrial infarct resulting from the deployment of the covered stent in the proximal segment of the LCX coronary artery was of variable size and location. However, the infarcted areas could be recognized on-line by local mapping of electrograms and local tissue impedance measurements. Spontaneous atrial arrhythmias are seldom in models of atrial infarction, though arrhythmia vulnerability to electrical stimulation can be successfully tested in these models. (Sinno et al., 2003; Nishida et al., 2011; Alasady et al., 2013). Moreover, an infarct healing period longer than that followed in our study (6 weeks) might be a more realistic substrate for spontaneous arrhythmia.

A close point-by-point merging analysis between the infarcted areas in the histological preparations and the regions of low-voltage in the endocardial mapping is challenged by the unpredictable magnitude of the changes in size and volume of the atria secondary to heart explantation and formaldehyde inclusion. A strict site-to-site correspondence of low-voltage electrograms and infarcted areas was not therefore performed in our model. However, we afforded evidence that regions with the low-voltage and low multifrequency impedance mainly corresponded with the areas with atrial infarct involvement.

4.5 Clinical implications

In the present work we have mapped the endocardial regions of healthy and infarcted left atrium and found that the areas with low voltage of electrograms depict greater range of variability than the multifrequency impedance values in the same areas. A likely explanation is that local multifrequency measurements explore the stable passive properties of the tissue while the endocardial voltage is affected by dynamic changes in the local activation front. Considering the similarities between human and swine cardiac ischemic electrophysiology, (Lelovas et al., 2014), a model of infarct atrial infarction like the developed in our study emerges as a reliable tool for further research on atrial electrophysiological mechanisms and development of atrial ablation techniques. A major goal for the success of electrical ablation of the arrhythmias is the accurate characterization of the target ablation structure. In this regard, recent studies have highlighted the advantages of the local measurement of tissue electrical impedance to achieve a better pulmonary vein isolation in the ablation of atrial arrhythmias. (Das et al., 2021; García-Bolao et al., 2022)

In these studies, only the magnitude component of the impedance was measured. In our study we have measured both, the magnitude and the phase angle components of the impedance at different frequencies. We have previously reported that multifrequency impedance mapping can detect different degrees of myocardial fibrosis (Amorós-figueras et al., 2016) and, remarkably, the impedance measurement will not be influenced by the changes in cardiac activation sequence. (Amorós-figueras et al., 2017)

Data availability statement

The raw data supporting the conclusion of this article will be made available by the authors, without undue reservation.

Ethics statement

The animal study was reviewed and approved by Comitè Ètica Experimentació Animal–IR Sant Pau.

Author contributions

GA-F, SC-R, GC-S, DA, EJ, AG-O, YM, DS-Q, JR-F, JG, and JC have made substantial contributions to the conception and design of the work, have participated in the acquisition, analysis and interpretation of the data, have drafted the manuscript, have given the final approval of the version to be published and the agreement to be accountable of all aspects of the work in ensuring that questions related to the accuracy or integrity of any part of the work are appropriately investigated and resolved.

Funding

This work was supported by the Spanish Ministerio de Economia y Competitividad, Instituto de Salud Carlos III (CB16/11/00276), FIS PI17/00069); and Fondo Europeo de Desarrollo Regional.

Conflict of interest

GA-F, EJ, JG, and JR-F received a research grant by the company Biosense-Webster. Biosense-Webster was not involved in the study design, collection, analysis, interpretation of data, the writing of this article, or the decision to submit it for publication.

The remaining authors declare that the research was conducted in the absence of any commercial or financial relationships that could be construed as a potential conflict of interest.

Publisher's note

References

Alasady, M., Shipp, N. J., Brooks, A. G., Lim, H. S., Lau, D. H., Barlow, D., et al. (2013). Myocardial infarction and atrial fibrillation: Importance of atrial ischemia. *Circulation Arrhythmia Electrophysiol.* 6 (4), 738–745. doi:10.1161/CIRCEP.113.000163

Amorós-figueras, G., Jorge, E., García-Sánchez, T., Bragós, R., Rosell-Ferrer, J., and Cinca, J. (2016). Recognition of fibrotic infarct density by the pattern of local systolic-diastolic myocardial. *Electr. Impedance'* 7. doi:10.3389/fphys.2016.00389

Amorós-figueras, G., Jorge, E., Alonso-Martin, C., Traver, D., Ballesta, M., Bragos, R., et al. (2017). Endocardial infarct scar recognition by myocardial electrical impedance is not in fluenced by changes in cardiac activation sequence. *Heart rhythm.* 15 (4), 589–596. doi:10.1016/j.hrthm.2017.11.031

Amoros-Figueras, G., Jorge, E., Alonso-Martin, C., Traver, D., Ballesta, M., Bragos, R., et al. (2018). Endocardial infarct scar recognition by myocardial electrical impedance is not influenced by changes in cardiac activation sequence. *Heart rhythm.* 15 (4), 589–596. doi:10.1016/j.hrthm.2017.11.031

Amorós-Figueras, G., Rosello-Diez, E., Sanchez-Quintana, D., Casabella-Ramon, S., Jorge, E., Nevado-Medina, J., et al. (2020). Changes in local atrial electrograms and surface ECG induced by acute atrial myocardial infarction. *Front. Physiology* 11, 264. doi:10.3389/fphys.2020.00264

Avula, U. M. R., Hernandez, J. J., Yamazaki, M., Valdivia, C. R., Chu, A., Rojas-Pena, A., et al. (2018). Atrial infarction-induced spontaneous focal discharges and atrial fibrillation in sheep role of dantrolene-sensitive aberrant ryanodine receptor calcium release. *Circulation Arrhythmia Electrophysiol.* 11 (3), e005659. doi:10.1161/CIRCEP.117.005659

Das, M., Luik, A., Shepherd, E., Sulkin, M., Laughner, J., Oesterlein, T., et al. (2021). Local catheter impedance drop during pulmonary vein isolation predicts acute conduction block in patients with paroxysmal atrial fibrillation: Initial results of the LOCALIZE clinical trial. *Europace* Feb (7), 1042–1051. doi:10.1093/europace/euab004

García-Bolao, I., Ramos, P., Luik, A., Sulkin, M. S., Gutbrod, S. R., and Oesterlein, T. (2022). Local impedance drop predicts durable conduction block in patients with paroxysmal atrial fibrillation. *JACC Clin. Electrophysiol.* 8, 1–10. doi:10.1016/j.jacep.2022.01.009

Guandalini, G. S., Liang, J. J., and Marchlinski, F. E. (2019). Ventricular tachycardia ablation: Past, present, and future perspectives. *JACC Clin. Electrophysiol.* 5 (12), 1363–1383. doi:10.1016/J.JACEP.2019.09.015

Hopman, L. H. G. A., Bhagirath, P., Mulder, M. J., Eggink, I. N., van Rossum, A. C., Allaart, C. P., et al. (2022). Quantification of left atrial fibrosis by 3D late gadolinium-enhanced cardiac magnetic resonance imaging in patients with atrial fibrillation: Impact of different analysis methods. *Eur. heart J. Cardiovasc. Imaging* 23 (9), 1182–1190. doi:10.1093/EHJCI/JEAB245

Kottkamp, H., Schreiber, D., Moser, F., and Rieger, A. (2017). Therapeutic approaches to atrial fibrillation ablation targeting atrial fibrosis. *JACC Clin. Electrophysiol.* 3 (7), 643–653. doi:10.1016/J.JACEP.2017.05.009

Lahuerta, A. A., Roberto, C., Saiz, F. J., Cano, O., Martinez-Mateu, L., Alonso, P., et al. (2022). Atrial low voltage areas: A comparison between atrial fibrillation and sinus rhythm. *Cardiol. J.* 29 (2), 252–262. doi:10.5603/CJ.A2021.0125

Laish-Farkash, A., Perelshtein Brezinov, O., Valdman, A., Tam, D., Rahkovich, M., Kogan, Y., et al. (2021). Evaluation of left atrial remodeling by 2D-speckle-tracking echocardiography versus by high-density voltage mapping in patients with atrial fibrillation. *J. Cardiovasc. Electrophysiol.* 32 (2), 305–315. doi:10.1111/jce.14837

Lelovas, P. P., Kostomitsopoulos, N. G., and Xanthos, T. T. (2014). A comparative anatomic and physiologic overview of the porcine heart. *J. Am. Assoc. Laboratory Animal Sci. JAALAS* 53 (5), 432–438.

Nishida, K., Qi, X. Y., Wakili, R., Comtois, P., Chartier, D., Harada, M., et al. (2011). Mechanisms of atrial tachyarrhythmias associated with coronary artery occlusion in a chronic canine model. *Circulation* 123 (2), 137–146. doi:10.1161/CIRCULATIONAHA.110.972778

Rivard, L., Sinno, H., Shiroshita-Takeshita, A., Schram, G., Leung, T. K., and Nattel, S. (2007). The pharmacological response of ischemia-related atrial fibrillation in dogs: Evidence for substrate-specific efficacy. *Cardiovasc. Res.* 74 (1), 104–113. doi:10.1016/j.cardiores.2007.01.018

Sanchez, B., Louarroudi, E., Jorge, E., Cinca, J., Bragos, R., and Pintelon, R. (2013). A new measuring and identification approach for time-varying bioimpedance using multisine electrical, 339. doi:10.1088/0967-3334/34/3/339

Schneider, C. A., Rasband, W. S., and Eliceiri, K. W. (2012). NIH image to ImageJ: 25 years of image analysis. *Nat. Methods* 9 (797), 671–675. doi:10.1038/nmeth.2089

Sinno, H., Derakhchan, K., Libersan, D., Merhi, Y., Leung, T. K., and Nattel, S. (2003). Atrial ischemia promotes atrial fibrillation in dogs. *Circulation* 107 (14), 1930–1936. doi:10.1161/01.CIR.0000058743.15215.03

frontiers | Frontiers in Physiology

TYPE Review
PUBLISHED 13 January 2023
DOI 10.3389/fphys.2023.1076261

OPEN ACCESS

EDITED BY
Fanny Vaillant,
Université de Bordeaux, France

REVIEWED BY
Jan Pavel Kucera,
University of Bern, Switzerland
Ndeye Rokhaya Faye,
Université de Bordeaux, France
Rushd Fadhil Mustafa Al-Shama,
Academic Medical Center, Netherlands

*CORRESPONDENCE
Yannick J. H. J. Taverne,
y.j.h.j.taverne@erasmusmc.nl

SPECIALTY SECTION
This article was submitted to Cardiac Electrophysiology, a section of the journal Frontiers in Physiology

RECEIVED 21 October 2022
ACCEPTED 04 January 2023
PUBLISHED 13 January 2023

CITATION
Amesz JH, Zhang L, Everts BR, De Groot NMS and Taverne YJHJ (2023), Living myocardial slices: Advancing arrhythmia research.
Front. Physiol. 14:1076261.
doi: 10.3389/fphys.2023.1076261

Living myocardial slices: Advancing arrhythmia research

Jorik H. Amesz[1,2], Lu Zhang[2], Bian R. Everts[1], Natasja M. S. De Groot[2] and Yannick J. H. J. Taverne[1]*

[1]Translational Cardiothoracic Surgery Research Lab, Lowlands Institute for Bioelectric Medicine, Department of Cardiothoracic Surgery, Erasmus University Medical Center, Rotterdam, Netherlands, [2]Translational Electrophysiology, Lowlands Institute for Bioelectric Medicine, Department of Cardiology, Erasmus University Medical Center, Rotterdam, Netherlands

Living myocardial slices (LMS) are ultrathin (150–400 μm) sections of intact myocardium that can be used as a comprehensive model for cardiac arrhythmia research. The recent introduction of biomimetic electromechanical cultivation chambers enables long-term cultivation and easy control of living myocardial slices culture conditions. The aim of this review is to present the potential of this biomimetic interface using living myocardial slices in electrophysiological studies outlining advantages, disadvantages and future perspectives of the model. Furthermore, different electrophysiological techniques and their application on living myocardial slices will be discussed. The developments of living myocardial slices in electrophysiology research will hopefully lead to future breakthroughs in the understanding of cardiac arrhythmia mechanisms and the development of novel therapeutic options.

KEYWORDS

living myocardial slices, 3D cardiac models, cardiac arrhythmia models, *in-vitro* electrophysiology, translational research

Introduction

In order to study electrophysiological phenomena of cardiac arrhythmias and evaluate treatment options, multiple *in-vitro* systems and *in-vivo* models have been developed over the past decades. Historically, the field of electrophysiology has greatly advanced based on animal studies, ranging from studies on *Caenorhabditis elegans* (Fischer et al., 2017) and zebrafish (Wilkinson et al., 2014) to large animals such as pigs and sheep. These animal models are still valuable for specific research questions. Yet, no model recapitulates the complete human interplay between electrophysiology, hemodynamics and cardiac morphology, so it is important to recognize species differences in cardiac action potentials, membrane currents and consequential calcium handling (Blackwell et al., 2022). Off note, animal models using for example pigs or goats are valuable due to their high resemblance to the human setting with similar cardiac size, anatomy and cardiac electrophysiology. However, use of such models is hampered due to increasing global ethical constraints, high costs and time to breed (Blackwell et al., 2022).

This prompted parallel exploration of other types of disease models. Two-dimensional cardiomyocyte cultures dominated the field of electrophysiological research for many years. Nonetheless, those *in-vitro* models fail to fully recapitulate the complex three-dimensional (3D) architecture of the heart despite the advances towards 3D cell cultures. The fact that stem-cell derived cardiomyocytes have relative immaturity in terms of their metabolic, contractile molecular and electrophysiological properties is still a major limitation of the field (Goldfracht et al., 2020). Furthermore, building 3D constructs cannot account for the complex adherence allowing bioelectric cell-cell communication between cells. Hence, there

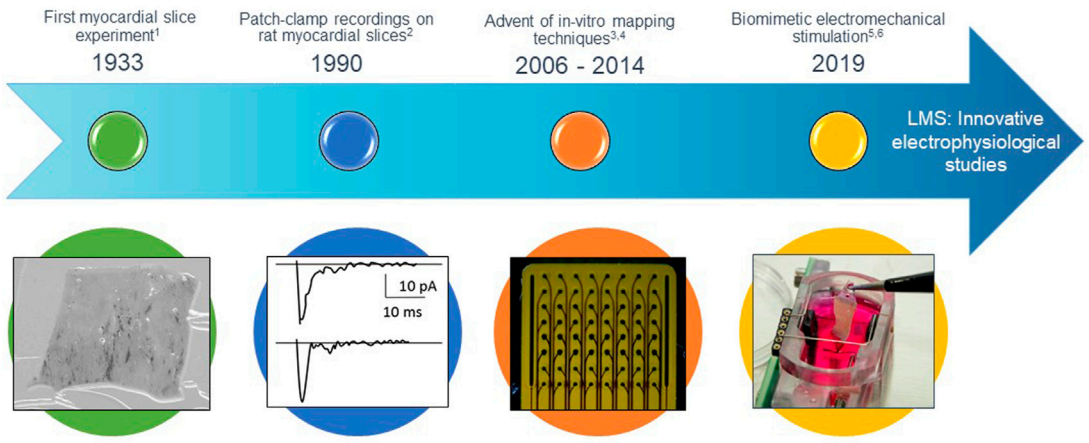

FIGURE 1
Timeline of major events for living myocardial slices (LMS) in electrophysiological research. 1 Pincus (1933), 2 Burnashev et al. (1990), 3 Halbach et al. (2006), 4 Wang et al. 2015, 5 Fischer et al. (2019), 6 Watson et al. (2019).

is still a growing demand for dedicated preclinical platforms that have a high degree of human cardiac electrophysiological mimicry.

Attention was therefore redirected to the use of living myocardial slices (LMS). The LMS technique is not new, but short-term cultivation of LMS and consequential interpretation and extrapolation of the results hampered its widespread use. Recent technological advances enabled the transition of LMS towards a more representative model of the human myocardium (Bursac et al., 2003; Camelliti et al., 2011). A major step forward in the myocardial slicing technique was achieved by the introduction of special electromechanical cultivation chambers (Fischer et al., 2019; Watson et al., 2019), enabling long-term cultivation of LMS cultures. The aim of this review is to present the potential of a biomimetic interface using LMS in electrophysiological studies outlining the advantages, disadvantages and future perspectives of the interface.

Living myocardial slices

LMS are ultrathin (150–400 µm and 6–17 cardiomyocyte layers) sections of cardiac tissue that are directly produced from cardiac specimens, leaving the native 3D microarchitecture and intracellular connections of the heart intact. The thin nature of the slices allows diffusion of oxygen and nutrients into the innermost cell layers, with a maximum diffusion distance of 200 µm from top and bottom surface of the slice (Shattock et al., 1983; Barclay, 2005). LMS have several advantages over cellular *in-vitro* cardiac models, in which the extracellular matrix with complex 3D architecture is lost. Moreover, cellular models often do not display all cell populations present in the heart and connections between cells are poorly expressed, while the *in-vivo* heart is characterized by a complex interplay of different cell types and communication between cells (Perbellini and Thum, 2019). Multicellularity and intercellular contact are important for proper investigation of myocardial propagation of electrical waves and should therefore be present in a representative electrophysiological model of the human heart. LMS maintain the native structure of the heart because they are directly 'cut' from intact cardiac tissue with a high-precision vibratome, and therefore present a model with a high degree of *in-vivo* mimicry suitable for electrophysiological research.

Brief history of myocardial slices in electrophysiological research

The use of myocardial slices dates back to 1933 when Pincus studied the effects of drugs on the oxygen consumption of several excised tissues, including cardiac ventricular tissue (Figure 1) (Pincus, 1933). Burnashev et al. (1990) were the first to use myocardial slices for cardiac electrophysiological research, demonstrating patch clamp recordings on rat cardiac muscle slices. However, broad interest in this technique remained scarce until Bursac et al. (2003) demonstrated that rat myocardial slices possessed more representative electrophysiological characteristics (connexin 43 expression and action potential characteristics) in comparison to cultured cardiomyocytes. From then on, more groups started employing cardiac slices for electrophysiological research, and especially the entrance of microelectrode arrays led to renewed interest in the myocardial slice as an electrophysiological model (Pillekamp et al., 2005; Camelliti et al., 2011). During that same period, experiments with optical mapping of myocardial slices were performed (Kang et al., 2016). The most important breakthrough in LMS culture was achieved in 2019 when two groups developed novel technologies that prevented significant and functional changes in LMS associated with chronic *in-vitro* culture, now allowing for LMS cultivation of several weeks to months (Fischer et al., 2019; Watson et al., 2019). Since then the number of articles published on experiments utilizing myocardial slices increased considerably (Pitoulis et al., 2020b).

TABLE 1 Overview of different biomimetic cultivation chamber interfaces for myocardial slices.

Biomimetic interface	Type of loading	Oxygenation	Electrical stimulation
Brandenburger et al. (2011)	No loading	Liquid-air interface	No stimulation
Watson et al. (2019)	Isometric 2D	Perfusion	Field
Fischer et al. (2019)	Auxotonic 2D	Agitation on rocker plate	Field
Pitoulis et al. (2022)	Dynamic 2D	Perfusion	Field
Miller et al. (2022)	Dynamic 3D	Daily oxygenated medium exchange	Field

Development of biomimetic cultivation chambers

Before 2011, culturing LMS was limited by the short period of cardiomyocyte viability in culture (≈24 h). This was first addressed with the development of culture systems with liquid-air interfaces (Brandenburger et al., 2011; Kang et al., 2016) and continuous electrical stimulation and oxygenation of the culture medium (Ou et al., 2019). As such, LMS cultivation was possible for 6–28 days. However, lack of mechanical loading of these slices still resulted in rapid decline of contractile force and altered cardiac expression *in-vitro*. In 2019, two groups presented novel biomimetic cultivation chambers that provide uniaxial mechanical loading and continuous electrical stimulation to LMS, improving cardiac phenotype and preserving contractile force of LMS (Fischer et al., 2019; Watson et al., 2019). Watson et al. (2019) developed custom-made stretchers for LMS which were placed in culture chambers with continuous flow and oxygenation of the culture medium. Electrical stimulation was performed with field stimulation in between two carbon electrodes. In this manner, isometric twitch forces were generated in the tissue. This resulted in highly functional LMS for 5 days. Fischer et al. (2019) choose a different approach with linear auxotonic loading of slices. Here, LMS were also mounted in a custom-made stretcher, but one end of the stretcher was able to move during contraction, resulting in elastic contractions. The movement of the flexible end of the stretcher was directly correlated to contractile force, allowing real-time measurement of LMS twitch force during culture. These culture chambers were placed on rocking plates for continuous agitation of the culture medium and electrical field stimulation was applied in between two graphite electrodes. As such, a stable beating state of LMS was reached for up to 4 months. However, adaptation in gene expression occurred during the first 8 days of culture, including components of excitation-contraction coupling and the extracellular matrix, and targets of adrenoceptor signalling. Later, Pitoulis et al. (2022) further optimized these static loading platforms by developing a system with dynamic mechanical loading, better simulating electromechanical events of the cardiac cycle with not only preload but also afterload. A 3-Element Windkessel operated in sync with the electrical stimulation to dynamically load LMS with force transducer feedback and a stretcher actuator. This resulted in force-length measurements, corresponding with pressure-volume loops *in-vivo*, and allowed for different (pathological) loading conditions (culture duration: 3 days). Recently, this concept was even taken further by not only providing dynamic loading in one axis, but in a more three-dimensional fashion with a pneumatically driven flexible membrane that induces stretch to the LMS on top of it (culture duration: 12 days) (Miller et al., 2022). Hence, cultivation in biomimetic cultivation chambers with electromechanical loading has proven to improve LMS culture conditions, and the community is still working on novel chambers to facilitate optimal physiological long-term cultures of LMS (Table 1). For electrophysiological research, the next step in the development of LMS cultivation chambers comprises the integration of electrodes and electrophysiological mapping techniques in the chambers.

LMS technique

The technique to produce LMS has been described in detail (Brandenburger et al., 2011; Watson et al., 2017; Fischer et al., 2019; Watson et al., 2019; Watson et al., 2020; Hamers et al., 2022). In this review, we will focus on the technique to produce LMS from human (residual) tissue, which we believe best mimics human (electro-)physiology because of cellular and structural differences between humans and animals. Yet, the technique to produce LMS from small mammals is rather similar (Watson et al., 2017) and has been important for the development of the technique. Moreover, small mammals present with easy access to cardiac tissue material, and the possibility to produce LMS from material of healthy controls.

Human tissue for the production of LMS is obtained from patients undergoing open-heart surgery, such as cardiac transplantations, assist device implantations, atrial appendage amputations, septal myectomies, or different types of congenital surgeries. Specimens are immediately submerged in cold 4°C Tyrode's solution with the addition of excitation-contraction uncoupler 2,3-butanedione monoxime (BDM), preventing the tissue from contracting during slicing. In the laboratory, excessive endocardial trabeculae and epicardial fat are removed from the cardiac tissue, and the tissue is submerged in 37°C low-melting agarose for structural support on the vibratome. This tissue block is mounted on the vibratome in 4°C Tyrode buffer supplemented with BDM and it is placed with the flat epicardium down to align fibers in the same plane within the tissue. It is of utmost importance that the myocardial fibre direction of the tissue is longitudinal to the moving direction of the vibratome blade in order to obtain viable slices. Watson et al. (2019) showed 97% viability of cardiomyocytes within slices if these critical steps of fibre orientation and alignment are applied. The vibratome then produces slices with a thickness of 150–400 µm coming from different layers within the myocardium. In general, vibratome speed should be lowered for atrial tissues in comparison with ventricular tissues, as atrial tissue is more fragile and therefore at higher risk for rupturing on the vibratome (Kang et al., 2016; Amesz et al., 2022). In addition, slices infiltrated with large amounts of fibrous

and adipose tissue often show separation of myocardial bundles and are therefore not routinely selected for culture.

Next, slices are mounted in special cultivation chambers filled with 37°C cell culture medium and superperfused with oxygen or placed on a rocking plate to provide diffusion of oxygen and nutrients to the cardiomyocytes. Medium-199 with insulin-transferrin selenium and antibiotics is the culture medium of choice for most groups working with LMS (Brandenburger et al., 2011; Kang et al., 2016), sometimes supplemented with antioxidants, growth factors and/or hormones (2-mercaptoethanol, fibroblast growth factor, vascular endothelial growth factor, (nor)adrenaline, triiodothyronine, and/or dexamethasone) (Fischer et al., 2019; Ou et al., 2019; Pitoulis et al., 2022). In the cultivation chambers, mechanical preload can be applied in different fashions (Fischer et al., 2019; Watson et al., 2019; Miller et al., 2022; Pitoulis et al., 2022). Electrical field or point stimulation results in cardiac contractions of the LMS, which can be monitored in real-time with dedicated force transducers. Electromechanical stimulation enables long-term cultivation of LMS and offers long-term analyses of LMS biomechanics, biochemistry, histology and electrophysiology.

Electrophysiological model

As mentioned before, LMS have a high-degree of *in-vivo* mimicry of electrophysiological properties of the human heart because of their intact native tissue structure. Hence, cardiomyocytes in LMS are well-aligned in a striated fashion and linked by gap junctions, and membrane bound connexins are preserved (Habeler et al., 2009). To date, LMS have been predominantly produced from ventricular specimens, but can also be produced from atrial tissue (Girmatsion et al., 2009; Biliczki et al., 2019; Amesz et al., 2022). In addition, Kang et al. (2016) produced slices from the sinoatrial node region and observed automaticity in these LMS. Hence, it could be of interest to produce slices from regions explicitly involved in cardiac arrhythmias, for better understanding of ectopic foci throughout the atria and underlying mechanisms of cardiac arrhythmias (Kang et al., 2016; Li et al., 2022). Next to that, one could produce LMS from patient material with and without history of cardiac arrhythmias, making LMS a disease-specific platform. Furthermore, anatomical differences in electrophysiology between the endocardial and epicardial layers can be addressed (Wen et al., 2018; Pitoulis et al., 2020a). For example, Wen et al. (2018) already showed longer action potential (AP) and calcium transient duration, and more calcium transient alternans in the endocardium compared to the epicardium.

As demonstrated by Pertsov et al. (1993) and Watanabe et al. (2017), LMS could be used to study the role of cardiac re-entry underlying tachyarrhythmias, induced by extrastimulation. This questions the widely accepted theory that re-entry is only possible in hearts exceeding a "critical mass" of more than ≈400 mm^2 and ≈12 g (Garrey, 1914; Winfree, 1994) as LMS present with a surface area of ≈80 mm^2. Yet, in order to obtain re-entry in such a small LMS, the refractory period has to be relatively short and/or conduction relatively slow. Next to that, investigating the role of electrical breakthrough waves in the pathophysiology of tachyarrhythmias seems more difficult with a LMS model. In theory, breakthrough waves could occur in LMS (150–400 μm) comprised of multiple (6–17) cell layers if cell layers are activated asynchronously due to the presence of intramural block, leading to dissociation in patterns of activation between the top and bottom layers of the LMS (Kharbanda et al., 2018). Yet, up to date, there has been no report on this phenomenon in LMS. This may be the result of lack of mapping technologies capable of detecting very small local activation time differences between the various layers. If such breakthrough waves would occur in LMS, they could be detected by simultaneous mapping of the top and bottom of the slice, if the sampling frequency of the recording system is high enough (Kharbanda et al., 2018).

The development of special biomimetic cultivation chambers also makes LMS a model with precise control of (patho-)physiological conditions. For example, mechanical overload can be induced by the application of extra stretch on myocardial tissue, leading to a fibrotic remodelling response (Nunez-Toldra et al., 2022; Pitoulis et al., 2022) associated with cardiac arrhythmias. At the same time, application of programmed electrical stimulation protocols in the cultivation chambers allows for mimicking arrhythmias, e.g., with programmed rapid electrical stimulation or frequent extrasystoles (Figure 2) (Amesz et al., 2022). Furthermore, viral transduction can be established in LMS (Ferrera et al., 2005; Kang et al., 2016; Thomas et al., 2016) for cardiac disease induction and gene therapy (Liu et al., 2020). Combining gene targeting technologies with mechanical conditioning and programmed electrical stimulation, LMS represent a potent system for the study of disease-specific activity including arrhythmias (Schneider-Warme et al., 2017).

This review mainly focuses on electrophysiological techniques applied to LMS. Yet, LMS also enable the possibility to perform comprehensive studies on the mechanistic understanding of arrhythmias. Fischer et al. (2019) developed a cultivation chamber with real-time measurement of contractile forces, without having to place the LMS on external force transducers. Such a platform can be used for continuous evaluation of contractile responses to different culture conditions, including tachypacing and induction of arrhythmias (Amesz et al., 2022). Moreover, structural and molecular analyses of LMS further supplement electrophysiological and mechanical assessments of LMS. Histology provides analysis of cellular and extracellular matrix organization, and specific biomolecules can be labeled and visualized. In addition, biochemical analyses at the genomic, proteomic and secrotomic level can be easily applied to LMS when snap-frozen after culture (Watson et al., 2020). These analyses can also be conducted on the spent culture medium to evaluate biochemical events in LMS, without termination of LMS cultivation. Although, analyses can be complicated due to the relatively small number of cells in LMS, resulting in low concentrations of secreted molecules in the culture medium. As such, LMS provide a platform with an easy assessment of different parameters using already available kits and techniques from other cardiac *in-vitro* research models. The next section of this review will specifically discuss the application of dedicated electrophysiological techniques on myocardial slices.

Intracellular action potential recording

The patch clamp technique has been the golden standard for basic electrophysiological experiments since its invention in the 1970s (Neher and Sakmann, 1976). The patch-clamp system is capable of measuring membrane voltages by attaching micron-sized diameter glass pipettes to the cell membrane. The membrane patch under the micropipette tip is broken and the electrode inside the micropipette is

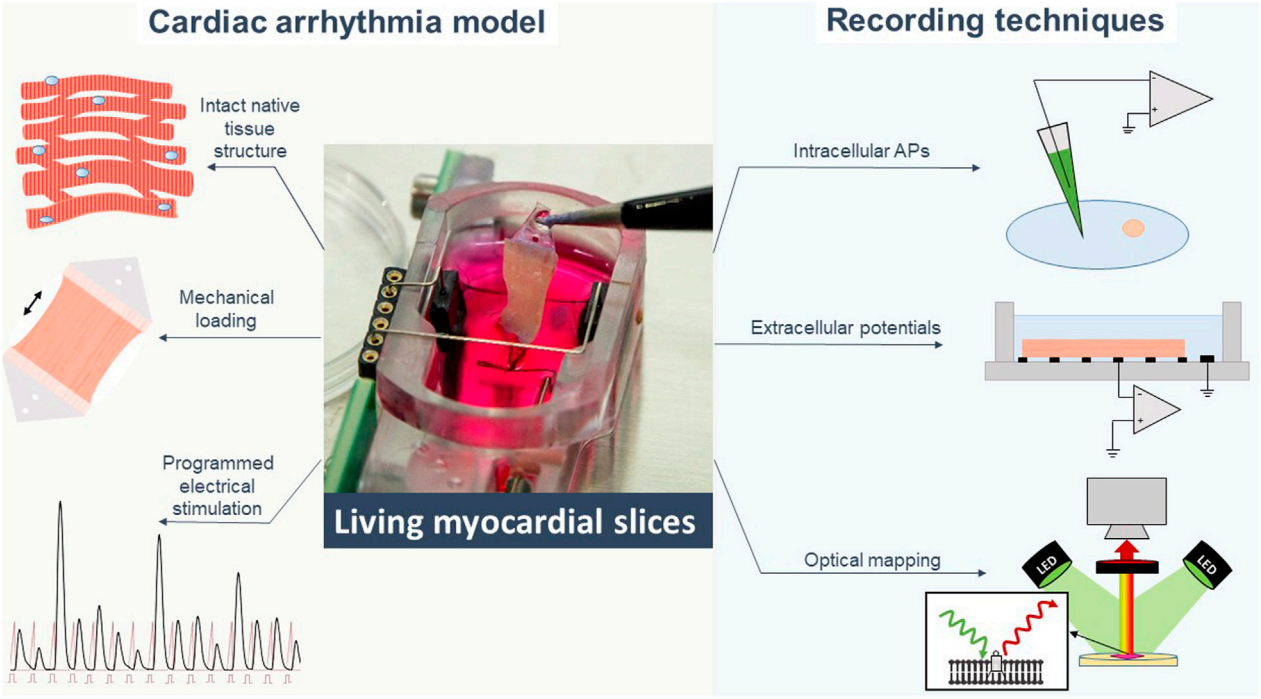

FIGURE 2
Living myocardial slices are a cardiac arrhythmia model with high degree of *in-vivo* mimicry to which different electrophysiological recording techniques can be applied. APs action potentials.

electrically connected to the cytoplasm to measure the intracellular transmembrane potential, resulting in an AP.

In 1990, Burnashev et al. (1990) were the first to apply the patch-clamp technique to rat cardiac slices. They reported resting membrane potentials (RMP) between −30 and −65 mV and sodium and inward rectifying potassium currents similar to isolated ventricular cells and proved single-channel recordings in LMS without the need for complicated cell isolation procedures. In addition, this technique showed proof-of-concept and avoided the possible alteration of channel properties caused by proteolytic enzymes during myocardial cell isolation, although, RMP of −30 mV indicate cellular damage to some extent.

Since then, the patch-clamp technique has been used in combination with LMS in a few studies. In 2011, Huang and Li explored the feasibility of whole-cell patch-clamp recordings from cardiac ventricular slices of newborn rats. The sodium current, outward potassium current, hyperpolarization-activated cyclic nucleotide–gated (HCN) channel, and AP all displayed features similar to those previously reported for isolated rat ventricular myocytes (Huang and Li, 2011). Consequently, Nong et al. (2013) performed patch-clamp recordings in ventricular slices from HCN4-gene transfected mice and found altered electrophysiological characteristics consisting of a greater negative amplitude and expression of funny currents.

The sharp electrode technique is an alternative approach for patch-clamping and is more commonly used on LMS. Here, a glass electrode with very small pore diameter is directly inserted in the cell to measure its membrane potential. Intracellular recordings of APs performed with sharp glass electrodes showed a fast upstroke, a high amplitude and short AP duration at 50%, characteristic for murine adult ventricular APs (Himmel et al., 2012), indicating that cardiomyocytes within the LMS were electrophysiologically intact. In 2016, Peinkofer et al. (2016) used this technique to study the AP differences between native murine atrial and ventricular cardiomyocytes from early embryonic development through adulthood. Measurements revealed significant changes in AP morphology between atria and ventricles and pre- and postnatal murine development. Next to that, they investigated the interaction between stem cell-derived cardiomyocytes and ventricular slices and showed electrical integration of the transplanted cardiomyocytes in the recipient slices (Peinkofer et al., 2017; Peinkofer et al., 2021).

For intracellular AP recording in LMS, the sharp electrode technique is more often used compared to the patch clamp technique, because the latter is more complicated in multicellular preparations with high amount of extracellular matrix proteins (Peinkofer et al., 2016). Yet, an advantage of the patch clamp technique is the possibility to record individual ion currents, which is not possible with sharp electrodes because membrane potentials cannot be clamped in the electrically well-coupled syncytium (Peinkofer et al., 2016). Hence, patch-clamps and sharp electrodes both have their perks and drawbacks and the technique of choice for intracellular measurements of APs in LMS depends on the research question. Additionally, non-invasive optical imaging techniques may provide an alternative solution for the disadvantages of these two techniques.

Optical mapping

Cardiac optical mapping is a fluorescent imaging technique to record electrical activity and calcium transients in the heart.

Measurements are performed with fluorescent dyes of which the emitted light is captured by an imaging system with high spatial and temporal resolution. To date, few studies have used optical mapping in combination with LMS.

Optical mapping allows the measurement of a multitude of parameters, including membrane potential with voltage sensitive dyes (VSDs) and intracellular free calcium ($[Ca^{2+}]_i$) dynamics with calcium dyes. Fast VSDs are often based on a styryl component (Efimov et al., 2004) and enable the recording of optical APs. In addition, AP duration, activation, conduction velocity, and repolarization maps can be acquired based on changes in fluorescence (O'Shea et al., 2020; Efimov et al., 2004; Kang et al., 2016; Berenfeld and Efimov, 2019). Based on these parameters, AP upstroke analysis, arrhythmia analysis, and phase mapping can be performed (Efimov et al., 2004; Laughner et al., 2012).

Calcium dyes are used to visualize spatial changes in the kinetics and amplitude of calcium transients (Del Nido et al., 1998; Laurita et al., 2003; Venkataraman et al., 2012). The binding of a high-affinity calcium dye to $[Ca^{2+}]_i$ can affect calcium handling by prolonging the calcium transient (Herron et al., 2012). Therefore, low-affinity dyes, such as Fura-4F, are preferred (Wokosin et al., 2004; Fast, 2005). Calcium dynamics are usually displayed in colour-coded maps (Jaimes et al., 2016) which are used to interpret the mechanisms of arrhythmias (Davidenko et al., 1992; Omichi et al., 2004; Warren et al., 2007) and heart failure (Lang et al., 2015). The calcium upstroke and extrusion phases, and calcium transient time to peak are used to study the activity of cellular exchangers, pumps and ryanodine receptors (RyR). Intracellular calcium transient duration is a Ca^{2+} analogue of the AP duration in optical mapping (Jaimes et al., 2016). Furthermore, calcium dyes are used to study calcium kinetics that influence contractility. A combination of VSDs and calcium dyes gives insights into excitation-contraction coupling and arrhythmia mechanisms (Jaimes et al., 2016).

The main advantages of optical mapping over currently available electrode measurements are the high spatial resolution, the ability to simultaneously measure several physiological parameters, and the absence of artefacts due to electrical stimulation (Efimov et al., 2004; Wang et al., 2015; Berenfeld and Efimov, 2019). Optical mapping also has several limitations and factors to consider. Firstly, optical mapping presents with the risk of illumination-induced phototoxicity caused by the production of reactive oxygen species (ROS) (Schaffer et al., 1994). This limits the study time for optical mapping and possibility to perform repeated measurements over time. However, phototoxicity is less pronounced in multicellular aggregates and tissue preparations, compared to single cells (Kanaporis et al., 2012). Moreover, recent developments in fluorescent dyes have resulted in dyes that can be excited at longer, red-shifted wavelengths, greatly reducing the necessary illumination intensity, which in turn reduces the risk of ROS-production (Matiukas et al., 2007). Secondly, a major limitation of optical mapping is the presence of motion artefacts caused by contraction. Commonly, these motion artefacts are suppressed with electromechanical uncouplers such as blebbistatin and BDM. However, this may result in alterations in AP duration and calcium handling (Kappadan et al., 2020). Another solution is the use of motion tracking algorithms in combination with ratiometric imaging, in which the ratio between two separate excitation or emission wavelengths is taken to attenuate noise (Bachtel et al., 2011; Kappadan et al., 2020). Thirdly, a complete optical mapping system can be very expensive, with prices of $40.000 for a CCD or CMOS camera. Finally, there has not been a consensus on the depth of field in optical mapping yet. However, ranges from 300–500 μm (Knisley, 1995; Girouard et al., 1996) and ranges up to 2 mm (Baxter et al., 2001) have been reported. In either case, it can be assumed that sufficient fluorescence can be measured from LMS with a thickness of ≈300 μm. It should be noted that every cell layer in a LMS contributes to the emitted fluorescence signal. Hence, the recorded fluorescence should be interpreted as an averaged signal throughout the slice thickness.

In the early 90s, optical mapping on cardiac slices was pioneered by the group of Jose Jalife et al. (Davidenko et al., 1990; Davidenko et al., 1992; Pertsov et al., 1993; Cabo et al., 1994; Davidenko et al., 1995). They showed initiation of sustained re-entrant excitation in small ventricular slices, which provided a major contribution to the understanding of spiral waves leading to re-entrant ventricular tachycardias (Davidenko et al., 1990; Davidenko et al., 1992; Pertsov et al., 1993; Davidenko et al., 1995). Now, optical mapping can be used for a variety of research questions and interventions. For example, Wang et al. (2014) showed the effects of axial stretch on action potential and calcium transient duration in LMS. Watanabe et al. (2017) investigated optogenetic manipulation of anatomical re-entry in ventricular LMS and showed effective termination by induction of local conduction block. And, Miller et al. (2020) and Li et al. (2022) showed cardiotoxicity of cancer drugs with use of optical mapping. Hence, cardiac optical mapping can be successfully performed on LMS for high-quality basic and translational research.

Extracellular field potential mapping

Cardiac extracellular potential mapping is an electrophysiological imaging technique to record electrical activity of cardiac tissue using multi-electrode arrays (MEAs). MEAs in contact with cardiac tissue record electrical activation waves propagating through the myocardium. The detected electrical signal results from the action potentials of cardiomyocytes located in the vicinity of the electrode (Sim et al., 2019). From these extracellular potentials, multiple parameters can be derived, including peak-to-peak amplitudes, potential duration and slope, and degree of fractionation. Comparison of local activation times between neighbouring electrodes provides information on conduction velocity and hence conduction disorders in the myocardial tissue (de Groot et al., 2022). Such electrophysiological mapping is performed in the clinical electrophysiology lab with bipolar catheters for detection of rhythm disorders and guidance of ablative therapies. Yet, MEAs applied for mapping can also be performed *in-vitro* for monitoring of electrical activity of cultured cardiomyocytes, and also LMS (Reppel et al., 2004).

The most commonly used MEA in LMS research consists of a 60-channel electrode array system with gold contacts (30 μm diameter) arranged in an 8 × 8 electrode grid with an inter-electrode distance range of 200 μm (Multi Channel Systems MCS GmbH, Reutlingen, Germany). This MEA was first used to record extracellular potentials of mouse ventricular slices, demonstrating conduction velocities of 21–24 cm/s (Pillekamp et al., 2005; Halbach et al., 2006; Pillekamp et al., 2006). Halbach et al. (2006) showed that LMS are (electro-) physiologically intact by measuring both APs and extracellular potentials at different stimulation frequencies and with the application of ion channel blockers. In addition. Himmel et al. (2012) demonstrated similar electrical signal characteristics of LMS

and other established *in-vitro* and animal models. As such, MEAs can be used for a variety of research questions and interventions. For example, the electrical integration of stem cells in myocardial tissue as cardiac regenerative therapy has been assessed using MEAs and LMS (Hannes et al., 2008; Pillekamp et al., 2009; Rubach et al., 2014). MEAs showed synchronized beating between transplanted stem cells and host LMS, hence demonstrating electrical coupling between both cell types (Hannes et al., 2008; Pillekamp et al., 2009). In addition, conduction block, induced with heptanol administration, could be visualized with colour-coded activation maps constructed with the use of MEAs (Pillekamp et al., 2009).

The simplicity of the MEA allows electrophysiological measurements to be performed without the need for sophisticated skills in complex electrophysiological techniques such as patch clamp (Spach et al., 1972; Chowdhury et al., 2018), or high computational power required for optical mapping signal analysis. The major contributor to successful extracellular potential mapping with MEAs on LMS is the contact between the myocardial tissue and the electrode. Furthermore, the density of the electrodes in the MEA determines its resolution, with a higher resolution providing more accurate information on cardiac conduction. Although the resolution of MEAs has improved over recent years with developments in MEA technology, it still presents with lower resolution as compared to optical mapping measurements (van der Does and De Groot, 2017; Hansen et al., 2018). Another factor to consider is the possible separation of myocardial bundles in LMS, reducing the representation of the *in-vivo* electrical activation patterns by LMS, especially if the tissue is infiltrated with fibrous and adipose tissue. Integrity of the slices can be improved if proper vibratome settings are applied, but data interpretation in these regions should be done carefully. Altogether, electrophysiological properties of LMS were verified using MEA techniques, promoting and broadening the potential of this technology for pharmacological drug testing and performing studies under (patho)physiological conditions (Bussek et al., 2009).

Current state and future perspectives

Most electrophysiological studies in this review are of methodological nature and describe intrinsic electrophysiological characteristics of LMS and techniques to reliably measure these features. These reports have shown that LMS present a valid platform with close *in-vivo* (electro)physiological resemblance, which is important for reliable interpretation and extrapolation of the results. Yet, as validity of the LMS model has been confirmed, we encourage the electrophysiological community to (further) incorporate this technique in her laboratories, in order to unravel detailed mechanistic properties of arrhythmias and test novel anti-arrhythmic therapies based on these insights. For example, Esfandyari et al. (2022) identified microRNAs that regulate the cardiac action potential and demonstrated that manipulation of these microRNAs in LMS can affect action potential duration and refractoriness. And, Watanabe et al. (2017) showed optogenetic manipulation of anatomical re-entry in ventricular LMS, being a potential therapeutic option for termination of reentrant tachyarrhythmias. These are examples of innovative therapies for cardiac arrhythmias, based on technological advances in cardiac cell biology and electrophysiology, which were tested in LMS.

The next step in LMS research should be the incorporation of dedicated mapping techniques into the biomimetic cultivation chambers. To date, optical and extracellular potential mapping has only been performed on unloaded slices, being less representative of the *in-vivo* volume loading of the heart which influences electrophysiological characteristics. Moreover, the incorporation of electrophysiological measurements in biomimetic cultivation chambers allows for direct correlation between electrical signal characteristics and force measurements (Fischer et al., 2019; Watson et al., 2019) to investigate excitation-contraction coupling mechanisms of cardiac arrhythmias (Grandi et al., 2012). The addition of biochemical and histological analyses to these force and electrical measurements makes LMS a platform capable of correlating different types of biological data coming from a single specimen with high-degree of *in-vivo* mimicry. As such, LMS will become an even more important player in the field of basic cardiac electrophysiology research.

Summary

LMS have been around for a few decades, but widespread use within the electrophysiological research community has been hampered due to functional degradation of LMS in culture. The introduction of biomimetic electromechanical cultivation chambers, enabled long-term cultivation and easy control of culture conditions of LMS. LMS provide a model with high-degree of human *in-vitro* electrophysiology mimicry, due to their native structure with conduction proteins and intact cell-cell interactions. Feasibility of intracellular AP and extracellular FP recording techniques has now been demonstrated extensively, showing similar conduction and potential characteristics to *in-vivo* and other *in-vitro* modalities. As such, LMS provide a valid model for mimicry of cardiac arrhythmias, and will hopefully lead to future breakthroughs in the understanding of cardiac arrhythmia mechanisms and development of novel therapeutic options.

Author contributions

JA wrote the manuscript with aid of LZ and BE, under supervision of NDG and YT.

Conflict of interest

The authors declare that the research was conducted in the absence of any commercial or financial relationships that could be construed as a potential conflict of interest.

Publisher's note

References

Amesz, J. H., Groot, N. M. S., Langmuur, S. J. J., Rooij, M. M. M. M., Tiggeloven, V. P. C., Bogers, A. J. J. C., et al. (2022). Biomimetic cultivation of atrial tissue slices: A novel platform for *in-vitro* atrial arrhythmia studies. *Research Square*. doi:10.21203/rs.3.rs-1799902/v1

Bachtel, A. D., Gray, R. A., Stohlman, J. M., Bourgeois, E. B., Pollard, A. E., and Rogers, J. M. (2011). A novel approach to dual excitation ratiometric optical mapping of cardiac action potentials with di-4-ANEPPS using pulsed LED excitation. *IEEE Trans. Biomed. Eng.* 58, 2120–2126. doi:10.1109/TBME.2011.2148719

Barclay, C. J. (2005). Modelling diffusive O(2) supply to isolated preparations of mammalian skeletal and cardiac muscle. *J. Muscle Res. Cell Motil.* 26, 225–235. doi:10.1007/s10974-005-9013-x

Baxter, W. T., Mironov, S. F., Zaitsev, A. V., Jalife, J., and Pertsov, A. M. (2001). Visualizing excitation waves inside cardiac muscle using transillumination. *Biophys. J.* 80, 516–530. doi:10.1016/S0006-3495(01)76034-1

Berenfeld, O., and Efimov, I. (2019). Optical mapping. *Card. Electrophysiol. Clin.* 11, 495–510. doi:10.1016/j.ccep.2019.04.004

Biliczki, P., Boon, R. A., Girmatsion, Z., Bukowska, A., Ördög, B., Kaess, B. M., et al. (2019). Age-related regulation and region-specific distribution of ion channel subunits promoting atrial fibrillation in human left and right atria. *Europace* 21, 1261–1269. doi:10.1093/europace/euz135

Blackwell, D. J., Schmeckpeper, J., and Knollmann, B. C. (2022). Animal models to study cardiac arrhythmias. *Circ. Res.* 130, 1926–1964. doi:10.1161/CIRCRESAHA.122.320258

Brandenburger, M., Wenzel, J., Bogdan, R., Richardt, D., Nguemo, F., Reppel, M., et al. (2011). Organotypic slice culture from human adult ventricular myocardium. *Cardiovasc. Res.* 93, 50–59. doi:10.1093/cvr/cvr259

Burnashev, N. A., Edwards, F. A., and Verkhratsky, A. N. (1990). Patch-clamp recordings on rat cardiac muscle slices. *Pflugers Arch.* 417, 123–125. doi:10.1007/BF00370782

Bursac, N., Papadaki, M., White, J. A., Eisenberg, S. R., Vunjak-Novakovic, G., and Freed, L. E. (2003). Cultivation in rotating bioreactors promotes maintenance of cardiac myocyte electrophysiology and molecular properties. *Tissue Eng.* 9, 1243–1253. doi:10.1089/10763270360728152

Bussek, A., Wettwer, E., Christ, T., Lohmann, H., Camelliti, P., and Ravens, U. (2009). Tissue slices from adult mammalian hearts as a model for pharmacological drug testing. *Cell Physiol. Biochem.* 24, 527–536. doi:10.1159/000257528

Cabo, C., Pertsov, A. M., Baxter, W. T., Davidenko, J. M., Gray, R. A., and Jalife, J. (1994). Wave-front curvature as a cause of slow conduction and block in isolated cardiac muscle. *Circ. Res.* 75, 1014–1028. doi:10.1161/01.res.75.6.1014

Camelliti, P., Al-Saud, S. A., Smolenski, R. T., Al-Ayoubi, S., Bussek, A., Wettwer, E., et al. (2011). Adult human heart slices are a multicellular system suitable for electrophysiological and pharmacological studies. *J. Mol. Cell Cardiol.* 51, 390–398. doi:10.1016/j.yjmcc.2011.06.018

Chowdhury, R. A., Tzortzis, K. N., Dupont, E., Selvadurai, S., Perbellini, F., Cantwell, C. D., et al. (2018). Concurrent micro-to macro-cardiac electrophysiology in myocyte cultures and human heart slices. *Sci. Rep.* 8, 6947. doi:10.1038/s41598-018-25170-9

Davidenko, J. M., Kent, P. F., Chialvo, D. R., Michaels, D. C., and Jalife, J. (1990). Sustained vortex-like waves in normal isolated ventricular muscle. *Proc. Natl. Acad. Sci. U. S. A.* 87, 8785–8789. doi:10.1073/pnas.87.22.8785

Davidenko, J. M., Pertsov, A. V., Salomonsz, R., Baxter, W., and Jalife, J. (1992). Stationary and drifting spiral waves of excitation in isolated cardiac muscle. *Nature* 355, 349–351. doi:10.1038/355349a0

Davidenko, J. M., Salomonsz, R., Pertsov, A. M., Baxter, W. T., and Jalife, J. (1995). Effects of pacing on stationary reentrant activity. Theoretical and experimental study. *Circ. Res.* 77, 1166–1179. doi:10.1161/01.res.77.6.1166

De Groot, N. M. S., Shah, D., Boyle, P. M., Anter, E., Clifford, G. D., Deisenhofer, I., et al. (2022). Critical appraisal of technologies to assess electrical activity during atrial fibrillation: A position paper from the European heart rhythm association and European society of cardiology working group on eCardiology in collaboration with the heart rhythm society, asia pacific heart rhythm society, Latin American heart rhythm society and computing in cardiology. *Europace* 24, 313–330. doi:10.1093/europace/euab254

Del Nido, P. J., Glynn, P., Buenaventura, P., Salama, G., and Koretsky, A. P. (1998). Fluorescence measurement of calcium transients in perfused rabbit heart using rhod 2. *Am. J. Physiol.* 274, H728–H741. doi:10.1152/ajpheart.1998.274.2.H728

Efimov, I. R., Nikolski, V. P., and Salama, G. (2004). Optical imaging of the heart. *Circ. Res.* 95, 21–33. doi:10.1161/01.RES.0000130529.18016.35

Esfandyari, D., Idrissou, B. M. G., Hennis, K., Avramopoulos, P., Dueck, A., El-Battrawy, I., et al. (2022). MicroRNA-365 regulates human cardiac action potential duration. *Nat. Commun.* 13, 220. doi:10.1038/s41467-021-27856-7

Fast, V. G. (2005). Simultaneous optical imaging of membrane potential and intracellular calcium. *J. Electrocardiol.* 38, 107–112. doi:10.1016/j.jelectrocard.2005.06.023

Ferrera, R., Cuchet, D., Zaupa, C., Revol-Guyot, V., Ovize, M., and Epstein, A. L. (2005). Efficient and non-toxic gene transfer to cardiomyocytes using novel generation amplicon vectors derived from HSV-1. *J. Mol. Cell Cardiol.* 38, 219–223. doi:10.1016/j.yjmcc.2004.11.014

Fischer, C., Milting, H., Fein, E., Reiser, E., Lu, K., Seidel, T., et al. (2019). Publisher Correction: Long-term functional and structural preservation of precision-cut human myocardium under continuous electromechanical stimulation *in vitro*. *Nat. Commun.* 10, 532. doi:10.1038/s41467-019-08510-9

Fischer, E., Gottschalk, A., and Schüler, C. (2017). An optogenetic arrhythmia model to study catecholaminergic polymorphic ventricular tachycardia mutations. *Sci. Rep.* 7, 17514. doi:10.1038/s41598-017-17819-8

Garrey, W. E. (1914). The nature of fibrillary contraction of the heart.—its relation to tissue mass and form. *Am. J. Physiology-Legacy Content* 33, 397–414. doi:10.1152/ajplegacy.1914.33.3.397

Girmatsion, Z., Biliczki, P., Bonauer, A., Wimmer-Greinecker, G., Scherer, M., Moritz, A., et al. (2009). Changes in microRNA-1 expression and Ik1 up-regulation in human atrial fibrillation. *Heart rhythm* 6, 1802–1809. doi:10.1016/j.hrthm.2009.08.035

Girouard, S. D., Laurita, K. R., and Rosenbaum, D. S. (1996). Unique properties of cardiac action potentials recorded with voltage-sensitive dyes. *J. Cardiovasc. Electrophysiol.* 7, 1024–1038. doi:10.1111/j.1540-8167.1996.tb00478.x

Goldfracht, I., Protze, S., Shiti, A., Setter, N., Gruber, A., Shaheen, N., et al. (2020). Generating ring-shaped engineered heart tissues from ventricular and atrial human pluripotent stem cell-derived cardiomyocytes. *Nat. Commun.* 11, 75. doi:10.1038/s41467-019-13868-x

Grandi, E., Workman, A. J., and Pandit, S. V. (2012). Altered excitation-contraction coupling in human chronic atrial fibrillation. *J. Atr. Fibrillation* 4, 495. doi:10.4022/jafib.495

Habeler, W., Pouillot, S., Plancheron, A., Pucéat, M., Peschanski, M., and Monville, C. (2009). An *in vitro* beating heart model for long-term assessment of experimental therapeutics. *Cardiovasc Res.* 81, 253–259. doi:10.1093/cvr/cvn299

Halbach, M., Pillekamp, F., Brockmeier, K., Hescheler, J., Müller-Ehmsen, J., and Reppel, M. (2006). Ventricular slices of adult mouse hearts--a new multicellular *in vitro* model for electrophysiological studies. *Cell Physiol. Biochem.* 18, 1–8. doi:10.1159/000095132

Hamers, J., Sen, P., Merkus, D., Seidel, T., Lu, K., and Dendorfer, A. (2022). Preparation of human myocardial tissue for long-term cultivation. *J. Vis. Exp.* doi:10.3791/63964

Hannes, T., Halbach, M., Nazzal, R., Frenzel, L., Saric, T., Khalil, M., et al. (2008). Biological pacemakers: Characterization in an *in vitro* coculture model. *J. Electrocardiol.* 41, 562–566. doi:10.1016/j.jelectrocard.2008.06.017

Hansen, B. J., Zhao, J., Li, N., Zolotarev, A., Zakharkin, S., Wang, Y., et al. (2018). Human atrial fibrillation drivers resolved with integrated functional and structural imaging to benefit clinical mapping. *JACC Clin. Electrophysiol.* 4, 1501–1515. doi:10.1016/j.jacep.2018.08.024

Herron, T. J., Lee, P., and Jalife, J. (2012). Optical imaging of voltage and calcium in cardiac cells & tissues. *Circ. Res.* 110, 609–623. doi:10.1161/CIRCRESAHA.111.247494

Himmel, H. M., Bussek, A., Hoffmann, M., Beckmann, R., Lohmann, H., Schmidt, M., et al. (2012). Field and action potential recordings in heart slices: Correlation with established *in vitro* and *in vivo* models. *Br. J. Pharmacol.* 166, 276–296. doi:10.1111/j.1476-5381.2011.01775.x

Huang, D., and Li, J. (2011). The feasibility and limitation of patch-clamp recordings from neonatal rat cardiac ventricular slices. *Vitro Cell Dev. Biol. Anim.* 47, 269–272. doi:10.1007/s11626-011-9387-6

Jaimes, R., 3R. D., Walton, R. D., Pasdois, P., Bernus, O., Efimov, I. R., and Kay, M. W. (2016). A technical review of optical mapping of intracellular calcium within myocardial tissue. *Am. J. Physiol. Heart Circ. Physiol.* 310, H1388–H1401. doi:10.1152/ajpheart.00665.2015

Kanaporis, G., Martisiene, I., Jurevicius, J., Vosyliute, R., Navalinskas, A., Treinys, R., et al. (2012). Optical mapping at increased illumination intensities. *J. Biomed. Opt.* 17, 096007. doi:10.1117/1.JBO.17.9.096007

Kang, C., Qiao, Y., Li, G., Baechle, K., Camelliti, P., Rentschler, S., et al. (2016). Human organotypic cultured cardiac slices: New platform for high throughput preclinical human trials. *Sci. Rep.* 6, 28798. doi:10.1038/srep28798

Kappadan, V., Telele, S., Uzelac, I., Fenton, F., Parlitz, U., Luther, S., et al. (2020). High-resolution optical measurement of cardiac restitution, contraction, and fibrillation dynamics in beating vs. Blebbistatin-uncoupled isolated rabbit hearts. *Front. Physiol.* 11, 464. doi:10.3389/fphys.2020.00464

Kharbanda, R. K., Garcia-Izquierdo, E., Bogers, A., and De Groot, N. M. S. (2018). Focal activation patterns: Breaking new grounds in the pathophysiology of atrial fibrillation. *Expert Rev. Cardiovasc Ther.* 16, 479–488. doi:10.1080/14779072.2018.1485488

Knisley, S. B. (1995). Transmembrane voltage changes during unipolar stimulation of rabbit ventricle. *Circ. Res.* 77, 1229–1239. doi:10.1161/01.res.77.6.1229

Lang, D., Holzem, K., Kang, C., Xiao, M., Hwang, H. J., Ewald, G. A., et al. (2015). Arrhythmogenic remodeling of β2 versus β1 adrenergic signaling in the human failing heart. *Circ. Arrhythm. Electrophysiol.* 8, 409–419. doi:10.1161/CIRCEP.114.002065

Laughner, J. I., Ng, F. S., Sulkin, M. S., Arthur, R. M., and Efimov, I. R. (2012). Processing and analysis of cardiac optical mapping data obtained with potentiometric dyes. *Am. J. Physiol. Heart Circ. Physiol.* 303, H753–H765. doi:10.1152/ajpheart.00404.2012

Laurita, K. R., Katra, R., Wible, B., Wan, X., and Koo, M. H. (2003). Transmural heterogeneity of calcium handling in canine. *Circ. Res.* 92, 668–675. doi:10.1161/01.RES.0000062468.25308.27

Li, G., Brumback Brittany, D., Huang, L., Zhang David, M., Yin, T., Lipovsky Catherine, E., et al. (2022). Acute glycogen synthase kinase-3 inhibition modulates human cardiac conduction. *JACC Basic Transl. Sci.* 0, 1001–1017. doi:10.1016/j.jacbts.2022.04.007

Liu, Z., Klose, K., Neuber, S., Jiang, M., Gossen, M., and Stamm, C. (2020). Comparative analysis of adeno-associated virus serotypes for gene transfer in organotypic heart slices. *J. Transl. Med.* 18, 437. doi:10.1186/s12967-020-02605-4

Matiukas, A., Mitrea, B. G., Qin, M., Pertsov, A. M., Shvedko, A. G., Warren, M. D., et al. (2007). Near-infrared voltage-sensitive fluorescent dyes optimized for optical mapping in blood-perfused myocardium. *Heart rhythm* 4, 1441–1451. doi:10.1016/j.hrthm.2007.07.012

Miller, J. M., Meki, M. H., Elnakib, A., Ou, Q., Abouleisa, R. R. E., Tang, X.-L., et al. (2022). Biomimetic cardiac tissue culture model (CTCM) to emulate cardiac physiology and pathophysiology *ex vivo*. *Commun. Biol.* 5, 934. doi:10.1038/s42003-022-03919-3

Miller, J. M., Meki, M. H., Ou, Q., George, S. A., Gams, A., Abouleisa, R. R. E., et al. (2020). Heart slice culture system reliably demonstrates clinical drug-related cardiotoxicity. *Toxicol. Appl. Pharmacol.* 406, 115213. doi:10.1016/j.taap.2020.115213

Neher, E., and Sakmann, B. (1976). Single-channel currents recorded from membrane of denervated frog muscle fibres. *Nature* 260, 799–802. doi:10.1038/260799a0

Nong, Y., Zhang, C., Wei, L., Zhang, Z., Cheng, J., Wen, L., et al. (2013). *In situ* investigation of allografted mouse HCN4 gene-transfected rat bone marrow mesenchymal stromal cells with the use of patch-clamp recording of ventricular slices. *Cytotherapy* 15, 905–919. doi:10.1016/j.jcyt.2013.03.010

Nunez-Toldra, R., Kirwin, T., Ferraro, E., Pitoulis, F. G., Nicastro, L., Bardi, I., et al. (2022). Mechanosensitive molecular mechanisms of myocardial fibrosis in living myocardial slices. *Esc. Heart Fail* 9, 1400–1412. doi:10.1002/ehf2.13832

O'Shea, C., Kabir, S. N., Holmes, A. P., Lei, M., Fabritz, L., Rajpoot, K., et al. (2020). Cardiac optical mapping - state-of-the-art and future challenges. *Int. J. Biochem. Cell Biol.* 126, 105804. doi:10.1016/j.biocel.2020.105804

Omichi, C., Lamp, S. T., Lin, S. F., Yang, J., Baher, A., Zhou, S., et al. (2004). Intracellular Ca dynamics in ventricular fibrillation. *Am. J. Physiol. Heart Circ. Physiol.* 286, H1836–H1844. doi:10.1152/ajpheart.00123.2003

Ou, Q., Jacobson, Z., Abouleisa, R. R. E., Tang, X. L., Hindi, S. M., Kumar, A., et al. (2019). Physiological biomimetic culture system for pig and human heart slices. *Circ. Res.* 125, 628–642. doi:10.1161/CIRCRESAHA.119.314996

Peinkofer, G., Burkert, K., Urban, K., Krausgrill, B., Hescheler, J., Saric, T., et al. (2016). From early embryonic to adult stage: Comparative study of action potentials of native and pluripotent stem cell-derived cardiomyocytes. *Stem Cells Dev.* 25, 1397–1406. doi:10.1089/scd.2016.0073

Peinkofer, G., Hescheler, J., and Halbach, M. (2017). Murine short Axis ventricular heart slices for electrophysiological studies. *J. Vis. Exp.*, 55725. doi:10.3791/55725

Peinkofer, G., Maass, M., Pfannkuche, K., Sachinidis, A., Baldus, S., Hescheler, J., et al. (2021). Persistence of intramyocardially transplanted murine induced pluripotent stem cell-derived cardiomyocytes from different developmental stages. *Stem Cell Res. Ther.* 12, 46. doi:10.1186/s13287-020-02089-5

Perbellini, F., and Thum, T. (2019). Living myocardial slices: A novel multicellular model for cardiac translational research. *Eur. Heart J.* 41, 2405–2408. doi:10.1093/eurheartj/ehz779

Pertsov, A. M., Davidenko, J. M., Salomonsz, R., Baxter, W. T., and Jalife, J. (1993). Spiral waves of excitation underlie reentrant activity in isolated cardiac muscle. *Circ. Res.* 72, 631–650. doi:10.1161/01.res.72.3.631

Pillekamp, F., Halbach, M., Reppel, M., Pfannkuche, K., Nazzal, R., Nguemo, F., et al. (2009). Physiological differences between transplanted and host tissue cause functional decoupling after *in vitro* transplantation of human embryonic stem cell-derived cardiomyocytes. *Cell Physiol. Biochem.* 23, 65–74. doi:10.1159/000204093

Pillekamp, F., Reppel, M., Brockmeier, K., and Hescheler, J. (2006). Impulse propagation in late-stage embryonic and neonatal murine ventricular slices. *J. Electrocardiol.* 39, 425 e1–e4. doi:10.1016/j.jelectrocard.2006.02.008

Pillekamp, F., Reppel, M., Dinkelacker, V., Duan, Y., Jazmati, N., Bloch, W., et al. (2005). Establishment and characterization of a mouse embryonic heart slice preparation. *Cell Physiol. Biochem.* 16, 127–132. doi:10.1159/000087739

Pincus, M. H. (1933). Effect of pitressin and pitocin on oxygen consumption of excised tissue. *Proc. Soc. Exp. Biol. Med.* 30, 1171–1174. doi:10.3181/00379727-30-6843

Pitoulis, F. G., Hasan, W., Papadaki, M., Clavere, N. G., Perbellini, F., Harding, S. E., et al. (2020a). Intact myocardial preparations reveal intrinsic transmural heterogeneity in cardiac mechanics. *J. Mol. Cell Cardiol.* 141, 11–16. doi:10.1016/j.yjmcc.2020.03.007

Pitoulis, F. G., Nunez-Toldra, R., Xiao, K., Kit-Anan, W., Mitzka, S., Jabbour, R. J., et al. (2022). Remodelling of adult cardiac tissue subjected to physiological and pathological mechanical load *in vitro*. *Cardiovasc Res.* 118, 814–827. doi:10.1093/cvr/cvab084

Pitoulis, F. G., Watson, S. A., Perbellini, F., and Terracciano, C. M. (2020b). Myocardial slices come to age: An intermediate complexity *in vitro* cardiac model for translational research. *Cardiovasc Res.* 116, 1275–1287. doi:10.1093/cvr/cvz341

Reppel, M., Pillekamp, F., Lu, Z. J., Halbach, M., Brockmeier, K., Fleischmann, B. K., et al. (2004). Microelectrode arrays: A new tool to measure embryonic heart activity. *J. Electrocardiol.* 37, 104–109. doi:10.1016/j.jelectrocard.2004.08.033

Rubach, M., Adelmann, R., Haustein, M., Drey, F., Pfannkuche, K., Xiao, B., et al. (2014). Mesenchymal stem cells and their conditioned medium improve integration of purified induced pluripotent stem cell-derived cardiomyocyte clusters into myocardial tissue. *Stem Cells Dev.* 23, 643–653. doi:10.1089/scd.2013.0272

Schaffer, P., Ahammer, H., Müller, W., Koidl, B., and Windisch, H. (1994). Di-4-ANEPPS causes photodynamic damage to isolated cardiomyocytes. *Pflügers Arch.* 426, 548–551. doi:10.1007/BF00378533

Schneider-Warme, F., Johnston, C. M., and Kohl, P. (2017). Organotypic myocardial slices as model system to study heterocellular interactions. *Cardiovasc. Res.* 114, 3–6. doi:10.1093/cvr/cvx215

Shattock, M. J., Bullock, G., Manning, A. S., Young, M., and Hearse, D. J. (1983). Limitations of the isolated papillary muscle as an experimental model: A metabolic, functional and ultrastructural study. *Clin. Sci.* 64, 4P. doi:10.1042/cs064004pa

Sim, I., Bishop, M., O'Neill, M., and Williams, S. E. (2019). Left atrial voltage mapping: Defining and targeting the atrial fibrillation substrate. *J. interventional cardiac Electrophysiol. Int. J. Arrhythm. pacing* 56, 213–227. doi:10.1007/s10840-019-00537-8

Spach, M. S., Barr, R. C., Serwer, G. A., Kootsey, J. M., and Johnson, E. A. (1972). Extracellular potentials related to intracellular action potentials in the dog Purkinje system. *Circulation Res.* 30, 505–519. doi:10.1161/01.res.30.5.505

Thomas, R. C., Singh, A., Cowley, P., Myagmar, B. E., Montgomery, M. D., Swigart, P. M., et al. (2016). A myocardial slice culture model reveals alpha-1A-adrenergic receptor signaling in the human heart. *JACC Basic Transl. Sci.* 1, 155–167. doi:10.1016/j.jacbts.2016.03.005

van der Does, L. J. M. E., and De Groot, N. M. S. (2017). Inhomogeneity and complexity in defining fractionated electrograms. *Heart rhythm* 14, 616–624. doi:10.1016/j.hrthm.2017.01.021

Venkataraman, R., Holcomb, M. R., Harder, R., Knollmann, B. C., and Baudenbacher, F. (2012). Ratiometric imaging of calcium during ischemia-reperfusion injury in isolated mouse hearts using Fura-2. *Biomed. Eng. Online* 11, 39. doi:10.1186/1475-925X-11-39

Wang, K., Lee, P., Mirams, G. R., Sarathchandra, P., Borg, T. K., Gavaghan, D. J., et al. (2015). Cardiac tissue slices: Preparation, handling, and successful optical mapping. *Am. J. Physiol. Heart Circ. Physiol.* 308, H1112–H1125. doi:10.1152/ajpheart.00556.2014

Wang, K., Terrar, D., Gavaghan, D. J., Mu-U-Min, R., Kohl, P., and Bollensdorff, C. (2014). Living cardiac tissue slices: An organotypic pseudo two-dimensional model for cardiac biophysics research. *Prog. Biophysics Mol. Biol.* 115, 314–327. doi:10.1016/j.pbiomolbio.2014.08.006

Warren, M., Huizar, J. F., Shvedko, A. G., and Zaitsev, A. V. (2007). Spatiotemporal relationship between intracellular Ca2+ dynamics and wave fragmentation during ventricular fibrillation in isolated blood-perfused pig hearts. *Circ. Res.* 101, e90–e101. doi:10.1161/CIRCRESAHA.107.162735

Watanabe, M., Feola, I., Majumder, R., Jangsangthong, W., Teplenin, A. S., Ypey, D. L., et al. (2017). Optogenetic manipulation of anatomical re-entry by light-guided generation of a reversible local conduction block. *Cardiovasc. Res.* 113, 354–366. doi:10.1093/cvr/cvx003

Watson, S. A., Dendorfer, A., Thum, T., and Perbellini, F. (2020). A practical guide for investigating cardiac physiology using living myocardial slices. *Basic Res. Cardiol.* 115, 61. doi:10.1007/s00395-020-00822-y

Watson, S. A., Duff, J., Bardi, I., Zabielska, M., Atanur, S. S., Jabbour, R. J., et al. (2019). Biomimetic electromechanical stimulation to maintain adult myocardial slices *in vitro*. *Nat. Commun.* 10, 2168. doi:10.1038/s41467-019-10175-3

Watson, S. A., Scigliano, M., Bardi, I., Ascione, R., Terracciano, C. M., and Perbellini, F. (2017). Preparation of viable adult ventricular myocardial slices from large and small mammals. *Nat. Protoc.* 12, 2623–2639. doi:10.1038/nprot.2017.139

Wen, Q., Gandhi, K., Capel, R. A., Hao, G., O'Shea, C., Neagu, G., et al. (2018). Transverse cardiac slicing and optical imaging for analysis of transmural gradients in membrane potential and Ca(2+) transients in murine heart. *J. Physiol.* 596, 3951–3965. doi:10.1113/JP276239

Wilkinson, R. N., Jopling, C., and Van Eeden, F. J. (2014). Zebrafish as a model of cardiac disease. *Prog. Mol. Biol. Transl. Sci.* 124, 65–91. doi:10.1016/B978-0-12-386930-2.00004-5

Winfree, A. T. (1994). Electrical turbulence in three-dimensional heart muscle. *Science* 266, 1003–1006. doi:10.1126/science.7973648

Wokosin, D. L., Loughrey, C. M., and Smith, G. L. (2004). Characterization of a range of fura dyes with two-photon excitation. *Biophys. J.* 86, 1726–1738. doi:10.1016/S0006-3495(04)74241-1

frontiers | Frontiers in Physiology

TYPE Review
PUBLISHED 13 February 2023
DOI 10.3389/fphys.2023.1132533

OPEN ACCESS

EDITED BY
Jolanda Van Der Velden,
VU Medical Center, Netherlands

REVIEWED BY
Louise Reilly,
University of Wisconsin-Madison,
United States
Anna Weinzinger,
University of Vienna, Austria

*CORRESPONDENCE
Barbara Ribeiro Oliveira-Mendes,
barbara.ribeiro@univ-nantes.fr

†These authors have contributed equally to this work

SPECIALTY SECTION
This article was submitted to Cardiac Electrophysiology,
a section of the journal
Frontiers in Physiology

RECEIVED 27 December 2022
ACCEPTED 30 January 2023
PUBLISHED 13 February 2023

CITATION
Alameh M, Oliveira-Mendes BR, Kyndt F, Rivron J, Denjoy I, Lesage F, Schott J-J, De Waard M and Loussouarn G (2023), A need for exhaustive and standardized characterization of ion channels activity. The case of $K_V11.1$.
Front. Physiol. 14:1132533.
doi: 10.3389/fphys.2023.1132533

A need for exhaustive and standardized characterization of ion channels activity. The case of $K_V11.1$

Malak Alameh[1,2†], Barbara Ribeiro Oliveira-Mendes[1*†], Florence Kyndt[1†], Jordan Rivron[1], Isabelle Denjoy[3], Florian Lesage[2], Jean-Jacques Schott[1], Michel De Waard[1,2†] and Gildas Loussouarn[1†]

[1]CNRS, INSERM, l'institut du thorax, Nantes Université, CHU Nantes, Nantes, France, [2]Labex ICST, INSERM, CNRS, Institut de Pharmacologie Moléculaire et Cellulaire, Université Côte d'Azur, Valbonne, France, [3]Service de Cardiologie et CNMR Maladies Cardiaques Héréditaires Rares, Hôpital Bichat, Paris, France

hERG, the pore-forming subunit of the rapid component of the delayed rectifier K^+ current, plays a key role in ventricular repolarization. Mutations in the *KCNH2* gene encoding hERG are associated with several cardiac rhythmic disorders, mainly the Long QT syndrome (LQTS) characterized by prolonged ventricular repolarization, leading to ventricular tachyarrhythmias, sometimes progressing to ventricular fibrillation and sudden death. Over the past few years, the emergence of next-generation sequencing has revealed an increasing number of genetic variants including *KCNH2* variants. However, the potential pathogenicity of the majority of the variants remains unknown, thus classifying them as variants of uncertain significance or VUS. With diseases such as LQTS being associated with sudden death, identifying patients at risk by determining the variant pathogenicity, is crucial. The purpose of this review is to describe, on the basis of an exhaustive examination of the 1322 missense variants, the nature of the functional assays undertaken so far and their limitations. A detailed analysis of 38 hERG missense variants identified in Long QT French patients and studied in electrophysiology also underlies the incomplete characterization of the biophysical properties for each variant. These analyses lead to two conclusions: first, the function of many hERG variants has never been looked at and, second, the functional studies done so far are excessively heterogeneous regarding the stimulation protocols, cellular models, experimental temperatures, homozygous and/or the heterozygous condition under study, a context that may lead to conflicting conclusions. The state of the literature emphasizes how necessary and important it is to perform an exhaustive functional characterization of hERG variants and to standardize this effort for meaningful comparison among variants. The review ends with suggestions to create a unique homogeneous protocol that could be shared and adopted among scientists and that would facilitate cardiologists and geneticists in patient counseling and management.

KEYWORDS

***KCNH2* gene, variants, electrophysiology, long QT syndrome, phenotyping**

hERG phenotyping, why?

The Long QT syndrome (LQTS) is a cardiac disorder characterized by abnormally prolonged ventricular repolarization that results in episodic ventricular tachyarrhythmias sometimes leading to ventricular fibrillation and sudden death in otherwise healthy persons (Charpentier et al., 2010). LQTS is thus a lethal disorder. Symptomatic patients left without therapy had a high mortality rate, 21% within 1 year from the first syncope (Schwartz, 1985). However, mortality rate in properly treated patients has now declined to around 1% over a 10-year period (Schwartz, 2013). Since LQTS is associated with sudden cardiac death, identifying patients at risk is instrumental. Uncovering a pathogenic variant, in one of the genes known to be associated with LQTS (e.g. *KCNH2* gene encoding hERG channel), allows identifying the relatives at risk, in the proband's family (Alders et al., 1993) (Figure 1A), even when ECGs are not always strongly evocative of the pathology (cf. patient III-1 and patient III-4 in Figure 1B). In absence of robust segregation data, determining the pathogenicity of the variant in the gene sequence of the proband may not be simple. Such variant may be a benign polymorphism that has nothing to do with the patient Long QT syndrome. Hence, *in vitro* functional studies confirming the pathogenicity of the variant will provide critical information.

The American College of Medical Genetics and Genomics (ACMG), the Association for Molecular Pathology (AMP) and the College of American Pathologists (CAP) proposed guidelines that compiles all the parameters that contribute to predict the potential pathogenicity of a given variant, namely the patient phenotype, the segregation data, the conservation of the varying sequence across species, the population data, the *in vitro* functional data, the nature of the amino acids implicated in the sequence variation, the position of the amino-acids, etc. (Richards et al., 2015). The final score classifies a given sequence variation according to five categories: "pathogenic," "likely pathogenic," "uncertain significance," "likely benign," and "benign."

The "uncertain significance" (VUS) usually occurs in two situations: when there are conflicting results from the different observables, or when there is insufficient evidence, as is often the case for novel missense variants. Intuitively, it seems reasonable that functional data will be significantly helpful to decrease the number of cases of "uncertain significance." A theoretical approach proposed by Brnich and collaborators used an algorithm to calculate all combinations of evidence. Using this systematic counting approach, they estimate how functional data allows decreasing the number of VUS. They convincingly illustrate that a majority of VUS could be reclassified with the addition of solid functional data (Brnich et al., 2018). This observation motivates functional studies of the variants identified so far. With the advent of the Next-Generation Sequencing (NGS), the number of variants affecting gene sequences are literally exploding: 99% of the 4.6 million reported missense variations in the Genome Aggregation Database (http://gnomad.broadinstitute.org/) (Lek et al., 2016) are rare (allele frequency <0.005). Interpreting these variants represents a significant roadblock. Only 2% of these variants have a clinical interpretation in ClinVar (Landrum et al., 2014). This observation urges the development of high-throughput and standardized methods for functional characterization of the variants.

At the writing of this review, 2434 *KCNH2* variants are referenced in Clinvar https://www.ncbi.nlm.nih.gov/clinvar/, of which 1832 are associated to LQTS. *KCNH2* gene is associated with type 2 Long QT syndrome, but also with Atrial Fibrillation (Hayashi et al., 2015) and short QT (Brugada et al., 2004). It represents the second most important genetic cause of Long QT syndrome, with an estimated prevalence between 25% and 30% of all cases (Schwartz et al., 2001; Kolder et al., 2015; Kutyifa et al., 2018). Figure 2 illustrates the acceleration of the publication of *KCNH2* variants over the years. As mentioned above, 2434 *KCNH2* variants are referenced in Clinvar, including 1135 missense variants. Since other variants (frameshift, non-sense, splice site) are most often pathogenic, we focused our analyses on missense variants. Among these 1135 missense variants, 962 are classified as VUS, representing approximately 85%.

This review aims at describing the nature of the functional assays undertaken so far and their limits, based on an exhaustive scan of these 1135 missense variants and additional 187 coming from the French network CARDIOGEN, not yet in ClinVar. We also looked at some specific details of the functional assays, in a smaller sample of 112 variants issued from the same French database for type 2 Long QT syndrome patients. This review then comes with new propositions to generate standardized protocols that will help cardiologists and geneticists for patient counseling in face of the increasing number of variants.

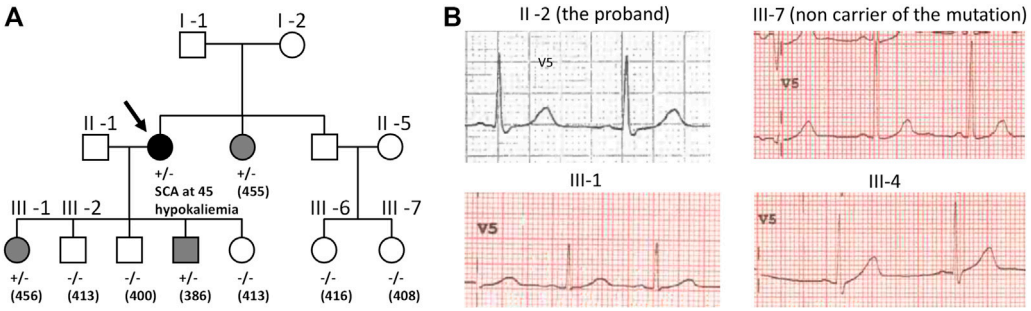

FIGURE 1
(A) Family pedigree harboring the c.2504G>C p.Arg835Pro *KCNH2* mutation that leads to hERG loss of function (Oliveira-Mendes et al., 2021). The proband (arrow) presented a sudden cardiac arrest (SCA) due to ventricular fibrillation at 45 during an episode of hypokalemia requiring an implantable cardiac defibrillator (ICD). Post-Resuscitation ECG was normal. Family members cascade screening detected the *KCNH2* variation in her sister and two children III-1 and III-4; QTc interval values (in ms) are shown between parentheses. Squares depict male subjects; circle, female subject; open symbols, unaffected members; solid black symbol, affected members; grey symbol, mild phenotype. **(B)** ECG tracings in lead V5 of the proband (II-2), a non-carrier niece (III-7), a daughter (III-1) and a son (III-4) who are both carriers of the variant and showing mild LQT2 phenotype (T waves: low amplitude amplitude for III-1 and very slightly bifid for III-4).

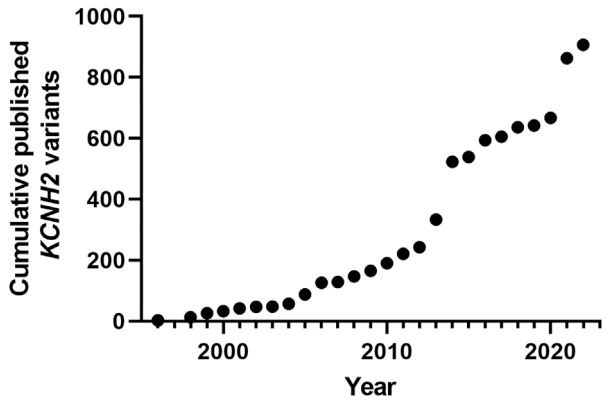

FIGURE 2
Cumulative published *KCNH2* variants. Years are Pubmed publication years. The two major increases correspond to high-throughput studies, the first focusing on membrane trafficking (Anderson et al., 2014), and the second focusing on ion channel activity with automated patch-clamp experiments (Ng et al., 2020).

Heterogeneity of the functional assays

As mentioned above, functional data being very helpful to reclassify the VUS, a functional evaluation of hundreds of variants is necessary. Also, the methods of acquisition of these functional data have to be scrupulously standardized to faithfully evaluate the pathogenicity of any variant. In this review, our aim was to establish how far we are from an extensive and standardized evaluation of hERG variants.

We performed an exhaustive scan of the literature on the 1322 missense variants (Figure 3A). We can distinguish two kind of functional assays: i) trafficking assays which are only estimating eventual alteration of hERG channel membrane targeting, without giving any keys on channel activity once at the membrane; these assays presented the advantage of between compatible with high-throughput characterization, early on (Anderson et al., 2014). ii) Electrophysiological assays, giving precise and global information on the ion channel activity, whatever the mechanistic nature of the alteration, trafficking and/or gating. We observed that functional assays were performed for only 37% (484/1322) of the variants. In 24% of cases, both trafficking and electrical activity of the variant were evaluated (311/1322) (Figure 3B). In 6% of cases, only electrophysiological experiments were performed, with no parallel trafficking study (74/1322).

Regarding functional studies, it is important to note that patch-clamp is the gold standard for assessing mutations affecting hERG functionality but to date, not all studies have extensively characterized all biophysical aspects. To understand this point, one should know that hERG channels present two gates (one activation gate and one inactivation gate) with specific voltage-dependence and kinetics. In the simplest case, maximal current is evaluated when both activation and inactivation gates are open. If this maximal current is lower in the variant as compared to WT hERG channel, there is a loss of function (Delisle et al., 2005). But despite preserved maximal currents, a potential loss of function of the channel activity may express as an alteration of the voltage-dependence of at least one of the gates: for example, a shift of the activation curve to positive potentials, necessitating greater depolarization to activate the channel, such as for the N470D mutation (Lin et al., 2010). It can also express as a change in channel opening or closing kinetics. For example, hERG N33T, R56Q, G903R, P1075L are associated with faster deactivation kinetics (closing of the activation gate) without any modification of the maximal current amplitude (Ng et al., 2020).

Thus, it is possible that a mutation alters a single parameter among all known biophysical parameters, namely the maximal current amplitude, the half-activation potential, the slope of the activation curve, the half-inactivation potential, the slope of the inactivation curve, activation and deactivation kinetics, inactivation and recovery from inactivation kinetics, and also the ion selectivity. This indicates how critical it is to study systematically all channel parameters of a given variant.

On a sample of 38 variants that were studied in electrophysiology, we examined how exhaustive all these parameters were characterized. These 38 variants were studied in electrophysiology among a total of 112 missense variants (i.e., 34%) collected in the national database of long QT patients constituted by a network of French Centers of Reference on cardiac arrhythmias (including the ones from Nantes

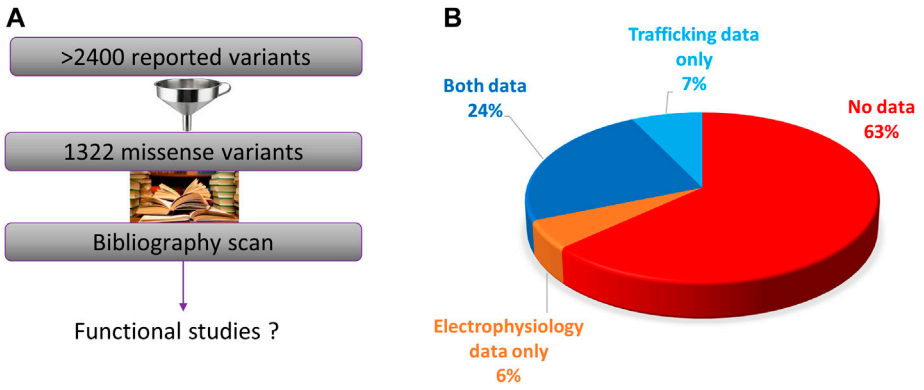

FIGURE 3
(A). Diagram presenting the principle of the present literature analysis of all the hERG missense variants. **(B)**. Pie chart presenting the percentage of the variants that were not studied at all, studied in electrophysiology only, trafficking studies only, or both (from analysis of Supplemental Table S1).

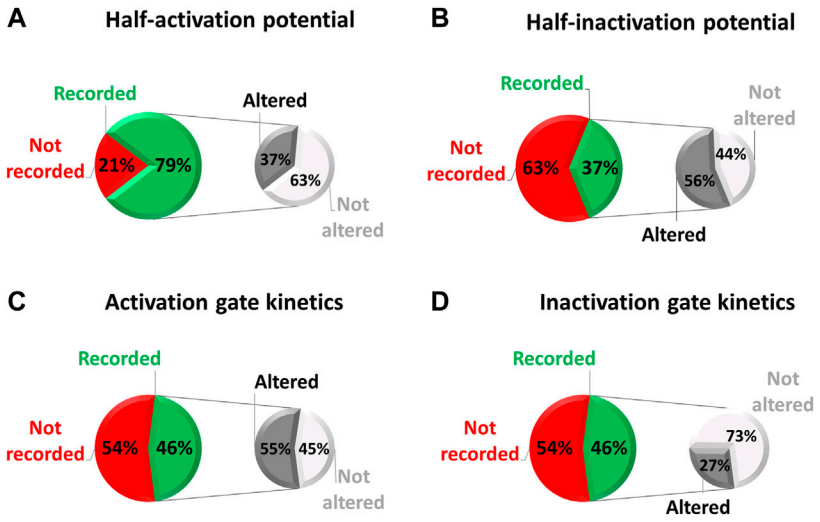

FIGURE 4
Pie chart presenting, among the missense variants referenced in the French network CARDIOGEN (n = 112) and studied in electrophysiology (n = 38), the percentage of which half-activation potential **(A)**, half-inactivation potential **(B)**, activation gate kinetics **(C)**, and inactivation gate kinetics **(D)** were studied, and when studied, the percentage of variants showing an alteration of the given parameter (from analysis of Supplemental Table S2).

University Hospital and the "Assistance Publique-Hôpitaux de Paris"). These Centers of Reference belong to the French network CARDIOGEN, which has developed a common database extensively reporting clinical and genetic information from all identified French cases. In the case of these 38 missense variants we are far from an extensive study of hERG biophysical parameters (red/green pie charts of Figure 4), despite the evidence that indeed all of the biophysical parameters can be affected individually (monochrome pie charts).

Experimental temperatures used for functional studies

A literature scan of electrophysiological studies of the 1135 missense variants also illustrates major variations in the temperature applied during two distinct steps of the evaluation of channel variants pathogenicity: 1) during hERG channel expression by the cultured cells, after introduction of the DNA/RNA encoding the channel and 2) during the electrophysiological characterization of the variants.

Temperature at which the cells are cultured during hERG channel expression mainly depends on the expression model used, the two main models being *Xenopus laevis* oocytes, which require incubation at low temperature (12°C–18°C) and mammalian cells, typically incubated at 37°C. Noteworthy, incubation at room temperature rescues the impaired trafficking of many hERG channel variants, as observed by hERG protein glycosylation which is an indicator of correct cell trafficking (Anderson et al., 2014). Functionally, incubation at room temperature may recover channel current amplitudes to values at least similar to WT values (Paulussen et al., 2002). With this knowledge in hand, it seems clear that, *Xenopus laevis* oocytes as the expression model, were not always able to make a logical link between the variant properties and Long QT syndrome.

For example, expression of the LQTS variant R534C, in *X. laevis* oocytes, surprisingly leads to a shift in the activation curve to negative value, predicting thus a shortening in the action potential by a computer model (Nakajima, 1999). In contrast, in mammalian CHO cells, kept at 37°C, R534C is associated with a major decrease in maximal current amplitude that is due to reduced trafficking (Oliveira-Mendes et al., 2021). To reconcile these data, it was shown in HEK293 cells that this reduced trafficking is rescued by incubating the cells at 27°C during the expression time course (Anderson et al., 2006). Since *X. laevis* oocytes are maintained at 12°C–18°C after cRNA injection, it is likely that this temperature favors membrane trafficking of the variant and hence masked the trafficking defect in the aforementioned study (Nakajima, 1999). Thus, the *X. laevis* oocyte model, which was used in 16% of the electrophysiology studies (cf. Figure 6 below) is clearly not the most relevant model to study the pathogenicity of hERG variants and should be avoided in the future.

Regarding the electrophysiological characterization of the variants, they are most frequently done at room temperature (Figure 5). For *Xenopus* oocytes, 37°C is largely above the physiological temperature and hardly tolerable by this cell type (Bienz and Gurdon, 1982). For mammalian cells, room temperature is paradoxically preferred for a technical reason: the success of the experiments (e.g., seal stability) is much higher at room temperature than at 37°C, as illustrated in a study using automated patch-clamp (Ranjan et al., 2019), which shows a success rate of 15% as compared to 80% at room temperature. However, hERG channel biophysical properties, and in particular kinetics such as activation and inactivation kinetics are highly temperature-dependent (Vandenberg et al., 2006). To properly report the biophysical properties of a given hERG variant, it would be wise to study it at 37°C. Alternatively, it would be interesting to keep studying the variant at room temperature and develop a method that would allow extrapolating the evolution of the channel properties with

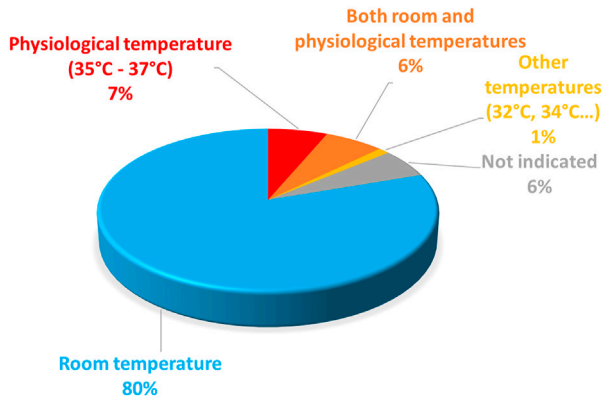

FIGURE 5
Pie chart presenting the percentage of hERG missense variants (among all the published missense variants), studied at room temperature, at physiological temperature, at both temperatures, or particular temperatures (32°C or 34°C). This chart includes all missense variants studied in patch-clamp experiment performed in mammalian cells (from analysis of Supplemental Table S1).

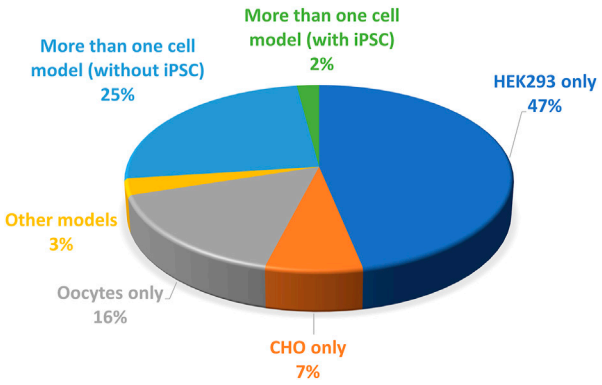

FIGURE 6
Pie chart presenting the percentage of the cell models used to study the *KCNH2* variants (from analysis of Supplemental Table S1).

rising temperatures from room temperature to physiological temperature.

Use of various cell models

Another source of variability is the cell model of study. Three categories of models are used for hERG variants phenotyping (Figure 6):

(i) A non-mammalian model, *X. laevis* oocytes which generate large currents, in the µA range, but have to be maintained at non-physiological temperature which may rescue some mutant impaired trafficking, as developed above. The validity of this model has already been discussed.

(ii) Mammalian cell lines that are easy to maintain and animal-free (van der Velden et al., 2022). Two cell lines are mainly used (CHO, HEK-293). They are cultured at physiological temperature, which represents a clear advantage over *X. laevis* oocytes. The presence of endogenous currents, in these models, but also in *X. laevis* oocytes, may interfere with measurements when studying mutants which generate currents of low amplitudes. To that respect CHO cells are a good model since they expressed minimal voltage-gated currents, when compared to other cells such as HEK-293 cells (Yu and Kerchner, 1998). On the down side, CHO cells proliferate twice faster as HEK-293 cells, potentially leading to much lower currents 48 h after transfection because transfected DNA would be split between more cells (Abaandou et al., 2021). This has to be considered, especially in automated patch-clamp experiments in which one cannot select efficiently transfected cells with a GFP-like reporter gene, as it is routinely done in conventional patch-clamp. Without reporter gene and with high rates of division such as in CHO cells, amplitude may then be too low in many cells for precise characterization of the biophysical parameters.

(iii) Induced pluripotent stem cells developed by Shinya Yamanaka (Takahashi and Yamanaka, 2006) allow the generation of human cardiomyocytes, iPS-CMs (Jouni et al., 2015) that constitute a very relevant model since their genotype is much closer to the patient's than transfected cells such as CHO or HEK-293 cells. These latter cell lines may be especially limited if the mutant phenotype depends on the presence of a specific auxiliary protein that is not expressed in the cell line, but would be present in native cardiomyocyte. For instance, a study on iPS-derived cardiomyocytes suggests the physiological relevance of the splice variant hERG 1b, which is shorter than the original isolate hERG 1a. hERG 1b, that lacks the N-terminal PAS domain, efficiently associates with hERG 1a, and modifies the generated IKr current (Jones et al., 2014). It remains possible that hERG 1b modifies to some extent the functional effect of at least some variants. For instance, in iPSC-derived cardiomyocytes, the H70R variant of the PAS domain leads to an approximately 50% decrease in current amplitude and an acceleration in deactivation (Feng et al., 2021). At the molecular level, the mutation induces a decrease in hERG 1a membrane trafficking but logically, there is a normal trafficking of hERG 1b lacking the PAS domain and thus the H70R mutation. Such an imbalance between hERG 1b (normal) and hERG 1a (decreased) may theoretically have an impact on the current characteristics.

Are the results obtained with iPS-CMs very different than those obtained in a simpler model and do they justify the use of the more complex, time consuming and costly iPS-derived cardiomyocytes? In *X. laevis* oocytes, the aforementioned mutation (H70R) led to similar deactivation alteration, but had a lower impact (around 25% decrease in homozygous condition) on current amplitude (Chen et al., 1999). Given that *X. laevis* oocytes are not the most relevant model for trafficking-deficient mutants, as mentioned above, the H70R mutation should be extensively studied in patch-clamp, using a simple mammalian model (HEK-293, CHO). So far H70R has only been studied by Western blots from HEK-293 cells, but this technique showed opposing results: one study suggests that H70R hERG is trafficking-deficient (Anderson et al., 2014), whereas another study suggests the opposite (Harley et al., 2012). Hence, it is critical to test whether or not the activities of a given hERG

TABLE 1 Major modifications induced by a variant across various models.

	Xenopus oocytes	CHO, HEK-293, COS-7	iPS-CMs	References
R56Q		2-3x acceleration in deactivation	2-3x acceleration in deactivation	Liu and Trudeau (2015)
H70R	25% decrease in current		50% decrease in current	Chen et al. (1999), Feng et al. (2021)
	2x acceleration in deactivation		2x acceleration in deactivation	
R534C	No decrease in current in heterozygous condition		50% decrease in current	Nakajima (1999), Mesquita et al. (2019)
A561P		70% decrease in current in heterozygous condition	50% decrease in current	Bellocq et al. (2004), Jouni et al. (2015)
		10-mV shift of the activation curve	No shift of the activation curve	
G601S	40% decrease in current	85% decrease in current		Furutani et al. (1999)

variant evaluated in transfected mammalian cells line and iPS-CMs hERG are very different. Table 1 compares major modifications induced by a variant across various models. More differences can be observed in the *X. laevis* oocytes model as compared to the iPS-CMs model, probably because of the temperature of incubation that rescues the mutation-induced impaired trafficking of the channel, thereby masking or underestimating the effect of the mutation.

Adding a level of complexity, it is possible that the current level is not always a quantitative marker of the pathology, even in iPS-CMs. One study identified two modifier genes in a family presenting a highly variable severity of the LQT among its members (carrying the R752W mutant), but similar hERG current levels in their corresponding iPS-CMs (Chai et al., 2018). Another study was also able to mimic, at the action potential level, the patient-dependent severity of the LQTS due to the L552S mutation in hERG despite similar current levels in asymptomatic vs. symptomatic patients iPS-CMs (Shah et al., 2020). Nevertheless, more studies are needed to firmly conclude on the added value of the more complex, time-consuming and costly iPS-derived cardiomyocytes in most of the variants. Noteworthy, patient-specific iPS-CMs is not a resource that all investigators have access to. Another option is to use commercially available iPS-CMs cell lines which can be infected with hERG variants to study their biophysical characteristics in a cardiac cell type (Liu and Trudeau, 2015).

The use of iPS-CMs may be more critical in other pathologies such as the Brugada syndrome in which the cell environment/patient's genome is more influent. For instance, iPS-CMs generated from six Brugada patients with different genetic backgrounds, revealed the same I_{Na} current abnormality in the six cell lines, independently of the presence (2 Brugada patients) or absence (4 Brugada patients) of a mutation in the *SCN5A* gene, coding for the sodium channel $Na_V1.5$ (Al Sayed et al., 2021). This suggests that iPS-CMs are critical to study the mechanisms implicated in complex polygenic pathologies such as the Brugada syndrome (Barc et al., 2022).

The generation of iPS-CMs may in the future allow identifying the impact of a variant in a hERG channel regulator, such as KCNE2 which has been proposed as a potential accessory subunit for hERG, but this remains to be confirmed (Eldstrom and Fedida, 2011). If KCNE2 is confirmed as an auxiliary subunit, co-transfection of hERG with this subunit in a mammalian cell line may add more precision to this kind of hERG phenotyping by allowing the system to be more similar to the patient cardiomyocyte. On the other hand, any hypothetical accessory subunit has to be carefully validated first. Moreover, relative expression of hERG vs. the auxiliary subunit has to be carefully calibrated since non-physiological overexpression of this subunit can rescue a loss of function mutation on the channel subunit, and underestimate the effect of a mutant, a story quite similar to the use of room temperature in *X. laevis* oocytes experiments described above (Liu et al., 2016).

At last, some articles use neonatal cardiomyocytes, as in a study which described similar effect of the G601S and N470D mutations on the current characteristics as in HEK-293 cells, for instance on the activation curve and deactivation kinetics (Lin et al., 2010).

Is it possible to easily mimic heterozygosity in high-throughput systems?

Importantly, most LQT2 mutation carriers are heterozygous. For instance, less than 1% of probands registered in the French database from the CARDIOGEN network are homozygous for a mutation. In order to mimic as much as possible, the condition of the patient, it is useful 1) to determine if there is an equal expression of both alleles, which seems to be the case (Shah et al., 2020), and 2) to be able to reproduce in the model of study this equal expression of both alleles.

In conventional patch-clamp study, equal expression of both alleles is achieved by transfecting cells with the equal amount of the two DNAs (Ficker et al., 2000; Chevalier, 2001; Saenen et al., 2007; Hayashi et al., 2009; McBride et al., 2013). Mimicking such heterozygosity is not always performed, some studies only comparing the WT and mutant condition, without testing the WT + mutant co-expression (22% of all variants studied in electrophysiology are only studied in the homozygote condition, cf. Supplemental Table S1). Classical transient transfections, such as FuGENE, Lipofectamine based transfections, are not very efficient in term of the percentage of transfected cells, requiring the co-expression of a reporter such as GFP to select the transgene expressing cells. In a high-throughput system, it is not possible to detect and select a transfected cell, leading to two major options: i) electroporation, which is much more efficient than chemical transfection in term of the percentage of transfected cells, has been successfully used for KCNQ1 high-throughput phenotyping (Vanoye et al., 2018). ii) A cell line stably expressing the WT or mutant channel

can overcome the need of transient transfection and was used for hERG high-throughput phenotyping (Ng et al., 2020). Yet, one first limit is that production of stable cell lines is time consuming (several steps of antibiotic selections). Second, such strategy allows the integration of a unique plasmid in cells, representing a limit as compared to transient transfection, which allows transfection of 2 (or more) plasmids, as mentioned above. Thus, the heterozygote situation can be mimicked only by the use of a plasmid with two expression cassettes, provided that expressions of the two cDNA are equivalent. This requirement does not seem to be respected in several studies that make use of bicistronic plasmids containing an Internal Ribosome Entry Site (IRES), in which expression of the first cassette is at least five time greater than expression in the second cassette (Mizuguchi et al., 2000). Of note, a study suggests it may be possible to reduce the difference by mutating the IRES (Al-Allaf et al., 2019). If this strategy is successfully applied for equal expression of hERG cDNA in the two cassettes, it would be a worthwhile recommendation for the study of hERG variants.

Artifactual heterogeneity of the recordings

It is critical to identify the potential artifacts leading to misevaluation of the effects of a given variant on the current characteristics and hence on the channel biophysical properties. A study using a mathematical model elegantly suggested that variability in hERG-channel-independent parameters (such as leak current, series resistance, etc.) is responsible for a major variability in the observed biophysical parameters (Lei et al., 2020). We also mathematically modeled the variability of the biophysical parameters of a voltage-dependent potassium channel, studied in conventional and high-throughput patch-clamp channels (Montnach et al., 2021). From the results we obtained, we proposed to reduce such variability, by limiting maximal current amplitude and series resistance. Beyond such maximal values, insufficient voltage-clamp generates variability in the voltage-dependence of activation. Our model also pinpoints that a phenomenon observed in several K_v channels and named "delayed repolarization" is in fact an artifactual property due to insufficient voltage-clamp. This strongly suggests that, in the case of transient transfection, the protocol has to be finely tuned to prevent currents larger than 10 nA (Montnach et al., 2021).

In the same vein, in order to limit the artifactual heterogeneity of the recordings, it is also critical to design the most adapted voltage simulation protocol specific to a given channel, since voltage-dependence and kinetics drastically vary from one channel type to another. For instance, a steady-state activation protocol in which the depolarizing pulse are too short in time may lead to erroneous effect of a given variant, such as the negative shift in the activation curve in the case of the R176W variant (Oliveira-Mendes et al., 2021).

Up to now, a majority of studies focused on a limited number of biophysical parameters among the following: the maximal current amplitude, the half-activation potential, the slope of the activation curve, the half-inactivation potential, the slope of the inactivation curve, activation and deactivation kinetics, inactivation and recovery from inactivation kinetics, and also the ion selectivity. Standardized and complete protocols, allowing a fast and quasi-exhaustive characterization of hERG channel activity, will prove more insightful than those studies. Such a protocol, used in (Oliveira-Mendes et al., 2021) can also be very short (35-s). This shortness is another criterion of robustness, giving little chance for cell characteristics such as the seal quality, series resistance, current amplitude, to vary during the course of the experiment. Another interest of such fast protocol is that it can be used to track concomitant variations of several parameters (e.g., amplitude, half-activation potential, deactivation). We used a simplified version of this complex protocol, to be able to follow the concomitant variations of several biophysical parameters caused by the variation in the membrane level of the membrane phospholipid PIP_2. Such a great deal of data allowed us to add many numerical constraints on a kinetic model and to demonstrate that PIP_2 stabilizes hERG channel open state (Rodriguez et al., 2010).

Another similar strategy to maximize the amount of information gathered with minimal time required is to use an unconventional protocol (such as a sinusoidal voltage-clamp protocol for conventional patch-clamp or a staircase protocol compatible with high-throughput system) generating enough information on the current characteristics, to use it to constrain a kinetic model that will be accurate enough to describe the properties of the activation and inactivation gates. Impressively, the protocol is able to predict the current obtained by the classical protocols (Beattie et al., 2018; Lei et al., 2019b). A major interest is that such approach may also be used to predict channel behavior at 37°C from experiments done at room temperature, which are much more successful than experiments at 37°C, as exposed above (Lei et al., 2019a). It remains to be determined if this unconventional protocol (sinusoidal; staircase), tested on the WT channel, is robust enough for the prediction of the biophysical behavior of channel variants. The 35-s protocol mentioned above, which does not need a kinetic model, has already been proven to be robust to study the electrophysiological activity of channel variants (Oliveira-Mendes et al., 2021).

In silico phenotyping

The guidelines proposed by the ACMG, AMP and CAP, mentioned above include criteria issued from *In Silico* pathogenicity prediction softwares, which are evaluating the evolutionary conservation of an amino acid or nucleotide, the location and context within the protein sequence, and the biochemical consequence of the amino acid substitution (Richards et al., 2015). Such tools are far from being 100% reliable (Riuró et al., 2015), but new effort have been engaged to improve the robustness of the prediction using deep learning (Qi et al., 2021).

The Cryo-EM structure of hERG channel in the open state represents an instrumental template on which molecular variants can be introduced to test their propensity to affect channel structure and hence function. One major limit is that the actual sequence lacks non-negligible intracellular regions of the channel (Wang and MacKinnon, 2017). It is though worth noting that hERG channel characteristics are not completely disturbed by the deletions operated in the cytoplasmic domain (Zhang et al., 2020). But it is clear that using such structure will be more predictive of a variant phenotype when the whole structure will be solved, in the different states (open, closed and inactivated) and in presence of potential hERG channel partners.

Conclusion

Our analysis of the large body of published work on hERG variants highlighted a lack of standardized analysis for hERG variants functional studies, which prevents an accurate comparison of the variants pathogenicity. In the future, a gold standard approach should use a single cell model, that must be a mammalian cell model (e.g., CHO or HEK293) and not *X. laevis* oocytes, and should mimic the heterozygote situation. iPS-derived human cardiomyocytes should be used as much as possible to further validate/invalidate such a simple heterologous expression system. In addition, electrophysiological recordings should be performed at physiological temperature, but it is still rarely the case, most probably due to the impact of temperature on seal quality, a problem that will be difficult to address. Also, standardized cell transfection protocols should be used to limit current amplitude and consequently incorrect voltage-clamp. Finally, standardized and optimized voltage-clamp protocol should be used to limit variability in the results. Recent initiatives using high-throughput electrophysiology are naturally going in that direction. This new tool represents a way to re-visit the body of variants in a much more standardized way. In complement to this standardization in the functional characterization, it is also important to standardize variant interpretation, as suggested by the Clinical Genome Resource Sequence Variant Interpretation Working Group and a laboratory working on *KCNH2* variant high-throughput phenotyping (Brnich et al., 2020; Jiang et al., 2022).

At last, development of *In Silico* methods will logically bring in parallel a standardized approach to predict the functional impact of a given variant.

Author contributions

MA, BO-M, GL, and MD contributed to conception and design of the study. MA, FK, JR, and GL organized the hERG variants database. MA, GL, and FK wrote the manuscript with support from MD and BO-M. ID, FL, and J-JS contributed to manuscript improvement. All authors contributed to manuscript revision, read, and approved the submitted version.

Funding

This work was supported by the Fondation Lefoulon Delande to BO-M, the Fédération Française de Cardiologie (DENJOY—Grands projets—2019 to ID, MD, and FL), and the Agence Nationale de la Recherche (grant number ANR-11-LABX-0015 to MD and FL; grant number ANR-21-CE17-0010-CarDiag to ID, MD, and FL).

Conflict of interest

The authors declare that the research was conducted in the absence of any commercial or financial relationships that could be construed as a potential conflict of interest.

Publisher's note

Supplementary material

The Supplementary Material for this article can be found online at: https://www.frontiersin.org/articles/10.3389/fphys.2023.1132533/full#supplementary-material

References

Abaandou, L., Quan, D., and Shiloach, J. (2021). Affecting HEK293 cell growth and production performance by modifying the expression of specific genes. *Cells* 10, 1667. doi:10.3390/cells10071667

Al Sayed, Z. R., Jouni, M., Gourraud, J., Belbachir, N., Barc, J., Girardeau, A., et al. (2021). A consistent arrhythmogenic trait in Brugada syndrome cellular phenotype. *Clin. Transl. Med.* 11, e413. doi:10.1002/ctm2.413

Al-Allaf, F. A., Abduljaleel, Z., Athar, M., Taher, M. M., Khan, W., Mehmet, H., et al. (2019). Modifying inter-cistronic sequence significantly enhances IRES dependent second gene expression in bicistronic vector: Construction of optimised cassette for gene therapy of familial hypercholesterolemia. *Non-coding RNA Res.* 4, 1–14. doi:10.1016/j.ncrna.2018.11.005

Alders, M., Bikker, H., and Christiaans, I. (1993). "Long QT syndrome," in *GeneReviews®*. Editors M. P. Adam, D. B. Everman, G. M. Mirzaa, R. A. Pagon, S. E. Wallace, L. J. Bean, et al. (Seattle, Seattle (WA: University of Washington).

Anderson, C. L., Delisle, B. P., Anson, B. D., Kilby, J. A., Will, M. L., Tester, D. J., et al. (2006). Most LQT2 mutations reduce Kv11.1 (hERG) current by a class 2 (Trafficking-Deficient) mechanism. *Circulation* 113, 365–373. doi:10.1161/CIRCULATIONAHA.105.570200

Anderson, C. L., Kuzmicki, C. E., Childs, R. R., Hintz, C. J., Delisle, B. P., and January, C. T. (2014). Large-scale mutational analysis of Kv11.1 reveals molecular insights into type 2 long QT syndrome. *Nat. Commun.* 5, 5535. doi:10.1038/ncomms6535

Barc, J., Tadros, R., Glinge, C., Chiang, D. Y., Jouni, M., and Simonet, F. (2022). Genome-wide association analyses identify new Brugada syndrome risk loci and highlight a new mechanism of sodium channel regulation in disease susceptibility. *Nat. Genet.* 54, 232–239. doi:10.1038/s41588-021-01007-6

Beattie, K. A., Hill, A. P., Bardenet, R., Cui, Y., Vandenberg, J. I., Gavaghan, D. J., et al. (2018). Sinusoidal voltage protocols for rapid characterisation of ion channel kinetics: Sinusoidal protocols to capture ion channel kinetics. *J. Physiol.* 596, 1813–1828. doi:10.1113/JP275733

Bellocq, C., Wilders, R., Schott, J.-J., Louérat-Oriou, B., Boisseau, P., Le Marec, H., et al. (2004). A common antitussive drug, clobutinol, precipitates the long QT syndrome 2. *Mol. Pharmacol.* 66, 1093–1102. doi:10.1124/mol.104.001065

Bienz, M., and Gurdon, J. B. (1982). The heat-shock response in xenopus oocytes is controlled at the translational level. *Cell* 29, 811–819. doi:10.1016/0092-8674(82)90443-3

Brnich, S. E., Abou Tayoun, A. N., Couch, F. J., Cutting, G. R., Greenblatt, M. S., Heinen, C. D., et al. (2020). Recommendations for application of the functional evidence PS3/BS3 criterion using the ACMG/AMP sequence variant interpretation framework. *Genome Med.* 12, 3. doi:10.1186/s13073-019-0690-2

Brnich, S. E., Rivera Muñoz, E. A., and Berg, J. S. (2018). Quantifying the potential of functional evidence to reclassify variants of uncertain significance in the categorical and Bayesian interpretation frameworks. *Hum. Mutat.* 39, 1531–1541. doi:10.1002/humu.23609

Brugada, R., Hong, K., Dumaine, R., Cordeiro, J., Gaita, F., Borggrefe, M., et al. (2004). Sudden death associated with short-QT syndrome linked to mutations in HERG. *Circulation* 109, 30–35. doi:10.1161/01.CIR.0000109482.92774.3A

Chai, S., Wan, X., Ramirez-Navarro, A., Tesar, P. J., Kaufman, E. S., Ficker, E., et al. (2018). Physiological genomics identifies genetic modifiers of long QT syndrome type 2 severity. *J. Clin. Investigation* 128, 1043–1056. doi:10.1172/JCI94996

Charpentier, F., Mérot, J., Loussouarn, G., and Baró, I. (2010). Delayed rectifier K+ currents and cardiac repolarization. *J. Mol. Cell. Cardiol.* 48, 37–44. doi:10.1016/j.yjmcc.2009.08.005

Chen, J., Zou, A., Splawski, I., Keating, M. T., and Sanguinetti, M. C. (1999). Long QT syndrome-associated mutations in the per-arnt-sim (PAS) domain of HERG potassium channels accelerate channel deactivation. *J. Biol. Chem.* 274, 10113–10118. doi:10.1074/jbc.274.15.10113

Chevalier, P., Rodriguez, C., Bontemps, L., Miquel, M., Kirkorian, G., Rousson, R., et al. (2001). Non-invasive testing of acquired long QT syndrome Evidence for multiple arrhythmogenic substrates. *Cardiovasc. Res.* 50, 386–398. doi:10.1016/S0008-6363(01)00263-2

Delisle, B. P., Slind, J. K., Kilby, J. A., Anderson, C. L., Anson, B. D., Balijepalli, R. C., et al. (2005). Intragenic suppression of trafficking-defective KCNH2 channels associated with long QT syndrome. *Mol. Pharmacol.* 68, 233–240. doi:10.1124/mol.105.012914

Eldstrom, J., and Fedida, D. (2011). The voltage-gated channel accessory protein KCNE2: Multiple ion channel partners, multiple ways to long QT syndrome. *Expert Rev. Mol. Med.* 13, e38. doi:10.1017/S1462399411002092

Feng, L., Zhang, J., Lee, C., Kim, G., Liu, F., Petersen, A. J., et al. (2021). Long QT syndrome *KCNH2* variant induces hERG1a/1b subunit imbalance in patient-specific induced pluripotent stem cell–derived cardiomyocytes. *Circ Arrhythmia Electrophysiol.* 14, e009343. doi:10.1161/CIRCEP.120.009343

Ficker, E., Thomas, D., Viswanathan, P. C., Dennis, A. T., Priori, S. G., Napolitano, C., et al. (2000). Novel characteristics of a misprocessed mutant HERG channel linked to hereditary long QT syndrome. *Am. J. Physiol. Heart Circ. Physiol.* 279, H1748–H1756. doi:10.1152/ajpheart.2000.279.4.H1748

Furutani, M., Trudeau, M. C., Hagiwara, N., Seki, A., Gong, Q., Zhou, Z., et al. (1999). Novel mechanism associated with an inherited cardiac arrhythmia: Defective protein trafficking by the mutant HERG (G601S) potassium channel. *Circulation* 99, 2290–2294. doi:10.1161/01.CIR.99.17.2290

Harley, C. A., Jesus, C. S. H., Carvalho, R., Brito, R. M. M., and Morais-Cabral, J. H. (2012). Changes in channel trafficking and protein stability caused by LQT2 mutations in the PAS domain of the HERG channel. *PLoS ONE* 7, e32654. doi:10.1371/journal.pone.0032654

Hayashi, K., Fujino, N., Uchiyama, K., Ino, H., Sakata, K., Konno, T., et al. (2009). Long QT syndrome and associated gene mutation carriers in Japanese children: Results from ECG screening examinations. *Clin. Sci.* 117, 415–424. doi:10.1042/CS20080528

Hayashi, K., Konno, T., Tada, H., Tani, S., Liu, L., Fujino, N., et al. (2015). Functional characterization of rare variants implicated in susceptibility to lone atrial fibrillation. *Circ. Arrhythm. Electrophysiol.* 8, 1095–1104. doi:10.1161/CIRCEP.114.002519

Jiang, C., Richardson, E., Farr, J., Hill, A. P., Ullah, R., Kroncke, B. M., et al. (2022). A calibrated functional patch-clamp assay to enhance clinical variant interpretation in KCNH2-related long QT syndrome. *Am. J. Hum. Genet.* 109, 1199–1207. doi:10.1016/j.ajhg.2022.05.002

Jones, D. K., Liu, F., Vaidyanathan, R., Eckhardt, L. L., Trudeau, M. C., and Robertson, G. A. (2014). hERG 1b is critical for human cardiac repolarization. *Proc. Natl. Acad. Sci. U.S.A.* 111, 18073–18077. doi:10.1073/pnas.1414945111

Jouni, M., Si Tayeb, K., Es Salah Lamoureux, Z., Latypova, X., Champon, B., Caillaud, A., et al. (2015). Toward personalized medicine: Using cardiomyocytes differentiated from urine derived pluripotent stem cells to recapitulate electrophysiological characteristics of type 2 long QT syndrome. *JAHA* 4, e002159. doi:10.1161/JAHA.115.002159

Kolder, I. C. R. M., Tanck, M. W. T., Postema, P. G., Barc, J., Sinner, M. F., Zumhagen, S., et al. (2015). Analysis for genetic modifiers of disease severity in patients with long-QT syndrome type 2. *Circ. Cardiovasc Genet.* 8, 447–456. doi:10.1161/CIRCGENETICS.114.000785

Kutyifa, V., Daimee, U. A., McNitt, S., Polonsky, B., Lowenstein, C., Cutter, K., et al. (2018). Clinical aspects of the three major genetic forms of long QT syndrome (LQT1, LQT2, LQT3). *Ann. Noninvasive Electrocardiol.* 23, e12537. doi:10.1111/anec.12537

Landrum, M. J., Lee, J. M., Riley, G. R., Jang, W., Rubinstein, W. S., Church, D. M., et al. (2014). ClinVar: Public archive of relationships among sequence variation and human phenotype. *Nucl. Acids Res.* 42, D980–D985. doi:10.1093/nar/gkt1113

Lei, C. L., Clerx, M., Beattie, K. A., Melgari, D., Hancox, J. C., Gavaghan, D. J., et al. (2019a). Rapid characterization of hERG channel kinetics II: Temperature dependence. *Biophysical J.* 117, 2455–2470. doi:10.1016/j.bpj.2019.07.030

Lei, C. L., Clerx, M., Gavaghan, D. J., Polonchuk, L., Mirams, G. R., and Wang, K. (2019b). Rapid characterization of hERG channel kinetics I: Using an automated high-throughput system. *Biophysical J.* 117, 2438–2454. doi:10.1016/j.bpj.2019.07.029

Lei, C. L., Clerx, M., Whittaker, D. G., Gavaghan, D. J., de Boer, T. P., and Mirams, G. R. (2020). Accounting for variability in ion current recordings using a mathematical model of artefacts in voltage-clamp experiments. *Phil. Trans. R. Soc. A* 378, 20190348. doi:10.1098/rsta.2019.0348

Lek, M., Karczewski, K. J., Minikel, E. V., Samocha, K. E., Banks, E., Fennell, T., et al. (2016). Analysis of protein-coding genetic variation in 60,706 humans. *Nature* 536, 285–291. doi:10.1038/nature19057

Lin, E. C., Holzem, K. M., Anson, B. D., Moungey, B. M., Balijepalli, S. Y., Tester, D. J., et al. (2010). Properties of WT and mutant hERG K^+ channels expressed in neonatal mouse cardiomyocytes. *Am. J. Physiology-Heart Circulatory Physiology* 298, H1842–H1849. doi:10.1152/ajpheart.01236.2009

Liu, L., Tian, J., Lu, C., Chen, X., Fu, Y., Xu, B., et al. (2016). Electrophysiological characteristics of the LQT2 syndrome mutation KCNH2-g572S and regulation by accessory protein KCNE2. *Front. Physiol.* 7, 650. doi:10.3389/fphys.2016.00650

Liu, Q., and Trudeau, M. C. (2015). Eag domains regulate LQT mutant hERG channels in human induced pluripotent stem cell-derived cardiomyocytes. *PLoS ONE* 10, e0123951. doi:10.1371/journal.pone.0123951

McBride, C. M., Smith, A. M., Smith, J. L., Reloj, A. R., Velasco, E. J., Powell, J., et al. (2013). Mechanistic basis for type 2 long QT syndrome caused by KCNH2 mutations that disrupt conserved arginine residues in the voltage sensor. *J. Membr. Biol.* 246, 355–364. doi:10.1007/s00232-013-9539-6

Mesquita, F. C. P., Arantes, P. C., Kasai-Brunswick, T. H., Araujo, D. S., Gubert, F., Monnerat, G., et al. (2019). R534C mutation in hERG causes a trafficking defect in iPSC-derived cardiomyocytes from patients with type 2 long QT syndrome. *Sci. Rep.* 9, 19203. doi:10.1038/s41598-019-55837-w

Mizuguchi, H., Xu, Z., Ishii-Watabe, A., Uchida, E., and Hayakawa, T. (2000). IRES-dependent second gene expression is significantly lower than cap-dependent first gene expression in a bicistronic vector. *Mol. Ther.* 1, 376–382. doi:10.1006/mthe.2000.0050

Montnach, J., Lorenzini, M., Lesage, A., Simon, I., Nicolas, S., Moreau, E., et al. (2021). Computer modeling of whole-cell voltage-clamp analyses to delineate guidelines for good practice of manual and automated patch-clamp. *Sci. Rep.* 11, 3282. doi:10.1038/s41598-021-82077-8

Nakajima, T., Furukawa, T., Hirano, Y., Tanaka, T., Sakurada, H., Takahashi, T., et al. (1999). Voltage-shift of the current activation in HERG S4 mutation (R534C) in LQT2. *Cardiovasc. Res.* 44, 283–293. doi:10.1016/S0008-6363(99)00195-9

Ng, C.-A., Perry, M. D., Liang, W., Smith, N. J., Foo, B., Shrier, A., et al. (2020). High-throughput phenotyping of heteromeric human ether-à-go-go-related gene potassium channel variants can discriminate pathogenic from rare benign variants. *Heart rhythm.* 17, 492–500. doi:10.1016/j.hrthm.2019.09.020

Oliveira Mendes, B., Feliciangeli, S., Ménard, M., Chatelain, F., Alameh, M., Montnach, J., et al. (2021). A standardised hERG phenotyping pipeline to evaluate *KCNH2* genetic variant pathogenicity. *Clin. Transl. Med.* 11, e609. doi:10.1002/ctm2.609

Paulussen, A., Raes, A., Matthijs, G., Snyders, D. J., Cohen, N., and Aerssens, J. (2002). A novel mutation (T65P) in the PAS domain of the human potassium channelchannel HERG results in the long QT syndrome by trafficking deficiency. *J. Biol. Chem.* 277, 48610–48616. doi:10.1074/jbc.M206569200

Qi, H., Zhang, H., Zhao, Y., Chen, C., Long, J. J., Chung, W. K., et al. (2021). MVP predicts the pathogenicity of missense variants by deep learning. *Nat. Commun.* 12, 510. doi:10.1038/s41467-020-20847-0

Ranjan, R., Logette, E., Marani, M., Herzog, M., Tâche, V., Scantamburlo, E., et al. (2019). A kinetic map of the homomeric voltage-gated potassium channel (Kv) family. *Front. Cell. Neurosci.* 13, 358. doi:10.3389/fncel.2019.00358

Richards, S., Aziz, N., Bale, S., Bick, D., Das, S., Gastier-Foster, J., et al. (2015). Standards and guidelines for the interpretation of sequence variants: A joint consensus recommendation of the American College of medical genetics and genomics and the association for molecular pathology. *Genet. Med.* 17, 405–424. doi:10.1038/gim.2015.30

Riuró, H., Campuzano, O., Berne, P., Arbelo, E., Iglesias, A., Pérez-Serra, A., et al. (2015). Genetic analysis, *in silico* prediction, and family segregation in long QT syndrome. *Eur. J. Hum. Genet.* 23, 79–85. doi:10.1038/ejhg.2014.54

Rodriguez, N., Amarouch, M. Y., Montnach, J., Piron, J., Labro, A. J., Charpentier, F., et al. (2010). Phosphatidylinositol-4,5-Bisphosphate (PIP2) stabilizes the open pore conformation of the Kv11.1 (hERG) channel. *Biophysical J.* 99, 1110–1118. doi:10.1016/j.bpj.2010.06.013

Saenen, J. B., Paulussen, A. D. C., Jongbloed, R. J., Marcelis, C. L., Gilissen, R. A. H. J., Aerssens, J., et al. (2007). A single hERG mutation underlying a spectrum of acquired and congenital long QT syndrome phenotypes. *J. Mol. Cell. Cardiol.* 43, 63–72. doi:10.1016/j.yjmcc.2007.04.012

Schwartz, P. J. (1985). Idiopathic long QT syndrome: Progress and questions. *Am. Heart J.* 109, 399–411. doi:10.1016/0002-8703(85)90626-X

Schwartz, P. J., Priori, S. G., Spazzolini, C., Moss, A. J., Vincent, G. M., Napolitano, C., et al. (2001). Genotype-phenotype correlation in the long-QT syndrome: Gene-specific triggers for life-threatening arrhythmias. *Circulation* 103, 89–95. doi:10.1161/01.cir.103.1.89

Schwartz, P. (2013). Practical issues in the management of the long QT syndrome: Focus on diagnosis and therapy. *Swiss Med. Wkly.* 143, w13843. doi:10.4414/smw.2013.13843

Shah, D., Prajapati, C., Penttinen, K., Cherian, R. M., Koivumäki, J. T., Alexanova, A., et al. (2020). hiPSC-derived cardiomyocyte model of LQT2 syndrome derived from asymptomatic and symptomatic mutation carriers reproduces clinical differences in aggregates but not in single cells. *Cells* 9, 1153. doi:10.3390/cells9051153

Takahashi, K., and Yamanaka, S. (2006). Induction of pluripotent stem cells from mouse embryonic and adult fibroblast cultures by defined factors. *Cell* 126, 663–676. doi:10.1016/j.cell.2006.07.024

van der Velden, J., Asselbergs, F. W., Bakkers, J., Batkai, S., Bertrand, L., Bezzina, C. R., et al. (2022). Animal models and animal-free innovations for cardiovascular research: Current status and routes to be explored. Consensus document of the ESC working Group on myocardial function and the ESC working Group on cellular biology of the heart. *Cardiovasc. Res. cvab370* 118, 3016–3051. doi:10.1093/cvr/cvab370

Vandenberg, J. I., Varghese, A., Lu, Y., Bursill, J. A., Mahaut-Smith, M. P., and Huang, C. L.-H. (2006). Temperature dependence of human *ether-à-go-go-* related gene K^+ currents. *Am. J. Physiology-Cell Physiology* 291, C165–C175. doi:10.1152/ajpcell.00596.2005

Vanoye, C. G., Desai, R. R., Fabre, K. L., Gallagher, S. L., Potet, F., DeKeyser, J.-M., et al. (2018). High-throughput functional evaluation of *KCNQ1* decrypts variants of unknown significance. *Circ Genomic Precis. Med.* 11, e002345. doi:10.1161/CIRCGEN.118.002345

Wang, W., and MacKinnon, R. (2017). Cryo-EM structure of the open human ether-à-go-go -related K + channel hERG. *Cell* 169, 422–430. doi:10.1016/j.cell.2017.03.048

Yu, S. P., and Kerchner, G. A. (1998). Endogenous voltage-gated potassium channels in human embryonic kidney (HEK293) cells. *J. Neurosci. Res.* 52, 612–617. doi:10.1002/(SICI)1097-4547(19980601)52:5<612::AID-JNR13>3.0.CO;2-3

Zhang, Y., Dempsey, C. E., and Hancox, J. C. (2020). Electrophysiological characterization of the modified hERG $_T$ potassium channel used to obtain the first cryo-EM hERG structure. *Physiol. Rep.* 8, e14568. doi:10.14814/phy2.14568

frontiers | Frontiers in Physiology

TYPE Review
PUBLISHED 16 February 2023
DOI 10.3389/fphys.2023.1132165

OPEN ACCESS

EDITED BY
Yoram Etzion,
Ben-Gurion University of the Negev,
Israel

REVIEWED BY
Antonio Carlos Campos De Carvalho,
Federal University of Rio De Janeiro,
Brazil
Yael Yaniv,
Technion Israel Institute of Technology,
Israel

*CORRESPONDENCE
Torsten Christ,
t.christ@uke.de

SPECIALTY SECTION
This article was submitted to Cardiac Electrophysiology,
a section of the journal
Frontiers in Physiology

RECEIVED 26 December 2022
ACCEPTED 06 February 2023
PUBLISHED 16 February 2023

CITATION
Ismaili D, Schulz C, Horváth A, Koivumäki JT, Mika D, Hansen A, Eschenhagen T and Christ T (2023), Human induced pluripotent stem cell-derived cardiomyocytes as an electrophysiological model: Opportunities and challenges—The Hamburg perspective.
Front. Physiol. 14:1132165.
doi: 10.3389/fphys.2023.1132165

Human induced pluripotent stem cell-derived cardiomyocytes as an electrophysiological model: Opportunities and challenges —The Hamburg perspective

Djemail Ismaili[1,2,3], Carl Schulz[1,3], András Horváth[4], Jussi T. Koivumäki[5], Delphine Mika[6], Arne Hansen[1,3], Thomas Eschenhagen[1,3] and Torsten Christ[1,3]*

[1]Institute of Experimental Pharmacology and Toxicology, University Medical Center Hamburg-Eppendorf, Hamburg, Germany, [2]Department of Cardiology, University Heart and Vascular Center Hamburg, University Medical Center Hamburg-Eppendorf, Hamburg, Germany, [3]DZHK (German Centre for Cardiovascular Research), Partner Site Hamburg/Kiel/Lübeck, Hamburg, Germany, [4]Translational Cardiology, Department of Cardiology, Inselspital, University Hospital Bern, University of Bern, Bern, Switzerland, [5]BioMediTech, Faculty of Medicine and Health Technology, Tampere University, Tampere, Finland, [6]Inserm, UMR-S 1180, Université Paris-Saclay, Orsay, France

Models based on human induced pluripotent stem cell-derived cardiomyocytes (hiPSC-CM) are proposed in almost any field of physiology and pharmacology. The development of human induced pluripotent stem cell-derived cardiomyocytes is expected to become a step forward to increase the translational power of cardiovascular research. Importantly they should allow to study genetic effects on an electrophysiological background close to the human situation. However, biological and methodological issues revealed when human induced pluripotent stem cell-derived cardiomyocytes were used in experimental electrophysiology. We will discuss some of the challenges that should be considered when human induced pluripotent stem cell-derived cardiomyocytes will be used as a physiological model.

KEYWORDS

hiPSC-CM, hESC-CM, human cardiomyocytes, ion currents, action potentials, computer modelling and simulation, automated patch clamp

Abbreviations: AP, action potential; APC, automated patch clamp; APD, action potential duration; APD_{20}, APD at 20% repolarization; APD_{90}, APD at 90% repolarization; CM, cardiomyocytes; EAD, early afterdepolarizations; EHT, engineered heart tissue; hESC-CM, human embryonic stem cell-derived cardiomyocytes; hiPSC-CM, human induced pluripotent stem cell-derived cardiomyocytes; $I_{BK,Ca}$, Big Conductance Calcium Activated Potassium Current; $I_{Ca,L}$, L-type Ca^{2+}-current; $I_{Ca,T}$, T-Type Ca^{2+}-current; I_f, hyperpolarization-activated funny current; $I_{K,ACh}$, Acetylcholine-activated potassium current; I_{Ks}, slow delayed rectifier potassium current; I_{Kr}, rapid delayed rectifier potassium current; I_{Kur}, ultrarapidly activating potassium current; I_{K1}, inward rectifier potassium current; I_{Na}, sodium current; I_{to}, transient potassium outward current; NCX, Na^+/Ca^{2+}-exchanger; NKA, Na^+/K^+-ATPase; RA, Retinoic acid; RMP, resting membrane potential; RF, repolarization fraction; 4-AP, 4-aminopyridine.

Introduction

The development of human induced pluripotent stem cell-derived cardiomyocytes (hiPSC-CM) is expected to become a relevant step for the translational aspect of cardiovascular basic research. HiPSC-CM provide human-based disease models for detailed functional studies of pathogenesis in a patient-specific manner. Importantly, hiPSC-CM-based models should allow to quantify the impact of genetic editing on an electrophysiological background close to the situation in humans. We share the enthusiasm on application of hiPSC-CM as a milestone in cardiovascular research. However, using hiPSC-CM in experimental electrophysiology during the past years, we have identified some challenges that we will discuss here and that are hopefully of interest to a broader readership.

Ion currents in hiPSC-CM: All aboard or even stowaways?

Data for a large number of ion channels in hiPSC-CM were published in 2011 (Ma et al., 2011) and following results were compared in detail to data obtained in the human adult heart (Figure 1; Casini et al., 2017). Given the importance of pump and exchanger currents for the electrical stability of cardiomyocytes (CM), data on Na^+/Ca^{2+}-exchanger (NCX) and Na^+/K^+-ATPase (NKA) in heart muscle, data for hiPSC-CM were reported as a following step in 2012 (Fine et al., 2013). Curiously, no data on NCX currents in human ventricular CM were available at that time. Data in hiPSC-CM fit nicely to the situation in native human atrial CM, when NCX was measured under the same experimental conditions (Christ et al., 2016). A recent study, directly comparing NCX currents in hiPSC-CM (cultured in engineered heart tissue, EHT) and adult human ventricular CM, found the NCX current density to be slightly higher in hiPSC-CM (Ismaili et al., 2022). However, the functional relevance of NCX cannot be predicted from current densities alone, since robust NCX currents were found consistently in ventricular myocytes of various species but functional consequences of pharmacological NCX-block on action potential duration (APD) and contractile force differ widely [for discussion see (Ismaili et al., 2022)]. Block of NCX shortened APD at 90% repolarization (APD_{90}) in EHT but not in human left ventricular tissue. In line with the APD data, force was increased by NCX-block in hiPSC-CM but not in human left ventricle (Ismaili et al., 2022). The lack of effect of NCX block on APD and force in human ventricular tissue is perplexing but fits well to earlier results in human atrial tissue (Christ et al., 2016). It should be noted that NCX block is devoid of effects on APD and force in many larger animals and we suppose that still more research is needed to better understand the physiological relevance of NCX in the adult heart (Eisner and Sipido, 2004). Inward currents by NCX resulting from Ca^{2+}-release should contribute to pacemaking in hiPSC-CM (Morad and Zhang, 2017). Newly developed, highly selective blockers of NCX are available (Otsomaa et al., 2020). However,

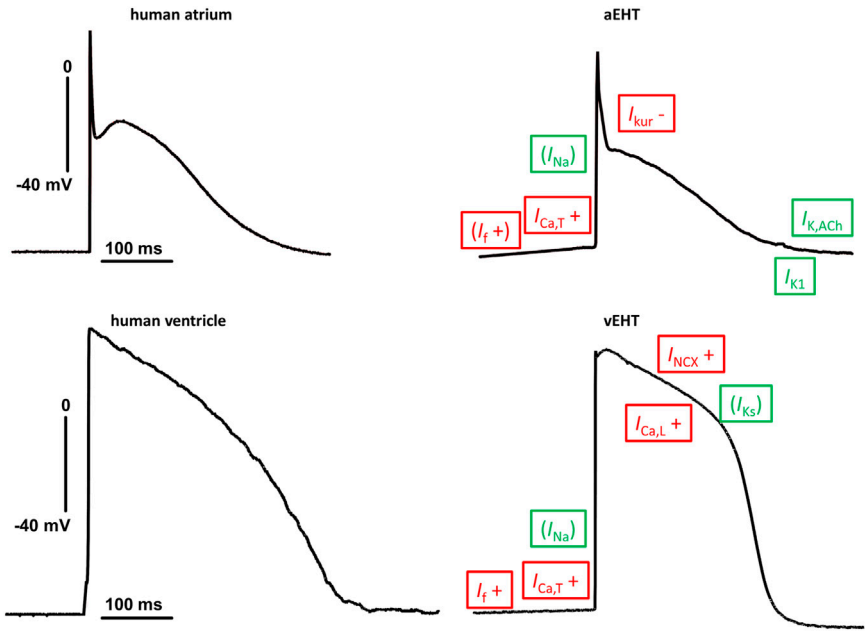

FIGURE 1
Similarities and differences in action potential shapes between adult human heart tissue and engineered heart tissue based on hiPSC-CM. Typical original traces of action potentials (AP) recorded in human adult (left) and engineered heart tissue (EHT, right) from atrium (top) and ventricle (bottom). Same scaling and zero voltage level for all four pictures. Differences in ion currents are indicated with red letter with + or – indicating changes related to adult tissue. Ion currents within the same range are indicated in green letter. Letters are given in brackets for ion currents where differences are suspected from AP recordings (no direct comparison of patch clamp data). Abbreviations: $I_{Ca,L}$, L-type Ca^{2+}-current; $I_{Ca,T}$, T-Type Ca^{2+}-current; I_f, hyperpolarization-activated funny current; $I_{K,ACh}$, Acetylcholine-activated potassium current; I_{Ks}, slow delayed rectifier potassium current; I_{Kur}, ultrarapidly activating potassium current; I_{K1}, inward rectifier potassium current; I_{Na}, sodium current; I_{NCX}, Na^+/Ca^{2+}-exchanger.

somewhat unexpectedly block of NCX has only marginally effects on beating rate in adult animal sinus node (Kohajda et al., 2020). Data on beating rate in hiPSC-CM are missing.

The situation regarding NKA is similarly suboptimal. The current densities for NKA in hiPSC-CM (Fine et al., 2013) fit nicely to data obtained in human atrial CM (Workman et al., 2003) but no data on NKA currents exist for human ventricular CM so far. As reported for human ventricular tissue (Prasad and Callaghan, 1970; Schwinger et al., 1990), inhibition of NKA by ouabain increased force in EHT (Mannhardt et al., 2016). Of note, ouabain exerted a biphasic inotropic response in EHT with an increase in force at low to medium (0.3–1 μM) and a sharp decrease at higher concentrations. In a study in human ventricular tissue, ouabain (200 nM) shortened APD_{90} (Prasad and Callaghan, 1970) and induced early afterdepolarizations (EAD) (Dangman et al., 1982). The n numbers are small and results were never confirmed. No data on effects of NKA-block on action potential (AP) are available for hiPSC-CM.

In the human ventricle, expression of transporters and ion channels show a transmural gradient (Soltysinska et al., 2009). Detailed biophysical characterization of potassium outward currents in human ventricular CM revealed an important role of the transient potassium outward current (I_{to}) for the transmural gradient of repolarization (more in subepicardial than in subendocardial layer) (Wettwer et al., 1994). I_{to} was reported in several hiPSC-CM cell lines (Ma et al., 2011; Lemme et al., 2018; Flenner et al., 2021). However, there is concern that I_{to} contributes less to AP shape in hiPSC-CM. That is, high concentrations of the prototypical I_{to} blocker 4-aminopyridine (4-AP) failed to affect AP shape in two of our in-house control hiPSC-CM cell lines (Lemme et al., 2018; Schulz et al., 2023). This finding may substantially limit the value of hiPSC-CM as a disease model that involves changes in I_{to} (Flenner et al., 2021) and indicate that actual hiPSC-CM preparations may represent a subendocardial ventricular CM phenotype (Wettwer et al., 1994). Thus, it remains open whether the generation of hiPSC-CM with a more subepicardial AP shape is a realistic goal.

Consequently, there is legitimate concern whether hiPSC-CM express all cardiac ion channels and transporters and whether their relative contribution fits the situation in the human heart (Casini et al., 2017). Conversely, hiPSC-CM clearly express ion channels that are absent in the adult human working myocardium.

Spontaneous beating and the sensitivity of hiPSC-CM beating rate to ivabradine strongly suggest substantial activity of the hyperpolarization-activated funny current (I_f) in hiPSC-CM EHT (Mannhardt et al., 2017). Accordingly, transcript abundance of HCN4 in hiPSC EHT is relatively high. In bulk RNA sequencing analysis, the mean of 28 control lines amounted to 3300 reads per million (=#807 most expressed gene; unpublished), while it is absent in normal human ventricles (Litviňuková et al., 2020). I_f density in standard ventricular-like hiPSC-CM was reported to be ~5 pA/pF, i.e., in the same range of human sinus node cells (Giannetti et al., 2021), but also in specifically differentiated sino-atrial hiPSC-CM (Protze et al., 2016). Biophysical properties of I_f and its autonomic modulation are very close to the situation in rabbit sinus node cells, making hiPSC-CM an attractive model to study cardiac pacemaking (Giannetti et al., 2021). A detailed study in hiPSC-CM revealed biochemical and electrophysiological changes in HCN4 in Coxsackievirus B3 (CVB3)-infected hiPSC-CM, a phenomenon that may contribute to the clinically observed myocarditis-induced bradycardia and cardiac arrest (Peischard et al., 2022). The latter study is remarkable, since it nicely illustrates that successful application of hiPSC-CM is not necessarily restricted to genetic studies.

Another current absent in the human working myocardium but occasionally found in hiPSC-CM is the T-Type Ca^{2+}-current ($I_{Ca,T}$) (Ivashchenko et al., 2013; Uzun et al., 2016). The presence of $I_{Ca,T}$ cannot necessarily be taken as an indication of immaturity, since this current has been found in the adult ventricular myocardium of many species (Uzun et al., 2016). The co-existence of T-type and L-type Ca^{2+}-channels in hiPSC-CM suggests that the additional inward current at potentials negative to the activation threshold for L-type Ca^{2+}-currents ($I_{Ca,L}$) likely contributes to pacemaking in hiPSC-CM. Moreover, it has to be taken into account that a substantial fraction (20%–30%) of peak Ca^{2+}-current can consist of $I_{Ca,T}$ in hiPSC-CM subjected to a typical test pulse potential used to measure $I_{Ca,L}$ (+10 mV) (Uzun et al., 2016). This finding can lead to overestimation of real Ca^{2+}-influx, since $I_{Ca,T}$ inactivates much faster than $I_{Ca,L}$. Thus it may be wise to quantify $I_{Ca,L}$ as dihydropyridine-sensitive currents in hiPSC-CM that possess $I_{Ca,T}$ (Prondzynski et al., 2019). Taken together, hiPSC-CM can express cardiac ion channels such as I_f and $I_{Ca,T}$ that are not expressed in adult human ventricular CM.

In addition, non-cardiac ion channels can be present in hiPSC-CM. An example are Big Conductance Calcium Activated Potassium Currents ($I_{BK,Ca}$) that were shown to be responsible for induced afterdepolarizations and oscillations in EHT of a specific hiPSC line (Horváth et al., 2020). Identification of $I_{BK,Ca}$ was rather easy because of a bizarre AP morphology and the availability of a selective blocker (iberiotoxin) (Horváth et al., 2020). Given that the current was not observed in EHTs from three other independent control lines and the transcript of the underlying channel (KCNMA1) was essentially absent in 44 other independent lines (unpublished data), a hiPSC artefact seems likely. Indeed, two independent reports demonstrated that iPSCs frequently acquire genetic alterations during cell culture. Kilpinen et al. (2017) showed that chromosome 10, harboring BKCa/KCNMA1, was among the most susceptible locus to copy number alterations. Another study searching for variants that provide mutated cells with a growth advantage in culture, identified KCNMA1 variants in two independent stem cell lines (Merkle et al., 2017). Thus, a genetic alteration leading to a reoccurring overgrowth of BK and misexpression in hiPSC is the most likely explanation for our finding. It remains open if this example may represent an exotic exception or if it is just the "tip of an iceberg." Anyhow, expression of non-cardiac sarcolemmal ion channels should be considered.

Action potentials recording in hiPSC-CM: Methodological issues

Initially, cultures of hiPSC-CM were interpreted as a mixture of ventricular, atrial and nodal CM. The interpretation was based on differences in resting membrane potential (RMP) and APD, which were analyzed in small numbers of cells (n ~ 20–30) by patch clamping (Itzhaki et al., 2010; Moretti et al., 2010; Ma et al., 2011;

Liang et al., 2013; Ma et al., 2013; Liang et al., 2016). However, analysis in a larger population (n = 320) of hiPSC-CM showed that the frequency distribution for APD_{90} followed a single Gaussian distribution, arguing against the idea of a truly mixed cell population and for a simple scatter of data (Du et al., 2015). Measurements were done by voltage-sensitive dyes that does not allow any conclusion on (diastolic!) membrane potential and it was argued that this limitation may have weakened the power to detect the mentioned above different populations (Giles and Noble, 2016). It is important to note that APD_{90} did not significantly differ between human right atrium and left ventricle (measured in intact tissue by sharp microelectrodes) (Horváth et al., 2018). In contrast, RMP was more negative in human left ventricle than in right atrium (measured by sharp microelectrodes) (Horváth et al., 2018). Nevertheless the difference was small (2.5 mV) and the groups showed substantial overlap (Horváth et al., 2018), making RMP less appropriate to distinguish between atrial and ventricular CM. The suitability of a parameter to distinguish between atrial and ventricular hiPSC-CM does not only depend on its power to discriminate between intact human adult atrial and ventricular tissue, but also on the method to measure action potentials. Most researchers have measured AP in isolated cells with patch electrodes. By using this approach, diastolic potentials are less negative in hiPSC-CM than in adult CM. Consequently, application of hyperpolarizing holding currents is mandatory in hiPSC-CM to bring the membrane potential in a range negative enough to elicit an AP. Clearly, such a "hold" diastolic membrane potential cannot be longer used as a discriminator between atrial and ventricular CM.

The less negative diastolic potential of hiPSC-CM has attracted much attention and is generally assumed a marker of immaturity of the CM and explained by abnormally low current densities of the inward rectifier current (I_{K1}) (Ma et al., 2011). However, I_{K1} densities are not necessarily too low in hiPSC-CM (Horváth et al., 2018). In fact, we measured mean values of barium (1 mM)-sensitive inward rectifying currents of 33 pA/pF in hiPSC-CM, compared with 41 pA/pF in left ventricular CM. We suspect technical issues may contribute. HiPSC-CM are much smaller than adult CM (Uzun et al., 2016). Even if a hiPSC-CM possesses physiological inward rectifier density, total membrane conductivity is much lower than in adult CM. Thus, membrane resistance is high and is close to the range of seal resistance, which is expected to generate substantial voltage errors. Such voltage errors can be avoided when membrane potential is measured by sharp microelectrodes in intact tissue. This approach became available with the introduction of EHT and was reported as early as in 2002 (Eschenhagen et al., 2002).

There are other advantages of sharp microelectrodes to measure AP. Proper cell-to-cell coupling may be critical for the generation of a correct diastolic potential in hiPSC-CM (Van de Sande et al., 2021). From a more general perspective, variability of APD is much lower when measured in intact tissue than in isolated CM measurements, because of high inter-cell variation of ion channel activity (Lachaud et al., 2022). This is not specific for hiPSC-CM, because the coefficient of variation was 2-fold and 3-fold higher for APD_{90} measured in isolated CM from human ventricle and atrium, respectively, than in intact tissue. Similarly, the variability was 5 times larger in hiPSC-CM than in EHT (Horváth et al., 2018), underscoring that AP recordings in isolated hiPSC-CM are particularly prone to methodological issues (Eschenhagen et al., 2002).

AP recordings in EHT also allow much longer lasting experiments (hours vs. minutes in case of hiPSC-CM) and thus application of several concentrations of a single test compound or application of different compounds (Lemoine et al., 2018) as routinely done in cardiac safety pharmacology on animal heart tissue (Himmel et al., 2012).

Atrial models: How much atrial-like is enough?

There is great interest in hiPSC-CM for studying atrial electrophysiology in the context of atrial fibrillation (AF). Strong associations are known between gene variants and the risk to develop AF. Atrial hiPSC-CM should be the model of choice to measure the impact of a distinct genetic background on human atrial electrophysiology. The Passier and Keller groups have shown that addition of retinoic acid (RA) in the differentiation protocol from hiPSC to CM suffices to induce atrial differentiation in stem cell derived CM (Lee et al., 2017). Here we will focus on RA´s ability to induce a true atrial-like AP shape in hiPSC-CM. Additionally, CRISPR/Cas9-based targeting of fluorescent reporters has been used to target ventricular hiPSC-CM (expressing myosin light chain 2) (Luo et al., 2021) or atrial hiPSC-CM (expressing sarcolipin) (Chirikian et al., 2021). In the absence of RA the percent of atrial cells was low (between 0.6% and 2.7%, depending on the culture duration). Cells identified as atrial cells showed an effect upon low concentrations (100 μM) of 4-AP. However, they missed the typical spike and dome shape and 4-AP prolonged but did not shortened APD_{90} (Wettwer et al., 2004), indicating a rather incomplete atrial AP phenotype (Schulz et al., 2023).

In order to estimate the efficacy of RA to induce an atrial-like AP shape, parameters are needed that allow clear discrimination between ventricular and atrial tissue. In contrast to APD_{90} and RMP (discussed above), the repolarization fraction (RF) is a powerful discriminator with human atrial tissue showing high and ventricular tissue low RF (Horváth et al., 2018). RF was uniformly low in hiPSC-CM/EHT not treated with RA (Itzhaki et al., 2010; Merkle et al., 2017), indicating a predominantly ventricular phenotype. RF was substantially higher in hiPSC-CM treated with RA, indicating a more atrial phenotype (Lemme et al., 2018). The high RF in atrium reflects stronger initial repolarization and relates to larger transient outward currents than in the human ventricle (Amos et al., 1996). Transient outward currents not only differ quantitatively between atrium and ventricle, but also qualitatively. The ultrarapidly activating potassium current (I_{Kur}) contributes to repolarization in the human atrium but not in the ventricle (Ravens et al., 2013). Pharmacological block of I_{Kur} by low concentrations of 4-AP (10–100 μM) allows detection of I_{Kur} in voltage clamp experiments (Amos et al., 1996). Furthermore, 4-AP enables to estimate contribution of I_{Kur} to AP shape, since a much higher concentration (millimolar range) is needed to block the transient outward current (present also in human ventricle). Thus, the sensitivity of the AP shape to low concentrations of 4-AP safely differentiates between the two regions. Finally,

acetylcholine activates the atrial-selective acetylcholine-activated potassium current ($I_{K,ACh}$), shorten APD_{90} and hyperpolarize the RMP in atrial, but not in ventricular tissue (Lemme et al., 2018). Of note, acetylcholine antagonizes effects of cAMP-dependent drugs such as isoprenaline in both tissues, the well-known indirect antiadrenergic effect (Méry et al., 1997).

In the seminal paper that showed the efficacy of RA to induce atrial differentiation in human embryonic stem cell (hESC)-derived CM, currents sensitive to 4-AP (50 μM) accounted to ~6 pA/pF (pulse potential of +50 mV) (Devalla et al., 2015), which is 2-fold lower than values for I_{Kur} in human atrial CM (Ford et al., 2013). A later study in hiPSC-CM showed even smaller currents (~2 pA/pF) (Hilderink et al., 2020), but they were sufficient to produce a short APD at 20% repolarization (APD_{20}; 20 ms), close to the situation in human atrium (7 ms) (Liang et al., 2016; Horváth et al., 2018). Furthermore, as in human atrium, plateau voltage was below 0 mV, and both short APD_{20} and negative plateau voltage were sensitive to 50 μM 4-AP (Devalla et al., 2015). However, the effects of I_{Kur} block on final repolarization differed. While in atrial hESC-CM block of I_{Kur} (with 4-AP or by knockout of $K_V1.5$) clearly prolonged APD_{90} (Devalla et al., 2015; Marczenke et al., 2017), it shortened APD_{90} in human atrium (4-AP and several newly developed I_{Kur} blockers) (Wettwer et al., 2004; Christ et al., 2008; Ford et al., 2013; Ford et al., 2016). This discrepancy, which is due to an indirect stimulation of I_{Kr} by the more positive plateau current (Wettwer et al., 2004), may have relevant consequences for the application of hiPSC-CM as a model for atrial drug screening. In fact, pharmacological blockers of I_{Kur} have gained great interest since they were believed to effectively terminate AF without the risk of life-threatening ventricular proarrhythmic effects. However, the inefficacy of I_{Kur} block to prolong atrial refractoriness *in vitro* (Du et al., 2015; Lemoine et al., 2018; Van de Sande et al., 2021; Lachaud et al., 2022) may explain the lack of antiarrhythmic efficacy in AF in patients (Shunmugam et al., 2018; Camm et al., 2019). Therefore, any pharmacological model where I_{Kur} block increases APD_{90} could be misleading (Devalla et al., 2015).

HiPSC-CM can be used to study tachypacing-induced remodeling in ventricular but also in atrial hiPSC-CM. In atrial tissues of patients with AF, I_{Kur} is smaller (Van Wagoner et al., 1997) and APD_{20} longer, resulting in a more triangulated (lower RF) AP. Importantly, APD_{90} is no longer shortened by 4-AP (Wettwer et al., 2004). One of our in-house RA-treated hiPSC-CM cell line shows some typical atrial characteristics (effect of 4-AP on APD), but the long APD_{20} resembles more the situation in chronic human AF (30 vs. 29 ms) (Ravens et al., 2015; Lemme et al., 2018). This finding could explain why we failed to induce remodeling in tachypaced atrial EHT (Lemoine et al., 2021).

Basal inward rectifier currents are smaller in human atrium than in ventricle (Varró et al., 1993; Horváth et al., 2018). There are no studies that compared basal inward rectifier currents between stem cell-derived CM treated with RA or not, but in small datasets activation of the $I_{K,ACh}$ was restricted to RA-treated stem cell-derived CM (Devalla et al., 2015; Lee et al., 2017; Argenziano et al., 2018). In one study, the effect of muscarinic receptor activation on APD_{90} in RA-treated atrial hESC-CM was hard to detect at all (Devalla et al., 2015), but accounted to ~20%–30% in atrial hiPSC-CM or atrial EHT (Lemme et al., 2018; Goldfracht et al., 2020), close to the situation in human atrium (Dobrev et al., 2001). $I_{K,ACh}$ is another atrial-selective potassium current that undergoes electrical remodeling. Shortening of APD_{90} upon activation of $I_{K,ACh}$ is lost in AF and constitutively active $I_{K,ACh}$ (Dobrev et al., 2005) is believed to contribute to increased inward rectifier in AF (Van Wagoner et al., 1997). Therefore, it is obvious that a substantial $I_{K,ACh}$ under control condition is necessary to study impact of tachycardic remodeling on inward rectifier currents.

In the human (but not rodent) heart, serotonin increases $I_{Ca,L}$ and force in the atrium but not in the ventricle (Jahnel et al., 1992; Pau et al., 2003). The physiological relevance still remains open. Under pathological conditions such as chronic AF, serotonin responses undergo complex remodeling: positive inotropic and proarrhythmic effects are diminished (Pau et al., 2007; Christ et al., 2014), while the increase in $I_{Ca,L}$ remains intact (Berk et al., 2016), underlining potential interest to use serotonin as a marker for AF-induced remodeling. It is not known whether atrial hiPSC-CM show an increase in $I_{Ca,L}$ and force in response to serotonin.

How specific and robust are computational models in recapitulating the hiPSC-CM phenotype(s)?

Biophysics-based computational modelling and simulations are a useful tool for quantitative characterization and understanding of the highly variable hiPSC-CM phenotype. To our knowledge, two different comprehensive approaches have thus far been employed in this context that we will refer to, for the sake of brevity, as data-based and population-based. Both approaches build a collection of virtual hiPSC-CMs by varying the model parameter values.

In the data-based approach that was first applied by Kernik et al. (2019), the parameter value ranges are derived directly from *in vitro* experiments. Whereas, in the population-based approach, which was introduced to hiPSC-CM realm by Paci et al. (2017), a chosen set of model parameter values are first varied in arbitrarily defined ranges, focusing on the maximum conductances and rates of ion channels and transporters. Then, the obtained virtual hiPSC-CM population is pruned by comparing a defined set of functional biomarkers to *in vitro* measurements. The fundamental limitation of the population-based approach is that despite the pruning the final collection will contain virtual hiPSC-CMs, whose parameter combinations are unphysiological in that they do not necessarily exist *in vitro*. The situation is analogous to using AP morphology as a marker for chamber specificity, because a ventricular- or atrial-like AP shapes can potentially be a result of underlying ion current strength combinations that do not exist in native human CMs. The data-based approach, on the other hand, is limited, well, by the available data. Despite the progress of high-throughput methods, measuring everything in one lab is not realistic. Thus, when the dataset is expanded to include measurements from multiple labs, the physiological variability will be exacerbated by inter-lab variability. More importantly, due to practical reasons, the depth of phenotype characterization in this approach will be limited, as it was in the Kernik et al. (2019)s study. Therefore, the model formulations need to be biophysically less detailed with fewer parameters so that their values can actually be measured *in vitro*. Thus, the model's application area is restricted to the phenotypic space, which the

data in question present—limited robustness. On the other hand, the more detailed hiPSC-CM models that have been employed in the population-based approach follow the common iterative modelling tradition, inheriting some model components and their parameters from previous, non-hiPSC-based, model generations—limited specificity.

Despite the limitations mentioned above, and others not discussed here, computational modelling is perhaps the only way to make sense of *in vitro* hiPSC-CM data, quantitatively. Although there are substantial and continuous methodology development efforts to narrowing the gap, the hiPSC-CM phenotype is different from native human CMs; a fact with which the cardiac research community has luckily come to terms with. The capabilities of the so-called computational maturation in translating the hiPSC-CM-based findings to the human context have already been shown in multiple independent studies (Gong and Sobie, 2018; Koivumäki et al., 2018; Tveito, Jæger, Huebsch, Charrez, Edwards, Wall, Healy; Jæger et al., 2020). Wider adoption of such frameworks would probably be fostered by transparent comparisons of the cell models as well as the inversion and regression approaches used in translation, as done recently for example, by Paci et al. (2021).

HiPSC-CM and automated patch clamp: The dream wedding in experimental cardiac electrophysiology?

The advent of hiPSC-CM coincides with the development of automated patch clamp (APC). The technique allows high-throughput experiments and has therefore successfully replaced the technically demanding and time-consuming conventional patch clamp in the field of drug screening in cellular expression systems. Besides the much higher throughput, APC offers the unique possibility to exchange the intracellular solution during an experiment, a procedure that is hard to achieve in manual patch clamp. In principle, APC in hiPSC-CM could be able to combine the benefits of hiPSC-CM (human background, genetically defined or even edited systems) with high-throughput measurements. Until very recently, APC had failed in large, elongated adult CM. In contrast, isolated ball-shaped hiPSC-CM resemble the cells (e.g., CHO, HEK) of commonly used heterologous expression systems and could therefore be better suited for APC. In fact, sodium current (I_{Na}) and $I_{Ca,L}$ are large in any type of CMs and can therefore routinely be measured by APC in hiPSC-CM (Goversen et al., 2018; Li et al., 2019). Ion current measurements by APC in hiPSC-CM bearing patient mutations could be of great interest and one recent study used hiPSC-CM derived from patients with Brugada-syndrome AP (Li et al., 2021). In contrast, we are not sure whether ion current measurements in hiPSC-CM from healthy donors will replace "traditional" measurements in expression system (Lemoine and Christ, 2021). The main reason lies in the fact that, even in human ventricular myocytes, repolarizing potassium outward currents are very small and difficult to detect. Delayed rectifier K^+ channel currents in adult human cardiac myocytes amount to less than 1 pA/pF (Jost et al., 2013) or remained undetectable [for detailed discussion compare (Ma et al., 2011)]. Moretti et al. (2010) were the first to demonstrate slow delayed rectifier currents (I_{Ks}) in hiPSC-CM. Ma et al. (2011) showed biophysical characteristics of delayed rectifier in hiPSC-CM close to the situation in humans. Interestingly, the authors found I_{Ks} currents in only 50% of hiPSC-CM, as reported earlier for human ventricular CM (Virág et al., 2001). Even with manual patch clamp only few studies report delayed currents (both I_{Ks} and I_{Kr}) in hiPSC-CM (Ma et al., 2013; Zhang et al., 2014). There is concern whether biophysical properties of I_{Kr} in hiPSC-CM resemble the situation in human CM (Zhang et al., 2014). It is unclear whether the issue relates to biological or methodological aspects (Christ et al., 2015). At present we are not aware of data on delayed rectifier currents in hiPSC-CM obtained by APC.

The shape of the AP represents a sum parameter of all ion channels active in a relatively intact cell/tissue. This may explain why (drug) effects on repolarization can be easily detected, making AP recording by APC highly attractive (Scheel et al., 2014). From the beginning, APD was consistently shorter in isolated hiPSC-CM when measured by APC than APD measured in intact adult human ventricular tissue by conventional sharp microelectrodes (Friedrichs et al., 2015). Holding currents (see above), essential to bring the diastolic potential in a range that allows Na^+-channel activation, could be responsible for the short APD. The issue with too small inward rectifier in hiPSC-CM could be fixed by dynamic clamping (Verkerk et al., 2017; Verkerk AO and Wilders, 2020). However, individual adjustment of dynamic clamp current density is limited to cell capacitance (Becker et al., 2020) but not to actual I_{K1} even in advanced APC systems. High membrane resistance of small cells like hiPSC-CM promotes voltage errors. The issue is of particular importance in case of improper seal resistances. Only one study using APC in ventricular-like hiPSC-CM reported some indirect information about seal resistance. The authors used a seal resistance >100 MΩ as a criterion for successful patching (Seibertz et al., 2022). Actual values in the data set were not reported. However, we would suspect that much higher values would be necessary to record the true membrane potential, values that are difficult to achieve even with manual patch clamp. In the same study authors had to apply continuous holding currents (mean value of −9.7 ± 1.5 pA/pF) to allow upstroke generation (Seibertz et al., 2022). Such holding currents are almost fivefold higher than peak I_{Kr} current in hiPSC-CM (Feng et al., 2021) and may at least in part explain the very short APD_{50} reported in this study [~70 ms, which compares with 220 ms in adult human ventricular tissue (Skibsbye et al., 2014)].

Thus, the high throughput in APC comes at a price. It is clearly an advantage if large numbers of compounds are to be tested during drug development. It also opens the possibility to phenotype hiPSC-CM from cell lines of larger patient populations. However, given the above considerations, such approaches are presently restricted to robustly measurable currents such as I_{Na} and $I_{Ca,L}$ (Seibertz et al., 2022). The log-fold increase in number of experiments will be helpful to cope with data scattering, a phenomenon whose basis we are just beginning to better understand (Ismaili et al., 2020). We are sceptical if APC is useful for AP recordings in hiPSC-CM. However, APC could help to increase the power of discrimination when ion currents are measured that differ only slightly between experimental groups.

Regulation of ion currents by cAMP

Ca^{2+}-handling in heart muscle is under strong control of the sympathetic nervous system. One of the many effectors, $I_{Ca,L}$, can be

easily monitored by patch clamp. Regulation of $I_{Ca,L}$ by cAMP/PKA pathway is described in high detail in adult CM from many mammalian species including humans (Liu et al., 2020; Hovey et al., 2022; Papa et al., 2022). Thus, measurements of $I_{Ca,L}$ in hiPSC-CM should help to elucidate how closely regulation resembles the situation in human adult myocardium.

As in the human heart, $I_{Ca,L}$ in hiPSC-EHT can be robustly increased by activation of both β_1-and β_2-adrenoceptors (Molenaar et al., 2014; Uzun et al., 2016). The potency of both epi- and norepinephrine to increase $I_{Ca,L}$ was close to the situation in human CM. $I_{Ca,L}$ increases were drastically smaller in hiPSC-CM cultured as monolayers than in EHT, while maximum cAMP increases (measured by Foerster energy transfer, FRET) were only slightly smaller (Uzun et al., 2016). Importantly, inhibition of PDE4 could bring increases in cAMP and $I_{Ca,L}$ values in monolayers to values measured in EHT, indicating that PDE4 strongly restricts cAMP and its coupling to Ca^{2+}-channels in hiPSC-CM cultured in monolayer format (Iqbal et al., 2021). Inhibition of PDE4 also potentiated inotropic responses to adrenergic stimulation in EHT, while inhibition of PDE3 did not (Saleem et al., 2020). The dominant impact of PDE4 seems to be a peculiarity of hiPSC-CM even in EHT format and contrasts with adult human myocardium, where PDE3 is the major PDE isoform restricting adrenergic responses (Eschenhagen, 2013; Molenaar et al., 2013).

As discussed above, I_f is consistently expressed in many hiPSC-CM cell lines and provides an opportunity to study regulation of ion currents by cAMP in hiPSC-CM. As in animal sinus node cells, I_f was increased by stimulation of β-adrenoceptors (by isoprenaline) but inhibited by stimulation of muscarinic receptors (by carbachol). Importantly, the potency of both compounds was close to values reported for rabbit sinus node cells (no data available from humans) (Giannetti et al., 2021), demonstrating that cAMP/PKA-dependent signaling is well developed in many hiPSC-CM.

Outlook

We discussed some aspects of electrophysiological measurements in hiPSC-CM and the substantial progress in electrophysiological characterization of hiPSC-CM. However, results still vary widely between different studies. Reasons are expected in methodological issues in the recording techniques, but also in biological differences between cell lines and culture techniques (e.g., monolayers vs. EHT, age of cultures, different culture media). The multitude of differences implies that the comparability between studies is more challenging in hiPSC-CM than in traditional studies on animal or human heart tissues. Experimental electrophysiologists can help to reduce scatter by critical application and interpretation of the various recording methods. The enthusiasm about application of hiPSC-CM in experimental cardiac electrophysiology seems unbroken. Thus, we expect that the concerted expertise of experimental electrophysiologists and stem cell experts will solve the challenges step by step.

Author contributions

Conceptualization: DI, TC; methodology: DI, TC; writing—original draft preparation: DI, CS, AnH, JK, TC; writing—review and editing: DM, ArH, TE; supervision: TE, TC; funding acquisition: ArH, TE, TC; All authors have approved the submission of this manuscript.

Funding

This study was supported by the German Ministry of Education and Research (BMBF, FKZ161L0236), by the German Centre for Cardiovascular Research (Grant No. 81Z0710110 to CS), European Research Council (ERC-AG IndivuHeart), Deutsche Forschungsgemeinschaft (DFG Es 88/12-1, DFG HA 3423/5-1), the Freie und Hansestadt Hamburg and the Fédération Française de Cardiologie (to DM).

Conflict of interest

TE and ArH were co-founders of EHT Technologies GmbH.

The remaining authors declare that the research was conducted in the absence of any commercial or financial relationships that could be construed as a potential conflict of interest.

The handling editor YE declared a past co-authorship with the author TE.

Publisher's note

References

Amos, G. J., Wettwer, E., Metzger, F., Li, Q., Himmel, H. M., and Ravens, U. (1996). Differences between outward currents of human atrial and subepicardial ventricular myocytes. *J. Physiol.* 491, 31–50. doi:10.1113/jphysiol.1996.sp021194

Argenziano, M., Lambers, E., Hong, L., Sridhar, A., Zhang, M., Chalazan, B., et al. (2018). Electrophysiologic characterization of calcium handling in human induced pluripotent stem cell-derived atrial cardiomyocytes. *Stem Cell Rep.* 10, 1867–1878. doi:10.1016/j.stemcr.2018.04.005

Becker, N., Horváth, A., De Boer, T., Fabbri, A., Grad, C., Fertig, N., et al. (2020). Automated dynamic clamp for simulation of Ik1 in human induced pluripotent stem cell–derived cardiomyocytes in real time using patchliner Dynamite8. *Curr. Protoc. Pharmacol.* 88, e70–e23. doi:10.1002/cpph.70

Berk, E., Christ, T., Schwarz, S., Ravens, U., Knaut, M., and Kaumann, A. J. (2016). In permanent atrial fibrillation, PDE3 reduces force responses to 5-HT, but PDE3 and PDE4 do not cause the blunting of atrial arrhythmias. *Br. J. Pharmacol.* 173, 2478–2489. doi:10.1111/bph.13525

Camm, A. J., Dorian, P., Hohnloser, S. H., Kowey, P. R., Tyl, B., Ni, Y., et al. (2019). A randomized, double-blind, placebo-controlled trial assessing the efficacy of S66913 in patients with paroxysmal atrial fibrillation. *Eur. Hear. J. - Cardiovasc. Pharmacother.* 5, 21–28. doi:10.1093/ehjcvp/pvy022

Casini, S., Verkerk, A. O., and Remme, C. A. (2017). Human iPSC-derived cardiomyocytes for investigation of disease mechanisms and therapeutic strategies in inherited arrhythmia syndromes: Strengths and limitations. *Cardiovasc. Drugs Ther.* 31, 325–344. doi:10.1007/s10557-017-6735-0

Chirikian, O., Goodyer, W. R., Dzilic, E., Serpooshan, V., Buikema, J. W., McKeithan, W., et al. (2021). CRISPR/Cas9-based targeting of fluorescent reporters to human iPSCs to isolate atrial and ventricular-specific cardiomyocytes. *Sci. Rep.* 11, 3026. doi:10.1038/s41598-021-81860-x

Christ, T., Horvath, A., and Eschenhagen, T. (2015). LQT1-phenotypes in hiPSC: Are we measuring the right thing? *Proc. Natl. Acad. Sci. U. S. A.* 112, E1968. doi:10.1073/pnas.1503347112

Christ, T., Kovács, P. P., Acsai, K., Knaut, M., Eschenhagen, T., Jost, N., et al. (2016). Block of Na+/Ca2+ exchanger by SEA0400 in human right atrial preparations from patients in sinus rhythm and in atrial fibrillation. *Eur. J. Pharmacol.* 788, 286–293. doi:10.1016/J.EJPHAR.2016.06.050

Christ, T., Rozmaritsa, N., Engel, A., Berk, E., Knaut, M., Metzner, K., et al. (2014). Arrhythmias, elicited by catecholamines and serotonin, vanish in human chronic atrial fibrillation. *Proc. Natl. Acad. Sci.* 111, 11193–11198. doi:10.1073/pnas.1324132111

Christ, T., Wettwer, E., Voigt, N., Hála, O., Radicke, S., Matschke, K., et al. (2008). Pathology-specific effects of the IKur/Ito/Ik,ACh blocker AVE0118 on ion channels in human chronic atrial fibrillation. *Br. J. Pharmacol.* 154, 1619–1630. doi:10.1038/bjp.2008.209

Dangman, K. H., Danilo, P., Hordof, A. J., Mary-Rabine, L., Reder, R. F., and Rosen, M. R. (1982). Electrophysiologic characteristics of human ventricular and Purkinje fibers. *Circulation* 65, 362–368. doi:10.1161/01.CIR.65.2.362

Devalla, H. D., Schwach, V., Ford, J. W., Milnes, J. T., El-Haou, S., Jackson, C., et al. (2015). Atrial-like cardiomyocytes from human pluripotent stem cells are a robust preclinical model for assessing atrial-selective pharmacology. *EMBO Mol. Med.* 7, 394–410. doi:10.15252/emmm.201404757

Dobrev, D., Friedrich, A., Voigt, N., Jost, N., Wettwer, E., Christ, T., et al. (2005). The G protein-gated potassium current Ik,ACh is constitutively active in patients with chronic atrial fibrillation. *Circulation* 112, 3697–3706. doi:10.1161/CIRCULATIONAHA.105.575332

Dobrev, D., Graf, E., Wettwer, E., Himmel, H. M., Hála, O., Doerfel, C., et al. (2001). Molecular basis of downregulation of G-protein–coupled inward rectifying K^+ current ($I_{K,ACh}$) in chronic human atrial fibrillation. *Circulation* 104, 2551–2557. doi:10.1161/hc4601.099466

Du, D. T. M., Hellen, N., Kane, C., and Terracciano, C. M. N. (2015). Action potential morphology of human induced pluripotent stem cell-derived cardiomyocytes does not predict cardiac chamber specificity and is dependent on cell density. *Biophys. J.* 108, 1–4. doi:10.1016/j.bpj.2014.11.008

Eisner, D. A., and Sipido, K. R. (2004). Sodium calcium exchange in heart: Necessity or luxury? *Circ. Res.* 95, 549–551. doi:10.1161/01.RES.0000143419.87518.9e

Eschenhagen, T., Didié, M., Heubach, J., Ravens, U., and Zimmermann, W. H. (2002). Cardiac tissue engineering. *Transpl. Immunol.* 9, 315–321. doi:10.1016/S0966-3274(02)00011-4

Eschenhagen, T. (2013). PDE4 in the human heart - major player or little helper? *Br. J. Pharmacol.* 169, 524–527. doi:10.1111/bph.12168

Feng, L., Zhang, J., Lee, C. H., Kim, G., Liu, F., Petersen, A. J., et al. (2021). Long QT syndrome KCNH2 variant induces hERG1a/1b subunit imbalance in patient-specific induced pluripotent stem cell-derived cardiomyocytes. *Circ. Arrhythmia Electrophysiol.* 14, E009343. doi:10.1161/CIRCEP.120.009343

Fine, M., Lu, F. M., Lin, M. J., Moe, O., Wang, H. R., and Hilgemann, D. W. (2013). Human-induced pluripotent stem cell-derived cardiomyocytes for studies of cardiac ion transporters. *Am. J. Physiol. - Cell Physiol.* 305, 481–491. doi:10.1152/ajpcell.00143.2013

Flenner, F., Jungen, C., Küpker, N., Ibel, A., Kruse, M., Koivumäki, J. T., et al. (2021). Translational investigation of electrophysiology in hypertrophic cardiomyopathy. *J. Mol. Cell. Cardiol.* 157, 77–89. doi:10.1016/j.yjmcc.2021.04.009

Ford, J., Milnes, J., El Haou, S., Wettwer, E., Loose, S., Matschke, K., et al. (2016). The positive frequency-dependent electrophysiological effects of the IKur inhibitor XEN-D0103 are desirable for the treatment of atrial fibrillation. *Hear. Rhythm.* 13, 555–564. doi:10.1016/j.hrthm.2015.10.003

Ford, J., Milnes, J., Wettwer, E., Christ, T., Rogers, M., Sutton, K., et al. (2013). Human electrophysiological and pharmacological properties of XEN-d0101: A novel atrial-selective kv1.5/IKur inhibitor. *J. Cardiovasc. Pharmacol.* 61, 408–415. doi:10.1097/FJC.0b013e31828780eb

Friedrichs, S., Malan, D., Voss, Y., and Sasse, P. (2015). Scalable electrophysiological investigation of ips cell-derived cardiomyocytes obtained by a lentiviral purification strategy. *J. Clin. Med.* 4, 102–123. doi:10.3390/jcm4010102

Giannetti, F., Benzoni, P., Campostrini, G., Milanesi, R., Bucchi, A., Baruscotti, M., et al. (2021). A detailed characterization of the hyperpolarization-activated "funny" current (I f) in human-induced pluripotent stem cell (iPSC)–derived cardiomyocytes with pacemaker activity. *Pflugers Arch. Eur. J. Physiol.* 473, 1009–1021. doi:10.1007/s00424-021-02571-w

Giles, W. R., and Noble, D. (2016). Rigorous phenotyping of cardiac iPSC preparations requires knowledge of their resting potential(s). *Biophys. J.* 110, 278–280. doi:10.1016/j.bpj.2015.06.070

Goldfracht, I., Protze, S., Shiti, A., Setter, N., Gruber, A., Shaheen, N., et al. (2020). Generating ring-shaped engineered heart tissues from ventricular and atrial human pluripotent stem cell-derived cardiomyocytes. *Nat. Commun.* 11, 75–15. doi:10.1038/s41467-019-13868-x

Gong, J. Q. X., and Sobie, E. A. (2018). Population-based mechanistic modeling allows for quantitative predictions of drug responses across cell types. *Npj Syst. Biol. Appl.* 414, 11. doi:10.1038/s41540-018-0047-2

Goversen, B., Becker, N., Stoelzle-Feix, S., Obergrussberger, A., Vos, M. A., van Veen, T. A. B., et al. (2018). A hybrid model for safety pharmacology on an automated patch clamp platform: Using dynamic clamp to join iPSC-derived cardiomyocytes and simulations of Ik1 ion channels in real-time. *Front. Physiol.* 8, 1094–1110. doi:10.3389/fphys.2017.01094

Hilderink, S., Devalla, H. D., Bosch, L., Wilders, R., and Verkerk, A. O. (2020). Ultrarapid delayed rectifier K+ channelopathies in human induced pluripotent stem cell-derived cardiomyocytes. *Front. Cell Dev. Biol.* 8, 536–614. doi:10.3389/fcell.2020.00536

Himmel, H. M., Bussek, A., Hoffmann, M., Beckmann, R., Lohmann, H., Schmidt, M., et al. (2012). Field and action potential recordings in heart slices: Correlation with established *in vitro* and *in vivo* models. *Br. J. Pharmacol.* 166, 276–296. doi:10.1111/j.1476-5381.2011.01775.x

Horváth, A., Christ, T., Koivumäki, J. T., Prondzynski, M., Zech, A. T. L., Spohn, M., et al. (2020). Case report on: Very early afterdepolarizations in HiPSC-cardiomyocytes—an artifact by Big conductance calcium activated potassium current (ibk,Ca). *Cells* 9, 253. doi:10.3390/cells9010253

Horváth, A., Lemoine, M. D., Löser, A., Mannhardt, I., Flenner, F., Uzun, A. U., et al. (2018). Low resting membrane potential and low inward rectifier potassium currents are not inherent features of hiPSC-derived cardiomyocytes. *Stem Cell Rep.* 10, 822–833. doi:10.1016/j.stemcr.2018.01.012

Hovey, L., Gamal El-Din, T. M., and Catterall, W. A. (2022). Convergent regulation of CaV1.2 channels by direct phosphorylation and by the small GTPase RAD in the cardiac fight-or-flight response. *Proc. Natl. Acad. Sci. U. S. A.* 119, e2208533119. doi:10.1073/PNAS.2208533119

Iqbal, Z., Ismaili, D., Dolce, B., Petersen, J., Reichenspurner, H., Hansen, A., et al. (2021). Regulation of basal and norepinephrine-induced cAMP and ICa in hiPSC-cardiomyocytes: Effects of culture conditions and comparison to adult human atrial cardiomyocytes. *Cell. Signal.* 82, 109970. doi:10.1016/J.CELLSIG.2021.109970

Ismaili, D., Geelhoed, B., and Christ, T. (2020). Ca2+ currents in cardiomyocytes: How to improve interpretation of patch clamp data? *Prog. Biophys. Mol. Biol.* 157, 33–39. doi:10.1016/J.PBIOMOLBIO.2020.05.003

Ismaili, D., Gurr, K., Horváth, A., Yuan, L., Lemoine, M. D., Schulz, C., et al. (2022). Regulation of APD and force by the Na+/Ca2+ exchanger in human-induced pluripotent stem cell-derived engineered heart tissue. *Cells* 11, 2424. doi:10.3390/cells11152424

Itzhaki, I., Maizels, L., Huber, I., Zwi-Dantsis, L., Caspi, O., Winterstern, A., et al. (2010). Modelling the long QT syndrome with induced pluripotent stem cells. *Nat* 471, 225–229. doi:10.1038/nature09747

Ivashchenko, C. Y., Pipes, G. C., Lozinskaya, I. M., Lin, Z., Xiaoping, X., Needle, S., et al. (2013). Human-induced pluripotent stem cell-derived cardiomyocytes exhibit temporal changes in phenotype. *Am. J. Physiol. - Hear. Circ. Physiol.* 305, H913–H922. doi:10.1152/ajpheart.00819.2012

Jæger, K. H., Charwat, V., Charrez, B., Finsberg, H., Maleckar, M. M., Wall, S., et al. (2020). Improved computational identification of drug response using optical measurements of human stem cell derived cardiomyocytes in microphysiological systems. *Front. Pharmacol.* 10, 1648. doi:10.3389/FPHAR.2019.01648/BIBTEX

Jahnel, U., Rupp, J., Ertl, R., and Nawrath, H. (1992). Positive inotropic response to 5-HT in human atrial but not in ventricular heart muscle. *J. Pharmacol. Exp. Ther.* 2, 482–485.

Jost, N., Virág, L., Comtois, P., Ordög, B., Szuts, V., Seprényi, G., et al. (2013). Ionic mechanisms limiting cardiac repolarization reserve in humans compared to dogs. *J. Physiol.* 591, 4189–4206. doi:10.1113/jphysiol.2013.261198

Kernik, D. C., Morotti, S., Di Wu, H., Garg, P., Duff, H. J., Kurokawa, J., et al. (2019). A computational model of induced pluripotent stem-cell derived cardiomyocytes incorporating experimental variability from multiple data sources. *J. Physiol.* 597, 4533–4564. doi:10.1113/JP277724

Kilpinen, H., Goncalves, A., Leha, A., Afzal, V., Alasoo, K., Ashford, S., et al. (2017). Common genetic variation drives molecular heterogeneity in human iPSCs. *Nature* 546, 370–375. doi:10.1038/nature22403

Kohajda, Z., Tóth, N., Szlovák, J., Loewe, A., Bitay, G., Gazdag, P., et al. (2020). Novel Na+/Ca2+ exchanger inhibitor ORM-10962 supports coupled function of funny-current and Na+/Ca2+ exchanger in pacemaking of rabbit sinus node tissue. *Front. Pharmacol.* 10, 1632. doi:10.3389/fphar.2019.01632

Koivumäki, J. T., Naumenko, N., Tuomainen, T., Takalo, J., Oksanen, M., Puttonen, K. A., et al. (2018). Structural immaturity of human iPSC-derived cardiomyocytes: *In silico* investigation of effects on function and disease modeling. *Front. Physiol.* 9, 80. doi:10.3389/fphys.2018.00080

Lachaud, Q., Aziz, M. H. N., Burton, F. L., Macquaide, N., Myles, R. C., Simitev, R. D., et al. (2022). Electrophysiological heterogeneity in large populations of rabbit ventricular cardiomyocytes. *Cardiovasc. Res.* 118, 3112–3125. doi:10.1093/cvr/cvab375

Lee, J. H., Protze, S. I., Laksman, Z., Backx, P. H., and Keller, G. M. (2017). Human pluripotent stem cell-derived atrial and ventricular cardiomyocytes develop from distinct mesoderm populations. *Cell Stem Cell* 21, 179–194. e4. doi:10.1016/j.stem.2017.07.003

Lemme, M., Ulmer, B. M., Lemoine, M. D., Zech, A. T. L., Flenner, F., Ravens, U., et al. (2018). Atrial-like engineered heart tissue: An *in vitro* model of the human atrium. *Stem Cell Rep.* 11, 1378–1390. doi:10.1016/J.STEMCR.2018.10.008

Lemoine, M. D., and Christ, T. (2021). Human induced pluripotent stem cell-derived cardiomyocytes: The new working horse in cardiovascular pharmacology? *J. Cardiovasc. Pharmacol.* 77, 265–266. doi:10.1097/FJC.0000000000000981

Lemoine, M. D., Krause, T., Koivumäki, J. T., Prondzynski, M., Schulze, M. L., Girdauskas, E., et al. (2018). Human induced pluripotent stem cell-derived engineered heart tissue as a sensitive test system for QT prolongation and arrhythmic triggers. *Circ. Arrhythmia Electrophysiol.* 11, e006035. doi:10.1161/CIRCEP.117.006035

Lemoine, M. D., Lemme, M., Ulmer, B. M., Braren, I., Krasemann, S., Hansen, A., et al. (2021). Intermittent optogenetic tachypacing of atrial engineered heart tissue induces only limited electrical remodelling. *J. Cardiovasc. Pharmacol.* 77, 291–299. doi:10.1097/FJC.0000000000000951

Li, W., Luo, X., Ulbricht, Y., and Guan, K. (2021). Blebbistatin protects iPSC-CMs from hypercontraction and facilitates automated patch-clamp based electrophysiological study. *Stem Cell Res.* 56, 102565. doi:10.1016/j.scr.2021.102565

Li, W., Luo, X., Ulbricht, Y., Wagner, M., Piorkowski, C., El-Armouche, A., et al. (2019). Establishment of an automated patch-clamp platform for electrophysiological and pharmacological evaluation of hiPSC-CMs. *Stem Cell Res.* 41, 101662. doi:10.1016/j.scr.2019.101662

Liang, P., Lan, F., Lee, A. S., Gong, T., Sanchez-Freire, V., Wang, Y., et al. (2013). Drug screening using a library of human induced pluripotent stem cell-derived cardiomyocytes reveals disease-specific patterns of cardiotoxicity. *Circulation* 127, 1677–1691. doi:10.1161/circulationaha.113.001883

Liang, P., Sallam, K., Wu, H., Li, Y., Itzhaki, I., Garg, P., et al. (2016). Patient-specific and genome-edited induced pluripotent stem cell–derived cardiomyocytes elucidate single-cell phenotype of Brugada syndrome. *J. Am. Coll. Cardiol.* 68, 2086–2096. doi:10.1016/J.JACC.2016.07.779

Litviňuková, M., Talavera-López, C., Maatz, H., Reichart, D., Worth, C. L., Lindberg, E. L., et al. (2020). Cells of the adult human heart. *Nature* 588, 466–472. doi:10.1038/s41586-020-2797-4

Liu, G., Papa, A., Katchman, A. N., Zakharov, S. I., Roybal, D., Hennessey, J. A., et al. (2020). Mechanism of adrenergic CaV1.2 stimulation revealed by proximity proteomics. *Nat* 577, 695–700. doi:10.1038/s41586-020-1947-z

Luo, X. L., Zhang, P., Liu, X., Huang, S., Le Rao, S., Ding, Q., et al. (2021). Myosin light chain 2 marks differentiating ventricular cardiomyocytes derived from human embryonic stem cells. *Pflugers Arch. Eur. J. Physiol.* 473, 991–1007. doi:10.1007/s00424-021-02578-3

Ma, D., Wei, H., Zhao, Y., Lu, J., Li, G., Sahib, N. B. E., et al. (2013). Modeling type 3 long QT syndrome with cardiomyocytes derived from patient-specific induced pluripotent stem cells. *Int. J. Cardiol.* 168, 5277–5286. doi:10.1016/j.ijcard.2013.08.015

Ma, J., Guo, L., Fiene, S. J., Anson, B. D., Thomson, J. A., Kamp, T. J., et al. (2011). High purity human-induced pluripotent stem cell-derived cardiomyocytes: Electrophysiological properties of action potentials and ionic currents. *Am. J. Physiol. - Hear. Circ. Physiol.* 301, 2006–2017. doi:10.1152/ajpheart.00694.2011

Mannhardt, I., Breckwoldt, K., Letuffe-Brenière, D., Schaaf, S., Schulz, H., Neuber, C., et al. (2016). Human engineered heart tissue: Analysis of contractile force. *Stem Cell Rep.* 7, 29–42. doi:10.1016/j.stemcr.2016.04.011

Mannhardt, I., Eder, A., Dumotier, B., Prondzynski, M., Kr-amer, E., Traebert, M., et al. (2017). Blinded contractility analysis in hipsc-cardiomyocytes in engineered heart tissue format: Comparison with human atrial trabeculae. *Toxicol. Sci.* 158, 164–175. doi:10.1093/toxsci/kfx081

Marczenke, M., Piccini, I., Mengarelli, I., Fell, J., Röpke, A., Seebohm, G., et al. (2017). Cardiac subtype-specific modeling of Kv1.5 ion channel deficiency using human pluripotent stem cells. *Front. Physiol.* 8, 469–511. doi:10.3389/fphys.2017.00469

Merkle, F. T., Ghosh, S., Kamitaki, N., Mitchell, J., Avior, Y., Mello, C., et al. (2017). Common genetic variation drives molecular heterogeneity in human iPSCs. *Nature* 545, 370–375. doi:10.1038/nature22403

Méry, P. F., Abi-Gerges, N., Vandecasteele, G., Jurevicius, J., Eschenhagen, T., and Fischmeister, R. (1997). Muscarinic regulation of the L-type calcium current in isolated cardiac myocytes. *Life Sci.* 60, 1113–1120. doi:10.1016/S0024-3205(97)00055-6

Molenaar, P., Christ, T., Berk, E., Engel, A., Gillette, K. T., Galindo-Tovar, A., et al. (2014). Carvedilol induces greater control of β2-than β1-adrenoceptor-mediated inotropic and lusitropic effects by PDE3, while PDE4 has no effect in human failing myocardium. *Naunyn. Schmiedeb. Arch. Pharmacol.* 387, 629–640. doi:10.1007/s00210-014-0974-4

Molenaar, P., Christ, T., Hussain, R. I., Engel, A., Berk, E., Gillette, K. T., et al. (2013). PDE3, but not PDE4, reduces β_1 - and β_2-adrenoceptor-mediated inotropic and lusitropic effects in failing ventricle from metoprolol-treated patients. *Br. J. Pharmacol.* 169, 528–538. doi:10.1111/bph.12167

Morad, M., and Zhang, X. H. (2017). Mechanisms of spontaneous pacing: Sinoatrial nodal cells, neonatal cardiomyocytes, and human stem cell derived cardiomyocytes1. *Can. J. Physiol. Pharmacol.* 95, 1100–1107. doi:10.1139/CJPP-2016-0743

Moretti, A., Bellin, M., Welling, A., Jung, C. B., Lam, J. T., Bott-Flügel, L., et al. (2010). Patient-specific induced pluripotent stem-cell models for long-QT syndrome. *N. Engl. J. Med.* 363, 1397–1409. doi:10.1056/NEJMoa0908679

Otsomaa, L., Levijoki, J., Wohlfahrt, G., Chapman, H., Koivisto, A.-P., Syrjanen, K., et al. (2020). Discovery and characterization of ORM-11372, a novel inhibitor of the sodium-calcium exchanger with positive inotropic activity. *Br. J. Pharmacol.* 177, 5534–5554. doi:10.1111/bph.15257

Paci, M., Koivumäki, J. T., Lu, H. R., Gallacher, D. J., Passini, E., and Rodriguez, B. (2021). Comparison of the simulated response of three *in silico* human stem cell-derived cardiomyocytes models and *in vitro* data under 15 drug actions. *Front. Pharmacol.* 12, 120. doi:10.3389/fphar.2021.604713

Paci, M., Passini, E., Severi, S., Hyttinen, J., and Rodriguez, B. (2017). Phenotypic variability in LQT3 human induced pluripotent stem cell-derived cardiomyocytes and their response to antiarrhythmic pharmacologic therapy: An *in silico* approach. *Hear. Rhythm.* 14, 1704–1712. doi:10.1016/j.hrthm.2017.07.026

Papa, A., Kushner, J., and Marx, S. O. (2022). Adrenergic regulation of calcium channels in the heart. *Annu. Rev. Physiol.* 84, 285–306. doi:10.1146/Annurev-Physiol-060121-04165310.1146/ANNUREV-PHYSIOL-060121-041653

Pau, D., Workman, A. J., Kane, K. A., and Rankin, A. C. (2007). Electrophysiological and arrhythmogenic effects of 5-hydroxytryptamine on human atrial cells are reduced in atrial fibrillation. *J. Mol. Cell. Cardiol.* 42, 54–62. doi:10.1016/j.yjmcc.2006.08.007

Pau, D., Workman, A. J., Kane, K. A., and Rankin, A. C. (2003). Electrophysiological effects of 5-hydroxytryptamine on isolated human atrial myocytes, and the influence of chronic β-adrenoceptor blockade. *Br. J. Pharmacol.* 140, 1434–1441. doi:10.1038/sj.bjp.0705553

Peischard, S., Möller, M., Disse, P., Ho, H. T., Verkerk, A. O., Strutz-Seebohm, N., et al. (2022). Virus-induced inhibition of cardiac pacemaker channel HCN4 triggers bradycardia in human-induced stem cell system. *Cell. Mol. Life Sci.* 79, 440–517. doi:10.1007/s00018-022-04435-7

Prasad, K., and Callaghan, J. C. (1970). Influence of glucose metabolism on ouabain-induced changes in the transmembrane potential and contraction of human heart *in vitro*. *Can. J. Physiol. Pharmacol.* 48, 801–812. doi:10.1139/y70-115

Prondzynski, M., Lemoine, M. D., Zech, A. T., Horváth, A., Di Mauro, V., Koivumäki, J. T., et al. (2019). Disease modeling of a mutation in α-actinin 2 guides clinical therapy in hypertrophic cardiomyopathy. *EMBO Mol. Med.* 11, e11115. doi:10.15252/EMMM.201911115

Protze, S. I., Liu, J., Nussinovitch, U., Ohana, L., Backx, P. H., Gepstein, L., et al. (2016). Sinoatrial node cardiomyocytes derived from human pluripotent cells function as a biological pacemaker. *Nat. Biotechnol.* 35135, 56–68. doi:10.1038/nbt.3745

Ravens, U., Katircioglu-Öztürk, D., Wettwer, E., Christ, T., Dobrev, D., Voigt, N., et al. (2015). Application of the RIMARC algorithm to a large data set of action potentials and clinical parameters for risk prediction of atrial fibrillation. *Med. Biol. Eng. Comput.* 53, 263–273. doi:10.1007/s11517-014-1232-0

Ravens, U., Poulet, C., Wettwer, E., and Knaut, M. (2013). Atrial selectivity of antiarrhythmic drugs. *J. Physiol.* 591, 4087–4097. doi:10.1113/jphysiol.2013.256115

Saleem, U., Ismaili, D., Mannhardt, I., Pinnschmidt, H., Schulze, T., Christ, T., et al. (2020). Regulation of ICa,L and force by PDEs in human-induced pluripotent stem cell-derived cardiomyocytes. *Br. J. Pharmacol.* 177, 3036–3045. doi:10.1111/BPH.15032

Scheel, O., Frech, S., Amuzescu, B., Eisfeld, J., Lin, K. H., and Knott, T. (2014). Action potential characterization of human induced pluripotent stem cell-derived cardiomyocytes using automated patch-clamp technology. *Assay. Drug Dev. Technol.* 12, 457–469. doi:10.1089/adt.2014.601

Schulz, C., Sönmez, M., Krause, J., Schwedhelm, E., Bangfen, P., Alihodzic, D., et al. (2023). *A critical role of retinoic acid concentration for the induction of a fully human-like atrial phenotype in hiPSC-CM*. BioRxiv. 2023.01.03.522611. doi:10.1101/2023.01.03.522611

Schwinger, R. H., Böhm, M., and Erdmann, E. (1990). Effectiveness of cardiac glycosides in human myocardium with and without "downregulated" beta-adrenoceptors. *J. Cardiovasc. Pharmacol.* 15, 692–697. doi:10.1097/00005344-199005000-00002

Seibertz, F., Rapedius, M., Fakuade, F. E., Tomsits, P., Liutkute, A., Cyganek, L., et al. (2022). A modern automated patch-clamp approach for high throughput electrophysiology recordings in native cardiomyocytes. *Commun. Biol.* 5, 969–1010. doi:10.1038/s42003-022-03871-2

Shunmugam, S. R., Sugihara, C., Freemantle, N., Round, P., Furniss, S., and Sulke, N. (2018). A double-blind, randomised, placebo-controlled, cross-over study assessing the use of XEN-D0103 in patients with paroxysmal atrial fibrillation and implanted pacemakers allowing continuous beat-to-beat monitoring of drug efficacy. *J. Interv. Card. Electrophysiol.* 51, 191–197. doi:10.1007/s10840-018-0318-2

Skibsbye, L., Poulet, C., Diness, J. G., Bentzen, B. H., Yuan, L., Kappert, U., et al. (2014). Small-conductance calcium-activated potassium (SK) channels contribute to action potential repolarization in human atria. *Cardiovasc. Res.* 103, 156–167. doi:10.1093/cvr/cvu121

Soltysinska, E., Olesen, S.-P., Christ, T., Wettwer, E., Varró, A., Grunnet, M., et al. (2009). Transmural expression of ion channels and transporters in human nondiseased and end-stage failing hearts. *Pflugers Arch. Eur. J. Physiol.* 459, 11–23. doi:10.1007/s00424-009-0718-3

Tveito, A., Jæger, K. H., Huebsch, N., Charrez, B., Edwards, A. G., Wall, S., et al. (2018). Inversion and computational maturation of drug response using human stem cell derived cardiomyocytes in microphysiological systems. *Sci. Rep.* 81, 176261–176314. doi:10.1038/s41598-018-35858-7

Uzun, A. U., Mannhardt, I., Breckwoldt, K., Horváth, A., Johannsen, S. S., Hansen, A., et al. (2016). Ca2+-currents in human induced pluripotent stem cell-derived cardiomyocytes effects of two different culture conditions. *Front. Pharmacol.* 7, 300. doi:10.3389/fphar.2016.00300

Van de Sande, D. V., Kopljar, I., Maaike, A., Teisman, A., Gallacher, D. J., Bart, L., et al. (2021). The resting membrane potential of hSC-CM in a syncytium is more hyperpolarised than that of isolated cells. *Channels* 15, 239–252. doi:10.1080/19336950.2021.1871815

Van Wagoner, D. R., Pond, A. L., McCarthy, P. M., Trimmer, J. S., and Nerbonne, J. M. (1997). Outward K+ current densities and Kv1.5 expression are reduced in chronic human atrial fibrillation. *Circ. Res.* 80, 772–781. doi:10.1161/01.RES.80.6.772

Varró, A., Nánási, P. P., and Lathrop, D. A. (1993). Potassium currents in isolated human atrial and ventricular cardiocytes. *Acta Physiol. Scand.* 149, 133–142. doi:10.1111/j.1748-1716.1993.tb09605.x

Verkerk Ao, W. R., and Wilders, R. (2020). Dynamic clamp in electrophysiological studies on stem cell-derived cardiomyocytes-why and how? *J. Cardiovasc Pharmacol.* 77, 267–279. doi:10.1097/FJC.0000000000000955

Verkerk, A. O., Veerman, C. C., Zegers, J. G., Mengarelli, I., Bezzina, C. R., and Wilders, R. (2017). Patch-clamp recording from human induced pluripotent stemcell-derived cardiomyocytes: Improving action potential characteristics throughdynamic clamp. *Int. J. Mol. Sci.* 18, 1873. doi:10.3390/ijms18091873

Virág, L., Iost, N., Opincariu, M., Szolnoky, J., Szécsi, J., Bogáts, G., et al. (2001). The slow component of the delayed rectifier potassium current in undiseased human ventricular myocytes. *Cardiovasc. Res.* 49, 790–797. doi:10.1016/S0008-6363(00)00306-0

Wettwer, E., Amos, G. J., Posival, H., and Ravens, U. (1994). Transient outward current in human ventricular myocytes of subepicardial and subendocardial origin. *Circ. Res.* 75, 473–482. doi:10.1161/01.RES.75.3.473

Wettwer, E., Hála, O., Christ, T., Heubach, J. F., Dobrev, D., Knaut, M., et al. (2004). Role of IKur in controlling action potential shape and contractility in the human atrium: Influence of chronic atrial fibrillation. *Circulation* 110, 2299–2306. doi:10.1161/01.CIR.0000145155.60288.71

Workman, A. J., Kane, K. A., and Rankin, A. C. (2003). Characterisation of the Na, K pump current in atrial cells from patients with and without chronic atrial fibrillation. *Cardiovasc. Res.* 59, 593–602. doi:10.1016/S0008-6363(03)00466-8

Zhang, M., D'Aniello, C., Verkerk, A. O., Wrobel, E., Frank, S., Ward-Van Oostwaard, D., et al. (2014). Recessive cardiac phenotypes in induced pluripotent stem cell models of Jervell and Lange-Nielsen syndrome: Disease mechanisms and pharmacological rescue. *Proc. Natl. Acad. Sci. U. S. A.* 111, E5383–E5392. doi:10.1073/pnas.1419553111

frontiers | Frontiers in Physiology

TYPE Review
PUBLISHED 11 April 2023
DOI 10.3389/fphys.2023.1149023

OPEN ACCESS

EDITED BY
Ruben Coronel,
University of Amsterdam, Netherlands

REVIEWED BY
Rajni Kant Thakur,
Dr. Yashwant Singh Parmar University of Horticulture and Forestry, India
Fernanda Bosada,
Academic Medical Center, Netherlands
Yoram Etzion,
Ben-Gurion University of the Negev, Israel

*CORRESPONDENCE
Katherine T. Murray,
kathy.murray@vumc.org

SPECIALTY SECTION
This article was submitted to Cardiac Electrophysiology, a section of the journal Frontiers in Physiology

RECEIVED 20 January 2023
ACCEPTED 31 March 2023
PUBLISHED 11 April 2023

CITATION
Murphy MB, Kannankeril PJ and Murray KT (2023), Overview of programmed electrical stimulation to assess atrial fibrillation susceptibility in mice.
Front. Physiol. 14:1149023.
doi: 10.3389/fphys.2023.1149023

Overview of programmed electrical stimulation to assess atrial fibrillation susceptibility in mice

Matthew B. Murphy, Prince J. Kannankeril and Katherine T. Murray*

Departments of Medicine, Pediatrics, and Pharmacology, Vanderbilt University School of Medicine, Nashville, TN, United States

Atrial fibrillation (AF) is the most common human arrhythmia and is associated with increased risk of stroke, dementia, heart failure, and death. Among several animal models that have been used to investigate the molecular determinants of AF, mouse models have become the most prevalent due to low cost, ease of genetic manipulation, and similarity to human disease. Programmed electrical stimulation (PES) using intracardiac or transesophageal atrial pacing is used to induce AF as most mouse models do not develop spontaneous AF. However, there is a lack of standardized methodology resulting in numerous PES protocols in the literature that differ with respect to multiple parameters, including pacing protocol and duration, stimulus amplitude, pulse width, and even the definition of AF. Given this complexity, the selection of the appropriate atrial pacing protocol for a specific model has been arbitrary. Herein we review the development of intracardiac and transesophageal PES, including commonly used protocols, selected experimental models, and advantages and disadvantages of both techniques. We also emphasize detection of artifactual AF induction due to unintended parasympathetic stimulation, which should be excluded from results. We recommend that the optimal pacing protocol to elicit an AF phenotype should be individualized to the specific model of genetic or acquired risk factors, with an analysis using several definitions of AF as an endpoint.

KEYWORDS

atrial pacing, intracardiac, transesophageal, mice, atrial fibrillation

Introduction

Afflicting >37 million people worldwide, atrial fibrillation (AF) is the most common sustained arrhythmia in the Western world (Lippi et al., 2021). AF increases the risk of stroke, dementia, heart failure, and death, including sudden cardiac death (Staerk et al., 2017). Unfortunately, existing therapies for the prevention and treatment of AF are suboptimal due to high recurrence rates and serious associated adverse events (Gupta et al., 2013; January et al., 2014). In order to develop novel AF therapies, animal models have been employed to investigate the molecular determinants of the AF substrate.

Large animals including dogs (Gerstenfeld et al., 2011), goats (Wijffels et al., 1995), and sheep (Anne et al., 2007) have been frequently used to model AF. However, housing costs, limited genetic manipulation, and poor social acceptance have prompted investigation of small animal models instead (Schuttler et al., 2020). While mouse models of AF risk factors

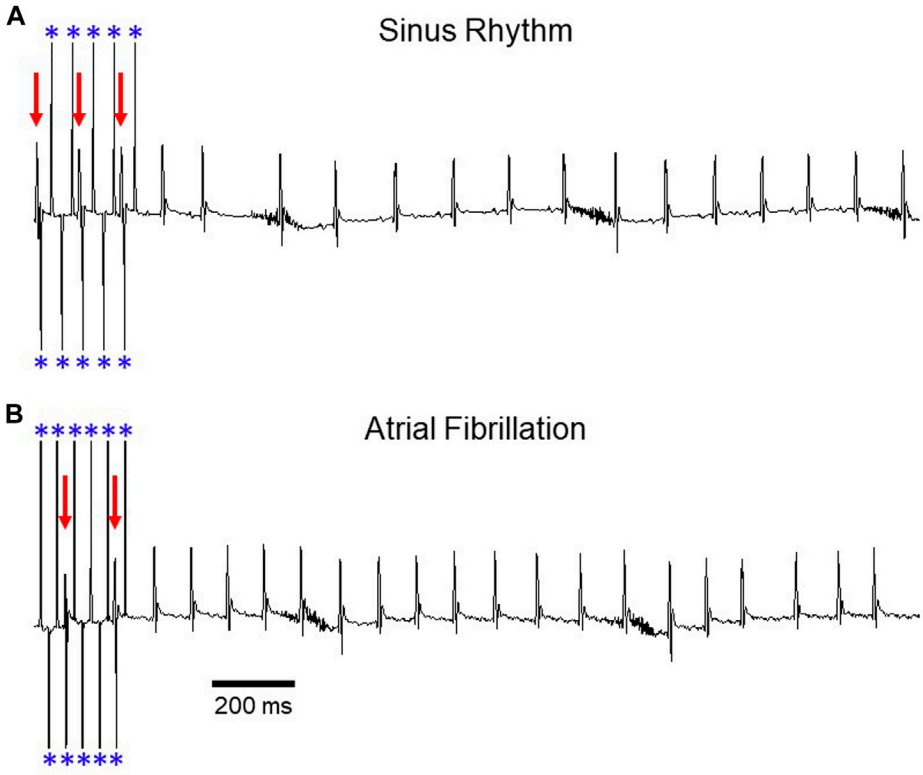

FIGURE 1
Induction of AF during transesophageal atrial pacing. Surface ECG recordings depicting **(A)** sinus rhythm and **(B)** atrial fibrillation after rapid atrial pacing. In panel **A**, pacing demonstrates 2:1 AV conduction (rate exceeds Wenckebach cycle length), with variable A:V conduction in panel **B**. Red arrows denote QRS complexes and blue asterisks denote atrial pacing spikes. The baseline artifact is related to mouse respiration. Adapted from Murphy MB, Kim K, Kannankeril PJ, Murray KT. Optimization of Transesophageal Atrial Pacing to Assess Atrial Fibrillation Susceptibility in Mice. *J Vis Exp*. (184), e64168, doi:10.3791/64168 (2022).

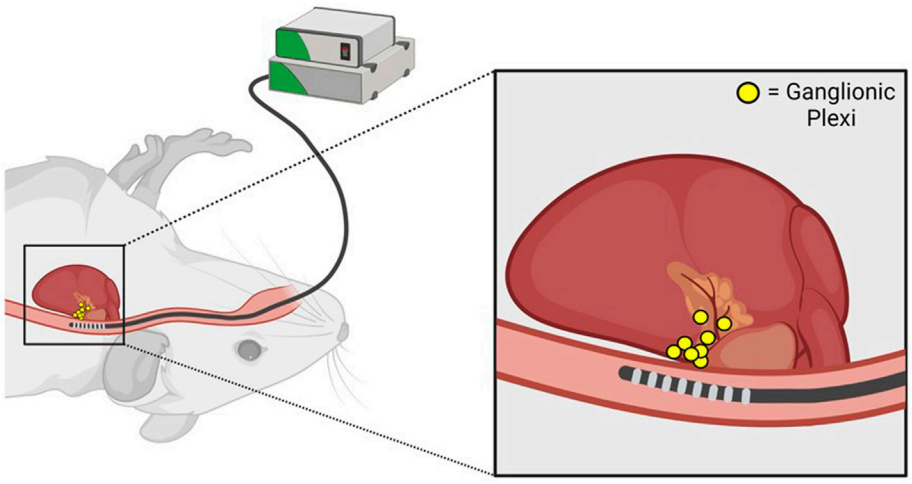

FIGURE 2
Anatomic basis for parasympathetic stimulation during transesophageal atrial pacing. Proximity of the transesophageal pacing catheter to posterior left atrial ganglionic plexi is illustrated. Adapted from Murphy MB, Kim K, Kannankeril PJ, Murray KT. Optimization of Transesophageal Atrial Pacing to Assess Atrial Fibrillation Susceptibility in Mice. *J Vis Exp*. (184), e64168, doi:10.3791/64168 (2022).

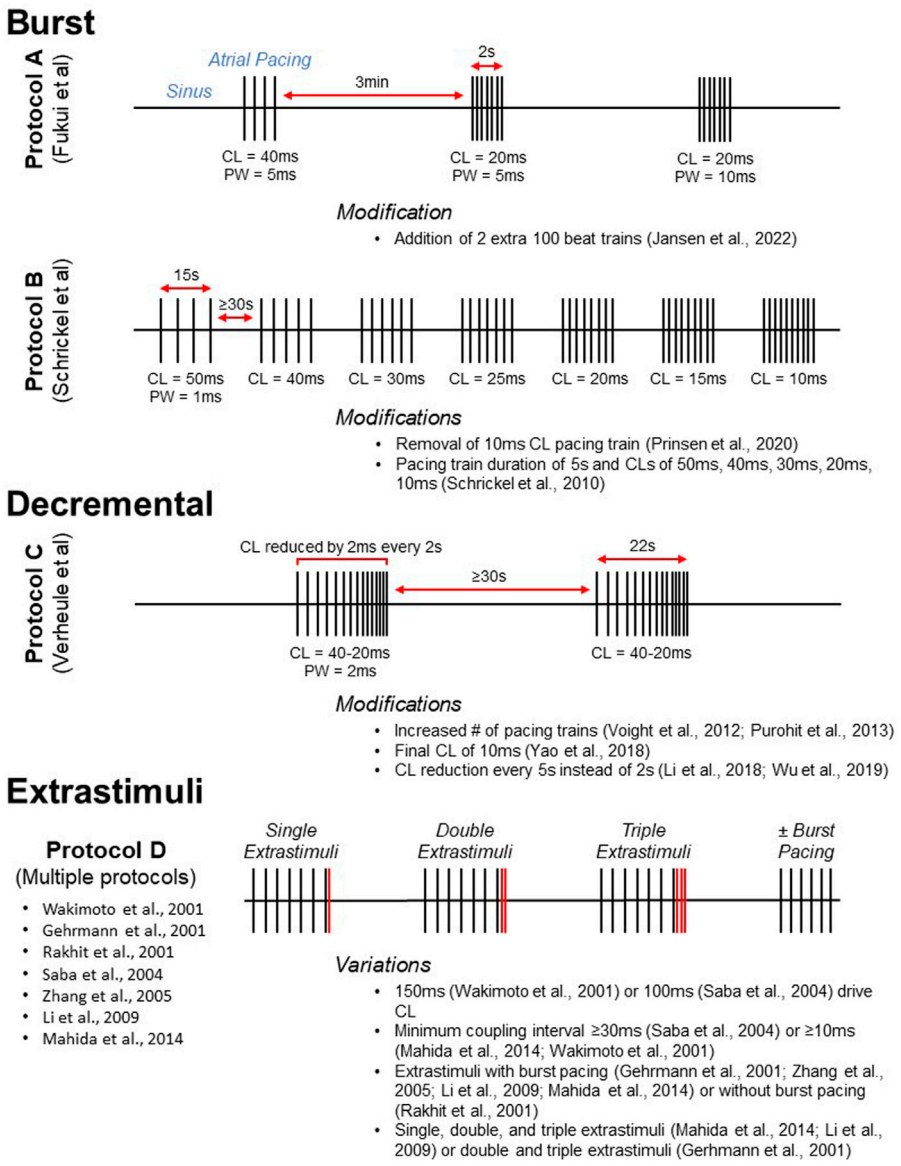

FIGURE 3
Visual representation of commonly used atrial pacing protocols. Protocols A, B, and C display the timing of stimulus delivery for three widely used burst (Schrickel et al., 2002; Fukui et al., 2013) and decremental (Verheule et al., 2004) atrial pacing protocols. Selected modifications are listed below. For conceptualization, Protocol D (multiple reported protocols) illustrates the delivery of extrastimuli after a pacing train. Protocols utilizing extrastimuli are often, but not always, accompanied by burst pacing. CL, cycle length; PW, pulse width.

are not without limitations (e.g., differences in ion channel expression and shorter action potential durations), they do address a number of limitations encountered with large animals and are often quite similar to human disease (Fukui et al., 2013; Guasch et al., 2013). However, few mouse models develop spontaneous AF (Keefe et al., 2022a) and, as a result, most require programmed electrical stimulation (PES) to assess AF susceptibility (Figure 1). Atrial pacing can be performed by either intracardiac stimulation of the right atrium using a multipolar catheter placed into the heart *via* an internal jugular vein, or by transesophageal pacing, given the close proximity of the esophagus to the posterior left atrium (Figure 2). Several basic pacing modes are used for stimulus delivery including: 1) burst pacing with a constant interstimulus interval, or cycle length (CL); 2) decremental pacing during which the pacing CL becomes progressively shorter (i.e., the rate faster) during the pacing train; and 3) the introduction of premature beats or extrastimuli during sinus rhythm or following a pacing train (Figure 3). Due to a lack of standardized methods, numerous PES protocols have been reported that differ with respect to multiple parameters such as pacing mode and protocol design, stimulus amplitude, and even the definition of AF (Murphy et al., 2022b). Given this complexity, the selection of an appropriate atrial pacing protocol for a specific model has remained arbitrary. Here, we review the development of intracardiac and transesophageal PES, including commonly used pacing protocols, representative experimental models, and advantages and disadvantages of both techniques. Rather than an exhaustive review of all published studies, we have focused on frequently

TABLE 1 Selected studies utilizing intracardiac PES to induce AF.

References	Intervention/Model	Pacing mode	Amplitude (mA)	Definition of AF		
				Episode	Regularity	Susceptibility
Wakimoto et al. (2001)	Parasympathetic stimulation	Extrastimuli, burst	NR	NR	Reg/Irreg	Incidence, duration
Gehrmann et al. (2001)	Myocardial infarction	Extrastimuli, burst	NR	NR	NR	Incidence
Rakhit et al. (2001)	eNOS deficiency	Extrastimuli, burst	NR	NR	NR	Incidence
Sood et al. (2008)	FKBP12.6 deficiency	Decremental	1.5x TH	≥1s	Irreg	Incidence, duration
Voight et al. (2012)	RyR2 S2814D knock-in	Decremental	1.5x TH	≥1s	NR	Incidence
Purohit et al. (2013)	Angiotensin II infusion	Decremental	NR	≥1s	Irreg	Incidence
Yao et al. (2018)	Constitutively active NLRP3	Decremental	1.5x TH	≥1s	Irreg	Incidence
Egom et al. (2008)	NPR-C deficiency	Burst	0.4 mA	≥1s	Irreg	Incidence, duration
Jansen et al. (2019)	Angiotensin II infusion, NPR-C deficiency	Burst	NR	≥1s	Irreg	Incidence, duration
Scott et al. (2021)	Obesity, NLRP3 deficiency	Decremental	NR	≥2s	NR	Incidence, duration
Jansen et al. (2017)	Aging	Burst	NR	≥1s	Irreg	Incidence, duration
Saba et al. (2005)	TNF-α overexpression	Extrastimuli, burst	2x TH	10 beats	NR	Incidence
Li et al. (2018)	Angiotensin II infusion, PSMB10 deficiency	Burst	NR	≥1s	Irreg	Incidence, duration
Wu et al. (2019)	Angiotensin II infusion	Burst	NR	NR	NR	Incidence, duration
Polina et al. (2020)	Akita - type 1 diabetes	Burst	NR	≥1s	Irreg	Incidence, duration
Bohne et al. (2021)	db/db - type 2 diabetes	Burst	NR	≥1s	Irreg	Incidence, duration
Jin et al. (2019)	Streptozotocin injection - type 1 diabetes	Burst	NR	≥1s	Irreg	Incidence, duration, episode
Wang et al. (2018)	Abdominal aortic constriction, ALK4 deficiency	Decremental	NR	≥1s	Irreg	Incidence, Duration
Campbell et al. (2020)	SPEG deficiency	Decremental	NR	>1s	NR	Incidence
Bapat et al. (2022)	Genetic inhibition of serum glucocorticoid kinase 1	Extrastimuli, burst	NR	>1s	NR	Incidence, duration, episode

Regularity refers to atrial signal. Reg, regular; Irreg, irregular; NR, not reported; TH, diastolic threshold; eNOS, endothelial nitric oxide synthase; RyR2, ryanodine receptor two; NLRP3, NOD-, LRR-, and pyrin domain-containing protein three; TNF-α, tumor necrosis factor alpha; PSMB10, proteasome 20S subunit beta 10; ALK4, activin receptor-like kinase 4; SPEG, striated muscle preferentially expressed protein kinase.

employed protocols described in sufficient detail that they can be easily reproduced, and examples of their modification. We then highlight studies using transesophageal PES that emphasize the development of reproducible pacing parameters for a specific model under study, as well as the detection of artifactual AF induction due to unintended parasympathetic stimulation.

Intracardiac PES

Development

Soon after AF was detected in the mouse (Wang et al., 1997; Sah et al., 1999), Wakimoto et al. (2001) used intracardiac PES for induction of AF. It was observed that a parasympathetic agonist, carbamylcholine, increased AF susceptibility in wild-type C57BL/6 mice subjected to atrial burst pacing. Moreover, the authors demonstrated that intracardiac stimulation could be used to determine electrophysiologic parameters including sinus node function (assessed by sinus node recovery time) and the effective refractory period (ERP, or non-conducting time period following a premature beat) of the atrium, atrioventricular (AV) node, and ventricle. These findings prompted the rapid development and widespread use of intracardiac PES in mouse models of AF risk factors (Gehrmann et al., 2001; Rakhit et al., 2001).

Common protocols

Multiple intracardiac atrial pacing protocols have been reported (Table 1). Despite differences in protocol parameters, many studies use a decremental mode of stimulus delivery as developed by

Verheule and coworkers (Figure 3, Protocol C). In the initial report, mice were subjected to two pacing trains with an initial pacing CL of 40 ms that was reduced by 2 ms every 2 s until termination at 20 ms (Verheule et al., 2004). Adaptations of this protocol have included an increased number of pacing trains (Voight et al., 2012; Purohit et al., 2013) as well as a final CL of 10 ms (Yao et al., 2018). Intracardiac PES can also be performed using burst pacing at a fixed CL, and several burst pacing protocols have been reported (Wakimoto et al., 2001). However, the methods developed by Fukui and coworkers for transesophageal PES are most commonly used (Fukui et al., 2013; Egom et al., 2015; Fukui et al., 2017; Jansen et al., 2019). In this protocol, pacing was delivered in three trains that were 2s in duration (Figure 3, Protocol A). The initial 2 s burst had a CL of 40 ms and a pulse width of 5 ms while the second and third bursts had CLs of 20 ms with pulse widths of 5 and 10 ms, respectively. A subsequent modification of this protocol was the addition of two 100 beat trains delivered at 20–25 ms pulse widths after the third 2 s burst (Jansen et al., 2022).

Examples of use

Intracardiac PES is routinely used in mouse models of AF risk factors such as inflammation, hypertension, and genetic variants. Using a decremental pacing protocol, Yao et al. (2018) found that activation of the cardiomyocyte NLRP3 (NACHT, LRR, and PYD domain containing protein 3) inflammasome increased AF susceptibility in mice. In this study, AF was considered to be an endpoint if two of the three pacing trains induced the arrhythmia. While some studies required similar reproducibility for a positive finding (Scott Jr et al., 2021), others reported all episodes of inducible AF (Jansen et al., 2017). It was reported that cardiomyocyte overexpression of tumor necrosis factor alpha (*Tnfa*) increased AF vulnerability after atrial burst pacing at CLs of 100–50 ms. However, pacing train duration was not reported limiting future applications of this protocol (Saba et al., 2005).

Angiotensin II (Ang II) infusion is a well-established mouse model of hypertension-mediated AF (Schluttler et al., 2020), and a variety of intracardiac atrial pacing protocols have been reported to elicit AF in these mice. One study determined that the decremental protocol initially described by Verheule could induce AF after a 3 weeks infusion of Ang II (Purohit et al., 2013). Others have modified the protocol in this model, including a reduction of the pacing CL by 2 ms every 5 s instead of every 2 s (Li et al., 2018; Wu et al., 2019). Using an atrial burst pacing protocol (Fukui et al., 2013; Fukui et al., 2017), it was demonstrated that activation of natriuretic peptide receptor-C (NPRC) protects against hypertension-mediated AF (Jansen et al., 2019). In addition to AF incidence, this study also characterized AF episodes as brief (<5 s), non-sustained (5–30 s), or sustained (>30 s). Using this classification, only sustained AF episodes were increased in Ang II-treated mice compared to controls, indicating the utility of a severity analysis in at least some AF models.

Multiple other AF risk factors have been modeled in mice, including diabetes and cardiomyopathy. Atrial burst pacing using the Fukui method demonstrated that loss of insulin signaling increased AF incidence and duration in type 1 diabetic Akita mice (Polina et al., 2020), as well as AF induction in type 2 diabetic db/db mice (Bohne et al., 2021). Another study reported that decremental pacing increased AF susceptibility in streptozocin-induced diabetes (Jin et al., 2019). Pacing was performed using a modified version of the Verheule protocol with CL reductions occurring every 5 s. In a mouse model of cardiomyopathy, Wang et al. found that haploinsufficiency of activin receptor-like kinase 4 (*Acvr1b*) reduced AF vulnerability. The authors also used an adaptation of the Verheule method with initial and final CLs of 50 and 10 ms, respectively (Wang et al., 2018). A series of burst pacing trains was used to determine that mice deficient in desmin (*Des*) were susceptible to AF and ventricular tachycardia (Schrickel et al., 2010). Atrial arrhythmias were induced by pacing in 5s intervals at CLs of 50, 40, 30, 20, and 10 ms, with the protocol performed initially with a stimulus amplitude of 1 mA, which was repeated using 2 mA.

In addition to ion channel mutations, genetic variants linked to AF have been studied in mice, including altered expression of genes encoding the paired-like homeodomain transcription factor 2 (*Pitx2*) and the potassium calcium-activated channel subfamily N member 3 (*Kcnn3*; Schuttler et al., 2020). Mice deficient in *Pitx2* were initially found to be susceptible to AF by decremental pacing using the Verheule protocol (Wang et al., 2010). Using both burst pacing as well as PES with extrastimuli, it was found that overexpression of *Kcnn3* resulted in atrial arrhythmias (Mahida et al., 2014; Figure 3, Protocol D). Burst pacing was performed at CLs of 50 or 30 ms for up to 1 min of stimulation. In addition, single, double, and triple extrastimuli were introduced following a drive CL of 100 ms, with a minimum coupling interval of 10 ms. This protocol has been used to induce AF in murine models by other investigators as well (Zhang et al., 2005; Li et al., 2009). Additional recent studies are included in Table 1 and Table 2 that represent further modifications of the studies illustrated in Figure 3 for both intracardiac and transesophageal pacing.

Advantages and disadvantages

One advantage of intracardiac PES is the ability to record a His potential, signifying the onset of ventricular conduction. This enables measurement of the AH interval, which is conduction from the right atrium to the His bundle and largely reflects AV nodal conduction, and the HV interval, representing conduction from the His bundle to ventricular myocardium. In addition, one can more precisely determine the atrial and AV nodal ERPs. During transesophageal pacing, stimulus artifacts are large and often obscure atrial signals (Etzion et al., 2008) which, in turn, prevents distinguishing between atrial capture with block in the AV node (AVNERP) or if atrial capture was lost (AERP). In contrast, stimulus artifacts are minimal during intracardiac PES so that atrial capture can generally be determined (Li and Wehrens, 2010; Hennis et al., 2022). Additionally, because a His potential is recorded, the AV nodal ERP can also be accurately determined. Another advantage of intracardiac PES is the ability to assess ventricular arrhythmia vulnerability (Hennis et al., 2022). However, this advantage may no longer be valid as recent reports indicate that the transesophageal approach can be used to induce ventricular tachyarrhythmias (Kim et al., 2021; Schmeckpeper et al., 2021). There are multiple disadvantages to intracardiac PES

TABLE 2 Selected studies using transesophageal PES to induce AF.

References	Intervention/Model	Pacing mode	Amplitude (mA)	Definition of AF		
				Episode	Regularity	Susceptibility
Hagendorff et al. (1999)	Connexin 40 deficiency	Burst	NR	NR	Reg/Irreg	Observation
Schrickel et al. (2002)	C57Bl/6 wild-type	Burst	1–4 mA	≥1s	Irreg	Incidence, duration
			2x TH			
Prinsen et al., 2020	Angiotensin II infusion	Burst	3 mA	≥1s	NR	Duration
Suita et al. (2020)	Occlusal disharmony	Burst	1.5 mA	≥2s	NR	Duration
Faggioni et al. (2014)	Calsequestrin deficiency	Burst	2x TH	≥0.15s	Irreg	Episode, duration
Suffee et al. (2022)	High-fat diet	Burst	NR	≥0s	NR	Incidence, duration
Fukui et al. (2017)	High-fat diet, leptin deficiency	Burst	NR	≥1s	Irreg	Incidence, duration
Sato et al. (2019)	Perilipin 2 overexpression	Burst	NR	≥5min	Irreg	Sustained AF
Aschar-Sobbi et al. (2015)	Endurance exercise	Decremental, burst	1.5x TH	≥10s	Irreg	Incidence, duration
Maria et al. (2020)	Insulin deficiency	Burst	NR	≥0s	NR	Incidence, duration
Verheule et al. (2004)	TGF-β1 overexpression	Decremental	1.5x TH	≥2s	Irreg	Incidence, duration
Zhan et al. (2020)	Angiotensin II infusion	Burst	NR	≥1s	Irreg	Incidence, duration
Xie et al. (2015)	RyR2-R2474S and RyR2-S2808D knock-in	Decremental	NR	≥1s	Irreg	Incidence
Fossier et al. (2022)	Metabolic syndrome	Burst	1 mA	≥1s	Irreg	Incidence
Mighiu et al. (2021)	NOX2 overexpression	Decremental	2x TH	≥2s	Irreg	Incidence, duration
Menon et al. (2019)	Frameshift *NPPA* mutation	Burst, decremental, other	NR	≥5s	Irreg	Episode, incidence, duration
Bosada et al. (2023)	TBX5 mutants	Decremental	2x TH	>1s	NR	Incidence, duration
Lai et al. (2022)	Cardiac-specific transgenic TGF-β	Burst	1.5x TH	>3s	Irreg	Incidence, duration
Gong et al. (2022)	Chronic pain	Decremental	NR	≥2s	Irreg	Incidence

Regularity refers to atrial signal. Reg, regular; Irreg, irregular; NR, not reported; TH, diastolic threshold; TGF-β, transforming growth factor beta; RyR2, ryanodine receptor two; NOX2, NADPH, oxidase two; NPPA, atrial natriuretic peptide gene; TBX5, T-box transcription factor 5.

including the amount of time required to study an individual mouse. Studies may last up to 2 h (Li and Wehrens, 2010) which can increase the risk of anesthetic influence on electrophysiologic parameters. Moreover, the required cardiac instrumentation is technically challenging and requires extensive training to avoid procedural errors such as excessive bleeding (Li and Wehrens, 2010). In addition, intracardiac PES is a terminal procedure in the mouse.

Transesophageal PES

Development

Hagendorff and coworkers were the first to use transesophageal PES in mice. Utilizing a burst protocol, the authors found that mice lacking connexin 40 (GJA5) were highly susceptible to atrial arrhythmias (Hagendorff et al., 1999). While AF incidence was reported, additional information including total AF duration and episode number was not described. Subsequently, a PES method was reported for AF induction in wild-type C57Bl/6 mice (Schrickel et al., 2002). This work demonstrated the importance of stimulus strength in promoting atrial arrhythmias, as induction of AF in wild-type mice was minimal at low stimulus amplitudes. Ultimately, these findings resulted in more widespread use of transesophageal PES for AF induction in mouse models.

Common protocols

As with intracardiac PES, transesophageal atrial pacing protocols have primarily used either a burst or decremental mode of stimulus delivery (Table 2). In a novel method, burst pacing was performed in sequential 15 s intervals at CLs of 50, 40, 30, 25, 20, 15, and 10 ms (Schrickel et al., 2002; Figure 3, Protocol B). While this initial study only included wild-type C57Bl/6 mice, the protocol was subsequently employed to demonstrate increased vulnerability to atrial arrhythmias in a mouse model of calsequestrin (*Casq2*) deficiency (Faggioni et al., 2014). A modification of this method was removal of the 10 ms CL pacing train (Prinsen et al.,

2020). Additional transesophageal burst pacing methods have been reported (Hagendorff et al., 1999; Fukui et al., 2013; Fukui et al., 2017). However, they were either not widely adopted for this mode of pacing (Hagendorff et al., 1999), or they have been primarily used for intracardiac PES (Fukui et al., 2013; Fukui et al., 2017). The most common decremental pacing protocol for transesophageal PES was that developed by Verheule and others described above, in which mice are subjected to two pacing trains with a gradual reduction in the pacing CL (Verheule et al., 2004).

Examples of use

Multiple metabolic disorders are linked to AF, including obesity as well as diabetes mellitus. Mice on a high-fat diet demonstrated increased AF vulnerability in response to transesophageal pacing using a single 3 s burst due to electrical and metabolic remodeling (Suffee et al., 2022; additional details such as pulse width not reported). Using their own method, Fukui and others demonstrated that hyperleptinemia increased AF susceptibility in mice maintained on a high-fat diet (Fukui et al., 2017). Another study reported that perilipin 2 (*Plin2*) overexpression increased sustained AF in mice due to atrial steatosis (Sato et al., 2019). While these authors defined sustained AF as an episode lasting longer than 5 min, other definitions have been more commonly used, including 10 s (Aschar-Sobbi et al., 2015), 15 s (Bruegmann et al., 2018), and 30 s (Jansen et al., 2017; Jansen et al., 2019). Transesophageal PES has also been used to induce AF in a mouse model of Type 1 diabetes (Maria et al., 2020).

As with intracardiac PES, several transesophageal atrial pacing protocols have been shown to induce AF in murine models of hypertension using chronic Ang II infusion, including the Fukui protocol (Fukui et al., 2013; Zhan et al., 2020). Reactive mediators of oxidative stress known as isolevuglandins were found to be drivers of AF in Ang II-infused hypertensive mice using a modification of the Schrickel protocol (Prinsen et al., 2020).

Using transesophageal PES, several studies have investigated the role of mitochondrial dysfunction and oxidative stress in AF pathogenesis. It was reported that mitochondrial oxidative stress drove AF due to oxidation of the type 2 ryanodine receptor (RYR2; Xie et al., 2015). The Verheule protocol was employed for AF induction, although the final pacing CL was lowered from 20 to 10 ms. Protocol details including the number of pacing trains delivered, pulse width, and stimulus amplitude were not described, hindering future use of this protocol. Another investigation attributed AF susceptibility during the metabolic syndrome to decreased mitochondrial calcium uptake (Fossier et al., 2022). Burst pacing trains were 30 s in duration, with an initial CL 30 ms shorter than the sinus RR interval. For subsequent pacing trains, the CL was reduced by 10 ms until termination at 30 ms. Overexpression of *NOX2* which encodes NADPH oxidase 2, a major source of reactive oxygen species, promoted inducibility of AF, but not its stability (Mighiu et al., 2021). This study employed an adaptation of the Verheule protocol, with atrial pacing initiated at a CL of 60 ms and subsequently reduced by 2 ms every 2 s until termination at 10 ms.

Transesophageal PES has also been successfully employed to investigate the molecular mechanisms of genetic causes of AF. Using a unique combination of burst and decremental pacing, it was determined that a frameshift mutation in the *NPPA* gene encoding natriuretic peptide precursor A increased AF vulnerability in mice due to electrical remodeling (Menon et al., 2019). Pacing was performed in sequential bursts of 300 cycles at CLs of 50, 40, 30, 25, 20, and 15 ms, followed by the Verheule decremental protocol. Mice were then subjected to burst pacing with 12 trains that were either 50 or 30 ms in length. As noted above, a modified version of the Schrickel method was used to demonstrate that loss of *Casq2* promoted murine AF susceptibility due to spontaneous diastolic Ca^{2+} elevations (Faggioni et al., 2014). Murphy and coworkers demonstrated that *Pitx2*-deficient mice were susceptible to AF using both burst and decremental transesophageal atrial pacing modes, suggesting that multiple methods can be useful to assess AF susceptibility in some models (Murphy et al., 2022b).

Advantages and disadvantages

A major advantage of transesophageal PES is the ability to perform repeated testing in the same animal (Schrickel et al., 2002). Unlike intracardiac PES, transesophageal atrial pacing is a survival procedure, allowing individual mice to be restudied over time or with different pacing protocols (Murphy et al., 2022a). Another advantage of transesophageal PES is a short study duration (~20 min). As described earlier, intracardiac pacing can last several hours which not only reduces the number of mice that can be studied at one time, but also increases the risk of confounding anesthetic effects (Constantinides et al., 2011). The disadvantages of transesophageal pacing include an inability to record the His potential, to accurately measure atrial and AV nodal ERP and, in some cases, to accomplish reliable ventricular stimulation (Hennis et al., 2022). Finally, excessive parasympathetic stimulation causing AV block during pacing may occur which can confound results (see below; Murphy et al., 2022b).

Protocol optimization for transesophageal PES

When using transesophageal PES, several factors can influence AF inducibility, including age, sex, and the pacing protocol employed. AF susceptibility increases as mice age (Luo et al., 2013; Jansen et al., 2017), and determining an age window when AF is inducible in the model under study but not in control mice is essential (Keefe et al., 2022b). In addition, only one sex may demonstrate an AF phenotype (Keefe et al., 2022b; Murphy et al., 2022b). Finally, we recently showed that for optimal reproducibility, pacing mode and parameters should be optimized in pilot studies for the specific model under investigation (Murphy et al., 2022b). For example, we found that *Pitx2*-deficient mice displayed AF inducibility using both burst and decremental pacing, whereas only burst pacing provoked AF in mice with systemic inflammation (Murphy et al., 2022b). In this investigation, male and female mice were subjected to decremental and burst pacing every other week beginning at 8 weeks of age to identify the ideal age, sex, and pacing mode for subsequent studies. Using this approach,

the optimal pacing conditions to elicit an AF phenotype in models of genetic and acquired risk factors were identified (Murphy et al., 2022a).

Another source of variability is the definition of AF as an endpoint (Table 2). The majority of studies define an AF episode as 1 s or more of rapid atrial activity with an irregularly irregular response (Voight et al., 2012; Xie et al., 2015; Fukui et al., 2017). However, AF susceptibility as an endpoint could potentially be defined as AF incidence (Fossier et al., 2022), total AF duration (Prinsen et al., 2020), sustained AF incidence (Jansen et al., 2019), and/or the number of AF episodes per mouse (Jin et al., 2019). Pilot studies can determine the number of pacing trains (typically at least 3) during decremental pacing that are optimal for AF detection, and whether short CLs below 20 ms during either decremental or burst pacing should be excluded due to excessive parasympathetic stimulation (see below). Depending upon the model studied, one or more specific definitions of AF susceptibility may reveal an AF phenotype (Mighiu et al., 2021; Murphy et al., 2022a). Therefore, it is essential to analyze AF susceptibility in multiple ways.

During transesophageal PES, inadvertent parasympathetic stimulation can occur due to pacing-induced excitation of ganglionic plexi on the posterior left atrium (Figure 2). This phenomenon is manifested by an excessive increase in the RR interval during pacing (as quantified in Murphy et al., 2022b), indicating the development of prominent slowing of AV nodal conduction and AV block, that is, often associated with artifactual AF induction in control mice. Notably, pacing-induced AV block can be minimized by using a stimulus amplitude ≤ twice diastolic threshold which should be optimized by careful catheter positioning (Murphy et al., 2022a), as well as longer pacing CLs. However, a subset of mice will inevitably experience parasympathetically-mediated AF induction. These animals should be excluded from analysis to increase specificity and facilitate reproducibility between studies.

Limitations of PES

Despite the widespread use of PES in mice, several challenges and limitations persist. A major issue is the frequency with which critical protocol details for published methods are not reported, including essential pacing parameters (e.g., stimulus intensity, pulse width, *etc.*). This not only prevents reproducibility but may limit the conclusions of the study. Another challenge is a lack of studies that compare PES protocols. Pacing protocols differ for multiple parameters, and it is largely unknown which strategies may be superior or inferior at inducing AF for a specific murine model. For transesophageal PES, we recently demonstrated that AF induction varies depending upon the protocol used (Murphy et al., 2022b) and provided an optimized strategy to develop transesophageal pacing methods. However, to the best of our knowledge no protocol comparisons have been reported for intracardiac PES and such studies would be valuable for future studies. An additional challenge of PES is interpretating the results with reference to the specific protocol used. For example, multiple iterations of the Verheule protocol are reported (Figure 3) with the number of pacing trains varying from 2 (Verheule et al., 2004) to 5 (Purohit et al., 2013). Recently, we demonstrated that an increased number of pacing trains in the Verheule protocol improved the statistical significance between experimental and control mice (Murphy et al., 2022b), suggesting that reproducibility may be enhanced by increasing pacing replicates.

Not infrequently, results obtained using PES do not report whether a regular tachycardia (i.e., atrial flutter or tachycardia) was observed. While a majority of studies define AF as a rapid and irregular atrial rhythm with an irregular ventricular response, many do not delineate regularity (Table 1; Table 2). This can be problematic given that at least in some rodents, atrial tachycardia can lead to prolonged episodes of regular arrythmias that may bias results. Nevertheless, only a handful of studies report regular atrial arrhythmias in mice (Table 1; Table 2), and these responses were most consistent with atrial flutter. Recent studies in rats suggest this limitation may be minimized by 1) quantifying AF with duration scores (Klapper-Goldstein et al., 2020) and 2) using a waveform complexity algorithm to objectively assess arrhythmia regularity (Murninkas et al., 2023).

Conclusion

Numerous intracardiac and transesophageal atrial pacing protocols have been described to induce AF in mice, with considerable variability in protocol parameters as well as the definition of AF susceptibility between studies. To increase the reproducibility of PES results, pilot studies are useful to optimize protocol design for each model under study.

Author contributions

MM and KM contributed to conception and design of the manuscript. MM, PK, and KM wrote sections of the manuscript. All authors contributed to manuscript revision, read, and approved the submitted version.

Funding

Supported by grants from the National Institutes of Health (HL096844 and HL133127 to KTM); the American Heart Association [18SFRN34230125 (KTM is the Basic Project PI); 903918 to MBM]; and the National Center for Advancing Translational Sciences of the National Institute of Health (UL1 TR000445).

Conflict of interest

The authors declare that the research was conducted in the absence of any commercial or financial relationships that could be construed as a potential conflict of interest.

Publisher's note

References

Anne, W., Willems, R., Holemans, P., Beckers, F., Roskams, T., Lenaerts, I., et al. (2007). Self-terminating AF depends on electrical remodeling while persistent AF depends on additional structural changes in a rapid atrially paced sheep model. *J. Mol. Cell Cardiol.* 43 (2), 148–158. doi:10.1016/j.yjmcc.2007.05.010

Aschar-Sobbi, R., Izaddoustdar, F., Korogyi, A. S., Wang, Q., Farman, G. P., Yang, F., et al. (2015). Increased atrial arrhythmia susceptibility induced by intense endurance exercise in mice requires TNFα. *Nat. Commun.* 6, 6018. doi:10.1038/ncomms7018

Bapat, A., Li, G., Xiao, L., Yeri, A., Hulsmans, M., Grune, J., et al. (2022). Genetic inhibition of serum glucocorticoid kinase 1 prevents obesity-related atrial fibrillation. *JCI Insight* 7 (19), e160885. doi:10.1172/jci.insight.160885

Bohne, L. J., Jansen, H. J., Daniel, I., Dorey, T. W., Moghtadaei, M., Belke, D. D., et al. (2021). Electrical and structural remodeling contribute to atrial fibrillation in type 2 diabetic db/db mice. *Heart rhythm.* 18 (1), 118–129. doi:10.1016/j.hrthm.2020.08.019

Bosada, F. M., van Duijvenboden, K., Giovou, A. E., Rivaud, M. R., Uhm, J., Verkerk, A. O., et al. (2023). An atrial fibrillation-associated regulatory region modulates cardiac *Tbx5* levels and arrhythmia susceptibility. *Elife* 12, e80317. doi:10.7554/eLife.80317

Bruegmann, T., Beiert, T., Vogt, C. C., Schrickel, J. W., and Sasse, P. (2018). Optogenetic termination of atrial fibrillation in mice. *Cardiovasc Res.* 114 (5), 713–723. doi:10.1093/cvr/cvx250

Campbell, H. M., Quick, A. P., Abu-Taha, I., Chiang, D. Y., Kramm, C. F., Word, T. A., et al. (2020). Loss of SPEG inhibitory phosphorylation of ryanodine receptor type-2 promotes atrial fibrillation. *Circulation* 142 (12), 1159–1172. doi:10.1161/CIRCULATIONAHA.120.045791

Constantinides, C., Mean, R., and Janssen, B. J. (2011). Effects of isoflurane anesthesia on the cardiovascular function of the C57BL/6 mouse. *ILAR J.* 52, e21–e31. PMID: 21677360.

Egom, E. E., Vella, K., Hua, R., Jansen, H. J., Moghtadaei, M., Polina, I., et al. (2015). Impaired sinoatrial node function and increased susceptibility to atrial fibrillation in mice lacking natriuretic peptide receptor C. *J. Physiol.* 593 (5), 1127–1146. doi:10.1113/jphysiol.2014.283135

Etzion, Y., Mor, M., Shalev, A., Dror, S., Etzion, O., Dagan, A., et al. (2008). New insights into the atrial electrophysiology of rodents using a novel modality: The miniature-bipolar hook electrode. *Am. J. Physiol. Heart Circ. Physiol.* 295 (4), H1460–H1469. doi:10.1152/ajpheart.00414.2008

Faggioni, M., Savio-Galimberti, E., Venkataraman, R., Hwang, H. S., Kannankeril, P. J., Darbar, D., et al. (2014). Suppression of spontaneous ca elevations prevents atrial fibrillation in calsequestrin 2-null hearts. *Circ. Arrhythm. Electrophysiol.* 7 (2), 313–320. doi:10.1161/CIRCEP.113.000994

Fossier, L., Panel, M., Butruille, L., Colombani, S., Azria, L., Woitrain, E., et al. (2022). Enhanced mitochondrial calcium uptake suppresses atrial fibrillation associated with metabolic syndrome. *J. Am. Coll. Cardiol.* 80 (23), 2205–2219. doi:10.1016/j.jacc.2022.09.041

Fukui, A., Ikebe-Ebata, Y., Kondo, H., Saito, S., Aoki, K., Fukunaga, N., et al. (2017). Hyperleptinemia exacerbates high-fat diet-mediated atrial fibrosis and fibrillation. *J. Cardiovasc Electrophysiol.* 28 (6), 702–710. doi:10.1111/jce.13200

Fukui, A., Takahashi, N., Nakada, C., Masaki, T., Kume, O., Shinohara, T., et al. (2013). Role of leptin signaling in the pathogenesis of angiotensin II-mediated atrial fibrosis and fibrillation. *Circ. Arrhythm. Electrophysiol.* 6 (2), 402–409. doi:10.1161/CIRCEP.111.000104

Gehrmann, F., Frantz, S., Maguire, C. T., Vargas, M., Ducharme, A., Wakimoto, H., et al. (2001). Electrophysiological characterization of murine myocardial ischemia and infarction. *Basic Res. Cardiol.* 96 (3), 237–250. doi:10.1007/s003950170054

Gerstenfeld, E. P., Lavi, N., Bazan, V., Gojraty, S., Kim, S. J., and Michele, J. (2011). Mechanism of complex fractionated electrograms recorded during atrial fibrillation in a canine model. *Pacing Clin. Electrophysiol.* 34 (7), 844–857. doi:10.1111/j.1540-8159.2011.03071.x

Gong, C., Ding, Y., Liang, F., Wu, S., Tang, X., Ding, H., et al. (2022). Muscarinic receptor regulation of chronic pain-induced atrial fibrillation. *Front. Cardiovasc Med.* 9, 934906. doi:10.3389/fcvm.2022.934906

Guasch, E., Benito, B., Qi, X., Cifelli, C., Naud, P., Shi, Y., et al. (2013). Atrial fibrillation promotion by endurance exercise: Demonstration and mechanistic exploration in an animal model. *J. Am. Coll. Cardiol.* 62 (1), 68–77. doi:10.1016/j.jacc.2013.01.091

Gupta, A., Perera, T., Ganesan, A., Sullivan, T., Lau, D. H., Roberts-Thomson, K. C., et al. (2013). Complications of catheter ablation of atrial fibrillation: A systematic review. *Circ. Arrhythm. Electrophysiol.* 6 (6), 1082–1088. doi:10.1161/CIRCEP.113.000768

Hagendorff, A., Schumacher, B., Kirchhoff, S., Luderitz, B., and Willecke, K. (1999). Conduction disturbances and increased atrial vulnerability in connexin 40-deficient mice analyzed by transesophageal stimulation. *Circulation* 99 (11), 1508–1515. doi:10.1161/01.cir.99.11.1508

Hennis, K., Rotzer, R. D., Rilling, J., Wu, Y., Thalhammer, S. B., Biel, M., et al. (2022). *In vivo* and *ex vivo* electrophysiological study of the mouse heart to characterize the cardiac conduction system, including atrial and ventricular vulnerability. *Nat. Protoc.* 17 (5), 1189–1222. doi:10.1038/s41596-021-00678-z

Jansen, H. J., Mackasey, M., Moghtadaei, M., Liu, Y., Kaur, J., Egom, E. E., et al. (2019). NPR-C (natriuretic peptide receptor-C) modulates the progression of angiotensin II-mediated atrial fibrillation and atrial remodeling in mice. *Circ. Arrhythm. Electrophysiol.* 12 (1), e006863. doi:10.1161/CIRCEP.118.006863

Jansen, H. J., McRae, M. D., Mackasey, M., and Rose, R. A. (2022). Regional and temporal progression of atrial remodeling in angiotensin II mediated atrial fibrillation. *Front. Physiol.* 13, 1021807. doi:10.3389/fphys.2022.1021807

Jansen, H. J., Moghtadaei, M., Mackasey, M., Rafferty, S. A., Bogachev, O., Sapp, J. L., et al. (2017). Atrial structure, function and arrhythmogenesis in aged and frail mice. *Sci. Rep.* 14 (7), 44336. doi:10.1038/srep44336

January, C. T., Wann, L. S., Alpert, J. S., Calkins, H., Cigarrao, J. E., Cleveland, J. C., et al. (2014). 2014 AHA/ACC/HRS guideline for the management of patients with atrial fibrillation: A report of the American college of cardiology/American heart association task force on practice guidelines and the heart rhythm society. *Circulation* 130 (23), e199–e267. doi:10.1161/CIR0000000000000041

Jin, X., Jiang, Y., Xue, G., Yuan, Y., Zhu, H., Zhan, L., et al. (2019). Increase of late sodium current contributes to enhanced susceptibility to atrial fibrillation in diabetic mice. *Eur. J. Pharmacol.* 857, 172444. doi:10.1016/j.ejphar.2019.172444

Keefe, J. A., Hulsurkar, M. M., Reilly, S., and Wehrens, X. H. T. (2022a). Mouse models of spontaneous atrial fibrillation. *Mamm. Genome*. doi:10.1007/s00335-022-09964-x

Keefe, J. A., Navarro-Garcia, J. A., Ni, L., Reilly, S., Dobrev, D., and Wehrens, X. H. T. (2022b). In-depth characterization of a mouse model of postoperative atrial fibrillation. *J. Cardiovasc Aging* 2, 40. doi:10.20517/jca.2022.21

Kim, K., Schmeckpeper, J., Blackwell, D. J., and Knollmann, B. C. (2021). Abstract B-PO01-017: RyR2 hyperactivity promotes susceptibility to ventricular tachycardia in structural heart disease. *Heart rhythm.* 18 (8), S57. doi:10.1016/j.hrthm.2021.06.163

Klapper-Goldstein, H., Murninkas, M., Gillis, R., Mulla, W., Levanon, E., Elyagon, S., et al. (2020). An implantable system for long-term assessment of atrial fibrillation substrate in unanesthetized rats exposed to underlying pathological conditions. *Sci. Rep.* 10 (1), 553. doi:10.1038/s41598-020-57528-3

Lai, Y., Tsai, F., Chang, G., Chang, S., Huang, C., Chen, W., et al. (2022). miR-181b targets semaphorin 3A to mediate TGF-β-induced endothelial-mesenchymal transition related to atrial fibrillation. *J. Clin. Invest.* 132 (13), e142548. doi:10.1172/JCI142548

Li, J., Wang, S., Bai, J., Yang, X. L., Zhang, Y. L., Che, Y. L., et al. (2018). Novel role for the immunoproteasome subunit PSMB10 in angiotensin II-induced atrial fibrillation in mice. *Hypertension* 71 (5), 866–876. doi:10.1161/HYPERTENSIONAHA.117.10390

Li, N., Timofeyev, V., Tuteja, D., Xu, D., Lu, L., Zhang, Q., et al. (2009). Ablation of Ca^{2+}-activated K^+ channel (SK2 channel) results in action potential prolongation in atrial myocytes and atrial fibrillation. *J. Physiol.* 587 (5), 1087–1100. doi:10.1113/jphysiol.2008.167718

Li, N., and Wehrens, X. H. T. (2010). Programmed electrical stimulation in mice. *J. Vis. Exp.* 39, 1730. doi:10.3791/1730

Lippi, G., Sanchis-Gomar, F., and Cervellin, G. (2021). Global epidemiology of atrial fibrillation: An increasing epidemic and public health challenge. *Int. J. Stoke* 16 (2), 217–221. doi:10.1177/1747493019897870

Luo, T., Chang, C., Zhou, X., Gu, S., Jiang, T., and Li, Y. (2013). Characterization of atrial histopathological and electrophysiological changes in a mouse model of aging. *Int. J. Mol. Med.* 32 (1), 138–146. doi:10.3892./ijmm.2012.1174

Mahida, S., Mills, R. W., Tucker, N. R., Simonson, B., Macri, V., Lemoine, M. D., et al. (2014). Overexpression of KCNN3 results in sudden cardiac death. *Cardiovasc Res.* 101 (2), 326–334. doi:10.1093/cvr/cvt269

Maria, Z., Campolo, A. R., Scherlag, B. J., Ritchey, J. W., and Lacombe, V. A. (2020). Insulin treatment reduces susceptibility to atrial fibrillation in type 1 diabetic mice. *Front. Cardiovasc Med.* 7, 134. doi:10.3389/fcvm.2020.00134

Menon, A., Hong, L., Savio-Galimberti, E., Sridhar, A., Youn, S., Zhang, M., et al. (2019). Electrophysiologic and molecular mechanisms of a frameshift NPPA mutation linked with familial atrial fibrillation. *J. Mol. Cell Cardiol.* 132, 24–35. doi:10.1016/j.yjmcc.2019.05.004

Mighiu, A. S., Recalde, A., Ziberna, K., Carnicer, R., Tomek, J., Bub, G., et al. (2021). Inducibility, but not stability, of atrial fibrillation is increased by NOX2 overexpression in mice. *Cardiovasc Res.* 117 (11), 2354–2364. doi:10.1093/cvr/cvab019

Murninkas, M., Gillis, R., Elyagon, S., Levi, O., Mulla, W., Katz, A., et al. (2023). An objective tool for quantifying atrial fibrillation substrate in rats. *Am. J. Physiol. Heart Circ. Physiol.* 324 (4), H461–H469. doi:10.1152/ajpheart.00728.2022

Murphy, M. B., Kim, K., Kannankeril, P. J., and Murray, K. T. (2022a). Optimization of transesophageal atrial pacing to assess atrial fibrillation susceptibility in mice. *J. Vis. Exp.* 184. doi:10.3791/64168

Murphy, M. B., Kim, K., Kannankeril, P. J., Subati, T., Van Amburg, J. C., Barnett, J. V., et al. (2022b). Optimizing transesophageal atrial pacing in mice to detect atrial fibrillation. *Am. J. Physiol. Heart Circ. Physiol.* 322 (1), H36–H43. doi:10.1152/ajpheart.00434.2021

Polina, I., Jansen, H. J., Li, T., Moghtadaei, M., Bohne, L. J., Liu, Y., et al. (2020). Loss of insulin signaling may contribute to atrial fibrillation and atrial electrical remodeling in type 1 diabetes. *Proc. Natl. Acad. Sci. U. S. A.* 114 (14), 7990–8000. doi:10.1073/pnas.1914853117

Prinsen, J. K., Kannankeril, P. J., Sidorova, T. N., Yermalitskaya, L. V., Boutaud, O., Zagol-Ikapitte, I., et al. (2020). Highly reactive isolevuglandins promote atrial fibrillation caused by hypertension. *JACC Basic Transl. Sci.* 5 (6), 602–615. doi:10.1016/j.jacbts.2020.04.004

Purohit, A., Rokita, A. G., Guan, X., Chen, B., Koval, O. M., Voigt, N., et al. (2013). Oxidized Ca(2+)/calmodulin-dependent protein kinase II triggers atrial fibrillation. *Circulation* 128 (16), 1748–1757. doi:10.1161/CIRCULATIONAHA.113.003313

Rakhit, A., Maguire, C. T., Wakimoto, H., Gehrman, J., Li, G. K., Kelly, R. A., et al. (2001). *In vivo* electrophysiologic studies in endothelial nitric oxide synthase (eNOS)-deficient mice. *J. Cardiovasc Electrophysiol.* 12 (11), 1295–1301. doi:10.1046/j.1540-8167.2001.01295.x

Saba, S., Janczewski, A. M., Baker, L. C., Shusterman, V., Gursoy, E. C., Feldman, A. M., et al. (2005). Atrial contractile dysfunction, fibrosis, and arrhythmias in a mouse model of cardiomyopathy secondary to cardiac-specific overexpression of tumor necrosis factor-{alpha}. *Am. J. Physiol. Heart Circ. Physiol.* 289 (4), H1456–H1467. doi:10.1152/ajpheart.00733.2004

Sah, V. P., Minamisawa, S., Tam, S. P., Wu, T. H., Dorn, G. W., Ross, J., et al. (1999). Cardiac-specific overexpression of RhoA results in sinus and atrioventricular nodal dysfunction and contractile failure. *J. Clin. Invest.* 103 (12), 1627–1634. doi:10.1172/JCI6842

Sato, S., Suzuki, J., Hirose, M., Yamada, M., Zenimaru, Y., Nakaya, T., et al. (2019). Cardiac overexpression of perilipin 2 induces atrial steatosis, connexin 43 remodeling, and atrial fibrillation in aged mice. *Am. J. Physiol. Endocrinol. Metab.* 317 (6), E1193–E1204. doi:10.1152/ajpendo.00227.2019

Schmeckpeper, J., Kim, K., Blackwell, D. J., Woodall, K., and Knollmann, B. C. (2021). Abstract 11402: Targeting RyR2 to suppress ventricular arrhythmias and improve left ventricular function in chronic ischemic heart disease. *Circulation* 144, A11402. doi:10.1161/circ.144.suppl_1.11402

Schrickel, J. W., Bielik, H., Yang, A., Schimpf, R., Shlevkov, N., Burkhardt, D., et al. (2002). Induction of atrial fibrillation in mice by rapid transesophageal atrial pacing. *Basic Res. Cardiol.* 97 (6), 452–460. doi:10.1007/s003950200052

Schrickel, J. W., Stockigt, F., Krzyzak, W., Paulin, D., Li, Z., Lubkemeier, I., et al. (2010). Cardiac conduction disturbances and differential effects on atrial and ventricular electrophysiological properties in desmin deficient mice. *J. Interv. Card. Electrophysiol.* 28 (2), 71–80. doi:10.1007/s10840-010-9482-8

Schuttler, D., Bapat, A., Kaab, S., Lee, K., Tomsits, P., Clauss, S., et al. (2020). Animal models of atrial fibrillation. *Circ. Res.* 127 (1), 91–110. doi:10.1161/CIRCRESAHA.120.316366

Scott, L., Jr, Fender, A. C., Saljic, A., Li, L., Chen, X., Wang, X., et al. (2021). NLRP3 inflammasome is a key driver of obesity-induced atrial arrhythmias. *Cardiovasc Res.* 117 (7), 1746–1759. doi:10.1093/cvr/cvab024

Sood, S., Chelu, M. G., van Oort, R. J., Skapura, D., Santonastasi, M., Dobrev, D., et al. (2008). Intracellular calcium leak due to FKBP12.6 deficiency in mice facilitates the inducibility of atrial fibrillation. *Heart rhythm.* 5 (7), 1047–1054. doi:10.1016/j.hrthm.2008.03.030

Staerk, L., Sherer, J. A., Ko, D., Benjamin, E. J., and Helm, R. H. (2017). Atrial fibrillation: Epidemiology, pathophysiology, and clinical outcomes. *Circ. Res.* 120 (9), 1501–1517. doi:10.1161/CIRCRESAHA.117.309732

Suffee, N., Baptista, E., Piquereau, J., Ponnaiah, M., Doisne, N., Ichou, F., et al. (2022). Impacts of a high-fat diet on the metabolic profile and the phenotype of atrial myocardium in mice. *Cardiovasc Res.* 118 (15), 3126–3139. doi:10.1093/cvr/cvab367

Suita, K., Yagisawa, Y., Ohnuki, Y., Umeki, D., Nariyama, M., Ito, A., et al. (2020). Effects of occlusal disharmony on susceptibility to atrial fibrillation in mice. *Sci. Rep.* 10, 13765. doi:10.1038/s41598-020-70791-8

Verheule, S., Sato, T., Everett, T., Engle, S. K., Otten, D., Rubart-von der Lohe, M., et al. (2004). Increased vulnerability to atrial fibrillation in transgenic mice with selective atrial fibrosis caused by overexpression of TGF-beta1. *Circ. Res.* 94 (11), 1458–1465. doi:10.1161/01.RES.0000129579.59664.9d

Voigt, N., Li, N., Wang, Q., Wang, W., Trafford, A. W., Abu-Taha, I., et al. (2012). Enhanced sarcoplasmic reticulum Ca2+ leak and increased Na+-Ca2+ exchanger function underlie delayed afterdepolarizations in patients with chronic atrial fibrillation. *Circulation* 125 (17), 2059–2070. doi:10.1161/CIRCULATIONAHA.111.067306

Wakimoto, H., Maguire, C. T., Kovoor, P., Hammer, P. E., Gehrmann, J., Triedman, J. K., et al. (2001). Induction of atrial tachycardia and fibrillation in the mouse heart. *Cardiovasc Res.* 50 (3), 463–473. doi:10.1016/s0008-6363(01)00264-4

Wang, J., Klysik, E., Sood, S., Johnson, R. L., Wehrens, X. H. T., and Martin, J. F. (2010). Pitx2 prevents susceptibility to atrial arrhythmias by inhibiting left-sided pacemaker specification. *Proc. Natl. Acad. Sci. U. S. A.* 107 (21), 9753–9758. doi:10.1073/pnas.0912585107

Wang, Q., Chen, Y., Zhang, D., Li, C., Chen, X., Hou, J., et al. (2018). Activin receptor-like kinase 4 haplodeficiency mitigates arrhythmogenic atrial remodeling and vulnerability to atrial fibrillation in cardiac pathological hypertrophy. *J. Am. Heart Assoc.* 7 (16), e008842. doi:10.1161/JAHA.118.008842

Wang, Y. X., Zheng, Y. M., Tan, Y. H., and Sheng, B. H. (1997). Effects of cycloprotobuxine-A on atrial fibrillation. *Zhongguo Yao Li Xue Bao* 18 (3), 245–250.

Wijffels, M. C., Kirchhof, C. J., Dorland, R., and Allessie, M. A. (1995). Atrial fibrillation begets atrial fibrillation. A study in awake chronically instrumented goats. *Circulation* 92 (7), 1954–1968. doi:10.1161/01.cir.92.7.1954

Wu, Y. X., Han, X., Chen, C., Zou, L. X., Dong, Z. C., Zhang, Y. L., et al. (2019). Time series gene expression profiling and temporal regulatory pathway analysis of angiotensin II induced atrial fibrillation in mice. *Front. Physiol.* 10, 597. doi:10.3389/fphys.2019.00597

Xie, W., Santulli, G., Reiken, S. R., Yuan, Q., Osborne, B. W., Chen, B., et al. (2015). Mitochondrial oxidative stress promotes atrial fibrillation. *Sci. Rep.* 5, 11427. doi:10.1038/srep11427

Yao, C., Veleva, T., Scott, L., Jr, Cao, S., Li, L., Chen, G., et al. (2018). Enhanced cardiomyocyte NLRP3 inflammasome signaling promotes atrial fibrillation. *Circulation* 138 (20), 2227–2242. doi:10.1161/CIRCULATIONAHA.118.035202

Zhan, Y., Abe, I., Nakagawa, M., Ishii, Y., Kira, S., Miyoshi, M., et al. (2020). A traditional herbal medicine rikkunshito prevents angiotensin II-induced atrial fibrosis and fibrillation. *J. Cardiol.* 76 (6), 626–635. doi:10.1016/j.jjcc.2020.07.001

Zhang, Z., He, Y., Tuteja, D., Xu, D., Timofeyev, V., Zhang, Q., et al. (2005). Functional roles of cav1.3(α_{1d}) calcium channels in atria: Insights gained from gene-targeted null mutant mice. *Circulation* 112 (13), 1936–1944. doi:10.1161/CIRCULATIONAHA.105.540070

frontiers | Frontiers in Physiology

TYPE Original Research
PUBLISHED 05 May 2023
DOI 10.3389/fphys.2023.1167524

OPEN ACCESS

EDITED BY
Igor R. Efimov,
George Washington University,
United States

REVIEWED BY
Matthew W. Kay,
George Washington University,
United States
Teun P. De Boer,
Utrecht University, Netherlands

*CORRESPONDENCE
Leonardo Sacconi,
leonardo.sacconi@cnr.it
Gerard A. Marchal,
marchal@lens.unifi.it

†These authors have contributed equally to this work and share first authorship

RECEIVED 16 February 2023
ACCEPTED 24 April 2023
PUBLISHED 05 May 2023

CITATION
Marchal GA, Biasci V, Loew LM, Biggeri A, Campione M and Sacconi L (2023), Optogenetic manipulation of cardiac repolarization gradients using sub-threshold illumination.
Front. Physiol. 14:1167524.
doi: 10.3389/fphys.2023.1167524

Optogenetic manipulation of cardiac repolarization gradients using sub-threshold illumination

Gerard A. Marchal[1,2,3*†], Valentina Biasci[1,4†], Leslie M. Loew[5], Annibale Biggeri[6], Marina Campione[7] and Leonardo Sacconi[3,8*]

[1]European Laboratory for Non-Linear Spectroscopy—LENS, Florence, Italy, [2]National Institute of Optics (INO-CNR), Florence, Italy, [3]Institute of Clinical Physiology (IFC-CNR), Pisa, Italy, [4]Department of Experimental and Clinical Medicine, University of Florence, Florence, Italy, [5]Center for Cell Analysis and Modeling, University of Connecticut, Farmington, CT, United States, [6]Department of Cardiac, Thoracic, Vascular Sciences and Public Health, University of Padua, Padua, Italy, [7]Institute of Neuroscience (IN-CNR) and Department of Biomedical Science University of Padua, Padua, Italy, [8]Institute for Experimental Cardiovascular Medicine, University Heart Center and Medical Faculty, University of Freiburg, Freiburg, Germany

Introduction: Mechanisms underlying cardiac arrhythmias are typically driven by abnormalities in cardiac conduction and/or heterogeneities in repolarization time (RT) across the heart. While conduction slowing can be caused by either electrophysiological defects or physical blockade in cardiac tissue, RT heterogeneities are mainly related to action potential (AP) prolongation or abbreviation in specific areas of the heart. Importantly, the size of the area with altered RT and the difference between the short RT and long RT (RT gradient) have been identified as critical determinators of arrhythmogenicity. However, current experimental methods for manipulating RT gradient rely on the use of ion channel inhibitors, which lack spatial and temporal specificity and are commonly only partially reversible. Therefore, the conditions facilitating sustained arrhythmia upon the presence of RT heterogeneities and/or defects in cardiac conduction remain to be elucidated.

Methods: We here employ an approach based on optogenetic stimulation in a low-intensity fashion (sub-threshold illumination), to selectively manipulate cardiac electrical activity in defined areas of the heart.

Results: As previously described, subthreshold illumination is a robust tool able to prolong action potentials (AP), decrease upstroke velocity as well as slow cardiac conduction, in a fully reversible manner. By applying a patterned sub-threshold illumination in intact mouse hearts constitutively expressing the light-gated ion channel channelrhodopsin-2 (ChR2), we optically manipulate RT gradients and cardiac conduction across the heart in a spatially selective manner. Moreover, in a proof-of-concept assessment we found that in the presence of patterned sub-threshold illumination, mouse hearts were more susceptible to arrhythmias. Hence, this optogenetic-based approach may be able to mimic conduction slowing and RT heterogeneities present in pathophysiological conditions.

KEYWORDS

optogenetics, sub-threshold illumination, optical mapping, electrophysiological modulation, repolarization gradients

1 Introduction

Cardiovascular diseases are the most common cause of death worldwide, and a substantial number of these deaths are caused by cardiac arrhythmias resulting in sudden cardiac death (Adabag et al., 2010). Mechanisms underlying cardiac arrhythmias are typically driven by abnormalities in cardiac conduction and/or repolarization. Conduction slowing can be caused by either electrophysiological defects such as reduced sodium current or physical blockade by myocardial fibrosis, and poses a well-established risk for generation of re-entrant arrhythmia (de Jong et al., 2011; Marchal and Remme, 2022). In addition, heterogeneities in repolarization time (RT) have been identified as pro-arrhythmic. RT heterogeneities are caused by action potential (AP) prolongation or abbreviation in specific areas of the heart, which can be caused by inherited disease (i.e., genetic disorders causing ion channel dysfunction), but also occur secondary to acquired heart disease such as myocardial infarction (Kelemen et al., 2022). Previously, the impact of RT heterogeneities on arrhythmia has been established in transgenic mouse models (Jeron et al., 2000; Salama et al., 2009), as well as upon infusion with RT-altering drugs (Fabritz et al., 2003) and/or blockade of the atrio-ventricular node in mouse, rabbit, and dog (Milberg et al., 2004; Loen et al., 2022). However, these approaches lack the ability to control the size of the affected area, often resulting in RT alterations across the whole ventricles. Importantly, the size of the area with altered RT and the difference between the short RT and long RT (RT gradient) have been identified as critical determinators of arrhythmogenicity (Cluitmans et al., 2021; Rivaud et al., 2021). However, current experimental methods to modulate repolarization locally rely on the infusion of AP duration (APD)-modulating drugs in single coronary arteries, limiting versatility of the spatial characteristics of the area with altered APD and restricting studies to larger animal models. In addition, the ion channel inhibitors presently used in most experimental methods for manipulating RT lack spatial and temporal specificity and are commonly only partially reversible. Therefore, aspects of the conditions facilitating sustained arrhythmia upon the presence of RT heterogeneities remain to be elucidated.

Recent optogenetic light-based pacing strategies enabled modulation of cardiac activity in a spatial- and temporal-specific manner, employing mice expressing the light-activated ion channel channelrhodopsin-2 (ChR2) (Entcheva and Kay, 2021). When activated by a light source, this unspecific ion channel allows positively charged ions to enter cardiomyocytes, inducing depolarization of the membrane potential (Nagel et al., 2005). Light-based pacing strategies have been proposed as an alternative for wired electrical stimulation for cardiac pacing (Bruegmann et al., 2010; Nussinovitch and Gepstein, 2015), as well as conventional internal cardioverters (Crocini et al., 2016; Nyns et al., 2017; Bruegmann et al., 2018). Moreover, optogenetics are a robust tool for investigating wave dynamics in cardiac tissue, studying the mechanisms underlying the induction, maintenance and control of cardiac arrhythmias (Burton et al., 2015; Feola et al., 2017). Importantly, optogenetic interventions have so far mostly been used for generating transient and intense depolarizing currents for triggering APs and cardioversion. Conversely, we and others recently described the ability of optogenetics for imposing a continuous depolarizing current with amplitudes that are too low to elicit APs (sub-threshold illumination), to modulate activation and repolarization characteristics in defined areas of the heart (Karathanos et al., 2014; Biasci et al., 2022). As such, this approach may be utilised to mimic conduction slowing and RT heterogeneities present in pathophysiological conditions.

Accordingly, to avoid misinterpretation of experimental readouts when applying sub-threshold illumination, cardiac electrical activity should be stable throughout the entire experiment. Since the mechanical uncoupler blebbistatin affects cardiac electrophysiology (Brack et al., 2013), we here first assessed the time-dependent impact of blebbistatin on cardiac repolarization and conduction characteristics when applied at a conventional concentration and a lower concentration in isolated murine hearts. Subsequently, we investigate the extent of RT gradients, local conduction slowing, and pro-arrhythmia upon application of sub-threshold optogenetic stimulation by using different illumination patterns.

2 Materials and methods

2.1 Mouse model generation

Transgenic mice (ChR2-mhc6-cre+) with cardiomyocyte-specific expression of ChR2 (H134R variant) were generated as previously described (Zaglia et al., 2015) and employed in this study. All animal handling and procedures were performed in accordance with the guidelines from Directive 2010/63/EU of the European Parliament on the protection of animals used for scientific purposes. The experimental protocol was approved by the Italian Ministry of Health (protocol number 531/2022-PR).

2.2 Isolated and perfused mouse hearts

Mice (6 months old) were heparinised (0.1 mL at 5,000 units/mL), anesthetised by isoflurane inhalation (5%), and euthanised by cervical dislocation. The excised heart was immediately bathed in Krebs-Henseleit (KH) solution and cannulated through the aorta. The KH buffer contained (in mM): 120 NaCl, 5 KCl, 2 MgS_2O_4–$7H_2O$, 20 $NaHCO_3$, 1.2 NaH_2PO_4–H_2O, 1.8 $CaCl_2$ and 10 glucose, pH 7.4 when equilibrated with carbogen (95% oxygen and 5% carbon dioxide). Cardiac contraction was inhibited during the entire experiment with 1 or 10 μM (±)-Blebbistatin (Enzo Life Sciences, Farmingdale, NY, United States) in the perfusion and bath solution. The cannulated heart was perfused through the aorta (using a horizontal Langendorff perfusion system) with KH solution and then transferred to a custom-built optical mapping chamber at a constant flow of 2.5 mL/min at 36°C ± 0.5°C. Two platinum electrodes were placed below the heart for monitoring cardiac electrical activity via electrocardiogram (ECG). 1 mL of perfusion solution containing the voltage sensitive dye (VSD) di-4-ANBDQPQ 6 μg/mL, University of Connecticut Health Center, Farmington, CT, United States (Matiukas et al., 2007), was bolus injected into the aorta. All the experiments were performed within 1 h after dye loading to avoid potential re-distribution of the dye and accumulation of phototoxic by-products.

2.3 All-optical imaging and manipulation platform

Optical mapping and control were performed using a custom-made mesoscope as previously described (Scardigli et al., 2018). In short, whole mouse hearts were illuminated by a light emitted diode (LED) operating at a wavelength centred at 625 nm (M625L3, Thorlabs, Newton, NJ, United States; maximum intensity of 0.875 mW/mm^2) in a wide-field configuration using a ×2 objective (TL2x-SAP, Thorlabs, Newton, NJ, United States). A ×20 objective (LD Plan-Neofluar ×20/0.4 M27, Carl Zeiss Microscopy, Oberkochen, Germany) was used to focus the fluorescent signal emitted by the VSD on the central portion (128 × 128 pixels) of the sensor of a sCMOS camera (OrcaFLASH 4.0, Hamamatsu Photonics, Shizuoka, Japan) operating at a frame rate of 1 kHz (1 ms actual exposure time). The detection path allows a field of view (at the object space) of 10.1 × 10.1 mm sampled with a pixel size of 80 µm. Optogenetic illumination was performed by employing a Lightcrafter 4500 projector (Texas Instruments, Dallas, TX, United States), operating at a wavelength of 470 nm, enabling projection of user-defined light patterns onto the cardiac surface. In order to illuminate in a sub-threshold fashion, the threshold for AP initiation was determined for each mouse heart, and illumination was applied a light intensity (LI) below the threshold. Overall, mouse hearts were illuminated with a mean LI of 0.136 ± 0.011 mW/mm^2. LIs were measured at sample site using a photodiode sensor (PD300-3W, Ophir Optronics, Jerusalem, Israel). User-defined illumination patterns (whole ventricular surface, apex, base, right ventricular area, and left ventricular area of the heart) were applied. Hearts were electrically paced by bipolar electrodes positioned at the apex and at the base attached to an isolated constant voltage stimulator (DS2A, Digitimer, Welwyn Garden City, Hertfordshire, United Kingdom).

2.4 Arrhythmia induction

To assess susceptibility to arrhythmia, we employed a stimulation protocol called "parasystole paradigm" where extra beats were electrically induced. Briefly, while leaving the sinus node (SN) intact, mouse hearts were electrically paced at the apex or at the base at a cycle length (CL) of 1.7 × (SN rate). Since each mouse heart has a different SN rate, the pacing CL and protocol duration varied between hearts. During the pacing protocol, cardiac activity was assessed using a two-lead pseudo-electrocardiogram. Arrhythmia was defined as irregular cardiac activity of longer than 250 ms.

2.5 Data and image analysis

All programs for data acquisition and analysis were developed with LabVIEW software (National Instruments). For optical recordings, ΔF/F0 imaging of cardiac electrical activity was performed by processing raw data: for each frame, the background was first subtracted, then the voltage-independent bleaching effect during each individual trace was corrected by normalising the fluorescent trace using either a linear or a non-linear polynomial fit applied to the diastolic phase. For each heart, AP kinetics parameters were measured, trace by trace, in order to get the mean values after averaging 5–10 subsequent trials. AP maximum rising slope (APRS), AP repolarization duration (APRD) at 50% of repolarization (APRD$_{50}$), 70% of repolarization (APRD$_{70}$), 90% of repolarization (APRD$_{90}$) were measured in a selected region of interest (ROI) of 10 × 10 pixels (≈1 mm^2). APRS -which is a measure of the velocity of the AP excitation phase- was normalised for AP amplitude. To dissect the effect of optogenetic stimulation on activation and repolarization kinetics, APRD was determined relative to the time of maximum depolarization. APRS, APRD$_{50}$ and APRD$_{90}$ maps were generated after a spatial binning of 4 × 4 pixels across the whole ventricle. APD$_{70}$ alternans was calculated using the following formula: $(\sum_{i=1}^{n-1} |APD_{70}, i+1, -, APD_{70}, i| / (n-1)$. Conduction velocity (CV) was calculated after a spatial binning of 6 × 6 pixels using a multi-vector approach: a seed reference pixel was arbitrarily chosen, and the cross-correlation of the fluorescence trace was calculated pixel by pixel, in order to estimate the temporal shift among every pixel (activation map). Next, local velocity maps were generated by calculating the delay between adjacent pixels divided by the pixel size. Since the local direction of the AP wavefront is represented by a vector for each pixel, the mean CV was calculated by averaging local CVs. Wavefront dispersion was determined using the standard deviation of the angle of local AP wavefront propagation vectors generated for each pixel.

In each mouse heart, motion artefact during optical recordings was assessed and reported as displacement of centre of mass (CM) of the heart and variation of heart area. In the first, we estimated the X; Y position of CM in each frame and the corresponding standard deviation (SD) in the stack. Subsequently, we found the displacement of CM in pixels with the following formula $\sqrt{(SDx)^2 + (SDy)^2}$ and we multiplied the result for the pixel size (80 µm). For the variation of heart area, we first calculated the heart area (in mm^2) in each frame as well as the mean area and the SD in the stack. Afterwards, we normalized the SD to the mean area, and we obtained the variation of heart area in %. Graphical representation of data was obtained using OriginPro 2018, version 9.5 64-bit (OriginLab Corporation, Northampton, MA United States).

2.6 Statistics

For each experimental condition, data from each heart was averaged, and this average was used for comparison and statistical analysis. Data is plotted as mean ± standard error of mean (SEM). Plots and statistical analyses were performed in GraphPad Prism software (version 9, GraphPad Software, San Diego, CA, United States) Two-way repeated measures (RM) analysis of variance (ANOVA), and in the case of missing values a Mixed Effects analysis, was used to compare changes in electrophysiological features between the illumination patterns. For the comparison of means at specific CLs, the Tukey's *post hoc* analysis was used. To investigate the general influence of time on electrophysiological features in 1 µM and 10 µM blebbistatin perfused-mouse hearts, a regression test was additionally applied: an ANOVA test was used to assess if the linear fitting function is significantly better than a

10.3389/fphys.2023.1167524

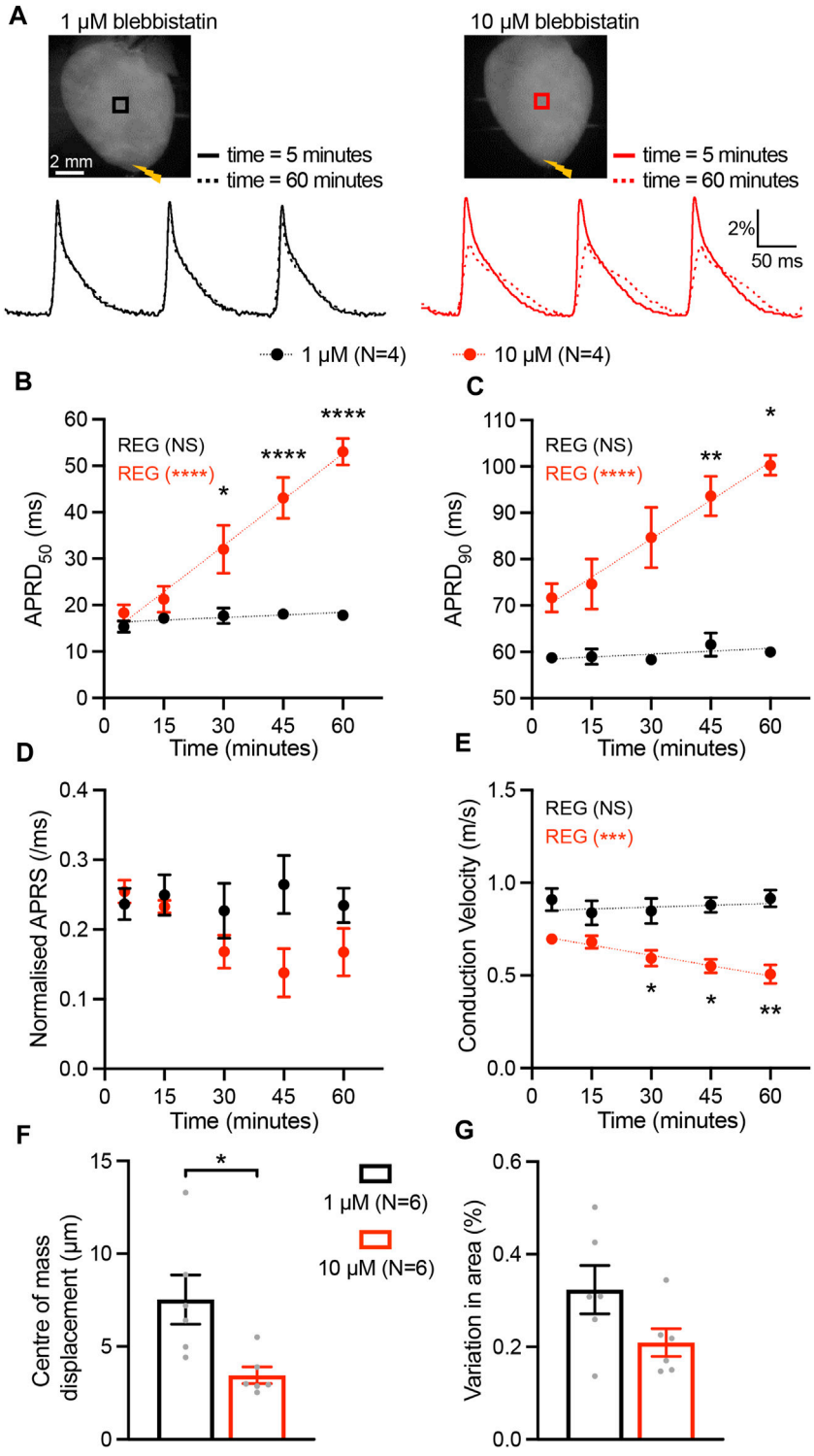

FIGURE 1
Time-dependent impact of blebbistatin at 1 µM (low) and 10 µM (high) concentrations. **(A)** Top, representative fluorescence images (F0) of mouse hearts perfused with blebbistatin at 1 µM (left) and 10 µM (right) concentrations. Mouse hearts were electrically paced at the apex (yellow bolt symbols) at a cycle length of 150 ms. Bottom, fluorescent signals (ΔF/F) representing action potentials (APs) extracted from the black and red ROIs at time 5 and 60 min after the hearts were stained with the VSD. **(B–E)** Time effect of blebbistatin on AP repolarization duration at 50% and 90% of repolarization ($APRD_{50}$, $APRD_{90}$), AP rising slope (APRS), and conduction velocity (CV). Parameters were measured in the ROIs shown in **(A)**. Data is reported as mean ± SEM and linear fit on experimental data was superimposed. Regression analysis results (REG; ANOVA test) are shown. A Mixed-Effects with RM analysis with Tukey's post-hoc test was also applied. **(F, G)** The motion artefact of the heart displayed as centre of mass displacement and variation of heart area at different concentrations at blebbistatin. Data is shown as mean ± SEM, N represents number of hearts assessed, and Student's t-test for mean comparison was applied. *$p < 0.05$, **$p < 0.01$, ****$p < 0.0001$.

constant function. For motion artefact analyses, unpaired Student's t-tests were used to compare 1 μM and 10 μM blebbistatin perfused mouse hearts.

To analyse arrhythmia susceptibility results, we first assessed the overall effect of sub-threshold illumination on arrhythmia inducibility. To this end, we estimated incidence rates of arrhythmia (total arrhythmia events/protocol duration in seconds) and 95% confidence intervals in the absence and presence of sub-threshold illumination. Subsequently, to evaluate the effect of each illumination pattern on arrhythmia inducibility, we estimated the incidence rate ratio (IRR) and 95% confidence intervals for each illumination pattern, taking absence of sub-threshold illumination as reference—i.e., the IRR was calculated as the incidence rate for each illumination pattern divided by the incidence rate for the control condition. Technically, we performed two comparisons: 1) presence versus absence of illumination, and 2) five illumination patterns versus absence of illumination. The comparisons were all conducted within hearts, since protocol duration differed between hearts. However, the type and number of illumination patterns were not constant among hearts, which created some imbalance and potential confounding. We therefore specified a Poisson mixed effect model (Skrondal and Rabe-Hesketh, 2004; Rabe-Hesketh and Skrondal, 2012), in which a random intercept was applied as an identifier for each heart. The inputs for this model are the frequency of arrythmias, the exposure time to the arrhythmia induction protocol, and the condition, which was the presence/absence of illumination (comparison 1) or the individual illumination patterns vs. control (compassion 2).

The frequency of arrythmias was reported as rate per second and 95% confidence interval based on Poisson likelihood (Clayton and Hills, 2013). Incidence Rate Ratios and 95% confidence intervals was obtained exponentiating the Poisson mixed effects regression coefficient and 95% confidence intervals. Statistical test on regression coefficients were performed by Wald test (Skrondal and Rabe-Hesketh, 2004).

3 Results

3.1 Blebbistatin at high concentration affects repolarization and conduction kinetics

To assess the time-dependent impact of the myosin inhibitor blebbistatin on cardiac excitation and repolarization characteristics, we applied blebbistatin at the commonly used (high) concentration of 10 μM as well as at the low concentration of 1 μM in murine hearts. Epicardial optical mapping was performed at 5, 15, 30, 45, and 60 min after VSD loading, during an electrical stimulation at the apex with 150 ms cycle length (CL). Blebbistatin at high concentration resulted in a significant time-dependent prolongation of action potential repolarization duration (APRD) at 50% and 90% of repolarization ($APRD_{50}$, $APRD_{90}$). By contrast, APRD at both repolarization stages remained unaffected when blebbistatin was applied at low dose (Figures 1A–C). Additionally, we found a slight but not significant time-dependent decrease in the AP rising slope (APRS) at high blebbistatin, while unchanged when applying low concentration (Figure 1D). Although only a trend for reduced APRS was observed, the related conduction velocity (CV) was highly significantly reduced over time when applying high concentration blebbistatin, while remaining stable upon low blebbistatin (Figure 1E). Assessment of cardiac movement during recordings revealed that the displacement of the centre of mass was significantly higher when applying low blebbistatin (Figure 1F), while the variation in cardiac surface (i.e., contractile movement) did not significantly differ between the two blebbistatin concentrations (Figure 1G).

3.2 Low-intensity illumination leads to reduced AP upstroke velocity and repolarization prolongation

We next investigated the impact of sub-threshold optogenetic stimulation on whole-heart electrophysiological characteristics as a function of the electrically-induced cycle length (CL), by quantifying the AP parameters APRS, $APRD_{50}$, and $APRD_{90}$ in the absence and upon optogenetic stimulation of the entire ventricular surface (Figures 2A, B). Given the time-dependent effect of blebbistatin on cardiac electrical activity, a low concentration of blebbistatin (1 μM) was applied during these experiments. Optogenetic stimulation induced a significant decrease in APRS, especially at faster pacing rates (Figure 2C). In addition, illumination induced a significant prolongation of $APRD_{50}$, but the magnitude of prolongation was not impacted by pacing rate (Figure 2D). Conversely, illumination-induced prolongation of $APRD_{90}$ was highly impacted by pacing rate, displaying decreasing prolongation at higher pacing rates (Figure 2E).

3.3 Patterned sub-threshold illumination manipulates ventricular excitation and repolarization gradients

Low-intensity optogenetic stimulation was subsequently applied in various patterns, illuminating the apical, basal, left, and right ventricular surface of hearts. Cardiac activation was initiated by an electrode placed at the apex, which stimulated at intervals of 150, 130, 110, and 90 ms.

In Figure 3, AP characteristics measured in the basal and apical area, are presented as gradients (*base minus apex*) in absence and presence of patterned sub-threshold illumination at either the apex or base (Figure 3A). APRS was similar between the base and apex when no illumination was applied, while significantly higher in the basal area during apical optogenetic stimulation and *vice versa* (Figure 3B). APRD at different stages of repolarization ($APRD_{50}$, $APRD_{90}$) was slightly longer at the apex when no optogenetic stimulation was applied, which was enhanced upon apical illumination and reversed when the base was illuminated (Figures 3C, D). Specifically, the effects of illumination on $APRD_{90}$ were diminished upon faster pacing. Meanwhile, application of the same illumination patterns while electrically stimulating at the base of the heart led to generally longer APRD at the base, which could be enhanced by basal illumination and diminished by illumination at the apex (Supplementary Figures S1A–C). Similar overall effects were observed when applying

10.3389/fphys.2023.1167524

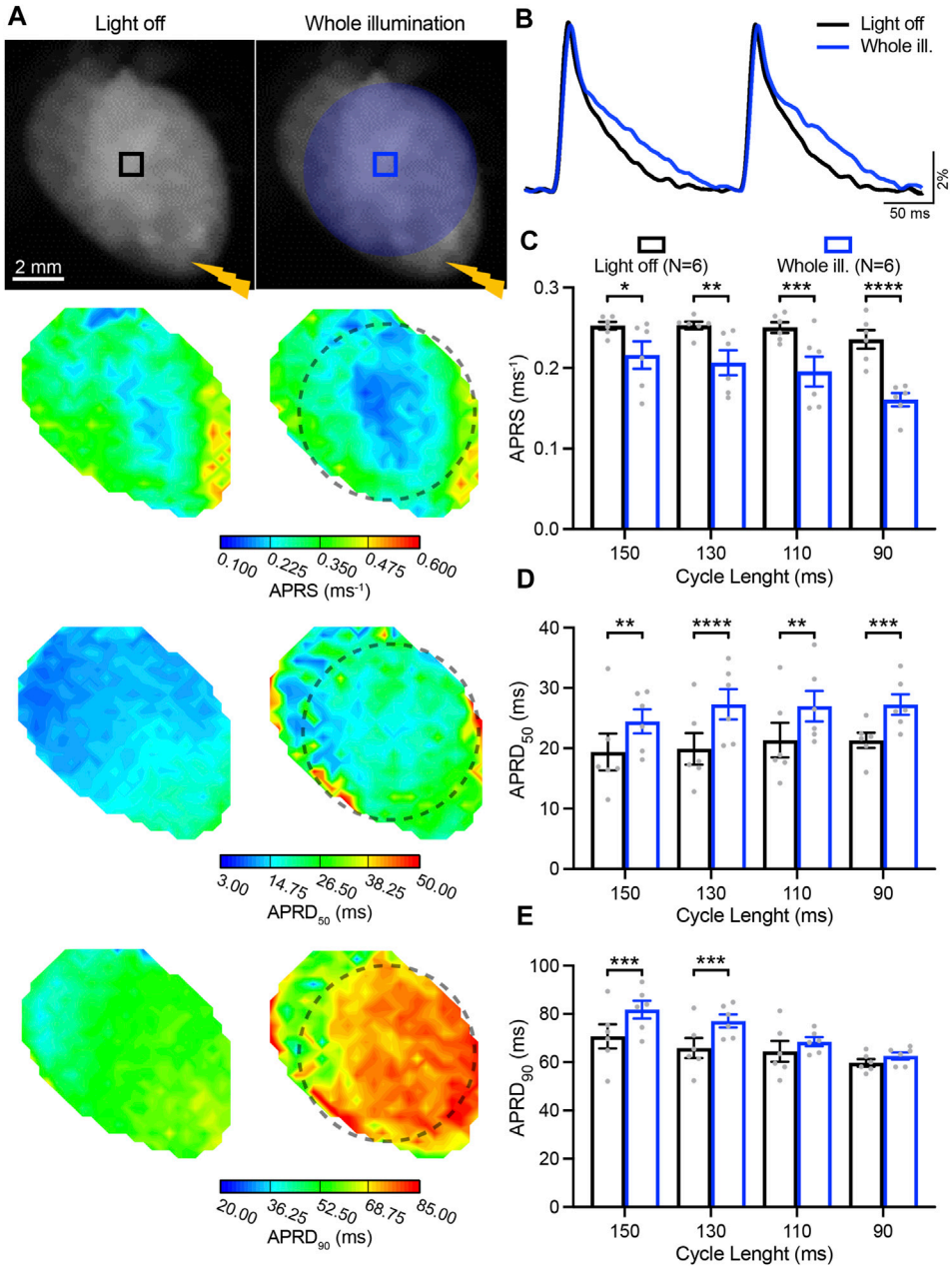

FIGURE 2
Low-intensity optogenetic stimulation of the entire ventricular surface reduces action potential (AP) upstroke velocity and prolongs AP repolarization duration (APRD). **(A)** Top: representative fluorescence images (F0) of mouse hearts perfused with 1 μM blebbistatin with the illumination pattern indicated. Mouse hearts were electrically paced at the apex (yellow bolt symbol) with a cycle length (CL) of 150, 130, 110, and 90 ms, in the absence (left) and in the presence of sub-threshold illumination of the entire ventricular surface (right). Bottom: representative AP rising slope (APRS) and APRD at 50% and 90% repolarization ($APRD_{50}$, $APRD_{90}$) maps recorded at a pacing CL of 130 ms, with the black dashed line indicating the border of the illumination pattern. **(B)** Representative AP traces recorded at pacing CL of 130 ms. **(C–E)** APRS, $APRD_{50}$ and $APRD_{90}$ as a function of the CL, in the absence and in the presence of sub-threshold illumination. The analysis of these parameters was performed in the ROIs shown in **(A)**. Data is reported as mean ± SEM, N represents number of hearts assessed, a two-way RM measurement ANOVA with Tukey's post-hoc test was applied. *$p < 0.05$, **$p < 0.01$, ***$p < 0.001$, ****$p < 0.0001$.

blebbistatin at higher concentration, although hearts generally were not able to follow faster pacing rates (Supplementary Figures S2, S3).

We also assessed light-mediated manipulation of gradients between the right- and left-ventricular area (*right minus left*) during illumination of either one of these regions of the heart (Figure 4A). In the absence of illumination, APRS was similar between the right and left. Illumination at the right resulted in a lower APRS at the right as compared to the left, while illumination of the left led to relative decrease in the left (Figure 4B). $APRD_{50}$ was slightly longer at the right, which was enhanced by illumination of the right, while illumination of

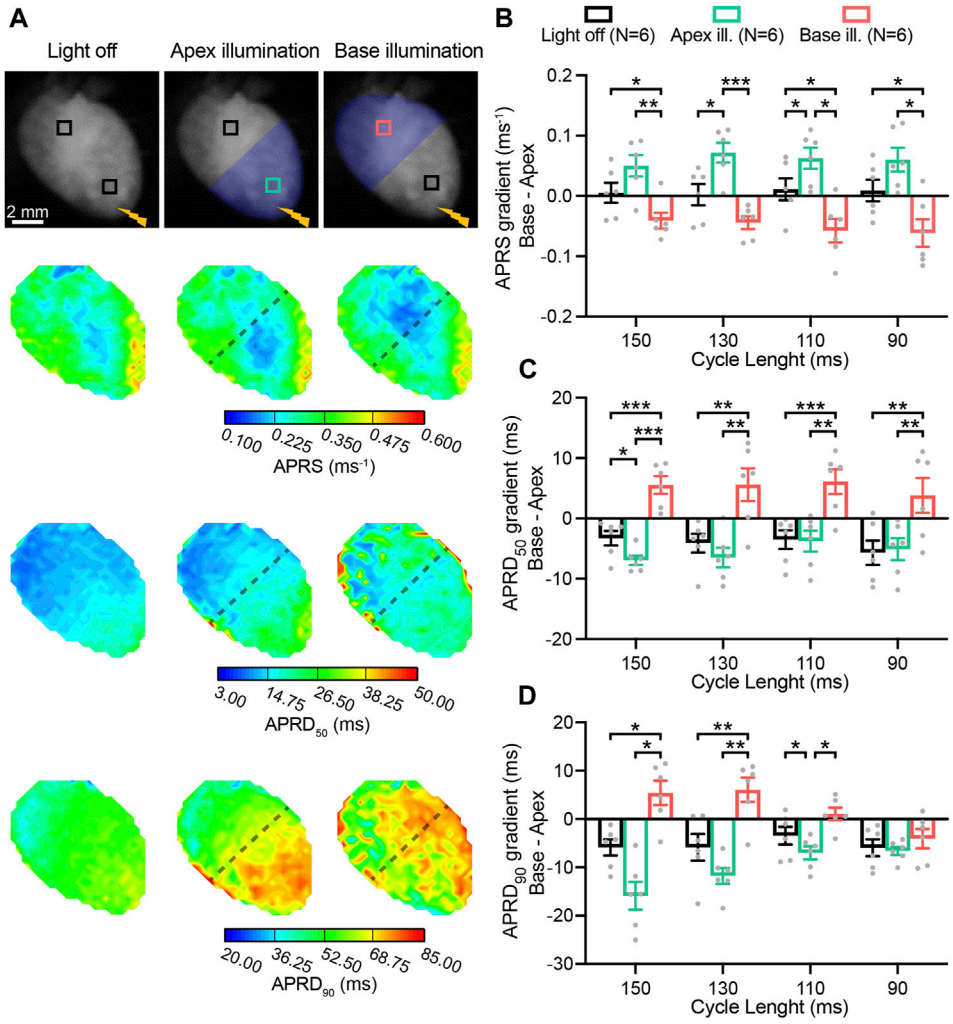

FIGURE 3
Patterned sub-threshold illumination induces base-to-apex gradients in action potential (AP) activation and repolarization characteristics. **(A)** Top: representative fluorescence images (F0) of mouse hearts perfused with 1 μM blebbistatin, with the illumination pattern indicated. Mouse hearts were electrically paced at the apex (yellow bolt symbol) at a cycle length (CL) of 150, 130, 110, and 90 ms, in the absence and in the presence of patterned sub-threshold illumination (apical or basal ventricular area). Bottom: representative AP rising slope (APRS) and AP repolarization duration at 50% and 90% repolarization ($APRD_{50}$, $APRD_{90}$) maps recorded at a pacing CL of 130 ms, with the black dashed lines indicating the border of the illumination patterns. **(B–D)** Base-to-apex gradient (*base minus apex*) of APRS, $APRD_{50}$ and $APRD_{90}$ as a function of the CL, in the absence and in the presence of patterned sub-threshold illumination. The analysis of these parameters was performed in the ROIs shown in **(A)**. Data is reported as mean ± SEM, N represents number of hearts assessed, a two-way RM measurement ANOVA with Tukey's post-hoc test was applied. *$p < 0.05$, **$p < 0.01$, ***$p < 0.001$, ****$p < 0.0001$.

the left abolished the gradient (Figure 4C). No gradient in $APRD_{90}$ was observed in the absence of illumination, while illumination at the right and left led to the emergence of a repolarization gradient with longer APRD in the illuminated area (Figure 4D). These light-induced gradients were significant at lower pacing rates but diminished at higher pacing rates. Moving electrical stimulation from the apex to the base and applying the same illumination patterns resulted in similar results for APRS, while less capable to induce gradients in APRD (Supplementary Figures S1E–G). Hearts perfused with solution containing high blebbistatin displayed similar right-to-left gradients in AP parameters (Supplementary Figures S2, S3).

In addition to inducing intraventricular gradients in AP activation and repolarization kinetics, patterned sub-threshold led to a trend to pattern-dependent localised alternans (beat-to-beat variations) in AP repolarization duration at 70% repolarization ($APRD_{70}$). These findings are presented in the Supplemental Material (Supplementary Figure S4).

3.4 Sub-threshold optogenetic modulation of conduction parameters

In addition to AP parameters, conduction characteristics were also assessed while performing electrical stimulation at the apex and applying various illumination patterns Figure 5A. Sub-threshold illumination of the entire ventricular surface induced a significant reduction of the CV at every pacing rate (Figure 5B),

10.3389/fphys.2023.1167524

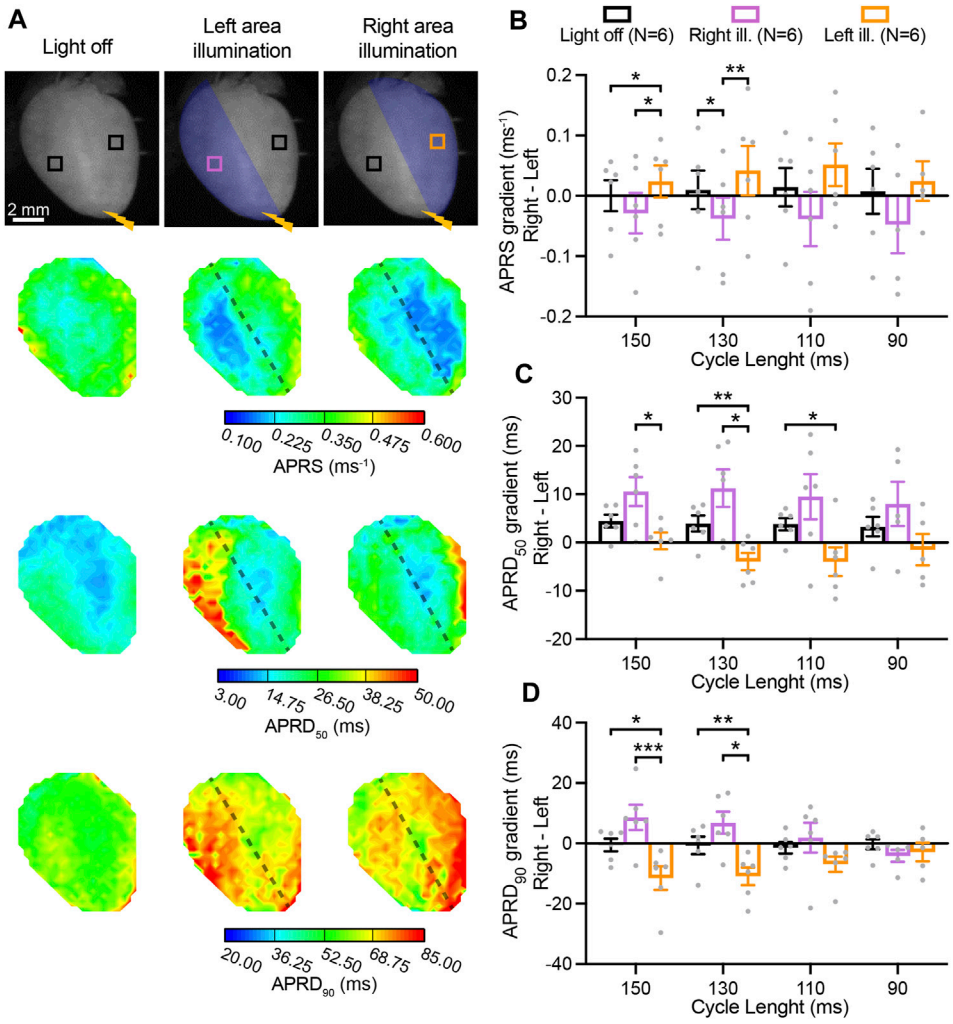

FIGURE 4
Right-to-left gradients in activation and repolarization action potential (AP) characteristics induced by patterned low-intensity optogenetic stimulation. **(A)** Top: representative fluorescence images (F0) of mouse hearts perfused with 1 μM blebbistatin, indicating the illumination pattern. Mouse hearts were electrically paced at the apex (yellow bolt symbol) with a cycle length (CL) of 150, 130, 110, and 90 ms, in the absence and in the presence of patterned sub-threshold illumination (right- and left- ventricular area). Bottom: representative AP rising slope (APRS) and AP repolarization duration at 50% and 90% repolarization ($APRD_{50}$, $APRD_{90}$) maps recorded at a pacing CL of 130 ms, with black dashed lines indicating the border of the illumination patterns. **(B–D)** Right-to-left gradient (*right minus left*) of APRS, $APRD_{50}$, and $APRD_{90}$ as a function of the CL, in the absence and in the presence of patterned sub-threshold illumination. The analysis of these parameters was performed in the ROIs shown in **(A)**. Data is reported as mean ± SEM, N represents number of hearts assessed, a Mixed-Effects with RM analysis with a Tukey's post-hoc test was applied. *$p < 0.05$, **$p < 0.01$, ***$p < 0.001$.

and was increasingly evident at higher pacing rates. AP wavefront dispersion, which is measure of conduction homogeneity, was overall significantly increased upon illumination, and was especially detectable at the fastest pacing rate (Figure 5C). Hence, sub-threshold illumination affects the speed as well as the directionality of wavefront propagation. Apical illumination had no effect on CV gradients between base and apex (*base minus apex*) which were already present in the absence of illumination, with relatively higher CV at the base. By contrast, illumination at the base did affect the gradient in CV, diminishing the pre-existing gradient (Figure 5D). While illumination at the right- or left-ventricular area led to a general effect on right-to-left (*right minus left*) CV gradients ($p < 0.05$), no significant differences between individual illumination patterns were observed (Figure 5E).

3.5 Pro-arrhythmogenic effects of low-intensity illumination

Finally, we performed a proof-of-concept assessment on the impact of patterned sub-threshold illumination on arrhythmia inducibility. Arrhythmia susceptibility was assessed by applying a parasystole pacing strategy, while imposing all the previously described illumination patterns (whole ventricular surface, apex, base, right ventricular area, and left ventricular area of the heart), and in the absence of optogenetic stimulation. Arrhythmic events per second in

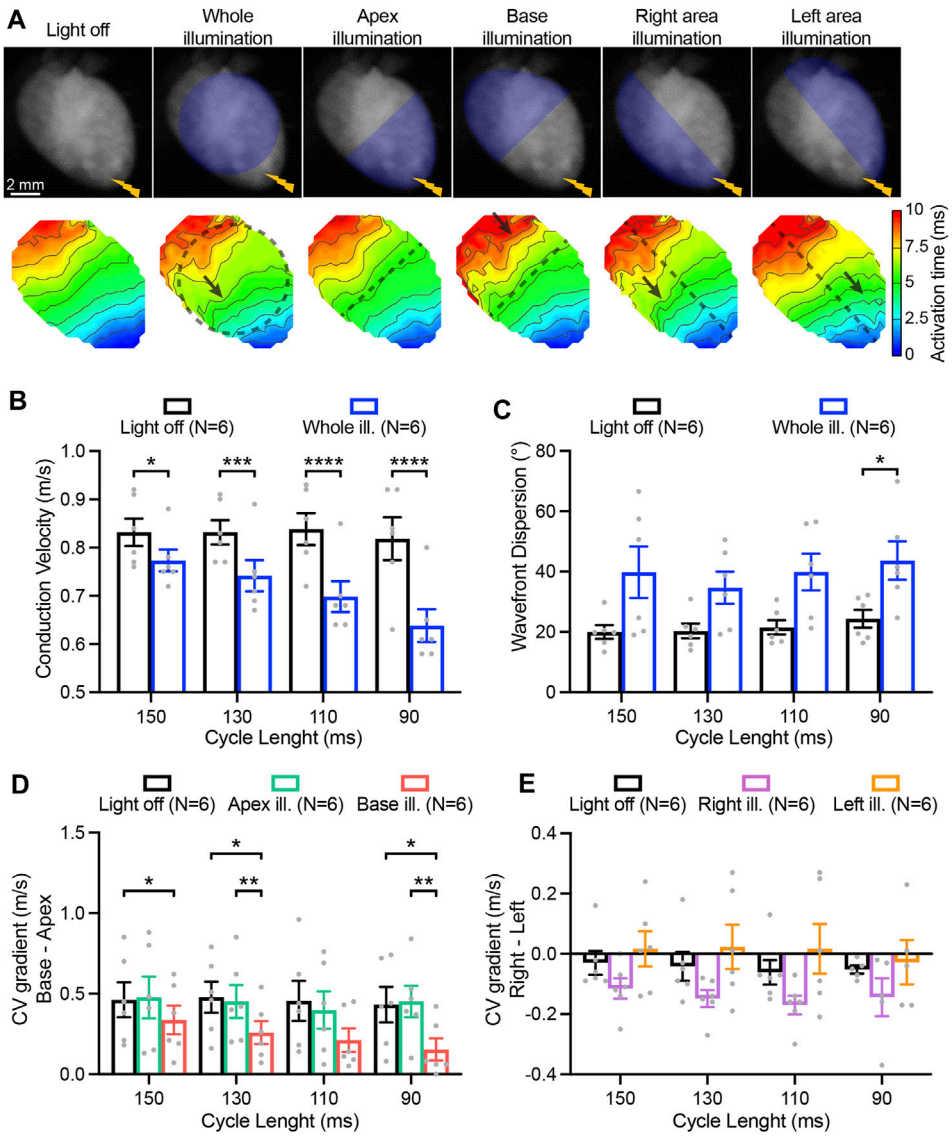

FIGURE 5
Impact of patterned sub-threshold illumination on ventricular conduction characteristics. **(A)** Top: representative fluorescence images (F0) of mouse hearts perfused with 1 μM blebbistatin showing the illumination protocol. Mouse hearts were electrically paced at the apex (yellow bolt symbol) at a cycle length (CL) of 150, 130, 110, and 90 ms, in the absence and in the presence of patterned sub-threshold illumination. Bottom: representative activation maps recorded at a pacing CL of 130 ms, with black dashed lines indicating the border of the illumination patterns and arrows highlighting wavefront abnormalities. **(B, C)** Conduction velocity (CV) and AP wavefront dispersion as a function of the CL during whole ventricular area illumination. **(D, E)** Base-to-apex and right-to-left gradient of CV as a function of the CL, in the absence and in the presence of patterned sub-threshold illumination. Data is reported as mean ± SEM, N represents number of hearts assessed. A two-way RM measurement ANOVA **(B–D)** or Mixed-Effects with RM analysis **(E)** with Tukey's post-hoc test was applied. *$p < 0.05$, **$p < 0.01$, ***$p < 0.001$, ****$p < 0.0001$.

each heart are presented in Figure 6A. Overall, 95% ± 2.7% of the arrhythmias observed were monomorphic, indicating ventricular tachycardia originating from a single rotor. Arrhythmia type was independent from the illumination pattern or stimulation site. Arrhythmia rate was increased when low-intensity illumination was applied, as compared to in the absence of illumination (Figure 6B). When taking individual illumination patterns into account, illumination at the apex resulted in a significant increase in arrhythmia rate (Figure 6C). Hence, patterned sub-threshold illumination results in increased susceptibility to arrhythmia.

4 Discussion

4.1 Blebbistatin time effect

In epicardial optical mapping experiments, the myosin inhibitor blebbistatin is commonly applied at a concentration of 10 μM as an electromechanical uncoupler to prevent motion artefacts and enhance the quality of the fluorescence traces obtained. We here demonstrate that blebbistatin alters cardiac electrophysiology in a time-dependent manner when applied the

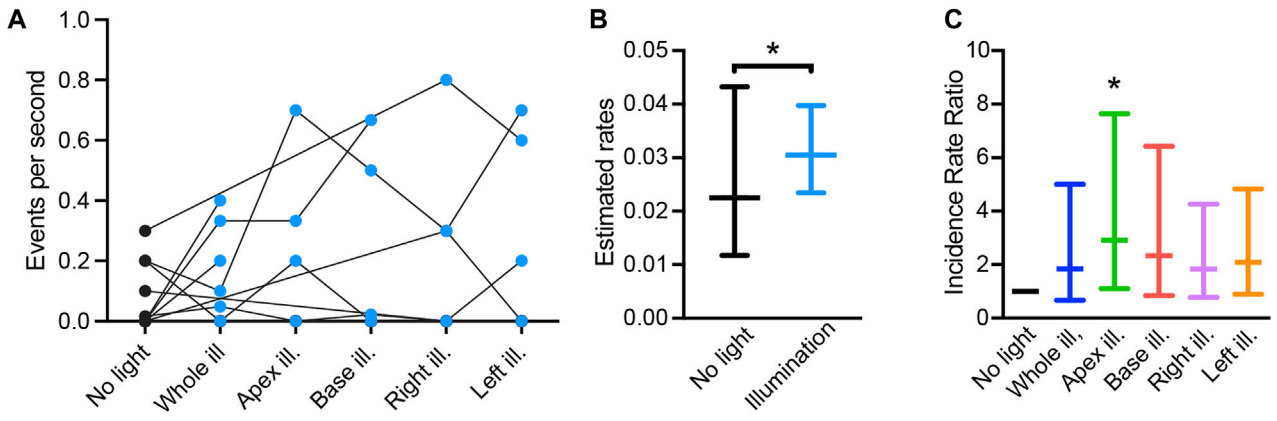

FIGURE 6
Pro-arrhythmic effect of patterned sub-threshold optogenetic stimulation. **(A)** Arrhythmia events per second recorded during the "parasystole paradigm" stimulation protocol, in the absence (black) and presence (blue) of patterned sub-threshold illumination. **(B)** Overall effect of patterned sub-threshold illumination in arrhythmia inducibility displayed as mean estimated rates of arrhythmia and lower/upper bounds of 95% confidence intervals. **(C)** Effect of individual illumination pattern on arrhythmia inducibility displayed as mean incidence rate ratio (IRR) and lower/upper bounds of 95% confidence intervals. Data was collected from 18 mouse hearts. Wald tests were performed for comparison, $*p < 0.05$.

commonly used concentration of 10 μM and did not at the lower concentration of 1 μM. Strikingly, previous research highlighted that blebbistatin can precipitate, blocking myocardial microvasculature and thereby inducing ischaemia and metabolic changes (Swift et al., 2012). In addition, a prolonging effect of blebbistatin on repolarization has been described in isolated hearts from rabbit (Brack et al., 2013) and pig (Lee et al., 2019), although other studies report no impact of blebbistatin on AP parameters (Fedorov et al., 2007; Marchant, et al., 2022). We here provide evidence of a time-dependent impact of high-dose blebbistatin on activation and repolarization kinetics in intact mouse hearts. While we did find a significant increase in displacement of centre of mass of the heart when applying blebbistatin at the low concentration, this displacement of ~4 μm can be considered negligible considering that the pixel size is 80 μm and movement is therefore minimal. Accordingly, we used a low concentration of blebbistatin during the patterned sub-threshold illumination experiments, since cardiac electrical activity should be stable and constant during the entire recording time to avoid misinterpretations of experimental results.

Importantly, even minor residual movement may severely impact signal quality in the setting of uneven staining or tissue heterogeneities (Zasadny et al., 2020). To counter this issue, motion-stabilising algorithms can be applied to correct for movement (Christoph and Luther, 2018). Alternatively, limitations of blebbistatin can potentially also be avoided by using a photostable nitro-derivate of blebbistatin which was recently synthesised and characterised both *in vitro* and *in vivo* (Képiró et al., 2014). Additionally, para-amino-blebbistatin was recently described, and has already been successfully applied to inhibit contraction of zebrafish hearts (Várkuti et al., 2016; van Opbergen et al., 2018). As these novel compounds showed neither phototoxic nor cytotoxic effects, they are promising replacements of blebbistatin for myosin inhibition.

4.2 Sub-threshold induced repolarization gradients: relevance for arrhythmia

For decades, it has been known that ventricular heterogeneities in conduction and RT predisposes to arrhythmia, and is specifically associated with idiopathic VF (Peeters et al., 1998). In addition, repolarization heterogeneities secondary to healed myocardial infarction have been identified as causal factors for ventricular tachycardia in porcine and human hearts (Callans and Donahue, 2022; Kelemen et al., 2022). Recent studies further elucidated the requirements to set the stage for re-entry arrhythmia secondary to repolarization heterogeneities, demonstrating the crucial balance between the ventricular area with short RT and long RT, as well as the steepness of the gradient in RT between these two areas (Cluitmans et al., 2021; Rivaud et al., 2021).

Utilising an optogenetic approach and applying sub-threshold illumination, we here identified several illumination patterns which were able to induce distinct gradients in $APRD_{90}$, which would also cause a gradient in effective refractory period (Knollmann et al., 2001). The largest gradient in $APRD_{90}$ was induced by illuminating the apex and resulted in a gradient of ~15 ms in $APRD_{90}$ between the apical and basal regions of the heart. Previous studies in a porcine model, in which RT gradients were induced by the infusion of drugs specific coronary arteries reported significantly larger RT gradients, with average gradients achieved reaching around 80 ms (Rivaud et al., 2021; van der Waal et al., 2022). However, total repolarization is also considerably longer in porcine hearts as compared to murine hearts. Remarkably, the relative gradient in RT achieved in porcine hearts was similar to the relative gradient in $APRD_{90}$ we achieved by sub-threshold illumination, with a difference of around 25% between the area with long RT and short RT. As such, while the absolute difference in RT achieved by sub-threshold optogenetic stimulation seems limited, it is still possible that the induced

RT gradient is sufficient to increase arrhythmia susceptibility and maintenance. Indeed, we observed an increase in arrhythmia susceptibility when sub-threshold illumination patterns were applied. Strikingly, the highest propensity to arrhythmias was observed upon illumination of the apex, the pattern which also resulted in the largest gradient in $APRD_{90}$. Hence, the findings of the present study indicate that the RT gradients induced by sub-threshold optogenetic stimulation is sufficient to enhance arrhythmogenicity.

4.3 Limitations and future directions

While we here demonstrate that patterned sub-threshold illumination enables optical manipulation of repolarization gradients and cardiac conduction, the generation of steep gradients proved challenging. An essential contributor to this limitation is the scattering of the stimulation light, resulting in contamination in the border area, as well as a higher degree of stimulation at the epicardial surface than at the endocardium, where the intensity drops with approximately 30% (Crocini et al., 2016). To overcome the limitations imposed by the scattering of blue light in the myocardial tissue, a red-shifted opsin could be adopted for optogenetic manipulation of transmural gradient. Another limiting factor is the non-uniform illumination due to the shape of the heart: although the projector produces light relatively homogeneously, light intensity at the epicardial surface will be heterogeneous due to the curvature of the heart.

Importantly, a recent study performed in pig hearts, demonstrate that a sharp border between the short and long repolarization regions is fundamental for arrhythmia maintenance (Rivaud et al., 2021). While the small dimension of murine hearts was potentially a limiting factor for the generation of gradients, we found an increase in arrhythmia susceptibility when the patterned sub-threshold illumination was applied. However, the driving mechanism and nature of the arrhythmias observed in the current investigation remain elusive. Therefore, a more in-depth analysis on the behaviour of these arrhythmia is required to further elucidate the impact of patterned sub-threshold illumination on arrhythmia maintenance.

We here propose the implementation of patterned sub-threshold stimulation for the modelling of cardiac arrhythmogenic syndromes. However, it is important to note the multifactorial nature of cardiac pathophysiology, which generally not only affects electrophysiological properties of the heart, but also structural, metabolic, and transcriptional aspects. Hence, while sub-threshold optogenetic stimulation models the RT prolongation observed in heart failure, other important pathological factors are lacking (Coronel et al., 2013). Moreover, while the introduced approach can be highly relevant for the investigation of RT gradients secondary to an ischaemic event -which leads to local shortening of RT-(Kelemen et al., 2022), the impact of local sub-threshold illumination is the reverse. Taken together, our findings petition for future investigations focussing on testing optogenetic manipulation of conduction and RT gradients in murine, as well as larger hearts and in more complex geometries. In this respect, panoramic (Qu et al., 2007) or volumetric (Sacconi et al., 2022) imaging could provide more comprehensive knowledge of RT gradient-based mechanisms underlying arrhythmia inducibility and maintenance. These techniques allow for investigation across the whole heart surface as well as within ventricle walls, expanding the epicardial observations reported in this study.

5 Conclusion

We here present a novel all-optical method as a robust tool to manipulate cardiac conduction and repolarization characteristics in a spatially-specific manner. An initial assessment indicated that this optogenetic-based strategy resulted in an increase of arrhythmia susceptibility. Hence, this approach represents a promising tool to create a pro-arrhythmogenic substrate driven by conduction slowing and RT heterogeneities. In addition, we provide evidence that the myosin inhibitor blebbistatin alters cardiac electrophysiological characteristics in a time-dependent manner, underlining that blebbistatin should be used in an as low as possible concentration.

Data availability statement

The original contributions presented in the study are included in the article/Supplementary Material, further inquiries can be directed to the corresponding author.

Ethics statement

The animal study was reviewed and approved by the Italian Ministry of Health (protocol number 531/2022-PR) and performed in accordance with the guidelines from Directive 2010/63/EU of the European Parliament on the protection of animals used for scientific purposes.

Author contributions

GM and VB contributed to conception and design of the study, performed experiments and statistical analyses, drafted the manuscript, and created images. LL provided fluorescent dyes. AB performed statistical analyses and wrote sections of the manuscript. MC provided transgenic mice. LS contributed to conception and design of the study, provided funding, and oversaw the study. All authors critically revised and approved the manuscript.

Funding

This study was funded by Fondazione CR Firenze, SALUS project. Additional funding was provided by the European Union's HORIZON programme through a MSCA postdoctoral fellowship awarded to GM (No. 101110977, OPTOCARD). LS is member of the German Research Foundation Collaborative Research Centre SFB1425 (DFG #422681845). We acknowledge support by the Open Access Publication Fund of the University of Freiburg.

Conflict of interest

The authors declare that the research was conducted in the absence of any commercial or financial relationships that could be construed as a potential conflict of interest.

Publisher's note

All claims expressed in this article are solely those of the authors and do not necessarily represent those of their affiliated organizations, or those of the publisher, the editors and the reviewers. Any product that may be evaluated in this article, or claim that may be made by its manufacturer, is not guaranteed or endorsed by the publisher.

Supplementary material

The Supplementary Material for this article can be found online at: https://www.frontiersin.org/articles/10.3389/fphys.2023.1167524/full#supplementary-material

References

Adabag, A. S., Luepker, R. V., Roger, V. L., and Gersh, B. J. (2010). Sudden cardiac death: Epidemiology and risk factors. *Nat. Rev. Cardiol.* 7, 216–225. doi:10.1038/nrcardio.2010.3

Biasci, V., Santini, L., Marchal, G. A., Hussaini, S., Ferrantini, C., Coppini, R., et al. (2022). Optogenetic manipulation of cardiac electrical dynamics using sub-threshold illumination: Dissecting the role of cardiac alternans in terminating rapid rhythms. *Basic Res. Cardiol.* 117, 25. doi:10.1007/s00395-022-00933-8

Brack, K. E., Narang, R., Winter, J., and Ng, G. A. (2013). The mechanical uncoupler blebbistatin is associated with significant electrophysiological effects in the isolated rabbit heart. *Exp. Physiol.* 98, 1009–1027. doi:10.1113/expphysiol.2012.069369

Bruegmann, T., Beiert, T., Vogt, C. C., Schrickel, J. W., and Sasse, P. (2018). Optogenetic termination of atrial fibrillation in mice. *Cardiovasc. Res.* 114, 713–723. doi:10.1093/cvr/cvx250

Bruegmann, T., Malan, D., Hesse, M., Beiert, T., Fuegemann, C. J., Fleischmann, B. K., et al. (2010). Optogenetic control of heart muscle *in vitro* and *in vivo*. *Nat. Methods* 7, 897–900. doi:10.1038/nmeth.1512

Burton, R. A. B., Klimas, A., Ambrosi, C. M., Tomek, J., Corbett, A., Entcheva, E., et al. (2015). Optical control of excitation waves in cardiac tissue. *Nat. Phot.* 9, 813–816. doi:10.1038/nphoton.2015.196

Callans, D. J., and Donahue, J. K. (2022). Repolarization heterogeneity in human post-infarct ventricular tachycardia. *JACC Clin. Electrophysiol.* 8, 713–718. doi:10.1016/j.jacep.2022.03.002

Christoph, J., and Luther, S. (2018). Marker-free tracking for motion artifact compensation and deformation measurements in optical mapping videos of contracting hearts. *Front. Physiology* 9, 1483. doi:10.3389/fphys.2018.01483

Clayton, D., and Hills, M. (2013). *Statistical models in epidemiology*. Oxford: OUP.

Cluitmans, M. J. M., Bear, L. R., Nguyên, U. C., van Rees, B., Stoks, J., ter Bekke, R. M. A., et al. (2021). Noninvasive detection of spatiotemporal activation-repolarization interactions that prime idiopathic ventricular fibrillation. *Sci. Transl. Med.* 13, eabi9317. doi:10.1126/scitranslmed.abi9317

Coronel, R., Wilders, R., Verkerk, A. O., Wiegerinck, R. F., Benoist, D., and Bernus, O. (2013). Electrophysiological changes in heart failure and their implications for arrhythmogenesis. *Biochimica Biophysica Acta (BBA) - Mol. Basis Dis.* 1832, 2432–2441. doi:10.1016/j.bbadis.2013.04.002

Crocini, C., Ferrantini, C., Coppini, R., Scardigli, M., Yan, P., Loew, L. M., et al. (2016). Optogenetics design of mechanistically-based stimulation patterns for cardiac defibrillation. *Sci. Rep.* 6, 35628. doi:10.1038/srep35628

de Jong, S., van Veen, T. A. B., van Rijen, H. V. M., and de Bakker, J. M. T. (2011). Fibrosis and cardiac arrhythmias. *J. Cardiovasc. Pharmacol.* 57, 630–638. doi:10.1097/FJC.0b013e318207a35f

Entcheva, E., and Kay, M. W. (2021). Cardiac optogenetics: A decade of enlightenment. *Nat. Rev. Cardiol.* 18, 349–367. doi:10.1038/s41569-020-00478-0

Fabritz, L., Kirchhof, P., Franz, M. R., Eckardt, L., Mönnig, G., Milberg, P., et al. (2003). Prolonged action potential durations, increased dispersion of repolarization, and polymorphic ventricular tachycardia in a mouse model of proarrhythmia. *Basic Res. Cardiol.* 98, 25–32. doi:10.1007/s00395-003-0386-y

Fedorov, V. V., Lozinsky, I. T., Sosunov, E. A., Anyukhovsky, E. P., Rosen, M. R., Balke, C. W., et al. (2007). Application of blebbistatin as an excitation–contraction uncoupler for electrophysiologic study of rat and rabbit hearts. *Heart rhythm.* 4, 619–626. doi:10.1016/j.hrthm.2006.12.047

Feola, I., Volkers, L., Majumder, R., Teplenin, A., Schalij, M. J., Panfilov, A. V., et al. (2017). Localized optogenetic targeting of rotors in atrial cardiomyocyte monolayers. *Circulation Arrhythmia Electrophysiol.* 10, e005591. doi:10.1161/CIRCEP.117.005591

Jeron, A., Mitchell, G. F., Zhou, J., Murata, M., London, B., Buckett, P., et al. (2000). Inducible polymorphic ventricular tachyarrhythmias in a transgenic mouse model with a long Q-T phenotype. *Am. J. Physiology-Heart Circulatory Physiology* 278, H1891–H1898. doi:10.1152/ajpheart.2000.278.6.H1891

Karathanos, T. V., Boyle, P. M., and Trayanova, N. A. (2014). Optogenetics-enabled dynamic modulation of action potential duration in atrial tissue: Feasibility of a novel therapeutic approach. *EP Eur.* 16, iv69–iv76. doi:10.1093/europace/euu250

Kelemen, K., Greener, I. D., Wan, X., Parajuli, S., and Donahue, J. K. (2022). Heterogeneous repolarization creates ventricular tachycardia circuits in healed myocardial infarction scar. *Nat. Commun.* 13, 830. doi:10.1038/s41467-022-28418-1

Képiró, M., Várkuti, B. H., Végner, L., Vörös, G., Hegyi, G., Varga, M., et al. (2014). para-Nitroblebbistatin, the non-cytotoxic and photostable myosin II inhibitor. *Angew. Chem. Int. Ed. Engl.* 53, 8211–8215. doi:10.1002/anie.201403540

Knollmann, B. C., Katchman, A. N., and Franz, M. R. (2001). Monophasic action potential recordings from intact mouse heart: Validation, regional heterogeneity, and relation to refractoriness. *J. Cardiovasc. Electrophysiol.* 12, 1286–1294. doi:10.1046/j.1540-8167.2001.01286.x

Lee, P., Quintanilla, J. G., Alfonso-Almazán, J. M., Galán-Arriola, C., Yan, P., Sánchez-González, J., et al. (2019). *In vivo* ratiometric optical mapping enables high-resolution cardiac electrophysiology in pig models. *Cardiovasc. Res.* 115, 1659–1671. doi:10.1093/cvr/cvz039

Loen, V., Vos, M. A., and van der Heyden, M. A. G. (2022). The canine chronic atrioventricular block model in cardiovascular preclinical drug research. *Br. J. Pharmacol.* 179, 859–881. doi:10.1111/bph.15436

Marchal, G. A., and Remme, C. A. (2022). Subcellular diversity of Nav1.5 in cardiomyocytes: Distinct functions, mechanisms and targets. *J. Physiology* 601, 941–960. doi:10.1113/JP283086

Marchant, J. L., Smith, F. M., and Farrell, P. (2022). The effective use of blebbistatin to study the action potential of cardiac pacemaker cells of zebrafish (*Danio rerio*) during incremental warming. *Curr. Res. Physiology* 5, 48–54. doi:10.1016/j.crphys.2022.01.002

Matiukas, A., Mitrea, B. G., Qin, M., Pertsov, A. M., Shvedko, A. G., Warren, M. D., et al. (2007). Near-infrared voltage-sensitive fluorescent dyes optimized for optical mapping in blood-perfused myocardium. *Heart rhythm.* 4, 1441–1451. doi:10.1016/j.hrthm.2007.07.012

Milberg, P., Ramtin, S., Mönnig, G., Osada, N., Wasmer, K., Breithardt, G., et al. (2004). Comparison of the *in vitro* electrophysiologic and proarrhythmic effects of amiodarone and sotalol in a rabbit model of acute atrioventricular block. *J. Cardiovasc. Pharmacol.* 44, 278–286. doi:10.1097/01.fjc.0000129581.81508.78

Nagel, G., Brauner, M., Liewald, J. F., Adeishvili, N., Bamberg, E., and Gottschalk, A. (2005). Light activation of channelrhodopsin-2 in excitable cells of *Caenorhabditis elegans* triggers rapid behavioral responses. *Curr. Biol.* 15, 2279–2284. doi:10.1016/j.cub.2005.11.032

Nussinovitch, U., and Gepstein, L. (2015). Optogenetics for *in vivo* cardiac pacing and resynchronization therapies. *Nat. Biotechnol.* 33, 750–754. doi:10.1038/nbt.3268

Nyns, E. C. A., Kip, A., Bart, C. I., Plomp, J. J., Zeppenfeld, K., Schalij, M. J., et al. (2017). Optogenetic termination of ventricular arrhythmias in the whole heart: Towards biological cardiac rhythm management. *Eur. Heart J.* 38, 2132–2136. doi:10.1093/eurheartj/ehw574

Peeters, H. A. P., Sippensgroenewegen, A., Wever, E. F. D., Potse, M., Daniëls, M. C. G., Grimbergen, C. A., et al. (1998). Electrocardiographic identification of abnormal ventricular depolarization and repolarization in patients with idiopathic ventricular fibrillation. *J. Am. Coll. Cardiol.* 31, 1406–1413. doi:10.1016/S0735-1097(98)00120-X

Qu, F., Ripplinger, C. M., Nikolski, V. P., Grimm, C., and Efimov, I. R. (2007). Three-dimensional panoramic imaging of cardiac arrhythmias in rabbit heart. *J. Biomed. Opt.* 12, 044019. doi:10.1117/1.2753748

Rabe-Hesketh, S., and Skrondal, A. (2012). *Multilevel and longitudinal modeling using stata*. 3rd ed. College Station, TX: Stata Press.

Rivaud, M. R., Bayer, J. D., Cluitmans, M., Waal, J. van der, Bear, L. R., Boukens, B. J., et al. (2021). Critical repolarization gradients determine the induction of reentry-based torsades de pointes arrhythmia in models of long QT syndrome. *Heart rhythm.* 18, 278–287. doi:10.1016/j.hrthm.2020.09.020

Sacconi, L., Silvestri, L., Rodríguez, E. C., Armstrong, G. A. B., Pavone, F. S., Shrier, A., et al. (2022). KHz-rate volumetric voltage imaging of the whole Zebrafish heart. *Biophys. Rep. (N Y)* 2, 100046. doi:10.1016/j.bpr.2022.100046

Salama, G., Baker, L., Wolk, R., Barhanin, J., and London, B. (2009). Arrhythmia phenotype in mouse models of human long QT. *J. Interv. Card. Electrophysiol.* 24, 77–87. doi:10.1007/s10840-008-9339-6

Scardigli, M., Müllenbroich, C., Margoni, E., Cannazzaro, S., Crocini, C., Ferrantini, C., et al. (2018). Real-time optical manipulation of cardiac conduction in intact hearts. *J. Physiology* 596, 3841–3858. doi:10.1113/JP276283

Skrondal, A., and Rabe-Hesketh, S. (2004). *Generalized latent variable modeling: Multilevel, longitudinal, and structural equation models*. United States: CRC Press.

Swift, L. M., Asfour, H., Posnack, N. G., Arutunyan, A., Kay, M. W., and Sarvazyan, N. (2012). Properties of blebbistatin for cardiac optical mapping and other imaging applications. *Pflugers Arch. - Eur. J. Physiol.* 464, 503–512. doi:10.1007/s00424-012-1147-2

van der Waal, J., Bear, L., Meijborg, V., Dubois, R., Cluitmans, M., and Coronel, R. (2022). Steep repolarization time gradients in pig hearts cause distinct changes in composite electrocardiographic T-wave parameters. *Ann. Noninvasive Electrocardiol.* 27, e12994. doi:10.1111/anec.12994

van Opbergen, C. J. M., Koopman, C. D., Kok, B. J. M., Knöpfel, T., Renninger, S. L., Orger, M. B., et al. (2018). Optogenetic sensors in the zebrafish heart: A novel *in vivo* electrophysiological tool to study cardiac arrhythmogenesis. *Theranostics* 8, 4750–4764. doi:10.7150/thno.26108

Várkuti, B. H., Képiró, M., Horváth, I. Á., Végner, L., Ráti, S., Zsigmond, Á., et al. (2016). A highly soluble, non-phototoxic, non-fluorescent blebbistatin derivative. *Sci. Rep.* 6, 26141. doi:10.1038/srep26141

Zaglia, T., Pianca, N., Borile, G., Da Broi, F., Richter, C., Campione, M., et al. (2015). Optogenetic determination of the myocardial requirements for extrasystoles by cell type-specific targeting of ChannelRhodopsin-2. *Proc. Natl. Acad. Sci.* 112, E4495–E4504. doi:10.1073/pnas.1509380112

Zasadny, F. M., Dyavanapalli, J., Dowling, N. M., Mendelowitz, D., and Kay, M. W. (2020). Cholinergic stimulation improves electrophysiological rate adaptation during pressure overload-induced heart failure in rats. *Am. J. Physiology-Heart Circulatory Physiology* 319, H1358–H1368. doi:10.1152/ajpheart.00293.2020

Frontiers in Physiology

Understanding how an organism's components work together to maintain a healthy state

The second most-cited physiology journal, promoting a multidisciplinary approach to the physiology of living systems - from the subcellular and molecular domains to the intact organism and its interaction with the environment.

Discover the latest Research Topics

See more →

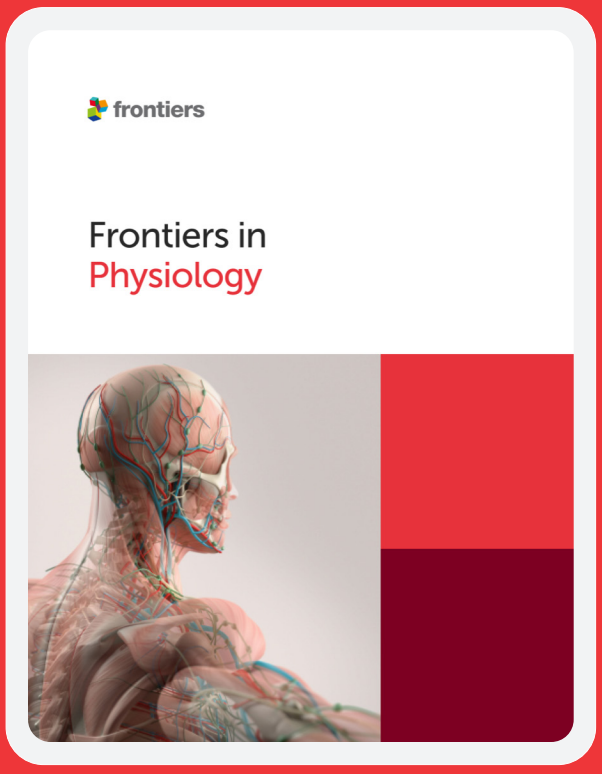

Frontiers

Avenue du Tribunal-Fédéral 34
1005 Lausanne, Switzerland
frontiersin.org

Contact us

+41 (0)21 510 17 00
frontiersin.org/about/contact